Quantum scalar field theory on a rotating black hole in five dimensions

Alessandro Monteverdi

Supervisor: Elizabeth Winstanley

A thesis submitted to The University of Sheffield for the degree of Doctor of Philosophy

in the

School of Mathematical and Physical Sciences

March 2025

University of Sheffield

Dedicata a mamma e papà...

'Aspettiamo le 18, aspettiamo il venerdì, aspettiamo l'amore perfetto, aspettiamo perfino il momento giusto per essere felici, aspettiamo una casa più bella, quel viaggio che ci cambia la vita, l'aumento, l'estate, il lunedì per iniziare la dieta e il sabato per il pasto libero, e intanto la vita ci scorre accanto come un treno mentre aspettiamo sul binario sbagliato e la perdiamo nei "quando avrò tempo" o "quando sarà il momento giusto". E se non fosse mai il momento giusto? Se tutto quello che avessimo fosse questo istante? Adesso, non c'è venerdì, non c'è estate, non c'è futuro che ti darà indietro ciò che stai vivendo oggi. La felicità è in tutta quella semplicità quotidiana che ignoriamo perché troppo impegnati ad aspettare; smettila di rimandare costantemente la vita a domani, perché domani potrebbe essere troppo tardi.'

- Alex Righi.

'We wait for 6 PM, for Friday, for the perfect love, we even wait for the right moment to be happy, we wait for a bigger house, for that life-changing trip, for a raise, for summer, for Monday to start the diet and for Saturday for the free meal, while life passes us by like a train as we wait on the wrong platform, losing it in the "when I have time" or "when the moment is right." But what if the right moment never comes? What if all we ever have is this very instant? Right now, there is no Friday, no summer, no future that will give you back what you're living today. Happiness lies in all that everyday simplicity we ignore because we're too busy waiting; stop constantly postponing life until tomorrow, because tomorrow might be too late.'

Contents

List of Tables

List of Figures

Abstract

In this thesis, we study a massive scalar field on a five-dimensional, rotating, asymptotically anti-de Sitter black hole spacetime. We introduce an enhanced symmetry in the spacetime by taking the two angular momentum parameters equal. We picked this setup because the geometry possesses additional symmetries that simplify analysis of mode solutions of the scalar field equation and the stress–energy tensor. In fact, when the angular momentum of the black hole is sufficiently small (so we are slowly rotating), we find that there is no speed-of-light surface. This allows us to identify a Killing vector field that is timelike everywhere outside the event horizon. Numerous advantages come from this setup, one of these is the absence of classical superradiance, which extremely simplifies the calculation. We then use quantum field theory on curved spacetime to perform the canonical quantisation of the massive scalar field on this background. We study separately the angular and radial parts of the Klein–Gordon equation. We identify the radial differential equation as a Heun equation, while the angular part takes the form of a spin-weighted spherical harmonics differential equation. We also present addition theorems for spin-weighted spherical harmonics, generalising previous results for scalar (spin-zero) spherical harmonics. These new results simplify the numerical analysis of the stress–energy tensor of a scalar field on a Kerr–AdS$_5$ black hole, but could be generalised to other scenarios. After this, we construct the quantum states to evaluate observables. In particular, we construct analogues of the Boulware and Hartle–Hawking quantum states for the quantum scalar field. Finally, we compute the differences in expectation values of the square of the quantum scalar field operator and the stress–energy tensor operator between these two quantum states, and present their numerical evaluation.

Declaration of Authorship

I hereby confirm that, except where clear reference is made to the work of others, this thesis is my own work. I am aware of the University's Guidance on the Use of Unfair Means (www.sheffield.ac.uk/ssid/unfair-means). This work has not been previously presented for an award at this, or any other, university. The following publications have arisen from work in this thesis:

- A. Monteverdi and E. Winstanley. Quantum scalar field theory on equal-angular-momenta Myers-Perry-AdS black holes. arXiv:2412.02814 [hep-th], December 2024.
- A. Monteverdi and E. Winstanley. Some addition theorems for spin-weighted spherical harmonics. Universe, 10(12):461, 2024. doi:10.3390/universe10120461, arXiv:2410.23201 [math-ph].

Alessandro Monteverdi

Acknowledgments

'Oscar Wilde said that if you know exactly what you want to be in life a teacher, or a grocer, or a judge, or a soldier you will become it that is your punishment. Actually not knowing what you want to be, reinventing yourself every morning, not being a noun but being a verb, being moving in life not being fixed in life is a privileged even though is a difficult one sometimes, don't feel bad about not knowing (...), be a permanent student if you can in the mind.'

- Stephen Fry.

'Oscar Wilde ha detto che se sai esattamente cosa vuoi essere nella vita – un insegnante, un commesso, un giudice o un soldato – lo diventerai: questa è la tua punizione. In realtà, non sapere cosa vuoi essere, reinventarti ogni mattina, non essere un sostantivo ma un verbo, essere in movimento nella vita anziché rimanere fermo, è un privilegio, anche se a volte è difficile. Non sentirti male per non sapere (...) sii sempre uno studente, se puoi, nella mente.'

First and foremost, I would like to thank my supervisor, Elizabeth Winstanley. I would not have reached the end of my PhD without her. Her patience, organisation, and availability were invaluable, along with all the useful discussions and explanations she provided during my PhD. If I have grown as a researcher, it is mainly thanks to her.

I would also like to thank the University of Sheffield, which provided me with the opportunity to pursue a PhD. The Hicks Building has been my second home for four years, and I am grateful to the university for providing this space for us students, as well as to all the administrative staff in F10 who helped me whenever I was in need. I would also like to thank the staff at the University of Sheffield High Performance Computing service, where most of the numerical computations in this thesis were performed.

I also want to thank UKRI and EPSRC for the scholarship and travel allowance, which not only enabled me to do a PhD but also allowed me to travel to conferences, meet new people, and present my research.

I wish to express my gratitude to my master's supervisor, Claudio Dappiaggi, for introducing me to the fascinating topics of semi-classical analysis and quantum field theory on curved backgrounds. Without him, I would never have progressed in my academic career or pursued a PhD. I am thankful for all his support during my master's and for the valuable lessons he taught me, as well as for his continued support during my PhD.

I would like to thank the CRAG group, who were very welcoming when I first moved in the UK after COVID. I am grateful to Siva, George, and Jacob for the engaging discussions and for being travel partners to conferences. I also want to thank Mary and Gaspard, who started the PhD journey with me, for all the memories we shared in the first months while discovering a new city together and joining the CRAG group as first-year PhD students. I am also thankful to the people I shared the H23 office with at the beginning of my PhD: Andrea, for helping me transition to a new country, and Elliot, for the amazing drawings on the blackboard and for the fun times playing Wordle together with Gaspard. I would like to thank Jonny for brightening up Wednesday mornings with his amazing stories, horrible jokes, and pictures of his cute dog, Spud.

I am grateful to Richard for all the good times we spent together and for introducing me to powerlifting—something I would never have thought of doing without his guidance. In two years at the gym, I reached milestones that I would never have achieved without him.

I also want to thank Elsa for being kind and always available when I needed help, for all the dinners she hosted at her place, for the amazing bread she baked, and for the most delicious hummus I have ever had. I want to thank her also for all the help she gave me at the beginning of my PhD, easing my transition to a new country and a new life, and for all the amazing hugs that always brightened my day.

I want to express my gratitude to Lisa, my office partner in G16. Part of why I have grown so much as a researcher—and why I managed to complete my PhD—is thanks to her. I am grateful for our scientific discussions in the office on various research topics, for the time spent together overcoming life's difficulties, and for her hospitality in inviting us to her place so often that it eventually felt like a second home. Thank you for always being there to help and for being my gym partner. I am truly glad we met and shared this journey as office partners.

I also want to thank my girlfriend, Lavi, who stayed with me throughout this journey in a different country, always by my side when times were tough and supporting me even from a distance. Thank you for your patience, for supporting me when it was not easy, and for always lending a sympathetic ear whenever I needed, as well as for always believing in me

on this journey that has been my PhD.

I would also like to thank my friends in Italy for always being just one phone call away, for coming to visit me, and for being present throughout my life even from a different country. You are a special and important part of my life.

Finally, I want to thank my family—my mom, dad, and sister—for always being there when I needed them, for helping me in this new step of my life, and for allowing me to pursue this mathematical journey. I would not be the person I am today without them. I also want to thank my grandma, who showed me how to be strong in the face of life's challenges, to always remain positive, and for being the most caring person I know.

Thank you to everyone who made my PhD so special; I am going to miss my life in Sheffield.

Part I

Fundamentals

Chapter 1

The beginning of the journey: general relativity

'Nel mezzo del cammin di nostra vita, Mi ritrovai per una selva oscura, Che la diritta via era smarrita.'

- Dante's Inferno (Canto I, lines 1–3).

'Midway upon the journey of our life, I found myself within a dark forest, For the straight path had been lost.'

General relativity was, and still is, one of the most successful theories in describing classical phenomena in the universe. Historically, the need for a new theory to describe gravity arose due to limitations in Newton's theory of gravity. An example of these limitations is that if we imagine moving the Sun to a different position further away from Earth, changing in an instant the distance between the two objects, Newton's theory implies that Earth would *instantly* experience a change in gravitational pull. The word "instantly" is incompatible with discoveries made at the beginning of the 20th century. Special relativity, introduced by Einstein in 1905 [52], postulates that electromagnetic interactions propagate at the finite speed of light, c, in all inertial frames. As a result, it became clear that a new theory was required, one that could reconcile these principles with gravity. This is where General Relativity came into play.

In the framework of General Relativity (GR), gravity is described not as a force, but rather as a consequence of the geometrical curvature of spacetime. We will introduce some of the mathematical tools to describe this theory in the following sections. However, the main goal of this thesis is to study and understand one of the most intriguing objects in the universe, theorised within this framework and imaged through a highly sophisticated

interferometry method almost 100 years after their theorisation: black holes. In this context, a black hole can be naively described as a region where gravity is so strong that nothing, neither particles nor radiation, can escape from it. The theory of GR predicts that a sufficiently compact mass can deform spacetime to create a black hole [53]. The origin of this theory can be traced back to 1784, when John Michell submitted a paper to *Philosophical Transactions* in which he attempted to describe light using Newtonian gravitational laws [100]. Long before the concepts of light speed invariance or photons were understood, Michell theorized the existence of a cosmological object with sufficient mass ($1.25 \times 10^8 M_\odot$) to attract light to its surface.

The first "modern" work describing a black hole was written in 1916 by Karl Schwarzschild [128], who derived the first static vacuum solution for Einstein's field equations (1.40), describing the behaviour of a gravitational field around a spherical body of mass M. The Schwarzschild solution illustrates how the curvature of spacetime around a massive object leads to phenomena such as event horizons. The event horizon can be thought of as the boundary that prevents an outside observer from seeing the singularity created by the collapsed mass. It is what fully characterizes a black hole and limits the spacetime in such a way that not even light can escape from it.

Another solution to Einstein's field equations was found by Roy Kerr in 1963 [80], describing a rotating black hole. This solution contains two free parameters: one, M, representing the mass of the source, and another, J, representing its angular momentum. When J is set to zero, the Kerr solution reduces to that of Schwarzschild. It has been proven that these are the only vacuum stationary families of solutions to Einstein's field equations, with associated spacetimes describing asymptotically flat black holes, in four dimensions [74, 75, 123]. Like the Schwarzschild solution, the Kerr solution has an event horizon and an inner curvature singularity. Kerr-like solutions represent the quintessential models for black holes, as these are the one that we have seen in the universe.

Any non-extremal Kerr black hole features an inner horizon, an outer horizon, and an ergosphere. The inner horizon is a Cauchy horizon, which, naively, represents a boundary in spacetime beyond which the laws of physics, as predicted by classical general relativity, break down in terms of predictability. The outer horizon, on the other hand, is a Killing horizon, with the Killing parameter associated with its Killing vector field interpretable, as in the Schwarzschild case, as a time coordinate. Lastly, in order to discuss the ergosphere, we introduce the concept of frame-dragging. Frame-dragging is a general relativistic phenomenon in which rotating massive objects twist the surrounding spacetime. The first direct measurement of this effect was conducted in 2011 by the Gravity Probe B experiment [55], which was able to detect it while orbiting the Earth. In the case of a rotating

black hole, frame-dragging becomes so extreme near the event horizon that it gives rise to a region called the ergosphere. Within this region, objects are compelled to co-rotate with the black hole, not due to any applied force, but because of the curvature of spacetime.

Black holes have been studied intensely by the scientific community, and the first experimental image of a black hole was released on 10 April 2019 by the Event Horizon Telescope (EHT) collaboration [5].

1.1 Geometrical tools

In this section we will present some core concepts of the theory of general relativity and differential geometry, which will be propaedeutical for the thesis and the study that we are going to present later on. We will follow [119, 147].

We start by giving the definition of manifold which is the building block of the theory [147].

1.1.1 Definition. *A manifold $\mathcal{M}$ is a Hausdorff, second countable, connected, orientable, smooth n-dimensional topological space, where **Hausdorff** means that for any two distinct points $p, q \in \mathcal{M}$, there exist disjoint open neighbourhoods U of p and V of q such that $U \cap V = \emptyset$.*

The Hausdorff property ensures that points can be "separated" in the topology of $\mathcal{M}$. In our context, we require that a causal structure exists on our background manifold. Let M be a smooth manifold. At each point $x \in M$, we denote the tangent space by T_xM and the cotangent space (the dual space of T_xM) by T_x^*M.

1.1.2 Definition. *A (p, q) tensor at a point $x \in M$ is defined as a multilinear map*

$$T : \underbrace{T_x^*M \times \cdots \times T_x^*M}_{p \text{ times}} \times \underbrace{T_xM \times \cdots \times T_xM}_{q \text{ times}} \longrightarrow \mathbb{R}, \tag{1.1}$$

that is, a map which takes p covectors and q vectors at x and returns a real number, linear in each of its arguments. The collection of all such tensors at x forms the tensor space $T_q^p(M)$.

The second object that we need to define is a distance between points on a manifold, such as the distance between p and q in $\mathcal{M}$. To this end we define a **metric** g on a manifold $\mathcal{M}$. This is a symmetric, nondegenerate tensor field of type $(0, 2)$. This means that a metric defines an inner product on the tangent space at each point in $\mathcal{M}$, though it is not necessarily positive definite.

In a coordinate basis, the metric g can be expanded in terms of its components $g_{\mu\nu}$ as:

$$g = \sum_{\mu,\nu} g_{\mu\nu}\, dx^\mu \otimes dx^\nu, \tag{1.2}$$

where $g_{\mu\nu}$ are the components of g in the chosen coordinate system. Alternatively, the notation ds^2 is sometimes used to represent the metric tensor. In this case, Equation (1.2) is written as:

$$ds^2 = \sum_{\mu,\nu} g_{\mu\nu}\, dx^\mu dx^\nu, \tag{1.3}$$

where, by convention, we omit the outer product symbol between dx^μ and dx^ν. This notation ds^2 reflects the interpretation of the metric as representing "infinitesimal squared distance" between points. This quantity is commonly refer to as the line element.

Given a metric g, we can construct an **orthonormal basis** $v_{(1)}, \ldots, v_{(n)}$ for the tangent space at each point $p \in \mathcal{M}$, such that:

- $g(v_{(a)}, v_{(b)}) = 0$ if $(a) \neq (b)$,
- $g(v_{(a)}, v_{(a)}) = \pm 1$,

where $v_{(n)}$ is a vector and the subscript (n) serves to label it. Although multiple orthonormal bases exist at each point p, the number of basis vectors with $g(v_{(a)}, v_{(a)}) = +1$ and those with $g(v_{(a)}, v_{(a)}) = -1$ does not depend on the chosen basis. This count of $+$ and $-$ signs is known as the **signature** of the metric.

In **Riemannian geometry**, we usually work with **positive definite metrics**, where the signature is $+ + \cdots +$. However, in spacetime, the metric has a **Lorentzian signature** $- + + + \cdots$, with one minus sign and the rest plus. Metrics of this type are called **Lorentzian metrics**.

We call the pair $(\mathcal{M}, g)$ a Lorentzian manifold if $\mathcal{M}$ is as per Definition 1.1.1, endowed with a Lorentzian metric g. Let us give an example:

1.1.3 Example. Consider Minkowski spacetime, $\mathcal{M} = \mathbb{R}^4$, with standard Cartesian coordinates with respects to which the metric tensor $\eta_{\mu\nu}$ is given by

$$\eta_{\mu\nu} = \mathrm{diag}(-1, 1, 1, 1).$$

For any point $p \in \mathbb{R}^4$, we can classify other points $q \in \mathbb{R}^4$ relative to p by the properties of the vector v_{pq}, which is the vector connecting the point p and q:

- q is **timelike separated** from p if $\eta(v_{pq}, v_{pq}) < 0$,
- q is **spacelike separated** from p if $\eta(v_{pq}, v_{pq}) > 0$,

- q is **lightlike separated** from p if $\eta(v_{pq}, v_{pq}) = 0$.

Using this classification, we define four sets of points, $I^{\pm}_{\mathbb{R}^4}(p)$ and $J^{\pm}_{\mathbb{R}^4}(p)$:

- $I^{+}_{\mathbb{R}^4}(p)$ and $I^{-}_{\mathbb{R}^4}(p)$ represent the **chronological future** and **chronological past** of p, respectively, while $I^{\pm}_{\mathbb{R}^4}(p)$ represents the set containing all points that are timelike separated from p.
- $J^{+}_{\mathbb{R}^4}(p)$ and $J^{-}_{\mathbb{R}^4}(p)$ represent the **causal future** and **causal past** of p, while, analogously $J^{\pm}_{\mathbb{R}^4}(p)$ represents the set containing all points that are causally separated from p (i.e., timelike or null separated).

This classification in Minkowski spacetime cannot be directly generalized to arbitrary manifolds. For a general point $p \in \mathcal{M}$ in a Lorentzian manifold, we examine the tangent space $T_p\mathcal{M}$. Using the metric g, a tangent vector $v \in T_p\mathcal{M}$ can be classified as:

- **timelike** if $g(v, v) < 0$,
- **spacelike** if $g(v, v) > 0$,
- **lightlike** if $g(v, v) = 0$.

We call $\mathcal{M}$ a **time-orientable manifold** if there exists a global vector field on $\mathcal{M}$ that is timelike at each point.

Now we introduce the concept of a **differentiable manifold** of dimension n. This is a pair $(\mathcal{M}, \mathcal{A})$, where:

- $\mathcal{M}$ is a manifold as in Definition 1.1.1, and:
  - it is locally Euclidean, meaning that each point in $\mathcal{M}$ has an open neighbourhood that is homeomorphic (a bijection that is continuous with a continuous inverse) to an open subset of $\mathbb{R}^n$.
- $\mathcal{A}$ is a collection of charts $\{(U_\alpha, \varphi_\alpha)\}$, where each chart consists of:
  - $U_\alpha \subset \mathcal{M}$ is an open subset of $\mathcal{M}$,
  - $\varphi_\alpha : U_\alpha \to \mathbb{R}^n$ is a homeomorphism from each open subset U_α to Euclidean space $\mathbb{R}^n$, called a chart. Each φ_α provides local coordinates on U_α.

We now introduce the concept of spacetime geometrically, following the definitions in [66, 119].

1.1.4 Definition. *A spacetime is a quadruple $\mathcal{S} = (\mathcal{M}, g, o, t)$ where:*

- *$(\mathcal{M}, g)$ is a time-orientable n-dimensional Lorentzian manifold,*
- *o is a choice of orientation on $\mathcal{M}$,*
- *t is a choice of time orientation.*

1.2 Differential geometry

In order to introduce the concepts of differential geometry we need a **smooth transition functions**: for any two charts $(U_\alpha, \varphi_\alpha)$ and (U_β, φ_β) with $U_\alpha \cap U_\beta \neq \emptyset$, the transition map $\varphi_\alpha \circ \varphi_\beta^{-1} : \varphi_\beta(U_\alpha \cap U_\beta) \to \varphi_\alpha(U_\alpha \cap U_\beta)$ must be a smooth (infinitely differentiable) function. Moreover, the collection of open sets $\{U_\alpha\}$ must cover the manifold M. This ensures that the manifold $\mathcal{M}$ is smooth in the sense that the coordinates can be transformed in a differentiable way between overlapping charts. We also need to define the derivative of a tensor. A rule must be provided to transport the tensor from one point to another, which is essential for defining the covariant derivative and for ensuring consistency in the differential structure of the manifold.

One such rule is **parallel transport**. Consider a curve γ, parametrized by λ, with tangent vector u^α and a vector field A^α defined in a neighbourhood of γ. Let a point p on the curve have coordinates x^α, and a nearby point q have coordinates $x^\alpha + dx^\alpha$. Then, the derivative operator should have the form

$$DA^\alpha = A^\alpha_T(p) - A^\alpha(p), \tag{1.4}$$

where $A^\alpha_T(p)$ is the vector obtained by *transporting* A^α from q to p.We can express this as:

$$DA^\alpha = dA^\alpha + \delta A^\alpha, \tag{1.5}$$

where

$$\delta A^\alpha = \Gamma^\alpha_{\mu\beta} A^\mu dx^\beta, \tag{1.6}$$

and $\Gamma^\alpha_{\mu\beta}$ is called the **connection**. The form of δA^α is motivated by the requirement that the covariant derivative be linear in both the vector field A^μ and the coordinate differential dx^β. This ensures that the total differential DA^α transforms tensorially under coordinate changes, despite the connection itself not being a tensor. The connection coefficients $\Gamma^\alpha_{\mu\beta}$ account for the variation of the basis vectors and capture how the components of a vector field change under parallel transport. We now have

$$DA^\alpha = \partial_\beta A^\alpha dx^\beta + \Gamma^\alpha_{\mu\beta} A^\mu dx^\beta, \tag{1.7}$$

and by dividing through by $d\lambda$, the increment in the curve's parameter, we obtain

$$\frac{DA^\alpha}{d\lambda} = u^\beta \nabla_\beta A^\alpha, \tag{1.8}$$

where $u^\beta = \frac{dx^\beta}{d\lambda}$ is the tangent vector, and

$$\nabla_\beta A^\alpha \equiv \partial_\beta A^\alpha + \Gamma^\alpha_{\mu\beta} A^\mu. \tag{1.9}$$

A vector field A^α is said to be **parallel transported** along a curve with tangent vector u^β if

$$\frac{DA^\alpha}{d\lambda} = 0 \tag{1.10}$$

everywhere along the curve. Equation (1.9) is the **covariant derivative** of the vector A^α. Other standard notations are:

$$\nabla_\beta A^\alpha \equiv A^\alpha_{;\beta} \quad \text{and} \quad \frac{DA^\alpha}{d\lambda} \equiv \nabla_u A^\alpha. \tag{1.11}$$

In general relativity, the connection is symmetric and metric-compatible:

$$\Gamma^\alpha_{\gamma\beta} = \Gamma^\alpha_{\beta\gamma}, \quad \nabla_\gamma g_{\alpha\beta} = 0, \tag{1.12}$$

these properties emerge as a consequence of Einstein's principle of equivalence. It is straightforward to demonstrate that Equations (1.12) yield the following expression for the connection:

$$\Gamma^\alpha_{\beta\gamma} = \frac{1}{2} g^{\alpha\mu} \left(\partial_\gamma g_{\mu\beta} + \partial_\beta g_{\mu\gamma} - \partial_\mu g_{\beta\gamma} \right). \tag{1.13}$$

We can see that the connection is completely determined by the metric, and the quantities $\Gamma^\alpha_{\beta\gamma}$ are known as the **Christoffel symbols**.

The connection in Equation (1.13) is known as the Levi-Civita connection. This will be the connection used throughout this thesis, as it forms the foundation of the theory of general relativity. Notably, it is possible to define different types of connections or to build a theory that revolves around this geometrical object rather than the metric (see [63]). However, this is beyond the scope of this thesis, and we should leave this to the proper mathematicians.

1.2.1 Definition. *A* causal curve *in M is a smooth, regular curve whose classification depends on its tangent vector. A curve is said to be causal if its tangent vector is always either timelike or null.*

We also want to introduce another important concept, namely **global hyperbolicity**.

1.2.2 Definition. *A spacetime $\mathcal{S}$ is globally hyperbolic if and only if there exists a Cauchy surface Σ that is a closed achronal subset of $\mathcal{S}$ such that $D_{\mathcal{S}}(\Sigma) = \mathcal{M}$, where:*

- *A subset $\Sigma \subset \mathcal{M}$ is called* ***achronal*** *if each timelike curve in $\mathcal{M}$ intersects Σ at most once;*
- *For any subset $\Sigma \subset \mathcal{S}$, we define the* ***future*** *$(+)$ and* ***past*** *$(-)$* ***domains of dependence*** *$D^\pm_{\mathcal{S}}(\Sigma)$ as the collection of all points $q \in \mathcal{M}$ such that every past $(+)$, respectively future $(-)$, inextensible causal curve passing through q intersects Σ. We denote the* ***domain of dependence*** *by $D_{\mathcal{S}}(\Sigma) := D^+_{\mathcal{S}}(\Sigma) \cup D^-_{\mathcal{M}}(\Sigma)$.*

We give the definition of inextensibility below.

1.2.3 Definition. *An inextensible causal curve is a causal curve that is maximally extended within the spacetime manifold. If we consider a causal curve*

$$\gamma : I \to \mathcal{M}, \tag{1.14}$$

where I is an interval in $\mathbb{R}$ and $\mathcal{M}$ is the spacetime manifold. The curve γ is called inextensible if there is no other causal curve

$$\widetilde{\gamma} : J \to \mathcal{M}, \tag{1.15}$$

with $I \subsetneq J$ such that

$$\widetilde{\gamma}|_I = \gamma. \tag{1.16}$$

In other words, γ cannot be "continued" to a larger domain while preserving its property of being a causal curve.

Global hyperbolicity not only ensures a well-defined notion of causality (second bullet point) but also provides a surface (first bullet point) on which we can specify initial data to solve the Klein-Gordon equation in a generic spacetime $\mathcal{S}$.

Within this framework, we now introduce the concept of Lie derivatives. Consider a curve γ with tangent vector $u^\alpha = \frac{dx^\alpha}{d\lambda}$ and a vector field A^α defined in a neighbourhood of γ. Let the point p have coordinates x^α, and let the point q be given by $x^\alpha + dx^\alpha$. The equation

$$x'^\alpha \equiv x^\alpha + dx^\alpha = x^\alpha + u^\alpha d\lambda \tag{1.17}$$

represents the infinitesimal coordinate transformation from the system x to the system x'. Under this transformation, the vector A^α becomes

$$A'^\alpha(x') = \frac{\partial x'^\alpha}{\partial x^\beta} A^\beta(x) = \left(\delta^\alpha_\beta + \partial_\beta u^\alpha d\lambda\right) A^\beta(x) = A^\alpha(x) + (\partial_\beta u^\alpha) A^\beta(x) d\lambda. \tag{1.18}$$

In other words,

$$A'^\alpha(q) = A^\alpha(p) + (\partial_\beta u^\alpha) A^\beta(p) d\lambda. \tag{1.19}$$

On the other hand, $A^\alpha(q)$, the value of the original vector field at the point q, can be expressed as

$$A^\alpha(q) = A^\alpha(x + dx) = A^\alpha(x) + \partial_\beta A^\alpha(x) dx^\beta = A^\alpha(p) + u^\beta \partial_\beta A^\alpha(p) d\lambda. \tag{1.20}$$

In general, $A'^\alpha(q)$ and $A^\alpha(q)$ will not be equal. Their difference defines the **Lie derivative** of the vector A^α along the curve γ:

$$\mathcal{L}_u A^\alpha(p) \equiv \frac{A^\alpha(q) - A'^\alpha(q)}{d\lambda}. \tag{1.21}$$

Combining Equations (1.19), (1.20), and (1.21), we obtain:

$$\mathcal{L}_u A^\alpha = u^\beta \partial_\beta A^\alpha - A^\beta \partial_\beta u^\alpha. \tag{1.22}$$

Notably, the Lie derivative $\mathcal{L}_u A^\alpha$ can be defined without reference to a connection, implying that Lie differentiation is a more fundamental operation than covariant differentiation. Furthermore, the definition of the Lie derivative can be extended to tensors of all types. For scalars, we have

$$\mathcal{L}_u f \equiv \frac{df}{d\lambda} = u^\alpha \partial_\alpha f. \tag{1.23}$$

Now that we have defined the Lie derivative, we can introduce the concept of Killing vector fields.

1.2.4 Definition. *A vector field X is called a Killing vector field if the Lie derivative of the metric g with respect to X vanishes:*

$$\mathcal{L}_X g = 0. \tag{1.24}$$

Using the Levi-Civita connection, this condition can be equivalently expressed as

$$g\left(\nabla_Y X, Z\right) + g\left(Y, \nabla_Z X\right) = 0, \tag{1.25}$$

for all vector fields Y and Z. In local coordinates, Equation (1.25) takes the form of the Killing equation:

$$\nabla_\mu X_\nu + \nabla_\nu X_\mu = 0, \tag{1.26}$$

which is valid in any coordinate system.

Killing vector fields are the infinitesimal generators of *isometries*, i.e. diffeomorphisms $\varphi : M \to M$ that preserve the metric, $\varphi^* g = g$. In other words, the flow generated by a Killing vector field corresponds to a continuous symmetry of the spacetime geometry.

Another important concept to introduce, which will be useful when discussing the Einstein field equations, is that of a geodesic. In curved spacetime, we call a curve a geodesic if it extremizes the spacetime interval between two fixed points.

Let a curve γ be described by the relations $x^\alpha(\lambda)$, where λ is an arbitrary parameter, and let p and q be two points on this curve. The distance between p and q along γ is given by

$$\Delta s = \int_p^q \sqrt{\pm g_{\alpha\beta} \dot{x}^\alpha \dot{x}^\beta}\, d\lambda, \tag{1.27}$$

where the positive or negative sign is chosen depending on whether the curve is spacelike or timelike, and $\dot{x}^\alpha = \frac{dx^\alpha}{d\lambda}$. If the curve is lightlike the distance is intrinsically zero, hence one cannot define a non-zero "distance" in the usual sense. The curve for which Δs is an extremum is determined by substituting into the Euler-Lagrange equations:

$$\frac{d}{d\lambda}\left(\frac{\partial L}{\partial \dot{x}^\alpha}\right) - \frac{\partial L}{\partial x^\alpha} = 0, \tag{1.28}$$

where L is the Lagrangian of the system. We find that $x^\alpha(\lambda)$ must satisfy the differential equation:

$$\ddot{x}^\alpha + \Gamma^\alpha_{\beta\gamma}\dot{x}^\beta\dot{x}^\gamma = \kappa(\lambda)\dot{x}^\alpha, \tag{1.29}$$

where $\kappa(\lambda) \equiv \frac{d\ln L}{d\lambda}$, and L is the Lagrangian associated with the curve. It is possible to assume an affine parametrisation so that $\kappa(\lambda) = 0$.

Geodesics are not only the curves that extremise the action but also those along which the tangent vector is parallel transported. This gives a geometric interpretation of the equation above. Introducing the tangent vector $u^\alpha \equiv \dot{x}^\alpha$, also known as the four-velocity, the geodesic equation can be equivalently written as:

$$u^\beta\nabla_\beta u^\alpha = \kappa(\lambda)u^\alpha, \tag{1.30}$$

which shows that the tangent vector is parallel transported along the curve up to a scaling governed by $\kappa(\lambda)$. In the case of affine parametrisation, this reduces to $u^\beta\nabla_\beta u^\alpha = 0$.

Now that we have also introduced the concept of distance in a curved spacetime, we can move our attention to defining the mathematical objects needed for us to write the Einstein field equations. We now introduce the Riemann tensor $R^\alpha{}_{\beta\gamma\delta}$, which may be defined by the relation:

$$R^\alpha{}_{\beta\gamma\delta} = \partial_\gamma\Gamma^\alpha_{\beta\delta} - \partial_\delta\Gamma^\alpha_{\beta\gamma} + \Gamma^\alpha_{\mu\gamma}\Gamma^\mu_{\beta\delta} - \Gamma^\alpha_{\mu\delta}\Gamma^\mu_{\beta\gamma}. \tag{1.31}$$

This tensor arises naturally when examining the non-commutativity of covariant derivatives. In curved spacetime, the covariant derivatives of a vector field do not generally commute; applying them in different orders yields a discrepancy that is precisely captured by the Riemann tensor. Specifically, for a vector V^α, the commutator of two covariant derivatives gives:

$$[\nabla_\gamma, \nabla_\delta]V^\alpha = R^\alpha{}_{\beta\gamma\delta}V^\beta. \tag{1.32}$$

This relation shows that the Riemann tensor encodes the intrinsic curvature of spacetime, reflecting how vectors are affected by parallel transport around an infinitesimal closed loop. The Riemann tensor is antisymmetric in the first, and in the last two indices. Its other symmetry properties are:

$$R_{\alpha\beta\gamma\delta} = -R_{\beta\alpha\gamma\delta} = -R_{\alpha\beta\delta\gamma} = R_{\gamma\delta\alpha\beta}, \tag{1.33}$$

and

$$R_{\mu\alpha\beta\gamma} + R_{\mu\gamma\alpha\beta} + R_{\mu\beta\gamma\alpha} = 0. \tag{1.34}$$

These are valid in any coordinate system. It is also possible to show that the Riemann tensor satisfies the Bianchi identities,

$$\nabla_\gamma R_{\mu\nu\alpha\beta} + \nabla_\beta R_{\mu\nu\gamma\alpha} + \nabla_\alpha R_{\mu\nu\beta\gamma} = 0. \tag{1.35}$$

A contraction of the Riemann tensor produces the Ricci tensor $R_{\alpha\beta}$ and the Ricci scalar R. These are defined by

$$R_{\alpha\beta} = R^{\mu}{}_{\alpha\mu\beta}, \quad R = R^{\alpha}{}_{\alpha}. \tag{1.36}$$

It is easy to show that $R_{\alpha\beta}$ is a symmetric tensor. The Einstein tensor is defined by

$$G_{\alpha\beta} = R_{\alpha\beta} - \frac{1}{2} R g_{\alpha\beta}, \tag{1.37}$$

which is also a symmetric tensor. The Einstein tensor satisfies

$$\nabla^{\beta} G_{\alpha\beta} = 0, \tag{1.38}$$

the contracted Bianchi identities.

Now we have all the tools to write the Einstein field equations (EFE),

$$G_{\alpha\beta} + \Lambda g_{\alpha\beta} = \frac{8\pi G}{c^4} T_{\alpha\beta}, \tag{1.39}$$

where G is Newton's gravitational constant, c is the speed of light in vacuum and where Λ is the cosmological constant. In what follows, we set $G = c = 1$, so that the Einstein field equations reduce to:

$$G_{\alpha\beta} + \Lambda g_{\alpha\beta} = 8\pi T_{\alpha\beta}. \tag{1.40}$$

These equations relate the curvature of spacetime, encoded in the Einstein tensor, with the distribution of matter, represented by the stress–energy tensor $T_{\alpha\beta}$. Consequently, Equation (1.38) implies that the stress–energy tensor must have zero divergence:

$$\nabla_{\beta} T^{\alpha\beta} = 0. \tag{1.41}$$

Because a symmetric 4×4 tensor has 10 independent components, one might expect there to be 10 independent equations. However, the Einstein tensor satisfies Equation (1.38), which impose 4 differential constraints on these equations. This means that, out of the 10 equations, only 6 are truly independent. Since the metric $g_{\mu\nu}$ in four dimensions has 10 independent components and the field equations determine only 6 of them independently, there remains the freedom to choose 4 arbitrary functions. The metric can therefore be determined up to four arbitrary functions, reflecting our complete freedom in choosing the coordinate system inherent in general relativity. This can be generalized to higher dimensions. We note that the field equations (1.40) can also be written in the form

$$R_{\alpha\beta} = 8\pi \left(T_{\alpha\beta} - \frac{1}{2} T g_{\alpha\beta} \right), \tag{1.42}$$

where $T \equiv T^{\alpha}_{\alpha}$ is the trace of the stress–energy tensor.

Now let us give a bit more detail on the stress-energy tensor. In the context of classical field theory and general relativity, the stress-energy tensor $T_{\alpha\beta}$ is defined as the functional

derivative of the matter part of the action S with respect to the metric $g^{\alpha\beta}$. The stress-energy tensor is given by:

$$T_{\alpha\beta} = -\frac{2}{\sqrt{-g}}\frac{\delta S_{\text{matter}}}{\delta g^{\alpha\beta}}, \tag{1.43}$$

where S is the action of the system, and g is the determinant of the metric tensor $g_{\alpha\beta}$. If we consider the Einstein-Hilbert action as our S:

$$S = \int d^4x\sqrt{-g}\left(\frac{R}{16\pi G} + \mathcal{L}_{\text{matter}}\right), \tag{1.44}$$

where R is the Ricci scalar, $\mathcal{L}_{\text{matter}}$ is the Lagrangian density for the matter fields, and G is Newton's gravitational constant, then Equation (1.43) shows the relation between the stress-energy tensor, the variation of the matter Lagrangian, and the geometry of spacetime. The first term in Equation (1.44) represents the contribution from the gravitational field in the Einstein field equations. The second term in Equation (1.44) is the variation of the matter Lagrangian, which gives the stress-energy tensor for the matter fields.

1.3 Black holes

We have now introduced all the geometrical tools needed for the introduction of the main topic of this thesis. We are going to focus exclusively on black holes. Black holes are specific solutions of the Einstein field equations in Equation (1.40), which exhibit a singular behaviour in the metric. These backgrounds are characterised by the presence of a singularity. Naively, a black hole can be thought of as a region of spacetime in which gravity is so strong that nothing, neither particles nor radiation, can escape from it. This creates a causal boundary dividing the interior of the black hole from its exterior. The delimiting boundary is called the event horizon.

As we mentioned in the introduction to this chapter, they were discovered in two kinds: the static case, the Schwarzschild black hole, and the rotating case, the Kerr black hole. Both of these are solutions of the Einstein field equation in the vacuum, which means that the stress-energy tensor is zero, $T_{\alpha\beta} = 0$, hence

$$R_{\alpha\beta} - \frac{1}{2}Rg_{\alpha\beta} = 0. \tag{1.45}$$

We are going to give a brief description of these known cases, which will serve as an introduction to Section 3.3.

1.3.1 Static black holes

Static black holes are black holes in which the line element does not depend explicitly on the time coordinate and which do not possess any angular momentum. More precisely, a spacetime is said to be *static* if it admits a timelike Killing vector field that is hypersurface-orthogonal everywhere. This formal definition ensures both time independence and the

absence of rotation in a coordinate-invariant manner, [30]. The Schwarzschild black hole in four dimensions is a static black hole. The metric can be understood by analysing the line element, which determines the distance between two neighbouring points. First, we pick a set of coordinates, also known as Schwarzschild coordinates, (t, r, θ, ϕ), and a signature $(-,+,+,+)$. Then, the line element is [128]:

$$ds^2 = -\left(1 - \frac{2M}{r}\right) dt^2 + \left(1 - \frac{2M}{r}\right)^{-1} dr^2 + r^2 d\theta^2 + r^2 \sin^2\theta \, d\phi^2, \tag{1.46}$$

where M is the mass of the black hole.
In the Schwarzschild case, the event horizon, the boundary of the black hole, can be evaluated by calculating what is known as the Schwarzschild radius r_{sc}:

$$r_{sc} = 2M. \tag{1.47}$$

At this radius, the coefficient of dt^2 in the line element goes to zero, and the dr^2 coefficient diverges. Hence, we observe two singular behaviours: one when $r \to 0$, and the other when $r \to 2M$. This requires closer examination. In fact, we can change the coordinate system we initially chose to another, thanks to the property of general relativity being diffeomorphism invariant. By switching to the so-called Kruskal coordinates, we can extend the solution. These coordinates have the advantage of covering the entire spacetime of the maximally extended Schwarzschild solution and being well-behaved everywhere outside the physical singularity. Let us denote the new coordinates as T and R. For $r > 2M$ (the exterior of the black hole), the transformation is defined as:

$$\begin{aligned} T &= \left(\frac{r}{2M} - 1\right)^{1/2} e^{r/4M} \sinh\left(\frac{t}{4M}\right), \\ R &= \left(\frac{r}{2M} - 1\right)^{1/2} e^{r/4M} \cosh\left(\frac{t}{4M}\right). \end{aligned} \tag{1.48}$$

For $0 < r < 2M$ (the interior of the black hole), the transformation is:

$$\begin{aligned} T &= \left(1 - \frac{r}{2M}\right)^{1/2} e^{r/4M} \cosh\left(\frac{t}{4M}\right), \\ R &= \left(1 - \frac{r}{2M}\right)^{1/2} e^{r/4M} \sinh\left(\frac{t}{4M}\right). \end{aligned} \tag{1.49}$$

Using these coordinates, the line element becomes:

$$ds^2 = -\frac{32M^3}{r} e^{-\frac{r}{2M}} dT^2 + \frac{32M^3}{r} e^{-\frac{r}{2M}} dR^2 + r^2 \, d\theta^2 + r^2 \sin^2\theta \, d\phi^2, \tag{1.50}$$

where r is implicitly defined in terms of the Kruskal coordinates T and R. From this form of the line element, we see that the only singularity left is the one as $r \to 0$, called the physical singularity, while the other one at $r \to 2M$ was merely a coordinate singularity arising from the choice of Schwarzschild coordinates. This can also be checked using the Kretschmann scalar:

$$K = R_{\alpha\beta\gamma\delta} R^{\alpha\beta\gamma\delta}, \tag{1.51}$$

where $R_{\alpha\beta\gamma\delta}$ is the Riemann curvature tensor. This quantity can help identify whether a singular behaviour defines a physical singularity or not. In the Schwarzschild black hole, K diverges when $r \to 0$, indicating a physical singularity, and is regular when $r \to 2M$, indicating that this is just a coordinate singularity.

Thanks to the definition of the Kruskal coordinates, we are able to describe the Schwarzschild spacetime with a Penrose diagram, see Figure 1.1. This picture is achieved by the compactification of the Kruskal coordinates, which makes it possible to represent infinities.

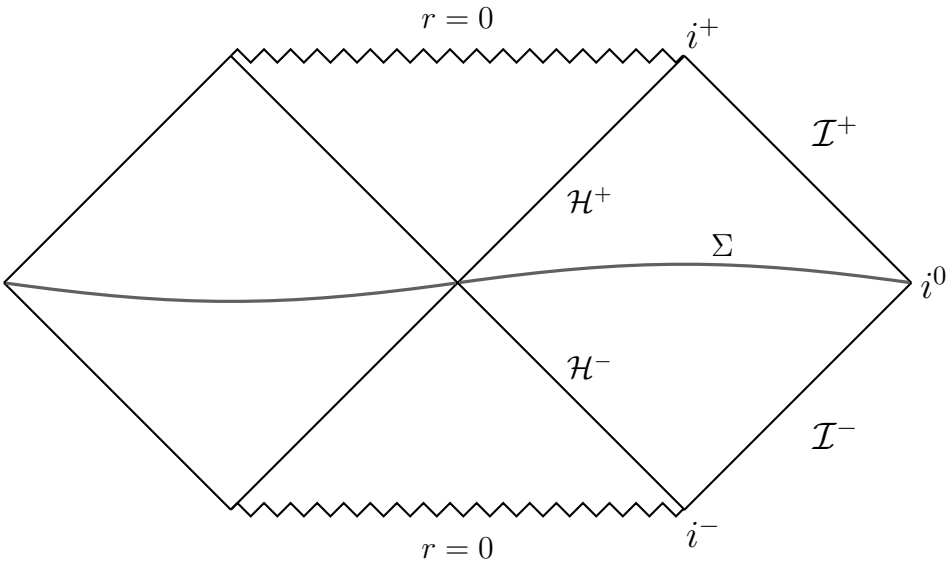

Figure 1.1: Penrose diagram for the maximal analytic extension of the Schwarzschild black hole.

In Figure 1.1:

- $\mathcal{I}^+$ represents future null infinity, where outgoing radiation reaches an observer at infinity,
- $\mathcal{I}^-$ represents past null infinity, where incoming radiation originates from infinity,
- i^+ is future timelike infinity,
- i^- is past timelike infinity,
- i^0 is spacelike infinity,
- $\mathcal{H}^+$ and $\mathcal{H}^-$ are the future and past event horizons, respectively, marking the boundaries of the black hole region.

- $r = 0$ corresponds to the singularity at the centre of the black hole, represented by the zigzag lines.
- Σ is a Cauchy surface.

This diagram encapsulates the causal structure of the Schwarzschild black hole spacetime.

1.3.2 Stationary black holes

Another possible solution to the vacuum EFE is the stationary black hole, also known as the rotating black hole. A spacetime is said to be *stationary* if it admits a timelike Killing vector field, indicating invariance under time translations. The Kerr solution is stationary because the line element does not depend explicitly on the time coordinate, reflecting the existence of such a symmetry. However, it possesses angular momentum $J \neq 0$, which reveals its rotating nature and distinguishes it from static spacetimes, where the timelike Killing vector is also required to be hypersurface-orthogonal. The line element for the Kerr black hole, with coordinates (t, r, θ, ϕ) and signature $(-, +, +, +)$, is:

$$ds^2 = -\left(1 - \frac{2Mr}{\Sigma}\right) dt^2 - \frac{4Mra\sin^2\theta}{\Sigma}\, dt\, d\phi + \frac{\Sigma}{\Delta} dr^2 + \Sigma\, d\theta^2 + \left(r^2 + a^2 + \frac{2Mra^2\sin^2\theta}{\Sigma}\right)\sin^2\theta\, d\phi^2, \quad (1.52)$$

where $\Sigma = r^2 + a^2\cos^2\theta$, $\Delta = r^2 - 2Mr + a^2$, and $a = J/M$ is the black hole's spin parameter. Here, M is the mass and J is the angular momentum. This expression does not contain a parameter for the charge of the black hole, which will be denoted as Q. This will not be treated in this thesis, but it is useful to note that charged black holes are also a branch of study [122]. For the metric in Equation (1.52), we can define the event horizon of the Kerr black hole as the surface

$$r_h = M + \sqrt{M^2 - a^2}, \quad (1.53)$$

which is obtained by solving $\Delta = 0$. More generally, the event horizon is a null hypersurface generated by a congruence of outgoing null geodesics whose expansion vanishes. This provides a coordinate-independent and physically meaningful characterisation: it is the boundary beyond which light cannot escape to future null infinity. Equivalently, in stationary spacetimes such as Kerr, the event horizon is also a Killing horizon, i.e. a null hypersurface where a suitable linear combination of the timelike and rotational Killing vectors becomes null. In the Kerr geometry, this condition corresponds precisely to the surface defined by $\Delta = 0$. We can also study other characteristic surfaces. First, the stationary limit surface r_s, which can be defined as the surface inside which an observer cannot remain at rest relative to infinity:

$$r_s = M + \sqrt{M^2 - a^2\cos^2\theta}, \quad (1.54)$$

which we obtain imposing $g_{tt} = 0$. This surface delimits a region in the Kerr spacetime known as the ergosphere. In the ergoregion of a rotating black hole, frame-dragging becomes so extreme that all observers following timelike trajectories are forced to co-rotate with the black hole, it is no longer possible to remain stationary relative to distant stars. This effect, known as frame-dragging, arises due to the curvature of spacetime caused by the black hole's rotation. The first direct measurement of frame-dragging in the vicinity of Earth was performed by the Gravity Probe B experiment in 2011 [55]. However, the presence of an ergoregion is not required for the formation of an accretion disc. An accretion disc forms when matter, such as gas or dust from a nearby star, is captured by the black hole's gravitational field and begins to orbit it. Through internal friction and viscous interactions within the disc, the material gradually loses angular momentum and spirals inward. As this infall proceeds, a portion of the gravitational potential energy is converted into electromagnetic radiation, causing the disc to shine brightly across a range of wavelengths, particularly in X-rays. It is this luminous accretion structure that was observed in the first image of a black hole captured by the Event Horizon Telescope in 2019 [5].

Two important surfaces around rotating black holes are central to much of the discussion in this thesis: the *stationary limit surface* and the *speed-of-light surface*.

The *stationary limit surface* is defined as the hypersurface on which the Killing vector field associated with time translations at infinity, usually denoted $\xi^{\mu}_{(t)}$, becomes null. Outside this surface, observers can remain at rest relative to infinity, but inside it, all timelike observers are forced to co-rotate with the black hole due to frame-dragging. This surface marks the boundary of the *ergoregion*, and it lies outside the event horizon for rotating black holes.

The *speed-of-light surface*, on the other hand, is the surface on which the Killing vector field that generates the outer event horizon, $\chi^{\mu} = \xi^{\mu}_{(t)} + \Omega_H \xi^{\mu}_{(\varphi)}$, becomes null. Here, Ω_H is the angular velocity of the horizon, $\xi^{\mu}_{(\varphi)}$ is the Killing vector field associated with axial symmetry, and $\xi^{\mu}_{(t)}$ is the Killing vector field associated with time translations at infinity. An observer moving with angular velocity Ω_H reaches the speed of light at this surface, and thus cannot exist beyond it.

We will explore the geometric and physical significance of these surfaces in more detail in Chapter 4, particularly in the context of quantum fields on rotating black hole backgrounds, where their presence or absence plays a crucial role.

Summary

In this chapter, we have introduced the main concepts of general relativity, explaining the mathematical tools necessary to define the Einstein field equations and providing a definition of the classical stress-energy tensor. We have also introduced some examples of the geometry of black holes. These foundational elements will be pivotal for our thesis, as the main topic involves the analysis of black hole solutions within the framework of quantum field theory in curved spacetime. This framework combines general relativity, which describes the geometry of spacetime, with quantum field theory, which explains the behaviour of matter in this background.

For this reason, in the next chapter, we will introduce the quantum tools needed for this semi-classical theory and provide a description of the theory itself.

Chapter 2

Quantum theory in curved spacetime arises

We now to introduce the second protagonist of this story: quantum field theory (QFT). This powerful framework governs the behaviour of the universe at small scales, describing the dynamics of quantum fields. The foundations of QFT were laid as early as the 1920s when Paul Dirac made the first attempt at quantizing the electromagnetic field [47]. Over the subsequent decades, QFT evolved from quantum mechanics into a comprehensive theory that describes the interactions of fundamental particles [117].

With QFT, we have a theory that successfully explains the microscopic world, while general relativity, introduced in Chapter 1, provides a complete description of macroscopic phenomena, such as the structure of spacetime and the behaviour of massive celestial bodies. However, a significant challenge emerges: these two theories are fundamentally incompatible. One of the scenarios where this incompatibility becomes apparent is in the proximity of black holes.

Black holes, which we mentioned in the previous chapter in Section 1.3, are solutions to Einstein's equations in GR. They can form when matter collapses, creating a singularity that curves spacetime so intensely that the effects of gravity become dominant. This scenario is unique in the universe because gravitational effects are so relevant that they can not be neglected near a black hole.

QFT, despite its remarkable success and predictive power, confirmed by numerous experiments [117], was developed under the assumption of flat spacetime. On Earth, where the curvature of spacetime due to gravity is negligible, this assumption holds true. However, near a black hole, spacetime curvature is extreme, and the "classical" QFT becomes inadequate. To study quantum fields in such environments, an extension of QFT to curved spacetime became necessary. This need led to the development of quantum field theory

on curved spacetime in the 1960s [113, 148].

One of the most successful predictions of QFT in curved spacetime is Hawking radiation [65], a theoretical result that suggests black holes can emit radiation and eventually evaporate. While this prediction awaits experimental confirmation, it has already been shown that an analogue of Hawking radiation can be measured experimentally [142].

In this theoretical framework, the semi-classical approach emerged. This approach aims to explore the behaviour of quantum matter in classical curved backgrounds by combining the successes of GR and QFT. It does not attempt to be a full theory of quantum gravity but rather seeks to uncover effects that could be instrumental in constructing such a theory. By relying on the mathematical foundations of QFT in curved spacetime, the semi-classical approach attempts to describe quantum phenomena in strong gravitational fields. This is achieved by solving the semi-classical Einstein field equations:

$$G_{\alpha\beta} + \Lambda g_{\alpha\beta} = 8\pi \langle \hat{T}_{\alpha\beta} \rangle, \tag{2.1}$$

where Λ is the cosmological constant, $g_{\alpha\beta}$ is the metric of the spacetime we are considering, $G_{\alpha\beta}$ is the Einstein tensor introduced in Chapter 1 and $\langle \hat{T}_{\alpha\beta} \rangle$ is the expectation value of the stress-energy tensor, which we will discuss in more detail later on in this chapter. In particular, the left side is classical, being unchanged from the Einstein field equations (1.40), and the right-hand side is quantum, containing the expectation value of the SET over a quantum state.

Throughout this thesis, we will explore these concepts in more detail. While this may seem like a lot to grasp, we will proceed step by step. First, we need to focus on what is required to provide a full description of a semi-classical theory. We need to define quantum states over the curved background, then discuss how to evaluate the expectation value of the stress-energy tensor, which will ultimately lead to solving the semi-classical Einstein field equations (2.1).

To achieve this, we will first introduce the fundamentals of QFT in flat spacetime, and then follow the historical progression, introducing the theory of QFT on curved spacetime. We will then discuss the semi-classical approach and the semi-classical Einstein equations. In particular, we will focus on black hole solutions.

2.1 Quantum field theory in flat spacetime

This will not be the place to summarize the entire scope of QFT, we leave that to standard textbooks such as [22, 117, 148, 149]. Instead, we will present an example to demonstrate how this theory can be applied. As mentioned earlier, we begin by introducing some basic

concepts of QFT in flat spacetime to set the foundation for formulating a QFT on a curved background. We consider a scalar field, which is not only the focus of this thesis but also serves as the simplest example for this introduction.

Hence, we begin with the study of a classical scalar field, $\Phi(x,t)$, in an n-dimensional spacetime, where x is a vector of dimension $n-1$, giving the spatial coordinates, and where we choose t as the time coordinate, with a Lagrangian density $\mathcal{L}(\Phi, \partial_\mu \Phi)$ given by

$$\mathcal{L}(\Phi, \partial_\mu \Phi) = -\frac{1}{2}\partial_\mu \partial^\mu \Phi - \frac{1}{2}\mu^2 \Phi^2, \tag{2.2}$$

where μ is the mass of the field. We can then define the action S as

$$S[\Phi, \eta_{\mu\nu}] = \int \mathcal{L}(\Phi, \partial_\mu \Phi)\, d^n x, \tag{2.3}$$

where $\eta_{\mu\nu}$ is the Minkowski metric. We can obtain the equation of motion for the scalar field by setting the variation of the action, δS, with respect to Φ, to zero giving

$$\begin{aligned} \delta S &= \int \left[\frac{\partial \mathcal{L}}{\partial \Phi}\delta\Phi + \frac{\partial \mathcal{L}}{\partial(\partial_\mu \Phi)}\delta(\partial_\mu \Phi) \right] d^n x \\ &= \int \delta\Phi \left[\frac{\partial \mathcal{L}}{\partial \Phi} - \partial_\mu \left(\frac{\partial \mathcal{L}}{\partial(\partial_\mu \Phi)} \right) \right] d^n x, \end{aligned} \tag{2.4}$$

where we have used integration by parts to go from the first line to the second one in Equation (2.4). We have also used Stokes' theorem, rewriting a term as a surface term, and we have assumed that the variation $\delta\Phi$ vanishes at the boundary. Requiring $\delta S = 0$, we find the Euler-Lagrange equation for the scalar field:

$$\partial_\mu \left(\frac{\partial \mathcal{L}}{\partial(\partial_\mu \Phi)} \right) - \frac{\partial \mathcal{L}}{\partial \Phi} = 0. \tag{2.5}$$

Substituting $\mathcal{L}$ from Equation (2.2) into (2.5), we find the Klein-Gordon equation:

$$\partial_\mu \partial^\mu \Phi - \mu^2 \Phi = 0. \tag{2.6}$$

A basis set of solutions to Equation (2.6) consist of the plane waves

$$\Phi_p(x,t) = A\, e^{-i\omega t + ip\cdot x}, \quad \omega^2 - |p|^2 = \mu^2, \tag{2.7}$$

where ω is the frequency, p is the momentum, and A is a normalization constant. We distinguish $\omega > 0$ for Φ_p to represent positive frequency modes, while the complex conjugate Φ_p^* gives the negative frequency modes when $\omega > 0$. This is pivotal in quantum field theory for canonical quantization, allowing us to define quantum states over a background. The theory requires us to find an orthonormal basis of solutions, in order to define an inner product. We define:

$$\langle \Phi_1, \Phi_2 \rangle = -i \int_\Sigma (\Phi_1 \partial_t \Phi_2^* - \Phi_2^* \partial_t \Phi_1)\, d^{n-1} x, \tag{2.8}$$

where Σ is an equal-time hypersurface. Due to the conservation of the current

$$j^\mu = -i\left(\Phi_1 \partial^\mu \Phi_2^* - \Phi_2^* \partial^\mu \Phi_1\right), \tag{2.9}$$

the value of the inner product is independent of the particular choice of Σ, provided that the field vanishes sufficiently rapidly at spatial infinity (which is typically ensured by appropriate boundary conditions). To determine A, we use this inner product for two solutions of the form in Equation (2.7). Substituting the plane wave solutions into (2.8) and enforcing orthonormality,

$$\langle \Phi_p, \Phi_{p'} \rangle = \delta(p - p') \text{ for } \omega > 0, \tag{2.10}$$

we obtain the normalization constant:

$$A = \frac{1}{\sqrt{2|\omega|(2\pi)^{n-1}}}. \tag{2.11}$$

To quantize the classical field, we promote it to an operator, "putting a hat on it",

$$\Phi(t, x) \to \hat{\Phi}(t, x), \tag{2.12}$$

and impose the equal-time commutation relations:

$$[\hat{\Phi}(t, x), \hat{\Phi}(t, x')] = 0, \tag{2.13}$$

$$[\hat{\pi}(t, x), \hat{\pi}(t, x')] = 0, \tag{2.14}$$

$$[\hat{\Phi}(t, x), \hat{\pi}(t, x')] = i\delta^{(n-1)}(x - x'), \tag{2.15}$$

where $\hat{\pi}(t, x)$ is the conjugate momentum:

$$\hat{\pi}(t, x) = \partial_t \hat{\Phi}(t, x) = \dot{\hat{\Phi}}(t, x). \tag{2.16}$$

We can expand the quantized field in terms of orthonormal modes:

$$\hat{\Phi}(t, x) = \sum_p \left[\hat{a}_p \Phi_p(t, x) + \hat{a}_p^\dagger \Phi_p^*(t, x)\right], \tag{2.17}$$

where the sum over p denotes a schematic decomposition into modes; in cases where the spectrum of the field is continuous, this summation should be understood as an integral over the relevant mode parameters. $\hat{a}_p$ and $\hat{a}_p^\dagger$ are the annihilation and creation operators, satisfying the canonical commutation relations (CCR):

$$[\hat{a}_p, \hat{a}_{p'}] = 0, \tag{2.18a}$$

$$[\hat{a}_p^\dagger, \hat{a}_{p'}^\dagger] = 0, \tag{2.18b}$$

$$[\hat{a}_p, \hat{a}_{p'}^\dagger] = \delta^{(n-1)}(p - p'). \tag{2.18c}$$

It is important to define now the difference between a ground state and a vacuum state. A ground state $|0\rangle$ is an eigenvector of the Hamiltonian $\hat{H}$ such that any other state $|\psi\rangle$ satisfies

$$\langle \psi | \hat{H} | \psi \rangle \geq \langle 0 | \hat{H} | 0 \rangle, \tag{2.19}$$

where $|\psi\rangle$ is any state in the Hilbert space and $\hat{H}$ is the Hamiltonian.

A vacuum state $|0\rangle$ is a ground state invariant under the Poincaré group:

$$U(a,\Lambda)|0\rangle = |0\rangle, \tag{2.20}$$

up to a phase (which can be set to 1), where $\{a,\Lambda\} \in \mathrm{ISO}(1,d-1)$ (inhomogeneous special orthogonal group or Euclidean group) and U is a unitary representation of the Poincaré group. In this sense, being a vacuum state is more restrictive than being just a ground state. For one thing, the former only exists in Poincaré invariant systems, while the latter exists for any physically meaningful system (that is, whenever $\hat{H}$ is bounded from below).

In Minkowski spacetime, there is a preferred vacuum state $|0\rangle$ defined by

$$\hat{a}_p|0\rangle = 0. \tag{2.21}$$

Due to the lack of invariance under the Poincaré group, a preferred vacuum state does not exist in curved spacetimes. Therefore, it becomes necessary to specify different ground states. This will be discussed in the next section, where we generalize the process of canonical quantization to quantum field theory in curved spacetime.

2.2 Quantum field theory in curved spacetime

In order to generalize what we have shown in the previous section to curved spacetimes, we need to modify the action we are studying. Specifically, we must introduce the concept of spacetime curvature into the action, which we achieve by incorporating the metric $g_{\mu\nu}$ into the action in Equation (2.3). Ordinary derivatives ∂_μ are replaced by covariant derivatives ∇_μ, and the covariant volume element changes from $d^n x$ to $\sqrt{-g}\, d^n x$, where $g = \det(g_{\mu\nu})$. These are all concepts introduced in Chapter 1. We reiterate that our aim is to present a practical example of applying the theory of quantum field theory in curved spacetime (QFTCS) to a scalar field, rather than providing a comprehensive description of the theory, which can be found in [22, 148]. The action then becomes

$$S[\Phi, g_{\mu\nu}] = \int \left[-\frac{1}{2} g^{\mu\nu} \nabla_\mu \Phi \nabla_\nu \Phi - \frac{1}{2}(\mu^2 + \xi R)\Phi^2 \right] \sqrt{-g}\, d^n x, \tag{2.22}$$

where R is the Ricci scalar, ξ is a coupling constant and $g_{\mu\nu}$ is the metric of the curved spacetime that we are considering. The coupling constant ξ determines the strength of the interaction between the curvature of spacetime and the quantum field. For minimal coupling, $\xi = 0$, while for conformal coupling,

$$\xi = \xi_c = \frac{n-2}{4(n-1)}. \tag{2.23}$$

In the previous section, we introduced all the ingredients needed to construct a real scalar field theory on a flat background. However, before we write the generalisation of the Klein-Gordon equation on (M, g), we need to make an important physical remark. In Minkowski spacetime $(\mathbb{R}^4, \eta)$, the presence of a large isometry group $SO(3,1) \ltimes \mathbb{R}^4$ provides a mathematical procedure that allows us to classify free fields through a map from $\mathbb{R}^4$ into a finite-dimensional Hilbert space transforming under a unitary and irreducible representation of the Poincaré group [19]. This procedure was introduced by Wigner [150], and it gives us the ability to build an unambiguous identification of a free field and construct the equations of motion. Hence, in Minkowski's spacetime, there is no arbitrariness when dealing with classical free theory. In a curved spacetime (M, g), the situation is not so straightforward. In principle, the metric g may possess no isometries, in which case we cannot apply the Wigner classification procedure, which relies on the existence of spacetime symmetries to label particles by mass and spin. Independently of this, in a general curved spacetime there may be ambiguities in constructing the Lagrangian for a free scalar field. These ambiguities can arise, for example, from the possible inclusion of curvature couplings such as $\xi R\phi^2$, where R is the Ricci scalar and ξ is an arbitrary dimensionless parameter. More generally, one can add any scalar function constructed from the scalar field and curvature tensors—such as the Ricci tensor or Riemann tensor—that vanishes in flat spacetime where $g = \eta$. Using Occam's razor, we wrote the action in Equation (2.22), from which the Klein-Gordon equation in a generic spacetime (M, g) can be written as:

$$\Box\Phi - (\mu^2 + \xi R)\Phi = 0, \tag{2.24}$$

where $\Box$ is the covariant d'Alembertian:

$$\Box\Phi = g^{\mu\nu}\nabla_\mu\nabla_\nu\Phi = g^{\mu\nu}\left(\partial_\mu\partial_\nu - \Gamma^\lambda_{\mu\nu}\partial_\lambda\right)\Phi. \tag{2.25}$$

Here, $\Gamma^\lambda_{\mu\nu}$ is the Christoffel symbol, defined by Equation (1.13). One of the key points of the theory is the assumption that the underlying background is globally hyperbolic (see Section 1.1). This condition on the geometry of spacetime guarantees that, given a wave equation such as the Klein–Gordon equation, the associated Cauchy problem is well posed, ensuring the existence of a unique solution once suitable initial data are assigned. This constraint can be loosened, which is what happens when we consider spacetimes that are asymptotically Anti-de-Sitter (AdS), which will be the main interest in this thesis. In these cases, the spacetime is not globally hyperbolic, but by assigning boundary conditions we can still ensure the existence of a unique solution when initial data are assigned. This will be discussed more in detail later on in the thesis.

As in the flat spacetime case, we need to define an inner product, in order to find an orthonormal basis of solutions of Equation (2.24). In curved spacetime, the scalar product is given by

$$\langle\Phi_1, \Phi_2\rangle = -i\int_\Sigma (\Phi_1\partial_\mu\Phi_2^* - \Phi_2^*\partial_\mu\Phi_1)\sqrt{-g}\, n^\mu d\Sigma, \tag{2.26}$$

where Σ is a spacelike hypersurface, n^μ is the unit normal vector to Σ, $d\Sigma$ is the volume element on Σ, and g is the determinant of $g_{\mu\nu}$. As discussed in the previous section, the scalar product $\langle \Phi_1, \Phi_2 \rangle$ does not depend on the choice of the hypersurface Σ.

We then proceed with the analysis, by performing a mode expansion of the scalar field in terms of an orthonormal basis of modes $f_j(t,x)$. In this expansion, the modes $f_j(t,x)$ are chosen to have positive frequency with respect to the time coordinate t, while their complex conjugates $f_j^*(t,x)$ correspond to the negative-frequency solutions. This yields

$$\Phi(\hat{t},x) = \sum_j \left[\hat{a}_j f_j(t,x) + \hat{a}_j^\dagger f_j^*(t,x)\right], \tag{2.27}$$

where the index j labels the modes, and the annihilation and creation operators $\hat{a}_j, \hat{a}_j^\dagger$ obey the CCR:

$$[\hat{a}_j, \hat{a}_{j'}] = 0, \tag{2.28a}$$
$$[\hat{a}_j^\dagger, \hat{a}_{j'}^\dagger] = 0, \tag{2.28b}$$
$$[\hat{a}_j, \hat{a}_{j'}^\dagger] = \delta^{(n-1)}(j - j'). \tag{2.28c}$$

Furthermore, similarly to the flat spacetime case, we define a vacuum state $|0_f\rangle$ that is annihilated by all the annihilation operators:

$$\hat{a}_j |0_f\rangle = 0. \tag{2.29}$$

Now, it might appear that we have extended the theory simply by introducing the concept of curvature into spacetime, modifying the action we start with, and replacing ordinary derivatives with covariant derivatives. However, consider a scenario where we have a different orthonormal set of basis modes $h_k(t,x)$, leading to an expansion of the field as

$$\hat{\Phi}(t,x) = \sum_k \left[\hat{b}_k h_k(t,x) + \hat{b}_k^\dagger h_k^*(t,x)\right], \tag{2.30}$$

where $\hat{b}_k$ and $\hat{b}_k^\dagger$ are a new set of annihilation and creation operators that satisfy the same CCR as in Equations (2.28). This allows us to define another vacuum state $|0_h\rangle$, such that

$$\hat{b}_k |0_h\rangle = 0. \tag{2.31}$$

Since both sets of modes are defined on the same background for the same field, they can be related. The f_j modes form an orthonormal basis, allowing the h_k modes to be expanded as

$$h_k = \sum_j \left[\alpha_{kj} f_j + \beta_{kj} f_j^*\right], \tag{2.32a}$$
$$f_j = \sum_k \left[\alpha_{kj}^* h_k - \beta_{kj} h_k^*\right]. \tag{2.32b}$$

These relations are known as Bogoliubov transformations, where α_{jk} and β_{jk} are the Bogoliubov coefficients, given by:

$$\alpha_{jk} = \langle h_j, f_k \rangle, \quad \beta_{jk} = -\langle h_j, f_k^* \rangle. \tag{2.33}$$

Using the orthonormality of the modes, the creation and annihilation operators can be related as:

$$\hat{a}_j = \sum_k \left(\alpha_{kj} \hat{b}_k + \beta_{kj}^* \hat{b}_k^\dagger \right), \tag{2.34a}$$

$$\hat{b}_k = \sum_j \left(\alpha_{kj}^* \hat{a}_j - \beta_{kj}^* \hat{a}_j^\dagger \right). \tag{2.34b}$$

The Bogoliubov coefficients satisfy the following normalization conditions [22]:

$$\sum_i (\alpha_{ji} \alpha_{ki}^* - \beta_{ji} \beta_{ki}^*) = \delta_{jk}, \tag{2.35a}$$

$$\sum_i (\alpha_{ji} \beta_{ki} - \beta_{ji} \alpha_{ki}) = 0. \tag{2.35b}$$

While this framework is well-defined in both Minkowski spacetime and curved spacetime, its implications in curved spacetime become particularly significant. We can notice this if we consider a system in the f-vacuum state $|0_f\rangle$, where no particles are detected using the f_j basis modes. Now, for the h-vacuum state, we can evaluate the number operator $\hat{N}_k = \hat{b}_k^\dagger \hat{b}_k$, given by:

$$\langle 0_f | \hat{N}_k | 0_f \rangle = \sum_j |\beta_{jk}|^2, \tag{2.36}$$

which evaluates the number of particles seen by an observer using the h_k basis modes. We can see that if any of the β_{jk} are non-zero, an observer employing the h_k basis will detect particles even in a vacuum defined by the f_j basis. This occurs because the Bogoliubov transformations mix creation and annihilation operators between the two bases, highlighting that the notion of particles in curved spacetime is observer-dependent. This becomes relevant when it is not possible to select a preferred vacuum state, as is the case in a general curved background.

In this thesis, we focus on the analysis of on a black hole background, which requires examining three possible ground states, depending on the set of coordinates used.

We have now provided a brief overview of quantum field theory in curved spacetime framework and developed mode-sum expressions for the quantum scalar field $\hat{\Phi}$. Next, we will turn our attention to computing expectation values. Throughout this thesis, we will evaluate the expectation values of the vacuum polarization $\langle \hat{\Phi}^2 \rangle$ and the stress-energy tensor $\langle \hat{T}_{\mu\nu} \rangle$. We will also show how to renormalize these quantities if possible. Additionally, we will introduce a method to compute finite, renormalized quantities by subtracting expectation values of the same observable in different ground states. These calculations will make use of Green's functions, which will be the subject of Section 2.3.

2.3 Green's functions

We now introduce what are known as Green's functions. These will be pivotal for the renormalization, as we will shortly see that these objects play an important role in this process. In this section, we consider a spacetime in which a vacuum state $|0\rangle$ exists (though it may not be unique) and where a time coordinate t is chosen to allow for proper time-ordering. This will be the case in the spacetimes that we will consider. In a general curved spacetime, the Green's functions satisfy the inhomogeneous equation:

$$\left[\Box - \left(\mu^2 + \xi R\right)\right] G(x, x') = -\frac{1}{\sqrt{-g}}\delta^{(n)}(x - x'), \tag{2.37}$$

where $\delta^{(n)}$ is the n-dimensional Dirac delta function, G refers to any one of a number of Green's functions, and x, x' represent two spacetime points, this is why the Green's functions are two-point functions. However, there are two-point functions that do not satisfy Equation (2.37), but instead only satisfy the Klein–Gordon equation (2.24) when considering a scalar field.

In the name of completeness, we mention some two-point functions of particular importance among the family of two-point functions. These are the Pauli-Jordan (Schwinger) two-point function G, the anticommutator function $G^{(1)}$, and the Feynman propagator G^F, [22]. In particular, the Feynman propagator G^F is defined as the time-ordered vacuum expectation value and is constructed so that it indeed solves equation (2.37); that is, when the differential operator $\Box - \left(\mu^2 + \xi R\right)$ acts on G^F, the delta function source is produced. On the other hand, the Pauli-Jordan (Schwinger) two-point function G and the anticommutator function $G^{(1)}$ are solutions of the corresponding homogeneous equation, they vanish when acted upon by the differential operator, reflecting the fact that they do not contain the delta function source. Hence, they are not solution of the inhomogeneous equation (2.37). Next, we provide a detailed construction of Green's functions.

The vacuum Pauli-Jordan and anticommutator two-point functions are given by [22]:

$$iG(x, x') = \langle 0|[\hat{\Phi}(x), \hat{\Phi}(x')]|0\rangle, \quad G^{(1)}(x, x') = \langle 0|\{\hat{\Phi}(x), \hat{\Phi}(x')\}|0\rangle, \tag{2.38}$$

where the anticommutator $\{\hat{A}, \hat{B}\}$ of two operators $\hat{A}$ and $\hat{B}$ is defined as

$$\{\hat{A}, \hat{B}\} = \hat{A}\hat{B} + \hat{B}\hat{A}. \tag{2.39}$$

They can be split into their respective positive and negative frequency parts as:

$$iG(x, x') = G_+(x, x') - G_-(x, x'), \quad G^{(1)}(x, x') = G_+(x, x') + G_-(x, x'), \tag{2.40}$$

where $G_\pm(x, x')$, the Wightman functions, are defined as:

$$G_+(x, x') = \langle 0|\hat{\Phi}(x)\hat{\Phi}(x')|0\rangle, \quad G_-(x, x') = \langle 0|\hat{\Phi}(x')\hat{\Phi}(x)|0\rangle. \tag{2.41}$$

The Feynman propagator $G^F(x,x')$ is defined as [22]:

$$iG^F(x,x') = \langle 0|T\left(\hat{\Phi}(x)\hat{\Phi}(x')\right)|0\rangle, \tag{2.42}$$

where T denotes time-ordering. For two spacetime points with time coordinates t and t', the time-ordering operation is defined as:

$$T\big(\hat{\Phi}(x)\hat{\Phi}(x')\big) = \begin{cases} \hat{\Phi}(x)\hat{\Phi}(x') & \text{if } t > t', \\ \hat{\Phi}(x')\hat{\Phi}(x) & \text{if } t' > t. \end{cases} \tag{2.43}$$

The Feynman propagator can be expressed as:

$$iG^F(x,x') = \Theta(t-t')\,G_+(x,x') + \Theta(t'-t)\,G_-(x,x'), \tag{2.44}$$

where Θ represents the Heaviside step function:

$$\Theta(t-t') = \begin{cases} 1 & \text{if } t > t', \\ 0 & \text{if } t < t'. \end{cases} \tag{2.45}$$

Two additional Green's functions of interest are the retarded G_R and advanced G_A Green's functions, which are defined as [22]:

$$G_R(x,x') = -\Theta(t-t')\,G(x,x'), \quad G_A(x,x') = \Theta(t'-t)\,G(x,x'). \tag{2.46}$$

Additionally, the Feynman propagator can be rewritten in terms of G_R and G_A as:

$$G^F(x,x') = -G_e(x,x') - \frac{i}{2}G^{(1)}(x,x'), \tag{2.47}$$

where G_e, the average of G_R and G_A, is given by:

$$G_e(x,x') = \frac{1}{2}\left[G_R(x,x') + G_A(x,x')\right]. \tag{2.48}$$

As we shall see later in this thesis, Green's functions are essential for determining the expectation values of the observables we wish to investigate, such as $\langle\hat{\Phi}^2\rangle$ and $\langle\hat{T}_{\mu\nu}\rangle$. In particular, they will prove useful for understanding Hadamard renormalization. However, we still need to introduce one last piece of the puzzle: the definition and concept of Hadamard quantum states.

2.4 Hadamard quantum states

If we look at Equation (2.37), we see that the right-hand side diverges when $x \to x'$. In order for us to find expectation values from the Green's functions and continue the analysis we need to renormalize. This can be addressed in flat spacetime by employing a technique known as normal ordering, denoted by ":": Normal ordering means that in any

product of creation and annihilation operators, the annihilation operators are placed to the right of the creation operators. For example,

$$: \hat{a}_p \hat{a}_p^\dagger :\rightarrow \hat{a}_p^\dagger \hat{a}_p. \tag{2.49}$$

However, renormalization in curved spacetime is considerably more challenging than in flat spacetime. This increased complexity arises because the quantum stress-energy tensor, $\langle \hat{T}_{\mu\nu} \rangle$, not only acts as a source of gravity, but also influences the curvature of the spacetime, see Equation (1.40). We need to apply a different procedure. Several renormalization schemes have been proposed in the literature, including the adiabatic approach [114], the DeWitt-Schwinger method [45], zeta-function regularisation [54], dimensional renormalization [134], and the Pauli-Villars method [115]. In this thesis, we employ a technique known as Hadamard renormalization [22]. Hadamard renormalization relies on expressing the Feynman propagator, $G^F(x, x')$ (the two-point function), in Hadamard form, which requires that the points x and x' are connected by a unique geodesic. It has been demonstrated [121] that if the two-point function exhibits Hadamard structure in an open neighbourhood of a Cauchy surface on a C^∞ globally hyperbolic manifold, then this structure persists everywhere.

First, we need to define when a quantum state is a Hadamard state, which constitutes the initial step towards discussing renormalization. We have already introduced the concept of ground states and vacuum states in curved spacetime, which arise from the lack of invariance under transformations of the Poincaré group in curved spacetimes. This implies that, unlike in Minkowski spacetime, there is no preferred unique vacuum state. In Minkowski spacetime, the vacuum is the state with the lowest energy and the absence of particles for an inertial observer. For this reason, we seek a quantum state possessing certain properties to mimic the features of the Minkowski vacuum. We require that a good physical state satisfies the following conditions [119, Chap. 3]:

- It yields finite quantum fluctuations for all observables, including the components of the stress-energy tensor.
- It mimics the ultraviolet behaviour of the Minkowski vacuum. This condition reflects the expectation that probing higher energies corresponds to performing measurements at smaller spacetime scales. Since, locally, the metric reduces to that of Minkowski spacetime, the underlying quantum state is expected to resemble the Poincaré ground state.

Additionally, when evaluating the product of two or more observables, such as fields at two or more distinct spacetime points (e.g., x and x'), it is crucial to control the structure of the singularities arising as $x \rightarrow x'$ in the two-point function. In Minkowski spacetime, we can control this using the normal ordering procedure, which relies on the creation and

annihilation operators. In curved spacetime we must identify a class of states that fulfil the mentioned conditions. These states are known as Hadamard states. Before presenting the formal expressions for Hadamard states, we need to introduce two essential quantities that are going to be useful for their construction.

The first one is Synge's world function, which can also be expressed as [22]:

$$\sigma(x,x') = \frac{1}{2}(\lambda_1 - \lambda_0)\int_z g_{\mu\nu}t^\mu t^\nu \, d\lambda, \tag{2.50}$$

where $t^\mu = \frac{dz}{d\lambda}$ is the tangent vector to the unique geodesic $z(\lambda)$ connecting x and x'. Assuming that x and x' lie within a normal neighbourhood, this ensures that any two points in the neighbourhood are connected by a unique geodesic lying entirely within that region. The parameter λ is affine, with $x = z(\lambda_0)$ and $x' = z(\lambda_1)$. The world function satisfies:

$$2\sigma = \sigma_{;\mu}\sigma^{;\mu}, \tag{2.51}$$

and it is important to note the following:

$$\begin{aligned} &\sigma(x,x') < 0 \quad \text{for timelike separation,} \\ &\sigma(x,x') = 0 \quad \text{for null separation,} \\ &\sigma(x,x') > 0 \quad \text{for spacelike separation.} \end{aligned} \tag{2.52}$$

The second quantity we need to introduce is the van Vleck–Morette determinant, $\Delta(x,x')$, which provides information on how geodesics originating from the point x converge or spread out at the point x'. It is defined as [22]:

$$\Delta(x,x') = [-g(x)]^{-\frac{1}{2}} \det\left[\sigma_{;\mu\nu'}(x,x')\right]\left[-g(x')\right]^{-\frac{1}{2}}. \tag{2.53}$$

In n dimensions, $\Delta(x,x')$ satisfies the differential equation:

$$\Box\sigma = n - 2\Delta^{-\frac{1}{2}}\Delta^{\frac{1}{2}}_{;\mu}\sigma^{;\mu}, \tag{2.54}$$

with the boundary condition:

$$\lim_{x\to x'}\Delta(x,x') = 1. \tag{2.55}$$

We now have all the ingredients to define the local Hadamard condition that characterises a Hadamard state and to describe how the two-point function of a Hadamard state can be written on a globally hyperbolic spacetime.

2.4.1 Definition. *Let (M,g) be a four dimensional spacetime. We say that a state and its two-point function are of local Hadamard form if, for every $x \in M$, we can write:*

$$G^F_{(4)}(x,x') = \lim_{\epsilon\to 0^+}\left\{\frac{i}{8\pi^2}\left(\frac{U_{(4)}(x,x')}{[\sigma_\epsilon(x,x')]} + V_{(4)}(x,x')\ln\left(\frac{\sigma_\epsilon(x,x')}{\lambda^2}\right) + W_{(4)}(x,x')\right)\right\}, \tag{2.56}$$

where x, x' are two arbitrary points in the spacetime that lie in a normal neighbourhood, ϵ is a regularisation parameter, λ is a reference length introduced to make the argument of the logarithm dimensionless, and $\sigma_\epsilon(x,x')$ is defined as $\sigma_\epsilon(x,x') = \sigma(x,x') + i\epsilon$, where $\sigma(x,x')$ is the Synge's function.

We have defined $\sigma_\epsilon(x,x')$ with the factor $i\epsilon$ because when $\epsilon \to 0^+$ we want to ensure that $G^F(x,x')$ has a singularity structure that resembles that of the Feynman propagator. The definition of the two-point function is strictly related to the dimension we are considering. Equation (2.56) applies in a general four-dimensional spacetime, and $U_{(4)}$, $V_{(4)}$, and $W_{(4)}$ are symmetric and regular biscalars in four dimensions. They can be found in Decanini and Folacci [41], where the general formula for $D \geq 2$ dimensions is also provided. In this thesis, we are concerned with spacetimes in five dimensions.

2.4.2 Definition. *The Hadamard form of the two-point function for a scalar field in general odd dimensions is given by:*

$$G^F(x,x') = \frac{i\alpha_D}{2}\left(\frac{U(x,x')}{[\sigma_\epsilon(x,x')]^{\frac{D}{2}-1}} + W(x,x')\right), \tag{2.57}$$

where $U(x,x')$ and $W(x,x')$ are symmetric and regular biscalar functions, which possess expansions of the form:

$$U(x,x') = \sum_{n=0}^{+\infty} U_n(x,x')\sigma^n(x,x'), \tag{2.58}$$

$$W(x,x') = \sum_{n=0}^{+\infty} W_n(x,x')\sigma^n(x,x'). \tag{2.59}$$

Notably, Equation (2.57) does not contain a $V(x,x')$ term, which was a source of divergence caused by the logarithmic term. This showcase once more why working in odd dimensions is beneficial and easier than working in even dimensions. The coefficient α_D is given by:

$$\alpha_D = \frac{\Gamma(D/2-1)}{(2\pi)^{D/2}}, \text{ with } D \text{ odd}, \tag{2.60}$$

The coefficients $U_n(x,x')$ satisfy the recursion relations:

$$\begin{aligned}&(n+1)(2n+4-D)U_{n+1} + (2n+4-D)U_{n+1;\mu}\sigma^{;\mu} \\ &- (2n+4-D)U_{n+1}\Delta^{-1/2}\Delta^{1/2}_{;\mu}\sigma^{;\mu} + (\Box - \mu^2 - \xi R)U_n = 0, \quad \text{for } n \in \mathbb{N},\end{aligned} \tag{2.61}$$

with the boundary condition:

$$U_0 = \Delta^{1/2}. \tag{2.62}$$

The coefficients $W_n(x,x')$ satisfy the recursion relations:

$$\begin{aligned}&(n+1)(2n+D)W_{n+1} + 2(n+1)W_{n+1;\mu}\sigma^{;\mu} \\ &- 2(n+1)W_{n+1}\Delta^{-1/2}\Delta^{1/2}_{;\mu}\sigma^{;\mu} + (\Box - \mu^2 - \xi R)W_n = 0, \quad \text{for } n \in \mathbb{N}.\end{aligned} \tag{2.63}$$

From the recursion relations (2.61) and (2.63), and the boundary condition (2.62), it is possible to prove that $G^F(x,x')$, as given by Equation (2.57), solves Equation (2.37). This follows straightforwardly from

$$(\Box - \mu^2 - \xi R)W(x,x') = 0. \tag{2.64}$$

It is important to notice that $W_n(x,x')$ is not uniquely defined. Indeed, the first coefficient of this sequence, $W_0(x,x')$, is not constrained by the recursion relations (2.63). If $W_0(x,x')$ is not fixed, the same holds for all $W_n(x,x')$ with $n \geq 1$. We can exploit this arbitrariness to show the quantum state dependence in the biscalar $W(x,x')$ by specifying the Hadamard coefficient $W_0(x,x')$. Once it has been specified, the recursion relations (2.63) uniquely determine the coefficients $W_n(x,x')$ for $n \geq 1$ and, therefore, the biscalar $W(x,x')$.

We now proceed by splitting $G^F(x,x')$ into the sum of two components, $H(x,x') + W(x,x')$, where the first term is called the Hadamard parametrix:

$$H(x,x') = \frac{i\alpha_D}{2} \frac{U(x,x')}{[\sigma(x,x') + i\epsilon]^{\frac{D}{2}-1}}. \tag{2.65}$$

In odd dimensions, this function encodes the full local singularity structure of the Feynman propagator of a Hadamard state. Hence, the singular part of the Feynman propagator, which depends only on the geometry and the field being considered, is known, allowing us to renormalize that quantity. We use states that fulfil the local Hadamard condition. The biscalars U and W can be determined via the Hadamard recursion relations given by (2.61) and (2.63), and all the relevant partial differential equations depend only on the spacetime metric and the equation of motion. Hence, we conclude that:

- The local singularity structure of the two-point function of a Hadamard state is fully determined by the spacetime geometry.

This being the case means that we have control over the singular structure of the Feynman propagator, and we can remove all unwanted pathologies with a suitable subtraction, because we can fully determine explicitly the expression of the divergent part once the geometry of the spacetime and the field under consideration are given. With the Hadamard states, we can describe one of the most important observables, namely, the stress-energy tensor for the Klein–Gordon scalar field, which will be discussed in the next section.

2.5 Stress-energy tensor

The stress-energy tensor (SET), $T_{\mu\nu}$, is the observable we will mainly focus on throughout this thesis, together with the vacuum polarisation, which is evaluated as an intermediate

step to determine the quantum stress-energy tensor. This is because the SET encodes information about matter and energy, a property true for both the classical and the quantum regimes. More specifically, the SET is a rank-two tensor that compactly describes how energy and momentum are distributed and flow through spacetime. To interpret the components of the energy-momentum tensor $T_{\mu\nu}$ physically, it is useful to introduce a locally orthonormal tetrad $\{e^{\mu}_{(a)}\}$, where Latin indices in parentheses label the local inertial frame components and $e^{\mu}_{(0)} = u^{\mu}$ is the 4-velocity of an observer at a given point. In this frame, the components of the energy-momentum tensor acquire the following interpretations:

- **Energy Density:** The component $T_{(0)(0)} = T_{\mu\nu}u^{\mu}u^{\nu}$ represents the energy density measured by an observer with 4-velocity u^{μ}. This gives the amount of energy per unit volume in the local rest frame of the observer.
- **Energy Fluxes:** The components $T_{(0)(i)} = T_{\mu\nu}u^{\mu}e^{\nu}_{(i)}$ describe the flux of energy in the spatial direction i, as measured in the observer's local rest frame. By symmetry, $T_{(i)(0)} = T_{(0)(i)}$.
- **Stresses (Pressure and Shear):** The purely spatial components $T_{(i)(j)} = T_{\mu\nu}e^{\mu}_{(i)}e^{\nu}_{(j)}$ encode the stresses in the system, including isotropic pressure when $i = j$, and shear stresses when $i \neq j$.

In the framework of general relativity, the SET acts as the source of the gravitational field in Einstein's field equations (1.40). This means that the distribution and flow of energy and momentum directly influence the curvature of spacetime, see Equation (1.40).

The quantum SET requires careful treatment when transitioning from classical theories. Notably, the quantum fluctuations modify the classical picture, necessitating renormalization procedures to extract meaningful physical predictions. We start our description by following the procedure outlined in [41] retrieving the formula for the classical stress-energy tensor from the action, for a massive scalar field.

The functional derivative of S in Equation (2.22) with respect to $g_{\mu\nu}$ allows us to define the stress-energy tensor $T_{\mu\nu}$ associated with a scalar field Φ, [22,148]. Specifically, we have

$$T_{\mu\nu} = \frac{2}{\sqrt{-g}}\frac{\delta S[\Phi, g_{\mu\nu}]}{\delta g_{\mu\nu}}, \tag{2.66}$$

and by considering the variation

$$g_{\mu\nu} \to g_{\mu\nu} + \delta g_{\mu\nu}, \tag{2.67}$$

the classical stress-energy tensor reads [41]:

$$\begin{aligned} T_{\mu\nu} =& (1-2\xi)\nabla_{\mu}\Phi\nabla_{\nu}\Phi + \left(2\xi - \frac{1}{2}\right) g_{\mu\nu}g^{\rho\sigma}\nabla_{\rho}\Phi\nabla_{\sigma}\Phi - \frac{1}{2}g_{\mu\nu}\mu^2\Phi^2 \\ & - 2\xi\Phi\nabla_{\mu}\nabla_{\nu}\Phi + 2\xi g_{\mu\nu}\Phi\Box\Phi + \xi\left(G_{\mu\nu}\right)\Phi^2, \end{aligned} \tag{2.68}$$

where we report the definition of the Einstein tensor introduced in Chapter 1 for simplicity:

$$G_{\mu\nu} = R_{\mu\nu} - \frac{1}{2} g_{\mu\nu} R, \tag{2.69}$$

with $R_{\mu\nu}$ being the Ricci tensor and R the scalar curvature. This tensor satisfies the conservation equation:

$$\nabla^{\nu} T_{\mu\nu} = 0. \tag{2.70}$$

If we consider a quantum field rather than a classical one, we need to be able to evaluate products of fields at the same spacetime point, namely: $:\Phi^2(x):$. If the quantum state $|\psi\rangle$ that we are considering is a Hadamard state, then the expression of the stress-energy tensor is given by:

$$\langle\psi|\hat{T}_{\mu\nu}(x)|\psi\rangle = \lim_{x'\to x} \left[\hat{\mathcal{T}}_{\mu\nu}(x,x') \left(-iG^F(x,x')\right)\right], \tag{2.71}$$

where $G^F(x,x')$ is the Feynman propagator or the two-point function, see Section 2.3 and $\hat{\mathcal{T}}_{\mu\nu}(x,x')$ is a differential operator which is constructed by point-splitting from the classical expression for the stress-tensor (2.68). It is a tensor of type $(0,2)$ in x and a scalar in x'. It is given by

$$\begin{aligned} T_{\mu\nu} = {} & (1-2\xi)\, g^{\nu'}_{\ \nu}\, \nabla_{\mu}\nabla_{\nu'} + \left(2\xi - \frac{1}{2}\right) g_{\mu\nu}\, g^{\rho\sigma'}\, \nabla_{\rho}\nabla_{\sigma'} \\ & - 2\xi\, g^{\mu'}_{\ \mu}\, g^{\nu'}_{\ \nu}\, \nabla_{\mu'}\nabla_{\nu'} + 2\xi\, g_{\mu\nu}\, \nabla_{\rho}\nabla^{\rho} \\ & + \xi \left(R_{\mu\nu} - \frac{1}{2} g_{\mu\nu} R\right) - \frac{1}{2}\, g_{\mu\nu}\mu^2\,, \end{aligned} \tag{2.72}$$

where $g_{\mu\nu'}$ denotes the bi-covector of parallel transport between x and x', which is defined by the partial differential equation

$$\partial_{\rho}(g_{\mu\nu'}\, \partial^{\rho}\sigma) = 0, \tag{2.73}$$

and the boundary condition

$$\lim_{x'\to x} g_{\mu\nu'} = g_{\mu\nu}. \tag{2.74}$$

The expectation value of the stress-energy tensor requires renormalization since the Feynman propagator diverges in the coincidence limit, $x \to x'$. This renormalization is made possible by the properties of Hadamard quantum states, see Section 2.4 and the concept of Hadamard renormalization, which we will explore further in Sections 2.6.

2.6 Hadamard renormalization of the stress-energy tensor

As we mentioned in Section 2.5 the expectation value of the stress-energy tensor operator with respect to a Hadamard quantum state $|\psi\rangle$ is formally given as the limit:

$$\langle\psi|\hat{T}_{\mu\nu}(x)|\psi\rangle = \lim_{x'\to x} \hat{\mathcal{T}}_{\mu\nu}(x,x') \left(-iG^F(x,x')\right), \tag{2.75}$$

where $G^F(x,x')$ is the Feynman propagator, as defined in Equation (2.42). This propagator is assumed to possess one of the Hadamard forms described in Section 2.4. $\hat{\mathcal{T}}_{\mu\nu}(x,x')$ in Equation (2.75) is a differential operator constructed via point-splitting from the classical expression of the stress-energy tensor.

For this formulation of the renormalization we follow the procedure outlined in [41]. Given the singular behaviour of the Feynman propagator when $x \to x'$, the expression for the expectation value of the stress-energy tensor operator in Equation (2.75) with respect to the Hadamard state $|\psi\rangle$ is divergent and therefore ill-defined. However, since we have taken an Hadamard state we know that this pathological behaviour arises from the purely geometrical part of the Hadamard expansion, for D odd as given in Equation (2.57):

$$G^F(x,x') \sim \frac{1}{\sigma(x,x')^{\frac{D}{2}-1}}, \tag{2.76}$$

where $\sigma(x,x')$ is the Synge world function. This divergence reflects the fact that the coincidence limit $x' \to x$ of the propagator is singular, which necessitates regularisation. It is possible to cure the pathological behaviour of $\langle\psi|\hat{T}_{\mu\nu}|\psi\rangle$ given by Equation (2.76) and to construct from it a meaningful expression that can act as a source in the semi-classical Einstein equations (2.82). This can also be regarded as the renormalized expectation value of the stress-energy tensor operator with respect to the Hadamard quantum state $|\psi\rangle$.

The Hadamard regularization prescription achieves this in odd dimensions as follows: we first discard the purely geometrical part of G^F, as given in Equation (2.57) from the right-hand side of Equation (2.75). Specifically, we apply the replacement:

$$\lim_{x'\to x} \hat{\mathcal{T}}_{\mu\nu}(x,x') \left(-iG^F(x,x')\right) \to \frac{\alpha_D}{2} \lim_{x'\to x} \hat{\mathcal{T}}_{\mu\nu}(x,x') W(x,x'), \tag{2.77}$$

where $W(x,x')$ is the regularized part of the Hadamard expansion. This ensures the conservation of the resulting expression. Therefore, the renormalized expectation value of the stress-energy tensor operator in the Hadamard state $|\psi\rangle$ is given by:

$$\langle\psi|\hat{T}_{\mu\nu}(x)|\psi\rangle_{\text{ren}} = \frac{\alpha_D}{2} \lim_{x'\to x} \hat{\mathcal{T}}_{\mu\nu}(x,x') W(x,x'). \tag{2.78}$$

We obtain the renormalized expectation value of the stress-energy tensor operator in the Hadamard state $|\psi\rangle$ as [41]:

$$\begin{aligned}\langle\psi|\hat{T}_{\mu\nu}|\psi\rangle_{\text{ren}} = \frac{\alpha_D}{2}\Bigg[&- \left(w_{\mu\nu} - \frac{1}{2}g_{\mu\nu}w^{\rho}{}_{\rho}\right) + \frac{1}{2}(1-2\xi)\nabla_\mu\nabla_\nu w \\ &+ \frac{1}{2}\left(2\xi - \frac{1}{2}\right) g_{\mu\nu}\Box w + \xi\left(R_{\mu\nu} - \frac{1}{2}g_{\mu\nu}R\right) w - \frac{1}{2}g_{\mu\nu}\mu^2 w\Bigg],\end{aligned} \tag{2.79}$$

where we define

$$w(x) = \lim_{x'\to x} W(x,x'), \tag{2.80a}$$

$$w_{\mu\nu}(x) = \lim_{x'\to x} W(x,x')_{;\mu\nu}, \tag{2.80b}$$

and we also report the results of [41] for the odd dimension case:

$$w^{\rho}{}_{\rho} = (\mu^2 + \xi R)w, \tag{2.81a}$$

$$\partial_\rho w^{\rho}{}_{a} = \frac{1}{4}\partial_a(\Box w) + \frac{1}{2}R^{\rho}{}_{a}\partial_\rho w + \frac{1}{2}\xi\partial_a R w. \tag{2.81b}$$

By subtracting the purely geometric, state-independent part of the Hadamard form of the propagator, the renormalized RSET becomes finite. Hence, we can use this expression to introduce the fundamental equations of the semi-classical theory, the semi-classical Einstein equations (2.83). It is important to note that the renormalisation procedure leaves a finite ambiguity in $\langle T_{\mu\nu}\rangle_{\text{ren}}$, corresponding to the freedom to add local, conserved, symmetric tensors constructed purely from the curvature of the background spacetime. These additional terms typically take the form of combinations of $g_{\mu\nu}R^2$, $R_{\mu\nu}R^{\mu\nu}$, $R_{\mu\nu\rho\sigma}R^{\mu\nu\rho\sigma}$, and their derivatives. Their presence reflects the fact that renormalisation is not unique, and must be fixed by physical considerations or renormalisation conditions.

2.7 Semi-classical Einstein field equations

Now that we have explained the renormalization procedure we are going to use it to introduce the semi-classical Einstein field equations:

$$G_{\mu\nu} + \Lambda g_{\mu\nu} = \langle\psi|\hat{T}_{\mu\nu}|\psi\rangle, \tag{2.82}$$

where the left-hand side is identical to the Einstein field equations (1.40), consisting of Λ, the cosmological constant, $G_{\mu\nu}$, the Einstein tensor, and $g_{\mu\nu}$, the metric of the spacetime under consideration. This encapsulates all the information about the geometry of the spacetime. The right-hand side, however, differs from the conventional formulation of general relativity, as it contains the expectation value of the stress-energy tensor operator evaluated in a quantum state ψ. This term encodes all the information regarding the energy and momentum of the system, which has been quantised using the procedure described in Section 2.2.

As we have seen, the right-hand side exhibits divergences when evaluated at the same point in spacetime, $x \to x'$. To properly define these equations, the right-hand side must be renormalized. There are various methods for achieving this, but in this thesis, we will use the Hadamard renormalization introduced in Section 2.6. Thus, the semi-classical Einstein field equations become:

$$G_{\mu\nu} + \Lambda g_{\mu\nu} = \langle\psi|T_{\mu\nu}|\psi\rangle_{\text{ren}}. \tag{2.83}$$

We will also demonstrate a clever way to evaluate a finite quantity that provides information about the behaviour of the spacetime and quantum fluctuations without employing

any renormalization procedure. This is possible due to the presence of multiple states in the theory of QFTCS, which arise from the lack of invariance under the Poincaré group. If we define two ground states for the same spacetime and quantum field, and if both states are Hadamard states (satisfying the decomposition presented in Equation (2.57)), we can subtract the expectation values of the same observable—in this case, the stress-energy tensor, obtaining a finite quantity. This is because, since the divergent part depends only on the spacetime and the type of field being considered, it is mathematically identical for both states. Therefore, subtracting these two expectation values cancels out the divergences, leaving the quantity of interest finite. This will be explored in more detail in Part II. This does not resolve the need to renormalize the right-hand side of Equation (2.83), but it provides a first step towards a full analysis, giving us a finite quantity that can be studied to extract physical information about the system.

2.7.1 Quantum corrected metric

The quantum-corrected metric is obtained by solving the problem of the backreaction. Let us suppose that we have evaluated the renormalized stress-energy tensor for a quantum field in a certain curved spacetime. To solve the semi-classical Einstein field equations (2.83), one must use this tensor as a source, making the unknown quantity the metric of the spacetime in Equation (2.83). This approach allows us to investigate, at the first perturbative level, how quantum perturbations affect the spacetime under consideration. Solving this is referred to as the backreaction problem, and the resulting metric is called the quantum-corrected metric. Two important assumptions underlie this calculation. First, it is assumed that quantum fluctuations of the matter fields are small, so that the semi-classical approximation remains valid. Second, it is typically assumed that the expectation value of the renormalised stress-energy tensor $\langle T_{\mu\nu}\rangle_{\text{ren}}$ respects the symmetries of the background spacetime, such as stationarity or spherical symmetry, ensuring consistency with the symmetries of the classical geometry. This implies that these fluctuations do not affect the symmetries of the spacetime being studied. For example, if we are considering the Schwarzschild metric, a spherically symmetric spacetime, its line element is given by:

$$ds^2 = -\left(1 - \frac{2M}{r}\right) dt^2 + \left(1 - \frac{2M}{r}\right)^{-1} dr^2 + r^2 d\theta^2 + r^2 \sin^2\theta \, d\phi^2, \tag{2.84}$$

where M is the mass of the black hole, and t, r, θ, and ϕ are the spherical coordinates (as introduced in Section 1.3). This symmetry is preserved in the quantum-corrected metric; hence, we can use the same form of the metric to find the new one:

$$ds^2 = -A(r)dt^2 + B(r)^{-1}dr^2 + r^2 d\theta^2 + r^2 \sin^2\theta \, d\phi^2, \tag{2.85}$$

where $A(r)$ is a general function that we need to determine. Substituting this metric into Equation (2.83) and solving for $A(r)$ and $B(r)$ provides the quantum-corrected metric of

the Schwarzschild black hole, which incorporates the quantum fluctuations of matter given by a scalar field.

Summary

In this chapter, we have introduced all the primary concepts related to quantum field theory, and its extension to quantum field theory on curved spacetime, that are necessary to proceed with this thesis. This is not a comprehensive description, which can be found in textbooks on the topic such as [22, 147, 148], but rather a condensed summary of the main topics that we will explore in the research chapters later on.

In particular, the Hadamard condition for a quantum state and Hadamard renormalization will be pivotal in studying the semi-classical analysis of the five dimensional Kerr-AdS later in the thesis. However, before delving into these analyses, we still need to provide a proper definition of what anti-de Sitter spacetimes are and what black holes in AdS entail. This will be the subject of the next chapter.

Chapter 3

Quantum field theory on anti-de Sitter black holes

In this chapter, we will discuss black holes that are asymptotically Anti-de Sitter (AdS). Before delving into this topic, we introduce the concept of AdS spacetime. AdS spacetime is a solution of the Einstein field equations obtained for negative values of the cosmological constant, Λ. Naively, it can be thought of as putting the universe in a "box." This analogy implies that, at infinity, we need to impose boundary conditions to solve the equations of motion for the quantum field considered in this spacetime. The type of boundary conditions depends on the differential equation governing the field's motion. For a scalar field, which is the focus of this thesis, the boundary conditions are the ones that we can impose on the solution of the Klein-Gordon equation which is a second-order homogeneous partial differential equation. These are the Dirichlet, Neumann, or Robin boundary conditions, see Section 3.2.

The reason for the focus on asymptotically AdS spacetimes in this thesis are twofold. First, the "box"-like nature of AdS simplifies the analysis [67]. For example, in AdS black hole spacetimes, problems related to superradiance disappear [68]. Second, the discovery of the AdS/CFT correspondence [93]. While this thesis does not present this theory, as it is not directly relevant to the QFTCS framework studied here, it remains a significant area of research. The AdS/CFT correspondence establishes a relationship between asymptotically Anti-de Sitter spacetimes and conformal field theories (CFT). This correspondence states an equivalence between the gravitational theory in the AdS spacetime and the conformal field theory on its boundary, such that there exists a dictionary to translate calculations between the two.

Nonetheless, we will focus on AdS spacetimes in the framework of QFTCS for our analysis. The structure of this chapter is outlined as follows: Section 3.1 will introduce the geometry of AdS spacetimes, focusing especially on the Poincaré patch and its significance

in simplifying the analysis of asymptotically AdS spacetimes. Section 3.2 will address the imposition of boundary conditions at the AdS boundary. Then, in Section 3.3, we will focus on the geometry and properties of AdS black holes, introducing some notable examples. Finally, in Section 3.4, we will introduce the different quantum states that can be studied on AdS black hole spacetimes for a scalar field.

3.1 Anti-de-Sitter spacetimes

We begin by introducing the AdS_{d+1} spacetime. The AdS spacetime can be visualised as a $(d+1)$-dimensional single-sheeted hyperboloid embedded in a $(d+2)$-dimensional flat Euclidean space, $\mathbb{E}^{(2,d)}$ [22, 25, 26], with the metric $\eta_{AB} = \mathrm{diag}(-1, 1, 1, \ldots, 1, -1)$. This spacetime is a maximally symmetric solution of the $(d+1)$-dimensional Einstein equations with a negative cosmological constant. Using the Cartesian coordinates X^A $(A = 0, 1, 2, \ldots, d+1)$, the hyperboloid in the embedding space satisfies the equation:

$$-(X^0)^2 + (X^1)^2 + (X^2)^2 + \cdots + (X^d)^2 - (X^{d+1})^2 = -L^2, \tag{3.1}$$

where $L > 0$ is the radius of the waist of the hyperboloid and is related to the cosmological constant by:

$$\Lambda = -\frac{d(d-1)}{2L^2}. \tag{3.2}$$

In Equation (3.1), there are two time-like coordinates, X^0 and X^{d+1}, while X^i, $i = 1, \ldots, d$, are space-like. The metric on the embedding space is given by

$$ds^2 = -(dX^0)^2 + (dX^1)^2 + (dX^2)^2 + \cdots + (dX^d)^2 - (dX^{d+1})^2. \tag{3.3}$$

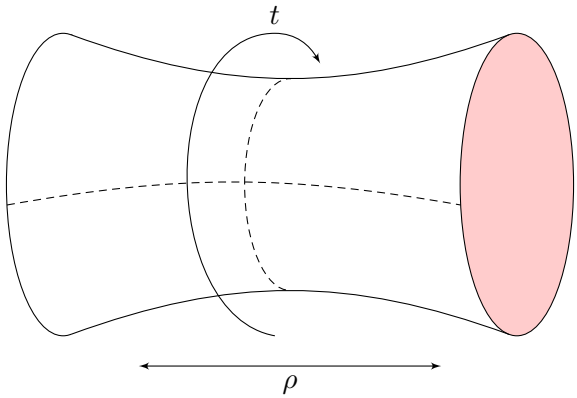

Figure 3.1: Schematic representation of AdS spacetime, with the $(n-2)$ angular coordinates omitted. This shows that pure AdS admits closed timelike curves (adapted from [10]).

We now choose a suitable set of dimensionless coordinates for AdS_{d+1} spacetime [79, 106]:

$$t, \quad -\pi \leq t \leq \pi, \tag{3.4a}$$
$$\rho, \quad 0 \leq \rho < \frac{\pi}{2}, \tag{3.4b}$$
$$\theta_j, \quad 0 \leq \theta_j \leq \pi, \quad j = 1, 2, \ldots, d-2, \tag{3.4c}$$
$$\phi, \quad 0 \leq \phi < 2\pi, \tag{3.4d}$$

where ρ is the radial coordinate, θ_j are polar coordinates, and ϕ is the azimuthal coordinate. The time coordinate t is periodic with a period of 2π, leading to closed timelike curves, see Figure 3.1. This can cause causality problems in our spacetime; however, these can be circumvented by considering the covering space, CAdS_{d+1}, where the time coordinate is extended to $t \in (-\infty, \infty)$. We can then pick the coordinate transformations that relate the dimensionless coordinates to the embedding space coordinates in $\mathbb{E}^{(2,d)}$ [10, 103, 104]:

$$\begin{aligned}
X^0 &= L \cos t \sec \rho, \\
X^1 &= L \tan \rho \cos \theta_1, \\
X^2 &= L \tan \rho \sin \theta_1 \cos \theta_2, \\
&\vdots \\
X^{d-1} &= L \tan \rho \sin \theta_1 \sin \theta_2 \cdots \sin \theta_{d-2} \cos \phi, \\
X^d &= L \tan \rho \sin \theta_1 \sin \theta_2 \cdots \sin \theta_{d-2} \sin \phi, \\
X^{d+1} &= L \sin t \sec \rho.
\end{aligned} \tag{3.5}$$

Taking derivatives of the embedding coordinates in Equation (3.5), we have:

$$\begin{aligned}
dX^0 &= L \left(-\sin t \sec \rho \, dt + \cos t \sec \rho \tan \rho \, d\rho \right), \\
dX^1 &= L \left(\sec^2 \rho \cos \theta_1 \, d\rho - \tan \rho \sin \theta_1 \, d\theta_1 \right), \\
&\vdots \\
dX^{d+1} &= L \left(\cos t \sec \rho \, dt + \sin t \sec \rho \tan \rho \, d\rho \right).
\end{aligned} \tag{3.6}$$

Substituting the derivatives from Equation (3.6) into the embedding in Equation (3.3) space metric gives the AdS_{d+1} metric:

$$ds^2 = L^2 \sec^2 \rho \left(-dt^2 + d\rho^2 + \sin^2 \rho \left[d\theta_1^2 + \sum_{i=2}^{d-2} \prod_{j=1}^{i-1} \sin^2 \theta_j \, d\theta_i^2 + \prod_{j=1}^{d-2} \sin^2 \theta_j \, d\phi^2 \right] \right). \tag{3.7}$$

In this thesis, we will focus on AdS black hole spacetimes in odd dimensions, so we will not treat the pure AdS case specifically. However, it is important to review this spacetime, as it will also serve as the asymptotic expression for the metric of the black holes we will

consider, specifically in the five-dimensional ($d = 4$) case. The corresponding metrics are given as follows:

$$ds^2 = L^2 \sec^2 \rho \left(-dt^2 + d\rho^2 + \sin^2 \rho \left[d\theta_1^2 + \sin^2 \theta_1 \, d\theta_2^2 + \sin^2 \theta_1 \sin^2 \theta_2 \, d\phi^2\right]\right), \tag{3.8}$$

for AdS_5 spacetime.

We present the Penrose diagram for the AdS_n spacetime, which is a useful example for understanding the difference between pure AdS_n and the covering $CAdS_n$. Notably, this is a pivotal point in the construction of the BTZ black hole that we will briefly introduce in Section 3.3. We suppress all the angular coordinates in order to show the diagram.

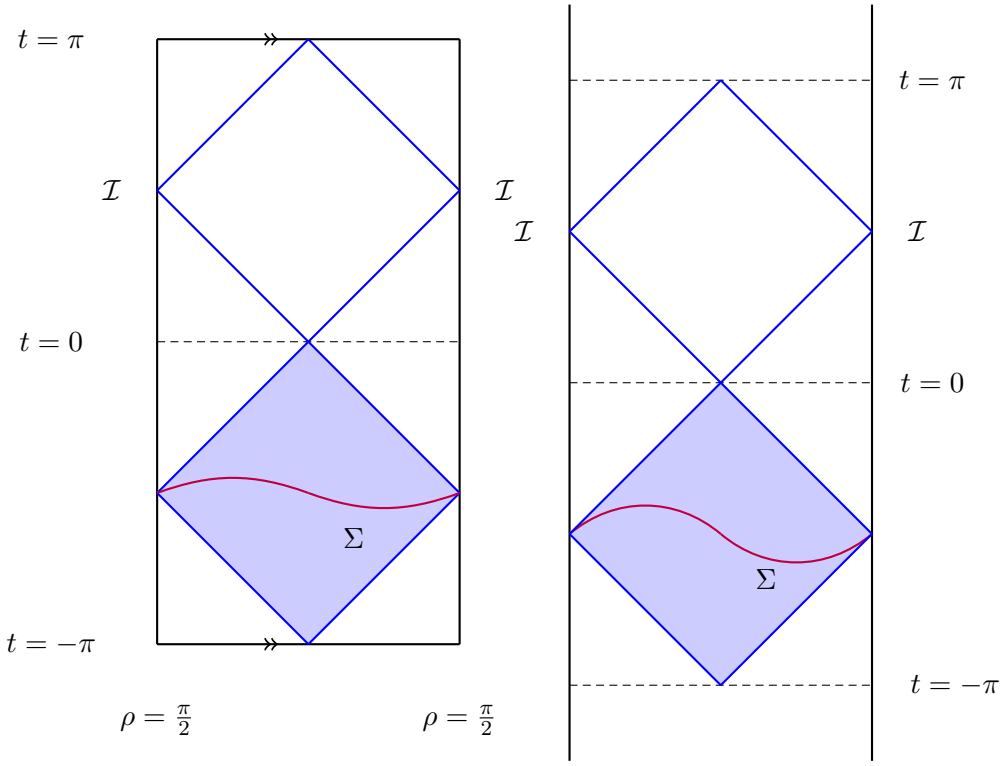

Figure 3.2: Penrose diagrams of the pure AdS_n spacetime (left), where the time coordinate has a period of 2π, allowing for the possibility of closed timelike curves. The radial coordinate ρ extends to a boundary at $\rho = \frac{\pi}{2}$. The covering space of this spacetime, $CAdS_n$ (right), has a time coordinate $t \in (-\infty, \infty)$. In the blue causal diamond, we take Σ as a spacelike hypersurface (red line). Given initial data on Σ, the evolution is determined only within the shaded region; to extend beyond this region, boundary conditions must be imposed (adapted from [14, 106]).

The timelike boundary in AdS and CAdS encloses the spacetimes in a "box". This means that, physically, null rays can reach the boundary in finite coordinate time. Hence, neither AdS nor CAdS are globally hyperbolic spacetimes. This implies that these spacetimes require boundary conditions because, in order to solve the equations of motion, we must

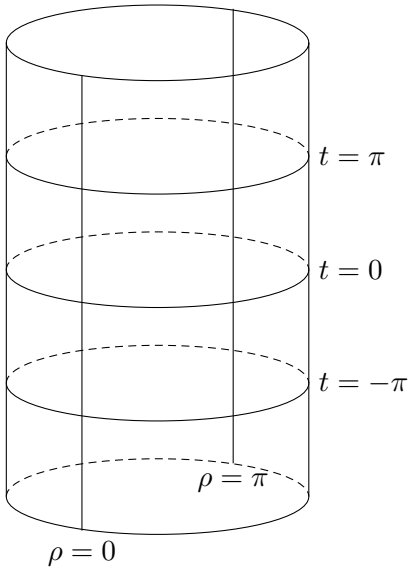

Figure 3.3: ESU with two dimensions suppressed. The cylinder extends to infinity in both directions (adapted from [10, 106]).

specify what happens to the field at the boundary $\mathcal{I}$. This is a mandatory requirement for constructing a meaningful quantum field theory [14, 18, 21, 34, 35, 37, 38, 59, 72, 73, 106, 146]. However, one problem arises: the boundary in AdS_4 spacetime at $\rho = \pi/2$ is not part of the AdS_4 spacetime itself; this can introduce some difficulties in imposing boundary conditions [72, 73, 106]. This problem can be overcome by mapping the AdS_4 spacetime into the Einstein Static Universe (ESU) [14]. We give the ESU metric as (see Figure 3.3)

$$ds^2 = L^2\Big(-dt^2 + d\rho^2 + \sin^2\rho\left[d\theta^2 + \sin^2\theta\, d\phi^2\right]\Big). \tag{3.9}$$

ESU is globally hyperbolic and its metric is conformal to that of the AdS metric in four dimensions,

$$ds^2 = L^2\sec^2\rho\Big(-dt^2 + d\rho^2 + \sin^2\rho\big[d\theta^2 + \sin^2\theta\, d\phi^2\big]\Big). \tag{3.10}$$

We can make a conformal transformation of the AdS metric (3.10) to that of the ESU (3.9),

$$g^{\text{AdS}}_{\mu\nu} = \Omega^2\, g^{\text{ESU}}_{\mu\nu}, \quad \Omega = \sec\rho. \tag{3.11}$$

As we can see from Figure 3.3, this spacetime can be thought of, in four dimensions, as a cylinder with no boundary, embedded in a five-dimensional Minkowski space. This eases the imposition of boundary conditions at the AdS boundary, because we have now made it part of the spacetime.

3.1.1 Poincaré patch

For our purposes, we will not work with the entire $CAdS_{d+1}$ spacetime. Instead, we focus on the Poincaré patch ($PAdS_{d+1}$), defined by selecting an appropriate coordinate

system [20]:

$$X^0 = \frac{1}{2z}\left(z^2 + L^2 + \bar{x}^2 - t^2\right), \tag{3.12}$$

$$X^i = \frac{Lx^i}{z}, \quad i = 1, 2, \ldots, (d-1), \tag{3.13}$$

$$X^d = \frac{1}{2z}\left(z^2 - L^2 + \bar{x}^2 - t^2\right), \tag{3.14}$$

$$X^{d+1} = \frac{Lt}{z}. \tag{3.15}$$

where $t, x^i \in \mathbb{R}$, $z \in (0, \infty)$, and

$$\bar{x}^2 = \sum_{i=1}^{d-1} (x^i)^2, \tag{3.16}$$

and z acts as the radial coordinate, given by

$$\frac{1}{z} = \frac{X^0 - X^d}{L^2}. \tag{3.17}$$

The Poincaré patch metric now takes the form

$$ds^2 = \frac{L^2}{z^2}\left(-dt^2 + d\bar{x}^2 + dz^2\right). \tag{3.18}$$

Thus, PAdS_{d+1} in Figure 3.4 is conformal to the upper half-plane:

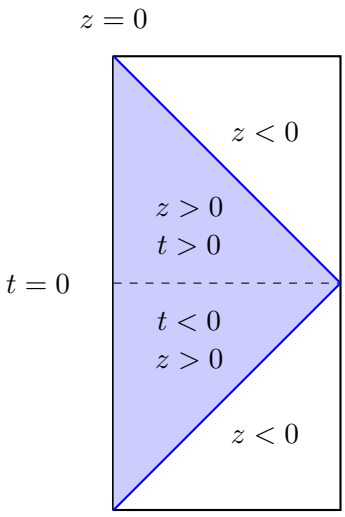

Figure 3.4: Penrose diagram for the Poincaré patch shown in blue, denoted by $z > 0$ (adapted from [106]).

$$H^{d+1} = \{(t, x_1, \ldots, x_{d-1}, z) \in \mathbb{R}^{d+1} \mid z > 0\}, \tag{3.19}$$

endowed with the Minkowski metric. The conformal factor is $\Omega = \frac{z}{L}$, i.e., $\Omega^2 g = \eta$. In this way, the Poincaré patch is identified with the Minkowski metric through a conformal transformation. This greatly simplifies the analysis of conformal fields on the curved

spacetime, as it allows the use of two-point functions in Minkowski space for calculations, taking into account the transition between metrics via the conformal factor. The radial coordinate z effectively divides CAdS spacetime into two regions, $z > 0$ and $z < 0$. Each of these regions represents half of the CAdS spacetime, with the Poincaré patch typically given by $z > 0$, see Figure 3.4. The plane $z = 0$ is a timelike boundary, which is not part of the PAdS spacetime, as evident from Equation (3.18). QFTCS formulated on PAdS still requires boundary conditions to be specified at the timelike boundary $z = 0$, which will be the topic of the next section.

3.2 Boundary conditions

As we mentioned in the previous section, CAdS spacetime can be naively thought of as placing the universe in a box. The "box" idea comes from the fact that the spacetime possesses a boundary at infinity, making it non-globally hyperbolic as explained in the previous section. One of the fundamental assumptions in quantum field theory in curved spacetime is that the underlying background is globally hyperbolic, see Definition 1.2.2. This condition on the spacetime geometry ensures that, for a wave equation such as the Klein-Gordon equation, the associated Cauchy problem is well-posed, with a unique solution existing once suitable Cauchy initial data are specified. However, in the case of CAdS spacetime, this issue can be addressed by prescribing appropriate boundary conditions [72, 73, 146]. The choice of boundary conditions is closely related to the differential equation under consideration. Since our primary focus is on the scalar field, for convenience, we recall the Klein-Gordon equation in curved spacetime:

$$\left(\Box - \mu^2 - \xi R\right) \Phi = 0, \tag{3.20}$$

where the implementation of boundary conditions depends on the type of differential equation, and hence on the type of field that we are studying. Notably, the d'Alembertian operator $\Box$ is metric-dependent, so if we were considering something other than asymptotically AdS spacetimes, we would also see a difference in the construction of this differential operator. However, this will not be the case, as we focus on asymptotically AdS spacetimes in this thesis.

For conformal fields, boundary conditions on AdS are broadly classified into two categories: transparent and reflective. With transparent boundary conditions, scalar field modes can freely pass through the CAdS boundary. For these boundary conditions to be properly defined, we need to embed the CAdS spacetime in the ESU, enabling the field modes to traverse the boundary and reappear on the opposite side within the ESU. This can be seen in Figure 3.5, where the left-hand image illustrates the embedding of spacetime in the ESU and the behaviour of scalar field modes under transparent boundary conditions. These boundary conditions were utilised in [92]. On the other hand, reflective boundary

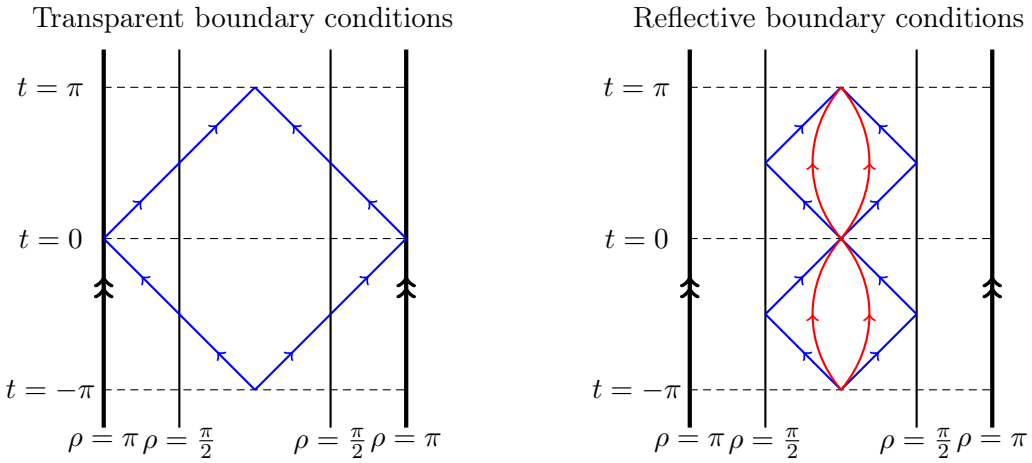

Figure 3.5: Representation of boundary conditions for a classical field on AdS. The diagrams show the ESU from Figure 3.3, with the cylinder opened up. The vertical lines marked with double arrows indicate where we cut, and once identified, they restore the cylinder. AdS spacetime lies between the interior vertical lines. The blue diagonal lines denote null geodesics (on the ESU in the left-hand figure and on AdS in the right-hand figure), while the red curved lines in the right-hand figure represent timelike geodesics (adapted from [10, 106]).

conditions correspond to Dirichlet, Neumann, and Robin (mixed) conditions, as shown in the right-hand image of Figure 3.5. In this case, the Dirichlet boundary condition imposes that the field modes vanish at the spacetime boundary,

$$\Phi = 0. \tag{3.21}$$

Neumann boundary condition, that the normal derivative of the field vanishes at the spacetime boundary,

$$\frac{\partial \Phi}{\partial \rho} = 0. \tag{3.22}$$

While Robin (mixed) boundary condition is a linear combination of Dirichlet and Neumann conditions, parameterised by the Robin parameter ζ, [73, 106],

$$\Phi \cos\zeta + \frac{\partial \Phi}{\partial \rho} \sin\zeta = 0, \quad \zeta \in [0, \pi]. \tag{3.23}$$

From the general Robin condition, it is evident that for $\zeta = 0$, the Dirichlet condition is recovered,

$$\Phi = 0, \tag{3.24}$$

and for $\zeta = \frac{\pi}{2}$, the Neumann condition is recovered,

$$\frac{\partial \Phi}{\partial \rho} = 0. \tag{3.25}$$

Furthermore, Dirichlet and Neumann boundary conditions are maximally symmetric, meaning they do not break the symmetry of the spacetime when imposed. Hence, in

pure AdS, which lacks a singularity, its maximal symmetry allows many quantities relevant to quantum field theory (QFT) to be derived in closed form when these boundary conditions are imposed.

This freedom in choosing the type of boundary condition to be imposed on an AdS background gives rise to a wide range of possible scenarios that can be studied. This could be an interesting branch of research, where one can investigate whether changing the boundary conditions modifies the final physical results of the evaluation of observables such as the SET. The possibility of changing boundary conditions is useful also for studies of the AdS/CFT correspondence. In fact, changing boundary conditions corresponds to new theories in the "bulk". We have only introduced a few possibilities for boundary conditions; the type of boundary condition also depends on the type of field that we are studying. For more general boundary conditions, see [34–38, 40, 59]. The analysis that we have presented focused mainly on the pure AdS spacetime without considering a singularity. The same approach and analysis can be applied to black hole spacetimes that are asymptotically AdS. In fact, the same boundary conditions can be imposed, depending only on the nature of the differential equation we are considering (in this case, the Klein–Gordon equation). We will now introduce some AdS black hole spacetimes.

3.3 Anti-de-Sitter black holes

Black holes in AdS spacetime have been extensively studied in the literature. In this thesis, we will present a study of the five-dimensional Kerr–AdS black hole in Part II. However, the BTZ black hole in three dimensions, as well as the Schwarzschild–AdS and Kerr–AdS black holes in four dimensions, have also been investigated in the literature [27, 67, 68], and we will provide a brief review of them in Sections 3.3.1, 3.3.2 and 3.3.3. Several advantages arise when working with AdS black holes.

Firstly, AdS black holes exhibit a unique thermal behaviour due to the presence of a boundary. Unlike their asymptotically flat counterparts, AdS black holes can reach thermal equilibrium with their surrounding radiation [67]. This leads to the existence of stable AdS black holes, whereas asymptotically flat black holes are generally unstable. In this thesis, we will be particularly interested in Hartle–Hawking states, which describe quantum fields in thermal equilibrium with a black hole. These states are well-suited for studying the thermodynamic properties of AdS black holes and their associated quantum field behaviour.

Secondly, the relevance of AdS black holes stems from the AdS/CFT correspondence [93], which hypothesizes a duality between gravity in asymptotically AdS spacetime and a con-

formal field theory (CFT) on its boundary. Hence, studying AdS black holes provides an opportunity to explore this duality, enabling researchers to probe aspects of quantum gravity and strongly coupled field theories [151].

Finally, AdS black holes are particularly useful in quantum studies, as they provide a simplified framework that facilitates analysis. For instance, the superradiant effect, which complicates the study of modes in asymptotically flat rotating black hole spacetimes, does not occur due to the presence of the boundary. We will see this more in detail in Part II.

In this thesis, we will explore various aspects of AdS black holes, providing a brief review of Schwarzschild-AdS, Kerr-AdS, and the BTZ black hole.

3.3.1 Schwarzschild-AdS

We will now introduce the Schwarzschild-AdS black hole, which is a static black hole in four dimensions, to highlight the differences between this case and the asymptotically flat Schwarzschild black hole metric introduced in Section 1.3. The Schwarzschild-AdS black hole is a solution of the Einstein field equations (1.40) when Λ is negative. This generates solutions that are asymptotically AdS.

The metric for the static Schwarzschild-AdS black hole can be written using Schwarzschild coordinates (t, r, θ, ϕ) and a signature $(-,+,+,+)$:

$$ds^2 = -\left(1 - \frac{2M}{r} + \frac{r^2}{L^2}\right) dt^2 + \left(1 - \frac{2M}{r} + \frac{r^2}{L^2}\right)^{-1} dr^2 + r^2 d\theta^2 + r^2 \sin^2\theta \, d\phi^2, \quad (3.26)$$

where M is the mass of the black hole, and L is the AdS radius, related to the cosmological constant Λ by $L^2 = -\frac{3}{\Lambda}$. The event horizon can still be determined through the Schwarzschild radius r_s, modified for the AdS case. This can be found by putting the coefficient of dt^2 in the metric equal to zero, and we find:

$$1 - \frac{2M}{r_s} + \frac{r_s^2}{L^2} = 0. \quad (3.27)$$

This can be rearranged into a cubic equation of the form:

$$r_s^3 - 2ML^2 + r_s L^2 = 0. \quad (3.28)$$

The nature of the solutions can be analysed using the discriminant Δ. Depending on the value of Δ, we have the following cases:

- When $\Delta > 0$, the cubic equation has three distinct real roots.
- When $\Delta < 0$, the equation has one real root and two complex conjugate roots.

- When $\Delta = 0$, the equation has at least two coincident roots, resulting in a multiple root.

The discriminant for a cubic polynomial $ax^3 + bx^2 + cx + d = 0$ is

$$\Delta = 18abcd - 4b^3d + b^2c^2 - 4ac^3 - 27a^2d^2, \tag{3.29}$$

in this case, Δ is:

$$\Delta = -4L^6 - 108L^4M^2, \tag{3.30}$$

which is negative for all L and M in $\mathbb{R}$. This means that we have only one real root, which corresponds to the value of the event horizon of this black hole. The real root of Δ is usually evaluated numerically. We can still introduce the coordinates for the Schwarzschild-AdS case, u and v, also introducing r_* as the tortoise coordinate for the AdS case, for which the explicit evaluation depends on the event horizon radius. The Kruskal coordinates (U, V) can then be defined, where we use the surface gravity of the Schwarzschild-AdS black hole. This coordinate transformation regularises the metric, showing once again that the only physical singularity is at $r \to 0$. Hence, the AdS case retains the essential features of the flat case, but the asymptotic behaviour of the spacetime is determined by the negative cosmological constant. Once defined the Kruskal coordinates as in the asymptotically flat case we show the Penrose diagram for this spacetime, see Figure 3.6.

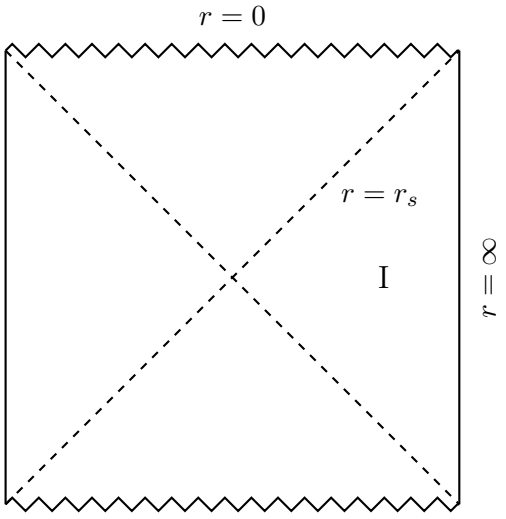

Figure 3.6: Penrose diagram for the maximal analytic extension of the Schwarzschild AdS black hole.

Another important difference is the one of thermodynamic stability which changes between the asymptotically flat and AdS case, see [67] for more detail. We will introduce the concept of quantum states on this background in Section 3.4.

3.3.2 Kerr-AdS

We will now introduce the corresponding rotating AdS black hole as in Section 1.3. The Kerr-AdS black hole is a stationary black hole, having mass M and angular momentum J. The Kerr-AdS black hole in four dimensions is a rotating black hole solution, whose line element, with coordinates (t, r, θ, ϕ) and signature $(-,+,+,+)$, is:

$$ds^2 = -\frac{\Delta_r}{\rho^2}\left(dt - \frac{a\sin^2\theta}{\Xi}d\phi\right)^2 + \frac{\rho^2}{\Delta_r}dr^2 + \frac{\rho^2}{\Delta_\theta}d\theta^2 + \frac{\Delta_\theta \sin^2\theta}{\rho^2}\left(a\, dt - \frac{r^2+a^2}{\Xi}d\phi\right)^2, \quad (3.31)$$

where

$$\Delta_r = \left(r^2+a^2\right)\left(1+\frac{r^2}{L^2}\right) - 2Mr, \quad (3.32)$$

$$\Delta_\theta = 1 - \frac{a^2}{L^2}\cos^2\theta, \quad (3.33)$$

$$\rho^2 = r^2 + a^2\cos^2\theta, \quad (3.34)$$

$$\Xi = 1 - \frac{a^2}{L^2}. \quad (3.35)$$

Here, $a = J/M$ represents the rotation parameter, L is the AdS radius related to the cosmological constant Λ by $L^2 = -3/\Lambda$, and Ξ accounts for the asymptotically AdS nature of the spacetime. The Kerr-AdS black hole in higher dimensions generalises to what is known as the Myers-Perry-AdS metric [105], where the metric solution includes multiple independent rotation parameters corresponding to each plane of rotation [61, 62]. We will now introduce the corresponding characteristic surfaces for the Kerr-AdS black hole, similar to those introduced for the asymptotically flat case in Section 1.3. For the Kerr-AdS metric, the position of the event horizon, defined as one of the roots of $\Delta_r = 0$, is no longer as straightforward as in the Kerr solution in flat spacetime. It requires the analysis of the discriminant of Δ_r to understand the nature of the solutions. The radii of the event horizon will depend not only on M and a, but also on L in a non-trivial way.

In addition, we can generalise the stationary limit surface to the AdS case. This surface retains its definition as the limit surface inside which an observer cannot remain at rest relative to infinity. In this case, the parameter L will also appear in the expression for the stationary limit surface. The ergosphere still exists in the Kerr-AdS case, and it is delimited by the stationary limit surface.

Lastly, the third characteristic surface, the light surface, is defined as the surface where the angular velocity of an observer co-rotating with the black hole matches the speed of light. The presence or absence of this surface in Kerr-AdS black holes significantly affects the analysis. This will be discussed extensively in Chapter 4, particularly in the context

of higher-dimensional Kerr-AdS spacetimes. We will see a direct example of these surfaces and how to analyse them for an AdS black hole in Chapter 4.

3.3.3 BTZ black hole

In this subsection, we present another important case of the AdS black hole scenario, the BTZ black hole [16, 17]. It is named after the authors who first analysed this black hole: Bañados, Teitelboim, and Zanelli. The BTZ black hole is a topological black hole in three dimensions that is asymptotically AdS and rotating. In this case, a topological black hole refers to a geometric construction obtained by identifying points in CAdS spacetime. This identification creates a situation in which we can define an event horizon that causally separates the rest of the spacetime. Since it is generated from CAdS, this is an asymptotically AdS black hole which, in its most general form, is also rotating. The resulting metric is a solution to the Einstein field equations and can be studied in the same way as the previous examples.

We will not provide an extensive analysis of this black hole in this thesis, even though it serves perfectly as a toy model to study new approaches and theories. We will present the line element and give some intuition on why it is an interesting case of study, even if it is a black hole in three dimensions, and how we can exploit this to our advantage.

The line element of the black hole is:

$$ds^2 = \left(M - \frac{r^2}{L^2}\right) dt^2 - J\ dt\ d\theta + \left(\frac{r^2}{L^2} - M + \frac{J^2}{4r^2}\right)^{-1} dr^2 + r^2 d\theta^2, \tag{3.36}$$

where (t, r, θ) is the coordinate system, with $-\infty < t < +\infty$, $0 < r < \infty$, and $0 \leq \theta < 2\pi$. M and J are, respectively, the mass and the angular momentum in these spacetimes. We will mainly follow the results shown in [92].

We will introduce, as in the other cases, the characteristic surfaces of this background, starting with the event horizon, at r_+. This spacetime also has an inner horizon at r_-. We define both as:

$$r_\pm = \frac{L|\alpha_\pm|}{2}, \quad \alpha_\pm = \sqrt{M + \frac{J}{L}} \pm \sqrt{M - \frac{J}{L}}, \tag{3.37}$$

where M and J can be written as

$$M = \frac{\alpha_+^2 + \alpha_-^2}{4} > 0, \quad J = \frac{L\ \alpha_+ \alpha_-}{2}, \tag{3.38}$$

with $\alpha_+ > 0$, $\alpha_+ \geq \alpha_-$, and

$$\alpha_+^2 - \alpha_-^2 = 4\sqrt{M^2 - \frac{J^2}{L^2}}. \tag{3.39}$$

This is the general solution for the rotating case of a BTZ black hole. The static black hole is obtained simply by setting $J = 0$, where $\alpha_+ = 2\sqrt{M} > 0$, $\alpha_- = 0$, and there is no inner horizon.

We can also define the stationary limit surface r_s. This is a Killing horizon, which is a null hypersurface where the norm of a Killing vector field vanishes. Looking at the component g_{tt} of Equation (3.36), we find that when it vanishes, we can define:

$$r_s = M^{1/2} L, \tag{3.40}$$

and the region between r_+ and r_s is called the ergosphere. Hence, Equation (3.40) defines a Killing horizon for the Killing vector ∂_t. We then have that ∂_t is timelike for $r > r_s$, lightlike at $r = r_s$, spacelike for $r_+ < r < r_s$, and no static observer can exist for $r < r_s$. Furthermore, we can define a Killing vector ξ as

$$\xi = \partial_t + \Omega_h \, \partial_\theta, \tag{3.41}$$

where Ω_h is the angular velocity of the event horizon, defined as

$$\Omega_h = \frac{J}{2r_+^2}. \tag{3.42}$$

The Killing vector in Equation (3.41) is the generator of the event horizon $r = r_+$. In addition, ξ is timelike everywhere outside the event horizon, which is what we need for the QFTCS analysis. Also, there is no speed-of-light surface as in the slowly rotating Kerr-AdS case.

This setup looks quite similar to the one we will encounter in Part II, where we study a Kerr-AdS five-dimensional black hole. However, in this case, the lower dimensionality makes every calculation significantly easier, allowing almost everything to be evaluated explicitly without resorting to numerical analysis. We report a few of the useful literature on this black hole which shows the multitude of possible avenues of research of this background [31, 33, 36, 39, 46, 84, 90, 92, 94–96, 133].

3.4 Quantum states on black holes and anti-de-Sitter black holes

We will now use the definition of quantum states given in Section 2.4, specifically looking at its application to black hole spacetimes. To define a quantum state, we need to quantise the field under consideration. As we mentioned before we will consider a scalar field. Following the framework of quantum field theory in curved spacetime, see Chapter 2, there are different ways to accomplish this.

One approach is known as the algebraic approach. This method utilises algebraic principles to construct an algebra that encapsulates all the information about the field and the spacetime under study. Quantum states are then defined as linear functionals on this algebra. The second approach is the more conventional method of canonical quantisation. In this method, the field is decomposed into sets of positive- and negative-frequency modes. The process involves constructing annihilation and creation operators: upon quantisation, positive-frequency modes are associated with annihilation operators, while negative-frequency modes are associated with creation operators. The ground state is then defined as the state for which the annihilation operator, constructed in this manner, acts to yield zero. These are the two primary methods of quantisation, we will explore the canonical quantisation in Part II.

For our purposes, we will consider the canonical quantisation procedure to define the following quantum states in this section. In Minkowski spacetime, which is a flat spacetime, it is possible to define a unique global vacuum state. However, in QFTCS, this is usually not the case. In fact, there is no preferred way to decompose the scalar field into positive- and negative-frequency modes. This arises from the fact that, in curved spacetimes, a unique vacuum state does not exist due to the lack of invariance under the Poincaré group. This translates into the fact that we can decompose the scalar field modes into positive and negative frequency modes with respect to different choices of time coordinate systems, allowing the definition of different vacuum states with different physical interpretations. We will now briefly review the possible ground states that can be defined on black hole spacetimes. In particular, we will first focus on the Schwarzschild black hole case for a scalar field and then explain the differences for a Schwarzschild-AdS black hole.

One major difference that will be common throughout the analysis and the construction of the quantum states can be seen by studying the Penrose diagrams of the Schwarzschild black hole spacetime, as shown in Figure 3.7 (which is reported from Section 1.3 for convenience), and the Penrose diagram for the Schwarzschild-AdS black hole, shown in Figure 3.6.

In an asymptotically flat Schwarzschild black hole spacetime, we have two sets of modes that we need to study in order to construct quantum states [143]. These are called the "in" and "up" modes, as shown in Figure 3.8. The "in" modes originate from past null infinity $\mathcal{I}^-$, while the "up" modes originate from the past horizon $\mathcal{H}^-$. The "in" and "up" modes form an orthonormal basis of the field modes, which can be used to decompose the scalar field and proceed with the canonical quantization procedure.

In the asymptotically Schwarzschild-AdS black hole spacetime, this scenario does not oc-

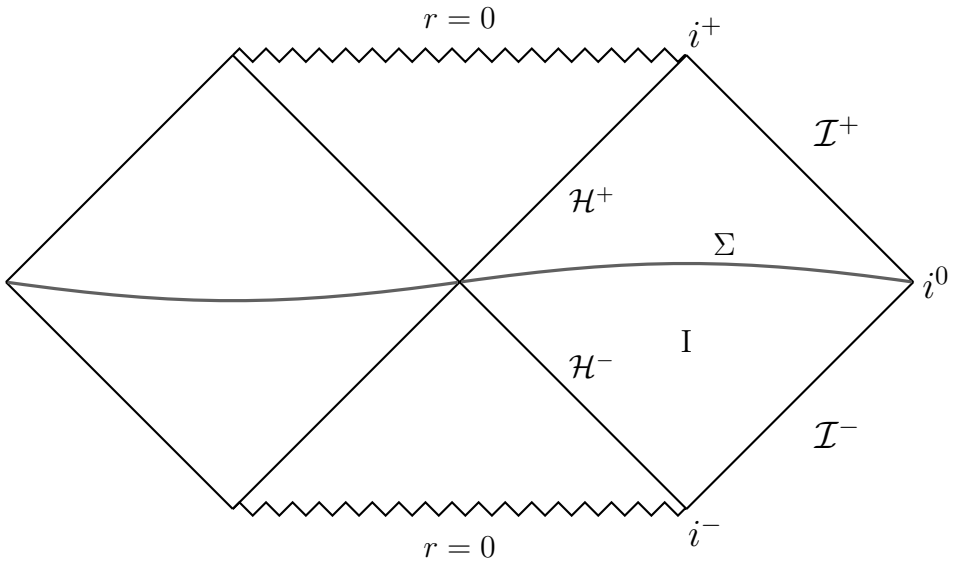

Figure 3.7: Penrose diagram for the maximal analytic extension of the Schwarzschild black hole.

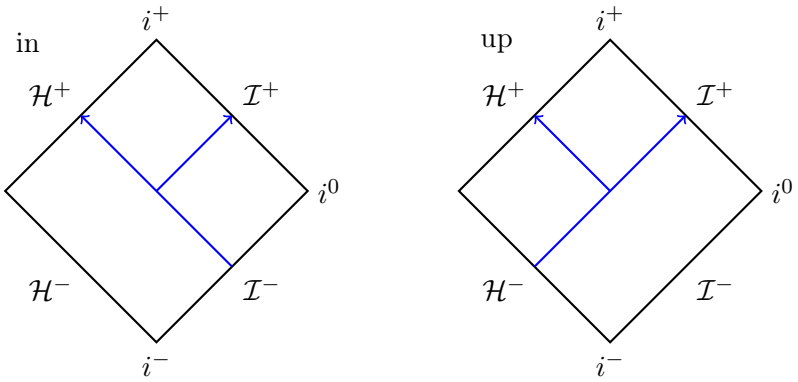

Figure 3.8: In/up modes (blue lines) depicted in Region I of the Schwarzschild black hole (adapted from [143]).

cur. In fact, the presence of the spacetime boundary at $r = \infty$ makes it that we only have one set of modes, as shown in Figure 3.9, when we impose reflective boundary conditions. This will simplify the construction of the quantum states as we will see more in detail in Part II.

In Schwarzschild spacetime, three primary quantum states have been defined: the Boulware state, $|B\rangle$ [23], the Unruh state, $|U\rangle$ [140,141], and the Hartle-Hawking state, $|H\rangle$ [64]. Each of these states is associated with a distinct choice of time coordinate, which is used to decompose the scalar field into positive and negative frequency modes. It will be possible to define the Boulware and Hartle-Hawking states also for the spacetimes that we will study in more detail in this thesis. We will now discuss each of these states, highlighting

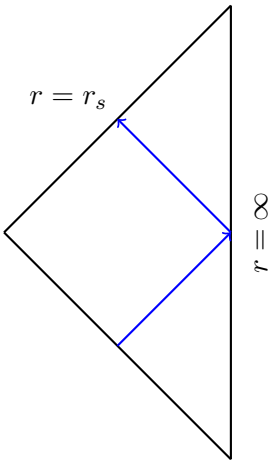

Figure 3.9: Penrose diagram of Region I in the Schwarzschild-AdS black hole with reflective boundary conditions, showing one set of modes (blue line).

the physical significance of the corresponding choice of time coordinate.

3.4.1 Boulware state

The Boulware state, $|B\rangle$ [23], is the ground state defined with respect to the Schwarzschild coordinate t. This has the physical interpretation of being as empty as possible for a static observer far from the black hole. This means that at both past $\mathcal{I}^-$ and future $\mathcal{I}^+$ null infinities in Figure 3.7, the state appears vacuum. In terms of the scalar field modes, this corresponds to an absence of particles.

The choice of time coordinate is motivated by the fact that the Schwarzschild spacetime is asymptotically flat. This means that as $r \to \infty$, the spacetime approaches Minkowski spacetime. At infinity, we can choose the time coordinate to be the Schwarzschild coordinate t. Consequently, we can define positive- and negative-frequency modes following the standard quantum field theory prescription in flat spacetime, utilizing the "in" and "up" modes as an orthonormal basis for the construction, see Figure 3.8. Another important aspect is that the Boulware state respects the underlying symmetries of the Schwarzschild spacetime. However, this state diverges on the event horizon [29].

The Boulware state can also be defined in asymptotically AdS black holes. A more detailed description of the canonical quantisation procedure will be provided for the five dimensional Kerr-AdS black hole in Part II. For now, this section offers only a brief review of the physical meaning of this quantum state.

3.4.2 Hartle-Hawking state

The Hartle–Hawking state $|H\rangle$ [64] is the thermal ground state, defined with respect to the Kruskal coordinates U and V. This choice is motivated by the fact that the Kruskal coordinate U serves as the affine parameter along the null generators of the past horizon $\mathcal{H}^-$, where an outgoing flux of Hawking radiation is observed. Similarly, the Kruskal coordinate V is the affine parameter along the null generators of the future horizon $\mathcal{H}^+$, where an incoming flux of Hawking radiation is present. For this reason, the Kruskal coordinates provide a natural choice for defining positive- and negative-frequency modes. Physically, this state corresponds to a scenario in which Hawking radiation is incoming from past null infinity $\mathcal{I}^-$ and outgoing at future null infinity $\mathcal{I}^+$, in Figure 3.7. This results in a thermal flux of particles at both past and future null infinity.

Another interpretation of the Hartle–Hawking state $|H\rangle$ is that of a black hole in an unstable thermal equilibrium with a heat bath at the Hawking temperature [76]. This ground state is regular on both the past and future horizons, $\mathcal{H}^{\pm}$.

The Hartle-Hawking state cannot be defined for a quantum scalar field in the Kerr black hole background [78]. Specifically, there is no quantum state that describes a Kerr black hole in thermal equilibrium with the spacetime at the Hawking temperature. This restriction can be intuitively understood by considering the simplified example of a rotating thermal state in Minkowski spacetime. In Minkowski spacetime, a rigidly rotating thermal state for a quantum scalar field does not exist [44]. However, we can define such a state if the Minkowski spacetime is confined within an infinite cylinder, symmetric around the axis of rotation, with a sufficiently small radius to avoid the formation of a speed-of-light surface [9]. We introduced the concept of the speed-of-light surface in Chapter 1 when discussing the Kerr metric. Similarly, if a Kerr black hole is enclosed by a perfectly reflecting mirror, such as in the case of a Kerr-AdS black hole, a Hartle-Hawking state can be defined for a quantum scalar field [51].

To summarise, this quantum state can be defined for the Schwarzschild-AdS black hole. While it does not exist for the Kerr black hole, it does for the Kerr-AdS black hole when specific condition are met. We will see its construction in more detail when studying the case of the Kerr–AdS five-dimensional black hole in Part II, where we will determine these specific conditions. An unfortunate side effect of introducing a reflecting boundary to construct such rotating thermal states is the emergence of Casimir divergences at the boundary [29, 50]. These divergences however are absent on asymptotically AdS black holes. Specifically, as we will see, in the Kerr-AdS case in five dimensions, these effects do not occur.

3.4.3 Unruh state

The Unruh state, $|U\rangle$, is the ground state defined with respect to both the Schwarzschild time t and the Kruskal coordinate U. This is because the Unruh state exhibits characteristics of both the Boulware and Hartle–Hawking states. It is a ground state that is as empty as possible at past null infinity, $\mathcal{I}^-$, like the Boulware state, while having a thermal flux of Hawking radiation at future null infinity, $\mathcal{I}^+$, similar to the Hartle–Hawking state. In terms of the scalar field modes, this state can be interpreted as an absence of particles in the in-modes at past null infinity and a thermalised flux of particles in the up-modes at future null infinity. Hence, we use the Schwarzschild time coordinate t to decompose the scalar field into positive- and negative-frequency modes for the in-modes at past null infinity $\mathcal{I}^-$, as done for the Boulware case. Meanwhile, for the up-modes which exhibit an outgoing Hawking radiation at future null infinity $\mathcal{I}^+$, we employ the Kruskal coordinate U, which serves as an affine parameter along the null generators of the past horizon $\mathcal{H}^-$, to decompose the field into positive- and negative-frequency modes. The Unruh state $|U\rangle$ is regular on the future horizon $\mathcal{H}^+$ but diverges on the past horizon $\mathcal{H}^-$. This state is often interpreted as describing a black hole formed by gravitational collapse.

For this reason, it would seem that the Unruh state is a suitable quantum state to study black holes and Hawking radiation. The construction of the Unruh state on a Kerr black hole spacetime is well-established [140, 141], and it is also possible to compute the expectation value of the renormalized stress-energy tensor [111]. However, the Unruh state does not preserve all the symmetries of the underlying spacetime, specifically, it lacks symmetry under the simultaneous inversion of the time and azimuthal angular coordinates. The literature usually prefers the use of the Hartle-Hawking state [11, 12, 69, 70, 137]. This is mainly because the Hartle-Hawking state is a thermal state in equilibrium that is also regular across both the future and past event horizons, and it respects the symmetries of the underlying black hole geometry. In addition, the Unruh state cannot be defined for asymptotically AdS black hole spacetimes. This arises from the fact that we cannot treat the "in" and "up" modes differently in the asymptotically AdS case, as we only have one set of modes, as shown in Figure 3.9, when we impose reflective boundary conditions. Therefore, the Unruh state will not be addressed in this thesis. For further details, we refer to [111, 141].

Summary

In this chapter, we have introduced the final main concepts needed before delving into the research parts of the thesis. We have explained what Anti-de Sitter spacetime is, with particular focus on the presence of a boundary, for which we have introduced some of the possible boundary conditions that can be imposed to solve the Klein-Gordon equation. We then introduced the main focus of the thesis: AdS black holes, providing a brief summary

of known cases.

Finally, we have given a physical interpretation of the quantum states that can be constructed over a black hole spacetime. These are the Boulware, the Hartle–Hawking, and the Unruh states. Specifically, we focus more on the Hartle–Hawking state since it is the preferred state for QFTCS analysis, due to its regularity across the event horizon when studying black holes, and because its symmetry properties make computations and numerical evaluations easier. This is particularly true for Euclideanized black holes, for which the evaluation of renormalized expectation values using the Hartle–Hawking state is simpler. However, in this thesis we will take advantage of the Hadamard properties and the fact that both the Boulware and the Hartle–Hawking state are Hadamard states; hence, we will not perform renormalization, because we will consider differences in the expectation values of observables in these two quantum states, more detail will be given in Part II.

Part II

Kerr-AdS, (4 + 1)-dimensional black hole

Introduction

'This project has completely confiscated my life, darling. Consumed me as only hero work can. My best work, I must admit. Simple, elegant, yet bold.'

- Edna, from "The Incredibles".

'Questo progetto mi ha completamente confiscato la vita, tesoro. Mi ha consumato come solo un lavoro da eroe riesce a fare. È il mio capolavoro, lo ammetto: semplice, elegante eppure importante.'

We now begin the description of the main protagonist of this thesis, and of my PhD, the Kerr-AdS 5D black hole spacetime. In Chapter 4 we introduce the geometry of this black hole, and then we start building a QFT on this curved spacetime, following the approach introduced in Chapters 1, 2, and 3. We do this by analysing a scalar field in Chapter 6. Before that, we provide a description of the spin-weighted spherical harmonics functions in Chapter 5, which will be propedeutical for the analysis later on. We then construct quantum states on this background in Chapter 7. Finally, we evaluate the two main observables of interest, the stress-energy tensor and the vacuum polarisation, presenting the numerical analysis and results in Chapter 8.

During Part II we will use an unconventional coordinate system array, permitted by GR theory, namely $(r, \theta, \phi, \psi, t)$ instead of the usual $(t, r, \theta, \phi, \psi)$ as typically utilised in the literature. This choice originates from my initial calculation of this metric at the start of my PhD, where I displayed all the spatial coordinates first and then the time coordinate. Although I did not expect this to be a significant choice at the time, it has stuck with me throughout my PhD. Hence, the space-time signature will be $(+,+,+,+,-)$ throughout Part II and we use units in which $8\pi G = c = \hbar = k_B = 1$.

This will be a comprehensive journey spanning three and a half years of my life, so buckle up, dear reader, there is much to discover. The first question that comes to mind is: why should someone study this black hole, in five dimensions and in AdS? This question inspired the titles of many of my talks and was a genuine puzzle at the start of my PhD.

I will try to show you why it is indeed interesting to study this black hole.

One of the main reasons for choosing this black hole is that, regardless of appearances, studying a quantum scalar field over this background is easier than on a rotating black hole in four dimensions. One of the many reasons why it is easier is that, thanks to the additional dimensions, we can introduce an enhanced symmetry in the metric, as we shall see in Chapter 4. Together with many other reasons that will be highlighted throughout the whole Part II.

Furthermore, an intuitive picture of why one might be "dragged" to study this black hole is provided by the light surface. We briefly introduced this characteristic surface in Part I, and it will be discussed in depth in Chapter 4. In order to grasp this "intuitive" picture, we have to dip our toes into the ocean of concepts that we will need to explore to fully understand this topic. Hence, if this is not clear, I promise it will be by the end of the thesis. We are interested in whether the light surface r_j exists, where, by abuse of notation, we use the same symbol to denote both the surface itself and its radial coordinate. This is because if this surface does not exist, we can define a time-like Killing vector field (see Equation (1.24)) that remains time-like everywhere outside the event horizon of the black hole under consideration, which means that we can properly define a QFT on this background.

Furthermore, we will mainly focus on the Hartle–Hawking state introduced in Section 3.4 and will be discussed more in detail in Section 7.3. The Hartle-Hawking state is a particular type of state in thermal equilibrium. From what we know thus far, the presence of r_j seems to have a significant impact on the existence of this state. Let us now consider a table of different black holes:

Black Holes	r_j	**Hartle–Hawking State**
BTZ	X	✓
Kerr-4D	✓	X
Kerr-4D-AdS	X (in some limit of L)	✓ (in some limit of L)
Kerr-5D-AdS	?	?

Thus, considering the special cases for the Kerr-4D-AdS black hole, we can see that the presence of the light surface is related to the existence of the Hartle–Hawking state. There is a theorem in four dimensions [60] which proves the existence of the Hartle–Hawking state on a stationary black hole spacetime if there is a globally timelike Killing vector and no speed-of-light surface. We would like to understand if this result holds in Kerr–5D–AdS. We will investigate whether r_j exists and, if so, in which limit of L it disappears, or if it

exists for every value of L. If r_j does not exist, then we will examine whether it is possible to construct the Hartle–Hawking state for that black hole. Hence, not only can we properly define a QFT over this background in the absence of r_j, but we can also specify the quantum state of interest, namely the Hartle-Hawking state. Spoiler alert: we will discover that in some regime the light surface does not exist, enabling us to construct the Hartle–Hawking state and carry out the remainder of the QFTCS analysis, which would have been impossible otherwise. The reader may have already noticed that there are more than ten pages left to read, which means that we have indeed managed to achieve something.

Hence, without further ado, let us begin our journey into the Kerr-AdS 5D black hole world by introducing its metric in three possible ways.

Chapter 4

The geometry of the spacetime

In this chapter, we introduce three possible coordinate choices for the 5D-Kerr-AdS black hole metric, namely the general metric of the 5D Kerr-AdS black hole (4.1), given in [58,109,125], the enhanced symmetry metric (4.6), given in [43], and the asymptotically flat metric (4.15), given in [57].

In the first section, we will introduce these three metrics and outline their differences. We will also show the coordinate transformations between them for later comparisons within the thesis. Furthermore, we present the Killing vectors (4.19), and symmetries associated with the metric (4.6), which is the one that we study throughout this thesis. Notably, we highlight the importance of ι (4.36), which acts as the null generator of the event horizon and can be also used to derive the expression for the light surface (4.44).

In the second section, we evaluate the three characteristic radii of the black hole: the event horizon, the light surface, and the stationary limit surface. We explore how they qualitatively change with variations in the rotational parameter of the black hole. In particular, we will focus our attention on the identification of a regime where the light surface ceases to exist. This leads us to define ι as a time-like Killing vector (see Equation (1.24) for the definition of a time-like Killing vector) everywhere in the spacetime outside the event horizon, providing a definition of time and also laying the foundations for later calculations on the scalar field. Additionally, we offer insights into some of the geometrical and thermodynamic properties of the black hole, including the evaluation of the Kretschmann scalar, the temperature, and the surface gravity.

4.1 The metric of the 5D-Kerr-AdS black hole

Thanks to the diffeomorphism invariance of general relativity, we can describe the same physical system using different sets of coordinates. Therefore, in this section, we will define three distinct line elements associated with the 5D Kerr-AdS black hole: the general line

element (4.1), as presented in [105, 109, 125], the enhanced symmetry line element (4.6), given in [43], and the asymptotically flat line element (4.15), shown in [57]. We will focus on their properties, in particular on the enhanced symmetry introduced in metric (4.6). Furthermore, we will show how to change between the coordinate systems associated with these line elements, which is going to be useful for later comparisons. Additionally, we will introduce the symmetries and Killing vectors specific to the line element (4.6), which is the one that we are going to study throughout Part II.

4.1.1 General metric of the 5D-Kerr-AdS black hole

The general metric for the 5D Kerr-AdS black hole, with coordinate system $(\varrho, \vartheta, \varphi_1, \varphi_2, t)$ is given in [105, 109, 125],

$$\begin{aligned} ds^2_{\rm NM} = &-\frac{\Delta_\varrho}{\varrho^2_\vartheta}\left(dt - \frac{a_1\sin^2\vartheta}{\Xi_1}d\varphi_1 - \frac{a_2\cos^2\vartheta}{\Xi_2}d\varphi_2\right)^2 + \frac{\varrho^2_\vartheta}{\Delta_\varrho}d\varrho^2 + \frac{\varrho^2_\vartheta}{\Delta_\vartheta}d\vartheta^2 \\ &+ \frac{\Delta_\vartheta\sin^2\vartheta}{\varrho^2_\vartheta}\left(a_1 dt - \frac{\varrho^2+a_1^2}{\Xi_1}d\varphi_1\right)^2 + \frac{\Delta_\vartheta\cos^2\vartheta}{\varrho^2_\vartheta}\left(a_2 dt - \frac{\varrho^2+a_2^2}{\Xi_2}d\varphi_2\right)^2 \\ &+ \frac{1+\varrho^2/L^2}{\varrho^2\varrho^2_\vartheta}\left(a_1a_2 dt - \frac{a_2(\varrho^2+a_1^2)\sin^2\vartheta}{\Xi_1}d\varphi_1 - \frac{a_1(\varrho^2+a_2^2)\cos^2\vartheta}{\Xi_2}d\varphi_2\right)^2, \end{aligned} \tag{4.1}$$

where

$$\begin{aligned} \varrho^2_\vartheta &= \varrho^2 + a_1^2\cos^2\vartheta + a_2^2\sin^2\vartheta, \\ \Delta_\varrho &= \frac{1}{\varrho^2}(\varrho^2+a_1^2)(\varrho^2+a_2^2)(1+\frac{\varrho^2}{L^2}) - 2\widetilde{M}, \\ \Delta_\vartheta &= 1 - \frac{a_1^2}{L^2}\cos^2\vartheta - \frac{a_2^2}{L^2}\sin^2\vartheta, \\ \Xi_{1,2} &= 1 - \frac{a_{1,2}^2}{L^2}, \end{aligned} \tag{4.2}$$

where $\vartheta \in (0, \frac{\pi}{2})$, $\varphi_1 \in (0, 2\pi)$ and $\varphi_2 \in (0, 2\pi)$. The metric in (4.1) is a solution of the vacuum Einstein field equations in five dimensions with a cosmological constant proportional to $-L^{-2}$, namely,

$$R_{\mu\nu} = -4L^{-2}g_{\mu\nu}, \qquad R = -\frac{20}{L^2}, \tag{4.3}$$

and the limit $L \to \infty$ reproduces the asymptotically flat case. Here, $\widetilde{M}$ is the mass of the black hole, a_1 is the rotational parameter associated with the coordinate φ_1, and a_2 is the rotational parameter associated with the coordinate φ_2. We denote this line element by $ds^2_{\rm NM}$, with NM referring specifically to Noda and Motohashi [109]. We want to exploit the fact that we are working in five dimensions and in order to do this we introduce an

enhanced symmetry in the system taking $a_1 = a_2 = a$ in the metric (4.1) which becomes:

$$\begin{aligned} ds^2_{\rm NM} = &- \frac{\Delta_\varrho}{\varrho^2_\vartheta}\left(dt - \frac{a\sin^2\vartheta}{\Delta_\vartheta}d\varphi_1 - \frac{a\cos^2\vartheta}{\Delta_\vartheta}d\varphi_2\right)^2 + \frac{\varrho^2_\vartheta}{\Delta_\varrho}d\varrho^2 + \frac{\varrho^2_\vartheta}{\Delta_\vartheta}d\vartheta^2 \\ &+ \frac{\sin^2\vartheta}{\varrho^2_\vartheta}\left(a\Delta_\vartheta dt - [\varrho^2+a^2]d\varphi_1\right)^2 + \frac{\cos^2\vartheta}{\varrho^2_\vartheta}\left(a\Delta_\vartheta dt - [\varrho^2+a^2]d\varphi_2\right)^2 \\ &+ \frac{1+\varrho^2/L^2}{\varrho^2\varrho^2_\vartheta}\left(a^2dt - \frac{a[\varrho^2+a^2]\sin^2\vartheta}{\Delta_\vartheta}d\varphi_1 - \frac{a[\varrho^2+a^2]\cos^2\vartheta}{\Delta_\vartheta}d\varphi_2\right)^2, \end{aligned} \tag{4.4}$$

where

$$\begin{aligned} &\varrho^2_\vartheta = \varrho^2 + a^2, \\ &\Delta_\varrho = \frac{1}{\varrho^2}(\varrho^2+a^2)^2(1+\frac{\varrho^2}{L^2}) - 2\widetilde{M}, \\ &\Delta_\vartheta = 1 - \frac{a^2}{L^2}, \\ &\Xi_{1,2} = 1 - \frac{a^2}{L^2} = \Delta_\vartheta. \end{aligned} \tag{4.5}$$

4.1.2 Enhanced symmetry metric of the 5D-Kerr-AdS black hole

In addition to the enhanced symmetry introduced in the metric (4.4), we introduce a particular set of coordinates that will aid us in the calculations later on, acting in synergy with the enhanced symmetry. We start our analysis by reporting the line element of the metric of the 5D Kerr-AdS black hole with the set of coordinates $(r, \theta, \phi, \psi, t)$ [43]:

$$\begin{aligned} ds^2 = -f(r)^2dt^2 + g(r)^2dr^2 + \frac{r^2}{4}\left[d\theta^2 + \sin^2\theta\, d\phi^2\right] \\ + h(r)^2\left[d\psi + \frac{1}{2}\cos\theta\, d\phi - \Omega(r)dt\right]^2, \end{aligned} \tag{4.6}$$

where $\theta \in [0, \pi)$, $\phi \in [0, 4\pi)$, $\psi \in [0, 2\pi)$. The metric in (4.6) is a solution of the vacuum Einstein field equations in five dimensions with a cosmological constant proportional to a length scale $-L^{-2}$, and the limit $L \to \infty$ reproduces the asymptotically flat case. We have that the metric functions are

$$\begin{aligned} g(r)^2 &= \left(1 + \frac{r^2}{L^2} - \frac{2M}{r^2} + \frac{2Ma^2}{r^2L^2} + \frac{2Ma^2}{r^4}\right)^{-1}, \\ h(r)^2 &= r^2\left(1 + \frac{2Ma^2}{r^4}\right), \\ \Omega(r) &= \frac{2Ma}{r^2h(r)^2}, \\ f(r) &= \frac{r}{g(r)h(r)}, \end{aligned} \tag{4.7}$$

where M and a stand for the mass and spin parameters, respectively. We take a to be non-negative, without loss of generality. We also display the value of the angular momentum

J of the black hole [43]:

$$J = 2\pi^2 aM. \tag{4.8}$$

We also write the transformation of coordinate with respect to the metric (4.4):

$$\begin{aligned} r &= \sqrt{\frac{(a^2+\varrho^2)}{1-\frac{a^2}{L^2}}} = \sqrt{\frac{\varrho_\vartheta}{\Delta_\vartheta}}, \\ \theta &= 2\vartheta, \\ \phi &= -(\varphi_1 - \varphi_2), \\ \psi &= \frac{a\ t}{L^2} + \frac{\varphi_2+\varphi_1}{2}, \end{aligned} \tag{4.9}$$

and

$$M = \frac{\widetilde{M}}{\Delta_\vartheta^3}. \tag{4.10}$$

Notably t in (4.4) is the same as in (4.6). We report also the matrix form of the metric $g_{\mu\nu}$ (4.6)

$$\begin{pmatrix} g^2(r) & 0 & 0 & 0 & 0 \\ 0 & \frac{r^2}{4} & 0 & 0 & 0 \\ 0 & 0 & \frac{1}{4}h^2(r)\cos^2(\theta) + \frac{1}{4}r^2\sin^2(\theta) & \frac{1}{2}h^2(r)\cos(\theta) & -\frac{1}{2}h^2(r)\cos(\theta)\Omega(r) \\ 0 & 0 & \frac{1}{2}h^2(r)\cos(\theta) & h^2(r) & -h^2(r)\Omega(r) \\ 0 & 0 & -\frac{1}{2}h^2(r)\cos(\theta)\Omega(r) & -h^2(r)\Omega(r) & h^2(r)\Omega(r)^2 - \frac{r^2}{g^2(r)h^2(r)} \end{pmatrix}, \tag{4.11}$$

its inverse $g^{\mu\nu}$

$$\begin{pmatrix} \frac{1}{g^2(r)} & 0 & 0 & 0 & 0 \\ 0 & \frac{4}{r^2} & 0 & 0 & 0 \\ 0 & 0 & \frac{4\csc^2(\theta)}{r^2} & -\frac{2\cot(\theta)\csc(\theta)}{r^2} & 0 \\ 0 & 0 & -\frac{2\cot(\theta)\csc(\theta)}{r^2} & -\frac{g^2(r)h^2(r)\Omega(r)^2}{r^2} + \frac{1}{h^2(r)} + \frac{\cot^2(\theta)}{r^2} & -\frac{g^2(r)h^2(r)\Omega(r)}{r^2} \\ 0 & 0 & 0 & -\frac{g^2(r)h^2(r)\Omega(r)}{r^2} & -\frac{g^2(r)h^2(r)}{r^2} \end{pmatrix}, \tag{4.12}$$

and its determinant

$$\mathsf{g} = \sqrt{-g} = \frac{1}{4}r^3\sin\theta. \tag{4.13}$$

It is important to note that the metric (4.6) depends on both r and θ in this form. This will be useful later, as it simplifies the computational analysis we will undertake. An alternative form of the same metric can be written, emphasizing its particular structure, as described in [85]. Using the same coordinate system $(r, \theta, \phi, \psi, t)$ in [43], we can write:

$$ds^2 = -f(r)^2dt^2 + g(r)^2dr^2 + h(r)^2\left[d\psi + A_\alpha dx^\alpha - \Omega(r)dt\right]^2 + r^2\hat{g}_{\alpha\beta}dx^\alpha dx^\beta, \tag{4.14}$$

where $\hat{g}_{\alpha\beta}$ is the Fubini–Study metric on $\mathbb{CP}^N$, where N is the dimension of the spacetime; in this case, $N = 1$. The coordinates (θ, ϕ) correspond to the $\mathbb{CP}^1$ sector. The two-dimensional Ricci tensor is $\hat{R}_{\alpha\beta} = 2(N+1)\hat{g}_{\alpha\beta}$, and $A = A_\alpha dx^\alpha$ is a 1-form such that

$\mathcal{J} = \frac{1}{2}dA$ is the Kähler form on $\mathbb{CP}^N$.

As explained in [85], this alternative formulation of the metric for the 5D-Kerr-AdS black hole arises from the geometrical property where S^{2N+1} can be written as an S^1 fibre over CP^N. We are going to use the metric (4.14) for comparison later on, see section 6.2.

4.1.3 Asymptotically flat metric of the 5D-Kerr-AdS black hole

We also present an alternative form of the metric (4.6) that will be useful for later results. In this case, where the spacetime is asymptotically flat rather than asymptotically AdS, the metric takes the following form, expressed in the coordinate system $(R, \vartheta, \Upsilon, \Psi, t)$ [57]:

$$ds^2_{\rm FS} = -dt^2 + (R^2+a^2)[\sin^2\vartheta\, d\Upsilon^2 + \cos^2\vartheta\, d\Psi^2] + \frac{R_0^2}{\rho_{FS}^2}\left[dt + a\sin^2\vartheta\, d\Upsilon + a\cos^2\vartheta\, d\Psi\right]^2 + \frac{R^2\rho_{FS}^2}{\Xi_{FS}}dR^2 + \rho_{FS}^2 d\vartheta^2, \quad (4.15)$$

where

$$\Xi_{FS} = (R^2+a^2)^2 - R_0^2R^2 \quad \text{and} \quad \rho_{FS}^2 = R^2 + a^2, \quad (4.16)$$

and the coordinates Υ and Ψ take values in the interval $[0, 2\pi]$, while the angle ϑ takes values $[0, \pi/2]$, and R_0 is a length parameter related to the mass of the black hole

$$M_{FS} = \frac{3R_0^2}{8\sqrt{\pi}G} \quad \text{if} \quad 8\pi G = 1 \quad \text{then} \quad M_{FS} = 3\sqrt{\pi}R_0^2, \quad (4.17)$$

where we reported the form in which $8\pi G \neq 1$ to facilitate comparison with the reference paper [57], which adopts this choice, in contrast to our convention of $8\pi G = 1$. Additionally, we use ϑ in (4.15) as it is the same as in (4.4). As in the previous case, we denote the line element by $ds^2_{\rm FS}$, where FS refers to Frolov and Stojkovic [57]. Finally, we state the relationship between the coordinates in the metrics (4.6) and (4.15):

$$\vartheta = \frac{\theta}{2}, \qquad \Upsilon = \frac{\phi}{2} - \psi, \qquad \Psi = -\frac{\phi}{2} - \psi, \qquad R^2 = r^2 - a^2. \quad (4.18)$$

In order to bring a bit more clarity to all these coordinates systems, we report a table (see Table 4.1) with all the changes to move from the metric (4.6) to the others. For convenience, we also provide a table representing the transformation of the black hole parameters, including mass, length scale, and rotational parameter, see Table 4.2. Now that we have brought peace into the world of different line elements and we have a good grasp on how to move between different papers, we can focus on the particular symmetries of this spacetime.

Metric (4.6)	Metric (4.15)	Metric (4.4)
r	$R^2 = r^2 - a^2$	$\varrho^2 = r^2(1 - \frac{a^2}{L^2}) - a^2$
θ	$\vartheta = \frac{\theta}{2}$	$\vartheta = \frac{\theta}{2}$
ϕ	$\Upsilon = \frac{\phi}{2} - \psi$	$\varphi_1 = -\frac{at}{L^2} + \psi - \frac{\phi}{2}$
ψ	$\Psi = -\frac{\phi}{2} - \psi$	$\varphi_2 = -\frac{at}{L^2} + \psi + \frac{\phi}{2}$
t	t	t

Table 4.1: The connections between the sets of coordinates in the metrics (4.4), (4.6) and (4.15).

Metric (4.6)	Metric (4.15)	Metric (4.4)
M	$M_{FS} = 3\sqrt{\pi}R_0^2$	$\widetilde{M} = \Delta_\vartheta^3 M$
L	$L \to \infty$	L
a	a	a

Table 4.2: The connections between the parameters in the metrics (4.4), (4.6) and (4.15).

4.1.4 Symmetries and Killing vectors

We report the Killing vectors, see Definition 1.2.4, of the metric (4.6), which is the one that we are going to use throughout this part of the thesis [43]:

$$\begin{aligned}
&\xi_0 = \frac{\partial}{\partial t}, \qquad \xi_1 = \frac{\partial}{\partial \phi}, \qquad \xi_2 = \frac{\partial}{\partial \psi}, \\
&\xi_3 = 2\cos\phi\frac{\partial}{\partial\theta} - 2\sin\phi\cot\theta\frac{\partial}{\partial\phi} + \sin\phi\csc\theta\frac{\partial}{\partial\psi}, \\
&\xi_4 = -2\sin\phi\frac{\partial}{\partial\theta} - 2\cos\phi\cot\theta\frac{\partial}{\partial\phi} + \cos\phi\csc\theta\frac{\partial}{\partial\psi}.
\end{aligned} \tag{4.19}$$

In addition, the metric (4.6) has other symmetries [112, 145], which will become more important when studying the separability of the Klein-Gordon equation in Chapter 6. One that can be seen manifestly is:

$$(t, \psi) \to (-t, -\psi). \tag{4.20}$$

4.2 Event horizon, stationary limit surface, speed of light surface

In this section, we now introduce the surfaces associated with the black hole described by the metric (4.6). We determine the event horizon, light surface, and stationary limit surface. Additionally, we provide an intuitive representation of the three radii after giving

a comprehensive analysis. Furthermore, we demonstrate the existence of two key values of the rotational parameter, denoted as $a_{\max}$ and $a_{\min}$.

4.2.1 Event horizon

Firstly, we are going to study the most important surface for a black hole to exist, this is the event horizon, which can be thought as a boundary between two non-causally related regions of spacetime. In order to find the event horizon r_+, we shall put the inverse matrix element g_{rr}^{-1} equal to zero, which, after some manipulation, gives the following cubic equation for r^2

$$\frac{r^6}{2a^2L^2M} + \frac{r^4}{2a^2M} + r^2\left(\frac{1}{L^2} - \frac{1}{a^2}\right) + 1 = 0. \tag{4.21}$$

As a rule, we know that if the discriminant Δ of the cubic is positive we will have three real solutions otherwise we will have two complex and one real solution, see Section 3.3. For this black hole:

$$\Delta = \frac{8M^2\left(L^2 - a^2\right)^3 + L^4M\left(L^4 - 8a^4 - 20a^2L^2\right) - 2a^2L^8}{4a^8L^8M^3}, \tag{4.22}$$

the sign of the discriminant determines whether the solution corresponds to a black hole or a naked singularity. When the discriminant is positive, it indicates the presence of an event horizon. However, for sufficiently large values of the spin parameter a, for example $a \gtrsim 0.7$ as shown in Figure 4.2, the discriminant can become negative. In such cases, no horizon exists and the solution describes a naked singularity. The extremal case, described below, corresponds to the boundary where the discriminant vanishes. In the following, we will focus exclusively on the black hole case. We have three real solutions r_+^2, r_-^2, and r_0^2. While the first two are positive, r_0^2 is negative. We find that our black hole has two event horizons, an inner r_- and an outer r_+ horizon:

$$r_+ = \frac{1}{\sqrt{3}}\left([B+C]^{1/3} + A\,[B+C]^{-1/3} - L^2\right)^{1/2}, \tag{4.23}$$

and the expressions for r_- and r_0 are

$$r_- = \frac{1}{\sqrt{6}}\left((-1-i\sqrt{3})\,[B+C]^{1/3} + A\,(-1+i\sqrt{3})\,[B+C]^{-1/3} - 2L^2\right)^{1/2}, \tag{4.24}$$

$$r_0 = \frac{1}{\sqrt{6}}\left((-1+i\sqrt{3})\,[B+C]^{1/3} + A\,(-1-i\sqrt{3})\,[B+C]^{-1/3} - 2L^2\right)^{1/2}, \tag{4.25}$$

where

$$C = i\sqrt{(A^3 - B^2)}, \tag{4.26}$$

and

$$A = -6a^2M + L^4 + 6L^2M, \tag{4.27}$$

$$B = -9L^2M\left(2a^2 + L^2\right) - L^6. \tag{4.28}$$

While there is an i in the definition of r_-, this is real, and it is because C is a purely imaginary number. This is not true for r_0, even though it has an i in the expression, as r_0^2 is a negative solution for the cubic. Therefore, r_0 is a purely imaginary variable of the black hole, which we use to simplify calculations later on.

However, the important result is that we have analytical expressions for all the solutions to Equation (4.21), that depend only on the three parameters characterizing the metric of the black hole, namely a, M, L. We show the behaviour of r_+ in Figure 4.1 and the combined behaviour of r_+ and r_- in Figure 4.2.

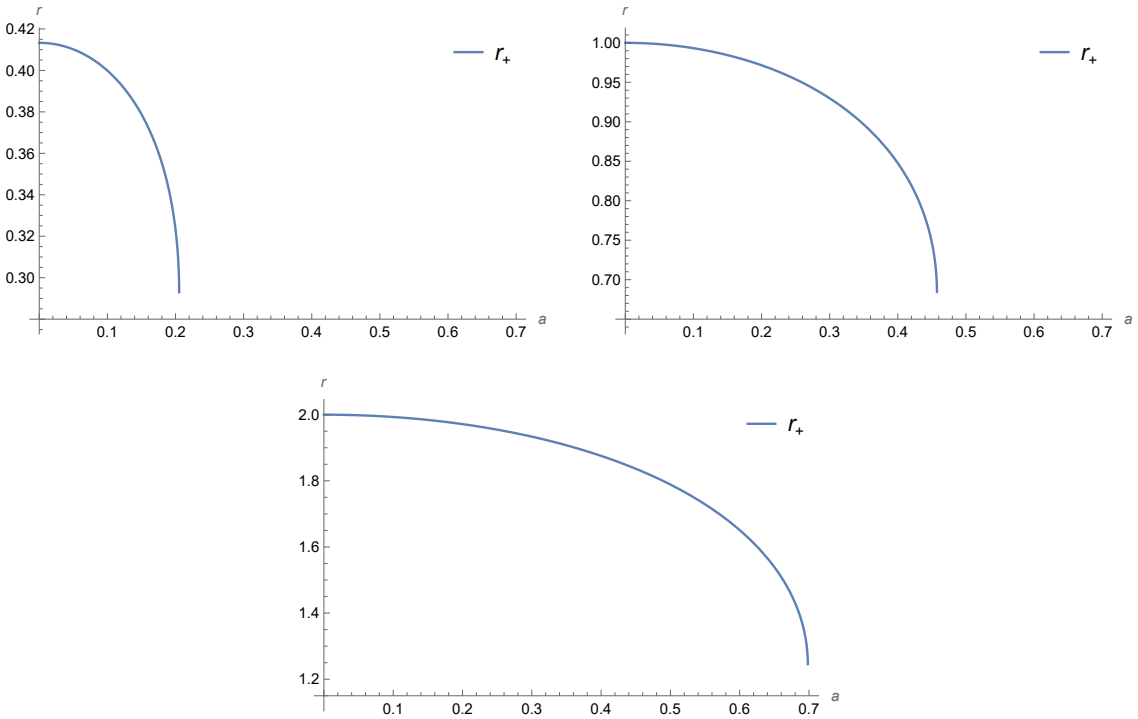

Figure 4.1: Event horizon radius r_+ for different masses: $M = 0.1$, $M = 1$, and $M = 10$ when $L = 1$.

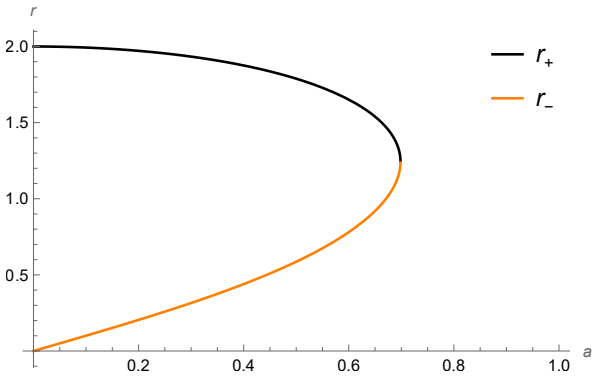

Figure 4.2: Representation of r_+ and r_- when $L = 1$ and $M = 10$.

From these plots (see Figures 4.1-4.2), it is clear that the radial coordinate r_+ exhibits qualitatively the same behaviour for different values of the mass M, while keeping L constant. Additionally, if we look at Figure 4.2, we can observe that for fixed values of M and L, both r_+ and r_- converge to the same value as a varies. This scenario occurs when the discriminant becomes zero, indicating a unique solution to Equation (4.21). This results in what is known as the extremal case of the 5D Kerr-AdS black hole. Furthermore, the plot reveals that r_+ persists up to a maximum value of a, beyond which the event horizon ceases to exist. We denote this maximum value as $a_{\max}$. We also observe similar qualitative behaviour for other values of M (see [43]).

We can show how to evaluate $a_{\max}$ analytically. We multiply the metric function g^{-2} (4.7) by r^4 in order to get a polynomial of order 6. We know that setting this equation equal to zero gives us the expressions for r_+, r_- and r_0. Hence, we can make a change of variable $x = r^2$ and $r_+^2 = x_+$. This will gives us a cubic polynomial $P(x)$,

$$P(x) = \frac{x^3}{L^2} + x^2 + 2M\left(\frac{a^2}{L^2} - 1\right)x + 2a^2M. \tag{4.29}$$

Since x_+ is a root of Equation (4.29) we know that this expression can be factorized as

$$P(x) = (x - x_+)Q(x), \tag{4.30}$$

where $Q(x)$ is

$$Q(x) = \frac{x^2}{L^2} + \left(\frac{x_+}{L^2} + 1\right)x + 2M\left(\frac{a^2}{L^2} - 1\right) + \left(\frac{x_+}{L^2} + 1\right)x_+. \tag{4.31}$$

At $a_{\max}$ as we can see from Figure 4.2, we have the extremal case for our black hole, in which the two horizons, the inner (r_-) and the outer (r_+), coalesce. This means that at $a_{\max}$ the polynomial $Q(x_+) = 0$. We can use this information to find the analytical expression of $a_{\max}$. We know that

$$P(x_+) = \frac{x_+^3}{L^2} + x_+^2 + 2M_{\text{ext}}\left(\frac{a_{\max}^2}{L^2} - 1\right)x_+ + 2a_{\max}^2M_{\text{ext}} = 0 \tag{4.32}$$

$$Q(x_+) = \frac{3x_+^2}{L^2} + 2x_+ + 2M_{\text{ext}}\left(\frac{a_{\max}^2}{L^2} - 1\right) = 0, \tag{4.33}$$

where M_{ext} is the value of the mass of the black hole, when $a = a_{\max}$. If we solve this system of equations for M_{ext} and $a_{\max}$ we find that

$$a_{\max}^2 = \frac{L^2x_+(L^2 + 2x_+)}{2(L^2 + x_+)^2}, \tag{4.34}$$

$$M_{\text{ext}} = \frac{x_+(x_+ + L^2)^2}{L^4}. \tag{4.35}$$

The last important object that we can define now that we have found the event horizon is ι. This is vector field defined as a linear combination of ξ_0 and ξ_2 (see Equation (4.19)),

$$\iota = \frac{\partial}{\partial t} + \Omega_H\frac{\partial}{\partial \psi}, \tag{4.36}$$

where Ω_H is the angular velocity of the black hole at the event horizon, which is the same as the function Ω in Equation (4.7) of the metric evaluated at the event horizon, r_+:

$$\Omega_H = \frac{2Ma}{r_+^4 + 2Ma^2}. \tag{4.37}$$

ι is the null generator of the event horizon and can also be used to evaluate the light surface as we will discuss later. Another notable property of ι is that it is a time-like Killing vector (1.24). Under certain conditions, it remains time-like throughout the entire spacetime outside the event horizon, which is pivotal for our analysis.

4.2.2 Stationary limit surface

The next characteristic surface is the stationary limit surface r_s, this can be defined as the surface inside which an observer cannot stay at rest relative to infinity. It is characterized by the Killing vector $\xi_0 = \frac{\partial}{\partial t}$, (4.19) and how it changes from time-like to space-like. In order to find the limit surface where the vector changes we must study:

$$g_{\mu\nu}\xi_0^\mu \xi_0^\nu = 0. \tag{4.38}$$

Given the Killing vector ξ_0 is associated with the time coordinate we are just asking when:

$$g_{tt} = -\frac{r^2}{L^2} + \frac{2M}{r^2} - 1 = 0, \tag{4.39}$$

which can be easily solved, and we find that the only real positive solution for this equation is:

$$r_s = \frac{L}{\sqrt{2}}\left[\left(1 + \frac{8M}{L^2}\right)^{\frac{1}{2}} - 1\right]^{\frac{1}{2}}. \tag{4.40}$$

As we can see the stationary limit surface is surprisingly independent of a.

4.2.3 Light surface

The same analysis can also be performed for the speed of light surface. This is the surface where an observer with the same angular velocity as the event horizon is moving at the speed of light. The light surface is connected to the Killing vector ι and following the result reported in the Appendix of [51] we must solve:

$$g_{\mu\nu}\iota^\mu \iota^\nu = 0, \tag{4.41}$$

from which we obtain:

$$g_{tt} + 2g_{\psi t}\Omega_H + g_{\psi\psi}\Omega_H^2 = 0, \tag{4.42}$$

where Ω_H is the angular velocity at the event horizon (4.37). We can rewrite expression (4.42) using the elements of the metric as:

$$-r^2\ g^{-2}(r) + h^4(r)\left(\ \Omega^2(r) - 2\ \Omega_H\ \Omega(r)\ + \Omega_H^2\ \right) = 0. \tag{4.43}$$

Solving this equation we have found an expression for the light surface (r_j):

$$r_j = \frac{L}{\sqrt{2}} \left(\frac{1 + \sqrt{1 - 8\frac{M}{L^2}(a\Omega_H - 1)^2 \left(L^2\Omega_H^2 - 1\right)}}{L^2\Omega_H^2 - 1} \right)^{\frac{1}{2}}. \tag{4.44}$$

We can see that r_j is real and positive real only when $L^2\Omega_H^2 - 1 > 0$, which corresponds to

$$\Omega_H > \frac{1}{L}, \tag{4.45}$$

hence we have found a bound for the existence of r_j. Notably, when L goes to infinity, in the asymptotically flat case, r_j becomes

$$r_j = \frac{1}{\sqrt{2}} \left(\frac{1 + \sqrt{1 - 8M\Omega_H^2(-1 + a\Omega_H)^2}}{\Omega_H^2} \right)^{\frac{1}{2}} \quad \text{when} \quad L \to \infty. \tag{4.46}$$

The analytical expression of r_j is pivotal for our future analysis, particularly because we will work in a regime where the light surface does not exist. Thanks to this, we can define a timelike Killing vector (1.24) in the exterior region to the event horizon. In particular, this result regarding the light surface directly comes from the fact that we are working in Anti-de Sitter (AdS) space, which intuitively corresponds to operating within a 'box,' given the presence of boundary in the spacetime.

We display Equation (4.44) in Figure 4.3. We can see that r_j also does not exist beyond $a_{\max}$, which acts as an asymptote for this quantity. In addition, we introduce a new quantity, denoted as $a_{\min}$, which is tailored to r_j and is related to the existence bound $\Omega_H > \frac{1}{L}$. In fact, r_j does not exist for values of a below $a_{\min}$.

In the same way, as we did for $a_{\max}$, we can also find an analytical solution for $a_{\min}$ which corresponds to the vertical asymptote for the function of r_j in Figure 4.3. We know that r_j exists only in the case of $\Omega_H > 1/L$. We can use the expression of the mass M in terms of the square event horizon $x_+ = r_+^2$

$$M = -\frac{x_+^2 \left(L^2 + x_+\right)}{2\left(a^2L^2 + a^2x_+ - L^2x_+\right)}, \tag{4.47}$$

if we substitute this into Equation (4.37) we obtain:

$$\Omega_H = a\left(\frac{1}{L^2} + \frac{1}{x_+}\right). \tag{4.48}$$

Now, if we approach $\Omega_H \to \frac{1}{L}$ we are approaching the asymptote, so:

$$\Omega_H = a\left(\frac{1}{L^2} + \frac{1}{x_+}\right) = \frac{1}{L}, \tag{4.49}$$

which implies

$$a_{\min} = \frac{Lx_+}{L^2 + x_+}. \tag{4.50}$$

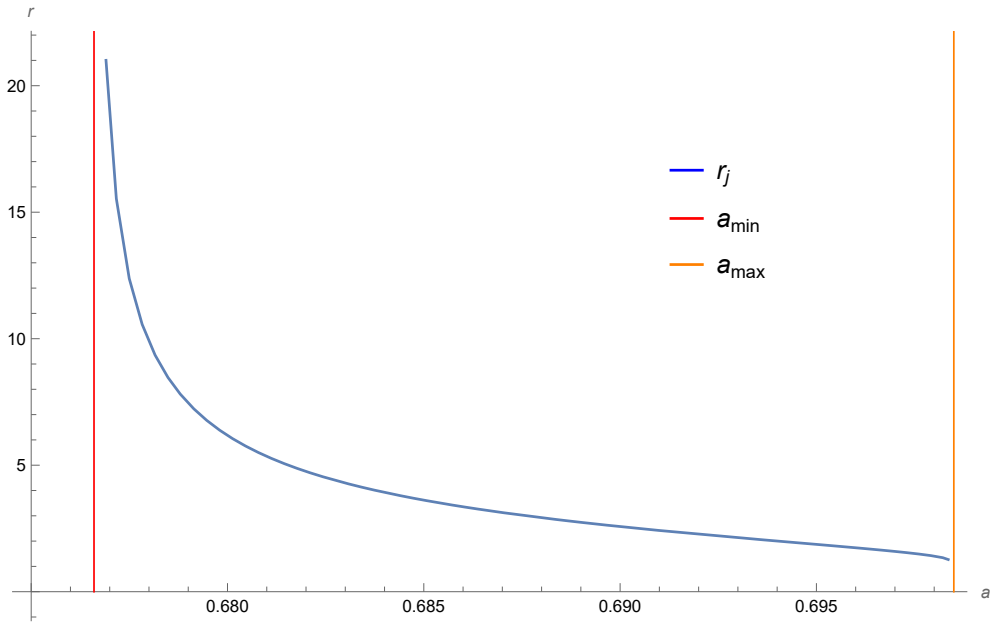

Figure 4.3: Light surface r_j for $L = 1$ and $M = 10$, with the two asymptotes $a_{\max}$ and $a_{\min}$.

4.2.4 Graphical representation of r_+, r_s and r_j

We now study the three radii r_+, r_s, and r_j for a Kerr-AdS-5D black hole. Since we have analytical expressions for these three radii, (4.23), (4.40), and (4.44), we can present a graphical analysis of them, Figure 4.4. We only report the specific case for $L = 1$ and $M = 10$ since the other cases, for different values of L and M present the same qualitative features [43].

We can see that r_s is always greater than r_+. We can also observe that as the rotation of the black hole increases (indicated by the parameter a), r_j collapses to the extremal case upon reaching $a_{\max}$, where $r_j = r_+$. Additionally, r_j crosses r_s and it becomes complex at $a_{\max}$.

In particular, both Figure 4.4 and Figure 4.5 illustrate how the black hole exhibits a specific geometry resembling a group of shells with different radii around the singularity. This structure appears much more like a Schwarzschild black hole than a Kerr black hole. This is due to the fact that the three surfaces have constant radius once we fix the black hole parameters, whereas in the Kerr black hole case, the stationary limit surface r_s and the speed-of-light surface r_j depends on the polar angle made with the axis of rotation. In the 5D case, as shown in the intuitive representation (Figure 4.5), the light surface r_j is dashed, reflecting the existence of a regime where the light surface is absent. Another important aspect is the difference between the 4D case and the 5D case which resides

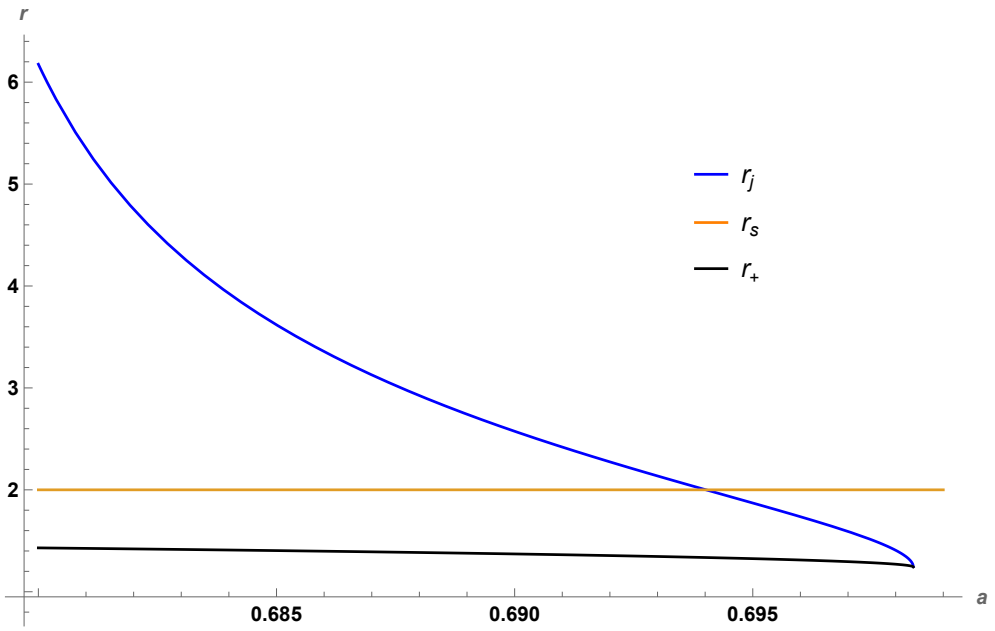

Figure 4.4: r_+, r_s and r_j for $L = 1$ and $M = 10$, see also [43].

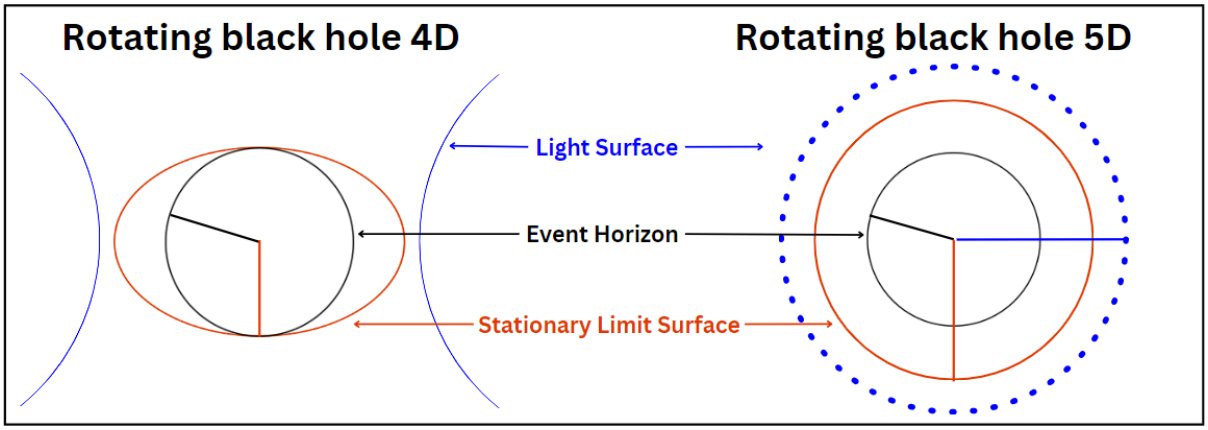

Figure 4.5: Schematic representation of the three radii r_+, r_j and r_s, and the difference between the 5D case and the 4D case, see also [91] for similar behaviour.

completely in the form of the light surface and the stationary limit surface. In the 4D case both these surfaces depend on the angular coordinate θ, while in the 5D case, thanks to the enhanced symmetry that we have introduced, they only depend on the parameters of the black hole, M, a, L. This makes the whole analysis a lot easier and it is one of the many reasons why we have decided to work with the 5D Kerr-AdS black hole.

From now on, we will confine our analysis to the case when a is restricted to lie between $(0, a_{\min})$, in the slow rotational regime, where r_j does not exist, while both r_+ and r_s do. Notably, within this framework, we can define a time-like Killing vector ι (4.36) throughout the region exterior to the event horizon. This vector is pivotal for later calculations and,

importantly, provides us with a consistent definition of time.

4.2.5 Surface gravity and temperature

In order to evaluate the temperature we compute the surface gravity κ_+ [147]:

$$\kappa_+^2 = -\frac{1}{2}(\nabla^\alpha \iota^\beta)(\nabla_\alpha \iota_\beta), \tag{4.51}$$

where ι is a Killing vector for our background (4.36). Notably, the normalization of κ_+ follows from the fact that the event horizon of a stationary black hole is a Killing horizon: a null hypersurface whose generators are tangent to a Killing vector field ι^μ. On the horizon, ι^μ becomes null and satisfies

$$\iota^\nu \nabla_\nu \iota^\mu = \kappa_+ \, \iota^\mu. \tag{4.52}$$

This equation defines κ_+ as the proportionality factor relating the derivative of the Killing vector along itself to itself on the horizon. In stationary, asymptotically flat spacetimes, one fixes the overall scale of ι^μ by requiring it to match the unit time translation at infinity, ensuring that κ_+ is uniquely defined and corresponds to the physical Hawking temperature via $T_H = \kappa_+/(2\pi)$ [147]. The explicit formula given above follows directly from manipulating this definition and using the Killing property of ι^μ together with the fact that it is null on the horizon.

We are using this Killing vector mainly because of its properties, being the null generator of the event horizon and the fact that is also a time-like Killing vector outside the event horizon. So this brings us to

$$\kappa_+^2 = \lim_{r \to r_+} \frac{4 \, f'(r)^2 - h(r) \, \Omega'(r)^2}{4 \, g(r)}$$

and the temperature of the black hole at the event horizon is:

$$T = \frac{\kappa_+}{2\pi}. \tag{4.53}$$

We can substitute the values of the metric functions (4.7) and obtain a polynomial expression that depends on r_+:

$$\kappa_+^2 = \frac{2M\left(L^2\Omega_H^2\left(2a^2+L^2\right)+a^2-6aL^2\Omega_H+2L^2\right)}{L^4 r_+^2} - \frac{8a^2M^2(a\Omega_H-1)^2}{r_+^8} + \\ + \frac{4M^2(L-a)(a+L)(a\Omega_H-1)^2}{L^2 r_+^6} + \frac{r_+^2\left(1-L^2\Omega_H^2\right)}{L^4} - 2\Omega_H^2. \tag{4.54}$$

4.2.6 Kretschmann scalar and Penrose diagram

We can also evaluate the Kretschmann scalar:

$$K = R_{\alpha\beta\gamma\delta} \cdot R^{\alpha\beta\gamma\delta} = \\ = \frac{8\left(192a^4L^4M^2 + 36M^2r^4\left(a^2 - L^2\right)^2 + 192a^2L^2M^2r^2(a-L)(a+L) + 5r^{12}\right)}{L^4r^{12}}, \tag{4.55}$$

which in the limit for $r \to \infty$ results in

$$\frac{40}{L^4} + O\left(\frac{1}{r^3}\right). \tag{4.56}$$

The Kretschmann scalar is utilized to verify if the singularities present in the spacetime are simply due to a choice of coordinates or real singularities. In this case, K makes it clear that the only singularity of this black hole with metric (4.6) is at $r = 0$. We can restrict our analysis to only the Kretschmann scalar because the Ricci scalar R is constant, and the Ricci tensor $R_{\mu\nu}$ is proportional to the metric $g_{\mu\nu}$, as shown in Equation (4.3).

We can also show the Penrose diagram of this black hole [2]. To do this, we first need to define the Kruskal coordinates as introduced in Section 1.3. For this purpose, we begin by introducing a corotating coordinate $\psi_\star$:

$$\psi_\star = \psi - \Omega_H\, t, \tag{4.57}$$

where Ω_H is defined in Equation (4.37). If we substitute $\psi_\star$ in Equation (4.6) the metric becomes

$$ds^2 = -f(r)^2\, dt^2 + g(r)^2\, dr^2 + \frac{r^2}{4}\left[d\theta^2 + \sin^2\theta\, d\phi^2\right] \\ + h(r)^2\left[d\psi_+ + \frac{1}{2}\cos\theta\, d\phi - \{\Omega(r) - \Omega_H\}\, dt\right]^2. \tag{4.58}$$

Next, we define the "tortoise" coordinate $r_\star$, which is given by [85]

$$\frac{dr_\star}{dr} = \frac{g(r)}{f(r)} = \frac{1}{r}\, g(r)^2\, h(r), \tag{4.59}$$

where $g(r)$, $f(r)$ and $h(r)$ are the metric functions in Equation (4.7). Finally, we define the change of coordinates to the Eddington–Finkelstein u and v coordinates, given by:

$$r_\star = \frac{v-u}{2}, \tag{4.60}$$

$$t = \frac{u+v}{2}. \tag{4.61}$$

Knowing that

$$dr_\star = \frac{dv - du}{2}, \tag{4.62}$$

$$dt = \frac{du + dv}{2}, \tag{4.63}$$

$$d\psi = d\psi_\star + dt\,\Omega_H, \tag{4.64}$$

$$dr = \frac{f(r)}{g(r)}\,dr_\star, \tag{4.65}$$

the line element in Equation (4.6) becomes

$$\begin{aligned} ds^2 = &-f(r)^2\,du\,dv + \frac{r^2}{4}\left(d\theta^2 + \sin^2\theta\,d\phi^2\right) \\ &+ \frac{h(r)^2}{4}\Big(2\,d\psi_\star + \Omega_H\,(du + dv) + \cos\theta\,d\phi - \Omega(r)\,(du + dv)\Big)^2. \end{aligned} \tag{4.66}$$

We then define the Kruskal coordinates U and V as:

$$U = -\frac{1}{\kappa_+}\,e^{-\kappa_+ u} \quad \text{and} \quad V = \frac{1}{\kappa_+}\,e^{\kappa_+ v}, \tag{4.67}$$

where κ_+ is the surface gravity at the event horizon, given in Equation (4.54). From this definition, we can write

$$dU = e^{-\kappa_+ u}\,du, \quad dV = e^{\kappa_+ v}\,dv, \tag{4.68}$$

and hence

$$dU\,dV = e^{\kappa_+(u-v)}\,du\,dv = e^{2\kappa_+ r_\star}\,du\,dv. \tag{4.69}$$

Thus, the line element can be written as

$$\begin{aligned} ds_{\mathrm{K}}^2 = &-\frac{f(r)^2}{\kappa_+^2 UV}\,dU\,dV + \frac{r^2}{4}\left[d\theta^2 + \sin^2\theta\,d\phi^2\right] \\ &+ h(r)^2\left[d\psi_+ + \frac{1}{2}\cos\theta\,d\phi - \frac{1}{2\kappa_+}\left\{\Omega(r) - \Omega_H\right\}\left(\frac{dV}{V} + \frac{dU}{U}\right)\right]^2. \end{aligned} \tag{4.70}$$

We also define the determinant of (4.70)

$$\mathrm{g}_{\mathrm{K}} = \sqrt{-g_{\mathrm{K}}} = \frac{r^2 h(r)}{8\kappa_+^2 UV}\left[2\kappa_+ f(r)^2 + \left\{\Omega(r) - \Omega_H\right\}^2 h(r)^2\right]\sin\theta. \tag{4.71}$$

Finally, we can construct the Penrose diagram of the Kerr–AdS five-dimensional black hole [2].

Summary

In this chapter, we introduced three key metrics for our analysis: the general metric of the 5D Kerr-AdS black hole (4.1), the enhanced symmetry metric (4.6), and the asymptotically flat metric (4.15). We provided a guide on transitioning between these metrics

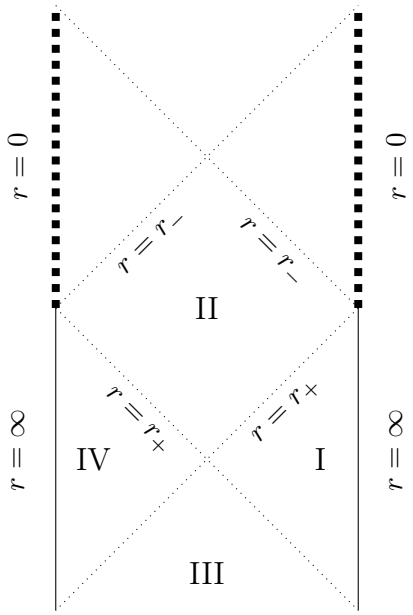

Figure 4.6: Penrose diagram of metric (4.6). The dotted lines represent the horizons: the event horizon is at $r = r_+$ and the inner horizon at $r = r_-$. Null infinity corresponds to the time-like boundary at $r = \infty$, and the dashed lines indicate the curvature singularity at $r = 0$ [2].

which is going to be useful for later comparisons within the thesis.

Furthermore, we have reported the Killing vectors and symmetries for the metric (4.6), which is the one that we are going to study throughout this thesis. Of particular interest is ι, serving as the null generator of the event horizon, and providing a means to also derive the expression for the light surface. We have evaluated the three characteristic radii of the black hole: the event horizon, the light surface, and the stationary limit surface, focusing on their bounds, limits, and their qualitative behaviour on changing a, the rotational parameter of the black hole.

Notably, we identify a regime for which the light surface does not exist. Consequently, ι is a time-like Killing vector everywhere in the spacetime outside the event horizon, which not only gives us a proper definition of time in our spacetime but it is also going to be pivotal for later calculations on the scalar field.

Moreover, we have also shown some of the geometrical and thermodynamic properties of the black hole evaluating the Kretschmann scalar, the temperature, and the surface gravity.

Chapter 5

Spin-weighted spherical harmonics

In this chapter, we present some properties of the spin-weighted spherical harmonics (swsh) [77, 108] and introduce new results. In particular, we discuss the addition theorem for this class of functions and a new generalisation with new addition theorems that we have derived. We also demonstrate how this knowledge can be advantageous in the analysis of a scalar field in this curved background in Chapter 8.

The spin-weighted spherical harmonics are used in different fields of physics; for this reason, we believe that the results we present could be useful not only for the study of a scalar field in a curved background but also in other branches of physics. For example, the spin-weighted spherical harmonics have been used to study anisotropies in the cosmic microwave background [3, 71, 129, 132, 154, 155], gravitational physics (including gravitational waves and perturbations of black hole space-times) [4,86,131,139]; geosciences [56,99]; anisotropic turbulence [120]; and electromagnetism [126]. We now give a brief summary of these functions, focusing on the properties that we need for our studies; for a more detailed description, we refer the reader to [15, 24, 28, 48, 49, 56, 99, 118].

5.1 Properties of spin-weighted spherical harmonics

In this section, we analyse the spin-weighted spherical harmonics, focusing in particular on their properties. We will examine the *edth*, $\eth$, and *edth–bar*, $\overline{\eth}$, differential operators [118]. The use of a different notation from that in [118] is intentional; indeed, we will also define the *edth–prime*, $\eth'$, and *edth–bar–prime*, $\overline{\eth}'$, operators for reasons that will soon become clear. We begin by presenting the definition of a spin-weighted spherical harmonic.

The spin-weighted spherical harmonics ${}_sY_\ell^m(\theta,\phi)$ are functions on the two-sphere $\mathbb{S}^2$ that have spin-weight s, where s is an integer or half-integer [77, 108]. We employ the usual spherical polar coordinates (θ,ϕ) on $\mathbb{S}^2$, with $\theta \in [0,\pi]$ and $\phi \in [0,2\pi)$. The spin-weighted spherical harmonics depend on three quantum numbers: s, ℓ, and m. The spin s is a pos-

itive or negative integer or half-integer. The orbital angular momentum quantum number ℓ then takes the values $\ell = |s|, |s|+1, |s|+2, \ldots$, and the azimuthal quantum number m takes the values $m = -\ell, -\ell+1, \ldots, \ell-1, \ell$.

There are many different ways to define the spin-weighted spherical harmonics in the literature. In this thesis, we follow the conventions of [99], which will serve well for our purposes in studying the scalar field in Chapter 6.

5.1.1 Definition. *The spin-weighted spherical harmonics ${}_sY_\ell^m(\theta,\phi)$ are defined in terms of the Wigner D-function by [99]*

$$ {}_sY_\ell^m(\theta,\phi) = (-1)^s \sqrt{\frac{2\ell+1}{4\pi}}\, D^{\ell *}_{m,-s}(\phi,\theta,0), \tag{5.1} $$

where the asterisk $*$ denotes complex conjugation.

Notably, s can be a half-integer; this does not compromise the procedure, but it introduces an i in front of some formulas, which can be accounted for.

The function $D^\ell_{m,-s}(\phi,\theta,0)$ is called the Wigner D-function and it is mainly used in quantum mechanics in order to describe the angular momentum together with the $d^\ell_{m,-s}(\theta)$, which is called lesser Wigner D-Function. We can define $D^\ell_{m,-s}(\phi,\theta,\psi)$ as [144]

$$ D^\ell_{m,-s}(\phi,\theta,\psi) = e^{-im\phi} d^\ell_{m,-s}(\theta) e^{is\psi}. \tag{5.2} $$

In addition, we can define the lesser Wigner D-functions through the Jacobi polynomials as [144]

$$ d^\ell_{m,-s}(\theta) = \mathcal{N}_{m,-s} \left[\frac{\mathcal{S}!(\mathcal{S}+\mathcal{M}+\mathcal{M}')!}{(\mathcal{S}+\mathcal{M})!(\mathcal{S}+\mathcal{M}')!}\right]^{\frac{1}{2}} \left(\sin\frac{\theta}{2}\right)^{\mathcal{M}} \left(\cos\frac{\theta}{2}\right)^{\mathcal{M}'} P_{\mathcal{S}}^{(\mathcal{M},\mathcal{M}')}(\cos\theta), \tag{5.3} $$

where $\mathcal{S}$, $\mathcal{M}$ and $\mathcal{M}'$ are related to m, s and ℓ by

$$ \mathcal{M} = |m+s|, \quad \mathcal{M}' = |m-s|, \quad \mathcal{S} = \ell - \frac{1}{2}(\mathcal{M}+\mathcal{M}'), \tag{5.4} $$

and $\mathcal{N}_{m,-s}$ is

$$ \mathcal{N}_{m,-s} = \begin{cases} 1 & \text{if } -s \geq m, \\ (-1)^{-(s+m)} & \text{if } -s < m. \end{cases} \tag{5.5} $$

We will focus on an addition theorem for these functions, as this is the main result that we will use later in the thesis. Its proof is based on the definitions of the operators ${}_s\eth$ and ${}_s\overline{\eth}$, as given below [118]:

5.1.2 Definition. *The operators ${}_s\eth$ and ${}_s\overline{\eth}$ act on the spin-weighted spherical harmonics as follows [77, 99, 108]:*

$$ {}_s\eth\, {}_sY_\ell^m(\theta,\phi) = -\left[\partial_\theta + \frac{\mathrm{i}}{\sin\theta}\partial_\phi - s\cot\theta\right] {}_sY_\ell^m(\theta,\phi), \tag{5.6a} $$

$$ {}_s\overline{\eth}\, {}_sY_\ell^m(\theta,\phi) = -\left[\partial_\theta - \frac{\mathrm{i}}{\sin\theta}\partial_\phi + s\cot\theta\right] {}_sY_\ell^m(\theta,\phi). \tag{5.6b} $$

The operators ${}_s\eth$, ${}_s\overline{\eth}$ respectively increase and decrease the spin-weight s of a spin-weighted spherical harmonics ${}_sY_\ell^m$ by one [77, 108]:

$$ {}_s\eth\, {}_sY_\ell^m = {}_{s+1}Y_\ell^m\sqrt{(\ell-s)(\ell+s+1)}, \tag{5.7a} $$

$$ {}_s\overline{\eth}\, {}_sY_\ell^m = -{}_{s-1}Y_\ell^m\sqrt{(\ell+s)(\ell-s+1)}. \tag{5.7b} $$

We now introduce the differential operators that we will use to prove the new addition theorems that were not previously defined in [118]. We denote by ${}_{s'}\eth'$ and ${}_{s'}\overline{\eth}'$ the operators ${}_s\eth$ and ${}_s\overline{\eth}$ where the coordinates (θ,ϕ) are replaced by (θ',ϕ') and the spin s by s':

$$ {}_{s'}\eth'\, {}_{s'}Y_\ell^m(\theta',\phi') = -\left[\partial_{\theta'} + \frac{\mathrm{i}}{\sin\theta'}\partial_{\phi'} + s'\cot\theta'\right] {}_{s'}Y_\ell^m(\theta',\phi'), \tag{5.8a} $$

$$ {}_{s'}\overline{\eth}'\, {}_{s'}Y_\ell^m(\theta',\phi') = -\left[\partial_{\theta'} - \frac{\mathrm{i}}{\sin\theta'}\partial_{\phi'} - s'\cot\theta'\right] {}_{s'}Y_\ell^m(\theta',\phi'), \tag{5.8b} $$

where, by replacing s with s', we obtain the same result for raising and lowering the spin s' as was previously found for s, thus obtaining

$$ {}_{s'}\eth\, {}_{s'}Y_\ell^m = {}_{s'+1}Y_\ell^m\sqrt{(\ell-s')(\ell+s'+1)}, \tag{5.9a} $$

$$ {}_{s'}\overline{\eth}\, {}_{s'}Y_\ell^m = -{}_{s'-1}Y_\ell^m\sqrt{(\ell+s')(\ell-s'+1)}. \tag{5.9b} $$

We can also show how derivatives with respect to the coordinates θ, ϕ, θ' and ϕ' act on the spin-weighted spherical harmonics. The following lemma, which follows directly from Definition 5.1.2, shows this and we will use this for the derivation of the addition theorems:

5.1.3 Lemma.

$$ \frac{\partial}{\partial\theta}\, {}_sY_\ell^m(\theta,\phi) = -\frac{1}{2}\left[{}_s\eth + {}_s\overline{\eth}\right] {}_sY_\ell^m(\theta,\phi), \tag{5.10a} $$

$$ \frac{\partial}{\partial\phi}\, {}_sY_\ell^m(\theta,\phi) = \frac{\mathrm{i}}{2}\sin\theta\left[{}_s\eth - {}_s\overline{\eth}\right] {}_sY_\ell^m(\theta,\phi) - \mathrm{i}\, s\cos\theta\, {}_sY_\ell^m(\theta,\phi), \tag{5.10b} $$

$$ \frac{\partial}{\partial\theta'}\, {}_{s'}Y_\ell^m(\theta',\phi') = -\frac{1}{2}\left[{}_{s'}\eth' + {}_{s'}\overline{\eth}'\right] {}_{s'}Y_\ell^m(\theta',\phi'), \tag{5.10c} $$

$$ \frac{\partial}{\partial\phi'}\, {}_{s'}Y_\ell^m(\theta',\phi') = \frac{\mathrm{i}}{2}\sin\theta'\left[{}_{s'}\eth' - {}_{s'}\overline{\eth}'\right] {}_{s'}Y_\ell^m(\theta',\phi') + \mathrm{i}\, s'\cos\theta'\, {}_{s'}Y_\ell^m(\theta',\phi'), \tag{5.10d} $$

where we can use Definition 5.1.2 and Equation (5.8) to find the right hand side for these equations.

Lastly, it is important to highlight that

$$\partial_\phi \left[{}_sY_\ell^m(\theta,\phi) \right] = \mathrm{i}\, m\, {}_sY_\ell^m(\theta,\phi), \tag{5.11}$$

which will become important in the calculation for the new addition theorems.

5.2 Addition theorem

We begin our analysis by recovering the well-known spin-weighted spherical harmonics addition theorem, before introducing the generalisations that we have found. We utilise the relationship in Definition 5.1.1 between the spin-weighted spherical harmonics and the Wigner D-functions to do this, and then we will apply the differential operators directly to the spin-weighted spherical harmonics using the *edth* and *edth–bar* operators to find the generalisations of the addition theorem.

We start by reporting the addition theorem for the Wigner D-functions [116, 144]:

$$\sum_{m=-\ell}^{\ell} D^\ell_{s,m}(\alpha_2,\beta_2,\gamma_2) D^\ell_{m,s'}(\alpha_1,\beta_1,\gamma_1) = D^\ell_{s,s'}(\alpha',\beta',\gamma'). \tag{5.12}$$

This result is valid whenever s and s' differ by an integer, and $\ell \geq \max\{|s|,|s'|\}$. Here α', β', γ' are Euler angles [116, 144], which satisfy the following relations:

$$\cot\left(\alpha'-\alpha_2\right) = \cos\beta_2 \cot\left(\alpha_1+\gamma_2\right) + \cot\beta_1 \sin\beta_2 \csc\left(\alpha_1+\gamma_2\right), \tag{5.13a}$$

$$\cos\beta' = \cos\beta_1\cos\beta_2 - \sin\beta_1\sin\beta_2\cos\left(\alpha_1+\gamma_2\right), \tag{5.13b}$$

$$\cot\left(\gamma'-\gamma_1\right) = \cos\beta_1 \cot\left(\alpha_1+\gamma_2\right) + \cot\beta_2 \sin\beta_1 \csc\left(\alpha_1+\gamma_2\right), \tag{5.13c}$$

and

$$\frac{\sin\left(\alpha'-\alpha_2\right)}{\sin\beta_1} = \frac{\sin\left(\gamma'-\gamma_1\right)}{\sin\beta_2} = \frac{\sin\left(\alpha_1+\gamma_2\right)}{\sin\beta'}. \tag{5.13d}$$

Since we know the relationship between the spin-weighted spherical harmonics and the Wigner D-functions (5.2), deriving the addition theorem for spin-weighted spherical harmonics is straightforward [71, 99, 131]:

$$\begin{aligned}
\sum_{m=-\ell}^{\ell} {}_sY_\ell^m(\theta,\phi)\, {}_{s'}Y_\ell^{m*}(\theta',\phi') &= \frac{2\ell+1}{4\pi} \sum_{m=-\ell}^{\ell} D^\ell_{m,-s'}(\phi',\theta',0) D^{\ell*}_{m,-s}(\phi,\theta,0) \\
&= \frac{2\ell+1}{4\pi} \sum_{m=-\ell}^{\ell} D^\ell_{m,-s'}(\phi',\theta',0) D^\ell_{-s,m}(0,-\theta,-\phi) \\
&= \frac{2\ell+1}{4\pi} D^\ell_{-s,-s'}(\alpha,\beta,\gamma) \\
&= \frac{2\ell+1}{4\pi} e^{-is\alpha} D^{\ell*}_{-s',-s}(\gamma,\beta,0),
\end{aligned} \tag{5.14}$$

where we have used Equation (5.12), (5.18) and the following property of the Wigner D-functions [144]:

$$D^{\ell*}_{s,m}(\phi,\theta,\chi) = D^\ell_{m,s}(-\chi,-\theta,-\phi). \tag{5.15}$$

5.2.1 Definition. *From (5.13), the Euler angles α, β, γ are now given in terms of the angles (θ, ϕ) and (θ', ϕ') as follows [99]:*

$$\cot\alpha = \cos\theta\cot\Delta\phi - \cot\theta'\sin\theta\csc\Delta\phi, \tag{5.16a}$$

$$\cos\beta = \cos\theta\cos\theta' + \sin\theta\sin\theta'\cos\Delta\phi, \tag{5.16b}$$

$$\cot\gamma = \cos\theta'\cot\Delta\phi - \cot\theta\sin\theta'\csc\Delta\phi, \tag{5.16c}$$

where $\Delta\phi$ is $\phi - \phi'$.

The Definitions (5.16) are, strictly speaking, valid only when $\phi - \phi'$ is not a multiple of π. The corresponding definitions of the Euler angles when $\phi - \phi'$ is a multiple of π can be found in [99]. For our purposes, we require only that $\alpha = \beta = \gamma = 0$ in the coincidence limit $\theta' = \theta$ and $\phi' = \phi$. We also have

$$-\frac{\sin\alpha}{\sin\theta'} = \frac{\sin\gamma}{\sin\theta} = \frac{\sin(\phi - \phi')}{\sin\beta}. \tag{5.17}$$

Next we use the result [144]

$$D^{\ell}_{s,s'}(\alpha, \beta, \gamma) = e^{-is\alpha} D^{\ell}_{s,s'}(0, \beta, \gamma) \tag{5.18}$$

to obtain the addition theorem for spin-weighted spherical harmonics [71, 99, 131].

5.2.2 Theorem. *The addition theorem for the spin-weighted spherical harmonics is:*

$$\begin{aligned}(-1)^s \sum_{m=-\ell}^{\ell} {}_sY^m_\ell(\theta,\phi)\,{}_{s'}Y^{m*}_\ell(\theta',\phi') &= \frac{2\ell+1}{4\pi} e^{-is\alpha} D^{\ell}_{s,s'}(0,\beta,\gamma) \\ &= \sqrt{\frac{2\ell+1}{4\pi}}\, e^{-is\alpha}\, {}_sY^{-s'}_\ell(\beta,\gamma).\end{aligned} \tag{5.19}$$

This result is valid whenever s and s' differ by an integer, and $\ell \geq \max\{|s|, |s'|\}$. The addition theorem is equivalent to the addition theorem for monopole harmonics [48, 49, 153]. We will be interested in the case when $s = s'$ that we will discuss later. In addition, we want to point out that several results have been retrieved when $s = 0$, see [143, 144]. We have written Equation (5.19) in an alternative, yet equivalent, form to that presented in [99]. Note that the addition theorem takes a slightly different form in some references [71, 131] due to variations in the definition of the spin–weighted spherical harmonics. In the coincidence limit $\theta' = \theta$ and $\phi' = \phi$, the Euler angles become $\alpha = \beta = \gamma = 0$ and the right-hand side of Equation (5.19) simplifies as follows

5.2.3 Lemma. *We have [99]*

$${}_sY^{-s'}_\ell(0,0) = \sqrt{\frac{2\ell+1}{4\pi}} D_{s,s'}(0,0,0) = \delta_{s,s'}\sqrt{\frac{2\ell+1}{4\pi}}, \tag{5.20}$$

where $\delta_{s,s'}$ is the usual Kronecker delta:

$$\delta_{s,s'} = \begin{cases} 1 & \text{if } s' = s, \\ 0 & \text{otherwise,} \end{cases} \tag{5.21}$$

and using the result [144]

$$D_{s,s'}(0,0,0) = \delta_{s,s'}. \tag{5.22}$$

5.2.4 Corollary. *The coincidence limit $\theta' = \theta$, $\phi' = \phi$ of the addition theorem (5.19) is:*

$$\sum_{m=-\ell}^{\ell} {}_sY_\ell^m(\theta,\phi)\,{}_{s'}Y_\ell^{m*}(\theta,\phi) = \frac{2\ell+1}{4\pi}\delta_{s,s'}. \tag{5.23}$$

This gives us the addition theorem for the spin-weighted spherical harmonics. In addition, given Definition 5.1.2 and Equation (5.8) we could also apply the differential operator directly, in doing so we can generalise this results to further addition theorems, which will be useful later in the thesis in the calculation for the Kerr–AdS five-dimensional black hole, specifically in Chapter 8.

5.3 New addition theorems

We now present our results for the new addition theorems. These results are valid under the same conditions on the quantum numbers s, s' and ℓ as for the original addition theorem; that is, the spins s and s' may differ only by an integer, and it must hold that $\ell \geq \max\{|s|, |s'|\}$. Our strategy for deriving these results is to apply appropriate combinations of the operators ${}_s\eth$, ${}_s\overline{\eth}$, ${}_{s'}\eth'$, and ${}_{s'}\overline{\eth}'$ (as defined in Definition 5.1.2) to the original addition theorem (5.19). We then utilise the "raising and lowering" properties of these operators given in Equations (5.7). We will go through the first two derivations step by step, while we will highlight the main differences in the calculation for the remaining results.

5.3.1 Theorem. *The new addition theorem obtained when taking a derivative with respect to θ on one term is:*

$$\begin{aligned}(-1)^s \sum_{m=-\ell}^{\ell} \left[\frac{\partial}{\partial\theta}{}_sY_\ell^m(\theta,\phi)\right] {}_{s'}Y_\ell^{m*}(\theta',\phi') \\ = \frac{1}{2}\sqrt{\frac{2\ell+1}{4\pi}}\Big\{\sqrt{(\ell-s)(\ell+s+1)}\,\mathrm{e}^{-\mathrm{i}(s+1)\alpha}\,{}_{s+1}Y_\ell^{-s'}(\beta,\gamma) \\ - \sqrt{(\ell+s)(\ell-s+1)}\,\mathrm{e}^{-\mathrm{i}(s-1)\alpha}\,{}_{s-1}Y_\ell^{-s'}(\beta,\gamma)\Big\}.\end{aligned} \tag{5.24}$$

Its derivation and proof can be obtained from the following calculation:

$$(-1)^s \sum_{m=-\ell}^{\ell} \left[\frac{\partial}{\partial\theta}\, {}_sY_\ell^m(\theta,\phi)\right] {}_{s'}Y_\ell^{m*}(\theta',\phi') = -\frac{(-1)^s}{2} \sum_{m=-\ell}^{\ell} \left[{}_s\eth\ {}_sY_\ell^m(\theta,\phi) + {}_s\bar{\eth}\ {}_sY_\ell^m(\theta,\phi)\right] {}_{s'}Y_\ell^{m*}(\theta',\phi'), \quad (5.25)$$

where we have used the result in Lemma 5.1.3 to introduce ${}_s\eth$ *and* ${}_s\bar{\eth}$*,*

$$= -\frac{(-1)^s}{2} \sum_{m=-\ell}^{\ell} \left[\sqrt{(\ell-s)(\ell+s+1)}\, {}_{s+1}Y_\ell^m(\theta,\phi) - \sqrt{(\ell+s)(\ell-s+1)}\, {}_{s-1}Y_\ell^m(\theta,\phi)\right] {}_{s'}Y_\ell^{m*}(\theta',\phi'), \quad (5.26)$$

where we have applied the properties in Equation (5.7),

$$= \frac{1}{2}\left\{\sqrt{(\ell-s)(\ell+s+1)} \sum_{m=-\ell}^{\ell} (-1)^{s+1} {}_{s+1}Y_\ell^m(\theta,\phi) {}_{s'}Y_\ell^{m*}(\theta',\phi') - \sqrt{(\ell+s)(\ell-s+1)} \sum_{m=-\ell}^{\ell} (-1)^{s-1} {}_{s-1}Y_\ell^m(\theta,\phi) {}_{s'}Y_\ell^{m*}(\theta',\phi')\right\}, \quad (5.27)$$

where we have multiplied the factor $(-1)(-1)^s$ *inside the parenthesis rearranging and exploiting the fact that* $(-1)^1 = (-1)^{-1} = (-1)$*,*

$$= \frac{1}{2}\sqrt{\frac{2\ell+1}{4\pi}}\left\{\sqrt{(\ell-s)(\ell+s+1)}\, \mathrm{e}^{-\mathrm{i}(s+1)\alpha} {}_{s+1}Y_\ell^{-s'}(\beta,\gamma) - \sqrt{(\ell+s)(\ell-s+1)}\, \mathrm{e}^{-\mathrm{i}(s-1)\alpha} {}_{s-1}Y_\ell^{-s'}(\beta,\gamma)\right\}, \quad (5.28)$$

where we have used the result of the addition theorem in Equation (5.19).

We will now present the second new result in the same manner.

5.3.2 Theorem. *The new addition theorem obtained when taking a derivative with respect to* ϕ *on one term is:*

$$(-1)^s \sum_{m=-\ell}^{\ell} m\, {}_sY_\ell^m(\theta,\phi) {}_{s'}Y_\ell^{m*}(\theta',\phi') = -\frac{1}{2}\sqrt{\frac{2\ell+1}{4\pi}}\left\{\sqrt{(\ell-s)(\ell+s+1)}\, \mathrm{e}^{-\mathrm{i}(s+1)\alpha} {}_{s+1}Y_\ell^{-s'}(\beta,\gamma) + \sqrt{(\ell+s)(\ell-s+1)}\, \mathrm{e}^{-\mathrm{i}(s-1)\alpha} {}_{s-1}Y_\ell^{-s'}(\beta,\gamma)\right\} \sin\theta - s\sqrt{\frac{2\ell+1}{4\pi}}\, \mathrm{e}^{-\mathrm{i}s\alpha} {}_sY_\ell^{-s'}(\beta,\gamma)\cos\theta. \quad (5.29)$$

Its derivation and proof can be obtained from the following calculation:

$$(-1)^s \sum_{m=-\ell}^{\ell} m\, {}_sY_\ell^m(\theta,\phi)\, {}_{s'}Y_\ell^{m*}(\theta',\phi') = -\mathrm{i}\,(-1)^s \sum_{m=-\ell}^{\ell} \left[\frac{\partial}{\partial\phi}\, {}_sY_\ell^m(\theta,\phi)\right] {}_{s'}Y_\ell^{m*}(\theta',\phi'), \quad (5.30)$$

where we have used the result in Equation (5.11),

$$= \frac{(-1)^s}{2} \sum_{m=-\ell}^{\ell} \left[{}_s\eth\, {}_sY_\ell^m(\theta,\phi) - {}_s\bar{\eth}\, {}_sY_\ell^m(\theta,\phi)\right] {}_{s'}Y_\ell^{m*}(\theta',\phi') \sin\theta - s\,(-1)^s \cos\theta \sum_{m=-\ell}^{\ell} {}_sY_\ell^m(\theta,\phi)\, {}_{s'}Y_\ell^{m*}(\theta',\phi'), \quad (5.31)$$

where we have used the result in Lemma 5.1.3,

$$= \frac{(-1)^s}{2} \sum_{m=-\ell}^{\ell} \Bigg\{ \Big[\sqrt{(\ell-s)(\ell+s+1)}\, {}_{s+1}Y_\ell^m(\theta,\phi) + \sqrt{(\ell+s)(\ell-s+1)}\, {}_{s-1}Y_\ell^m(\theta,\phi)\Big] {}_{s'}Y_\ell^{m*}(\theta',\phi') \Bigg\} \sin\theta - s\,(-1)^s \cos\theta \sum_{m=-\ell}^{\ell} {}_sY_\ell^m(\theta,\phi)\, {}_{s'}Y_\ell^{m*}(\theta',\phi'), \quad (5.32)$$

where we have applied the results in Equation (5.7),

$$= \frac{1}{2} \Bigg\{ -\sqrt{(\ell-s)(\ell+s+1)} \sum_{m=-\ell}^{\ell} (-1)^{s+1}\, {}_{s+1}Y_\ell^m(\theta,\phi)\, {}_{s'}Y_\ell^{m*}(\theta',\phi') - \sqrt{(\ell+s)(\ell-s+1)} \sum_{m=-\ell}^{\ell} (-1)^{s-1}\, {}_{s-1}Y_\ell^m(\theta,\phi)\, {}_{s'}Y_\ell^{m*}(\theta',\phi') \Bigg\} \sin\theta - s\,\cos\theta \sum_{m=-\ell}^{\ell} (-1)^s\, {}_sY_\ell^m(\theta,\phi)\, {}_{s'}Y_\ell^{m*}(\theta',\phi'), \quad (5.33)$$

where we have multiplied the factor $(-1)(-1)^s$ inside the parenthesis rearranging and again exploiting the fact that $(-1)^1 = (-1)^{-1} = (-1)$, displaying everything in order to apply the addition theorem,

$$= -\frac{1}{2}\sqrt{\frac{2\ell+1}{4\pi}} \Bigg\{ \sqrt{(\ell-s)(\ell+s+1)}\, \mathrm{e}^{-\mathrm{i}(s+1)\alpha}\, {}_{s+1}Y_\ell^{-s'}(\beta,\gamma) + \sqrt{(\ell+s)(\ell-s+1)}\, \mathrm{e}^{-\mathrm{i}(s-1)\alpha}\, {}_{s-1}Y_\ell^{-s'}(\beta,\gamma) \Bigg\} \sin\theta - s\sqrt{\frac{2\ell+1}{4\pi}}\, \mathrm{e}^{-\mathrm{i}s\alpha}\, {}_sY_\ell^{-s'}(\beta,\gamma)\cos\theta, \quad (5.34)$$

where we applied the result in Equation (5.19).

In both of these derivations we can see the procedure that we will also apply to the other results, utilising the properties of the differential operators ${}_s\eth$ and ${}_s\overline{\eth}$, that we can introduce thanks to Lemma 5.1.3. Notably, we can see how the label $-s'$ stays unchanged throughout the analysis; this is because the operation of raising and lowering the spin s happens when applying ${}_s\eth$ and ${}_s\overline{\eth}$, as shown in Equation (5.7). In Theorem 5.3.2, the evaluation is a bit more convoluted because the result in Lemma 5.1.3 introduces an additional factor depending on θ. In the following analysis we will not proceed step by step but we will highlight main differences on the derivation.

5.3.3 Theorem. *The new addition theorem obtained when taking a derivative with respect to θ on one term and θ' on the other term is:*

$$
\begin{aligned}
&(-1)^s \sum_{m=-\ell}^{\ell} \left[\frac{\partial}{\partial\theta}{}_sY_\ell^m(\theta,\phi)\right]\left[\frac{\partial}{\partial\theta'}{}_{s'}Y_\ell^{m*}(\theta',\phi')\right] \\
&\quad = -\frac{1}{4}\sqrt{\frac{2\ell+1}{4\pi}}\Bigg[\sqrt{(\ell-s)(\ell+s+1)(\ell-s')(\ell+s'+1)}\,\mathrm{e}^{-\mathrm{i}(s+1)\alpha}{}_{s+1}Y_\ell^{-s'-1}(\beta,\gamma) \\
&\qquad - \sqrt{(\ell-s)(\ell+s+1)(\ell+s')(\ell-s'+1)}\,\mathrm{e}^{-\mathrm{i}(s+1)\alpha}{}_{s+1}Y_\ell^{-s'+1}(\beta,\gamma) \\
&\qquad - \sqrt{(\ell+s)(\ell-s+1)(\ell-s')(\ell+s'+1)}\,\mathrm{e}^{-\mathrm{i}(s-1)\alpha}{}_{s-1}Y_\ell^{-s'-1}(\beta,\gamma) \\
&\qquad + \sqrt{(\ell+s)(\ell-s+1)(\ell+s')(\ell-s'+1)}\,\mathrm{e}^{-\mathrm{i}(s-1)\alpha}{}_{s-1}Y_\ell^{-s'+1}(\beta,\gamma)\Bigg], \qquad (5.35)
\end{aligned}
$$

Its derivation and proof can be obtained from the following calculation:

$$
\begin{aligned}
&(-1)^s \sum_{m=-\ell}^{\ell} \left[\frac{\partial}{\partial\theta}{}_sY_\ell^m(\theta,\phi)\right]\left[\frac{\partial}{\partial\theta'}{}_{s'}Y_\ell^{m*}(\theta',\phi')\right] \\
&\qquad = \frac{(-1)^s}{4}\sum_{m=-\ell}^{\ell}\left[{}_s\eth\,{}_sY_\ell^m(\theta,\phi) + {}_s\overline{\eth}\,{}_sY_\ell^m(\theta,\phi)\right] \\
&\qquad\qquad \times \left[{}_{s'}\eth'\,{}_sY_\ell^m(\theta',\phi') + {}_{s'}\overline{\eth}'\,{}_sY_\ell^m(\theta',\phi')\right]^* \\
&= \frac{(-1)^s}{4}\sum_{m=-\ell}^{\ell}\left[\sqrt{(\ell-s)(\ell+s+1)}\,{}_{s+1}Y_\ell^m(\theta,\phi) - \sqrt{(\ell+s)(\ell-s+1)}\,{}_{s-1}Y_\ell^m(\theta,\phi)\right] \\
&\quad \times \left[\sqrt{(\ell-s')(\ell+s'+1)}\,{}_{s'+1}Y_\ell^{m*}(\theta',\phi') - \sqrt{(\ell+s')(\ell-s'+1)}\,{}_{s'-1}Y_\ell^{m*}(\theta',\phi')\right] \\
&= -\frac{1}{4}\sum_{m=-\ell}^{\ell}\Bigg\{\sqrt{(\ell-s)(\ell+s+1)(\ell-s')(\ell+s'+1)}\,(-1)^{s+1}{}_{s+1}Y_\ell^m(\theta,\phi){}_{s'+1}Y_\ell^{m*}(\theta',\phi') \\
&\qquad - \sqrt{(\ell-s)(\ell+s+1)(\ell+s')(\ell-s'+1)}\,(-1)^{s+1}{}_{s+1}Y_\ell^m(\theta,\phi){}_{s'-1}Y_\ell^{m*}(\theta',\phi') \\
&\qquad - \sqrt{(\ell+s)(\ell-s+1)(\ell-s')(\ell+s'+1)}\,(-1)^{s-1}{}_{s-1}Y_\ell^m(\theta,\phi){}_{s'+1}Y_\ell^{m*}(\theta',\phi') \\
&\qquad + \sqrt{(\ell+s)(\ell-s+1)(\ell+s')(\ell-s'+1)}\,(-1)^{s-1}{}_{s-1}Y_\ell^m(\theta,\phi){}_{s'-1}Y_\ell^{m*}(\theta',\phi')\Bigg\}
\end{aligned}
$$

$$
\begin{aligned}
&= -\frac{1}{4}\sqrt{\frac{2\ell+1}{4\pi}}\Big[\sqrt{(\ell-s)(\ell+s+1)(\ell-s')(\ell+s'+1)}\,\mathrm{e}^{-\mathrm{i}(s+1)\alpha}{}_{s+1}Y_\ell^{-s'-1}(\beta,\gamma)\\
&\quad-\sqrt{(\ell-s)(\ell+s+1)(\ell+s')(\ell-s'+1)}\,\mathrm{e}^{-\mathrm{i}(s+1)\alpha}{}_{s+1}Y_\ell^{-s'+1}(\beta,\gamma)\\
&\quad-\sqrt{(\ell+s)(\ell-s+1)(\ell-s')(\ell+s'+1)}\,\mathrm{e}^{-\mathrm{i}(s-1)\alpha}{}_{s-1}Y_\ell^{-s'-1}(\beta,\gamma)\\
&\quad+\sqrt{(\ell+s)(\ell-s+1)(\ell+s')(\ell-s'+1)}\,\mathrm{e}^{-\mathrm{i}(s-1)\alpha}{}_{s-1}Y_\ell^{-s'+1}(\beta,\gamma)\Big], \quad (5.36)
\end{aligned}
$$

where we can see that we have used for the first time the differential operators ${}_{s'}\eth'$ and ${}_{s'}\overline{\eth}'$ defined in Equation (5.9).

5.3.4 Theorem. *The new addition theorem obtained when taking a derivative with respect to ϕ on one term and ϕ' on the other term is:*

$$
\begin{aligned}
&(-1)^s\sum_{m=-\ell}^{\ell} m^2\,{}_sY_\ell^m(\theta,\phi)\,{}_{s'}Y_\ell^{m*}(\theta',\phi') = (-1)^s\sum_{m=-\ell}^{\ell}\left[\frac{\partial}{\partial\phi}{}_sY_\ell^m(\theta,\phi)\right]\left[\frac{\partial}{\partial\phi'}{}_{s'}Y_\ell^{m*}(\theta',\phi')\right]\\
&= -\sqrt{\frac{2\ell+1}{4\pi}}\Bigg\{\frac{1}{4}\sin\theta\,\sin\theta'\Big[\sqrt{(\ell-s)(\ell+s+1)(\ell-s')(\ell+s'+1)}\,\mathrm{e}^{-\mathrm{i}(s+1)\alpha}{}_{s+1}Y_\ell^{-s'-1}(\beta,\gamma)\\
&\quad+\sqrt{(\ell-s)(\ell+s+1)(\ell+s')(\ell-s'+1)}\,\mathrm{e}^{-\mathrm{i}(s+1)\alpha}{}_{s+1}Y_\ell^{-s'+1}(\beta,\gamma)\\
&\quad+\sqrt{(\ell+s)(\ell-s+1)(\ell-s')(\ell+s'+1)}\,\mathrm{e}^{-\mathrm{i}(s-1)\alpha}{}_{s-1}Y_\ell^{-s'-1}(\beta,\gamma)\\
&\quad+\sqrt{(\ell+s)(\ell-s+1)(\ell+s')(\ell-s'+1)}\,\mathrm{e}^{-\mathrm{i}(s-1)\alpha}{}_{s-1}Y_\ell^{-s'+1}(\beta,\gamma)\Big]\\
&\quad-\frac{s'}{2}\sin\theta\,\cos\theta'\Big[\sqrt{(\ell-s)(\ell+s+1)}\,\mathrm{e}^{-\mathrm{i}(s+1)\alpha}{}_{s+1}Y_\ell^{-s'}(\beta,\gamma)\\
&\quad+\sqrt{(\ell+s)(\ell-s+1)}\,\mathrm{e}^{-\mathrm{i}(s-1)\alpha}{}_{s-1}Y_\ell^{-s'}(\beta,\gamma)\Big]\\
&\quad+\frac{s}{2}\cos\theta\,\sin\theta'\Big[\sqrt{(\ell-s')(\ell+s'+1)}\,\mathrm{e}^{-\mathrm{i}s\alpha}{}_sY_\ell^{-s'-1}(\beta,\gamma)\\
&\quad+\sqrt{(\ell+s')(\ell-s'+1)}\,\mathrm{e}^{-\mathrm{i}s\alpha}{}_sY_\ell^{-s'+1}(\beta,\gamma)\Big]-ss'\,\mathrm{e}^{-\mathrm{i}s\alpha}{}_sY_\ell^{-s'}(\beta,\gamma)\cos\theta\,\cos\theta'\Bigg\}.
\end{aligned}
$$

Its derivation and proof can be obtained from the following calculation:

$$
\begin{aligned}
&(-1)^s\sum_{m=-\ell}^{\ell} m^2\,{}_sY_\ell^m(\theta,\phi)\,{}_{s'}Y_\ell^{m*}(\theta',\phi') = (-1)^s\sum_{m=-\ell}^{\ell}\left[\frac{\partial}{\partial\phi}{}_sY_\ell^m(\theta,\phi)\right]\left[\frac{\partial}{\partial\phi'}{}_{s'}Y_\ell^{m*}(\theta',\phi')\right]\\
&\quad=(-1)^s\sum_{m=-\ell}^{\ell}\left\{\frac{\mathrm{i}}{2}\sin\theta\left[{}_s\eth\,-{}_s\overline{\eth}\right]{}_sY_\ell^m(\theta,\phi)-\mathrm{i}\,s\cos\theta\,{}_sY_\ell^m(\theta,\phi)\right\}\\
&\quad\times\left\{\frac{\mathrm{i}}{2}\sin\theta'\left[{}_{s'}\eth'-{}_{s'}\overline{\eth}'\right]{}_{s'}Y_\ell^m(\theta',\phi')-\mathrm{i}\,s'\cos\theta'\,{}_{s'}Y_\ell^m(\theta',\phi')\right\}^*\\
&\quad=(-1)^s\sum_{m=-\ell}^{\ell}\left\{\frac{\mathrm{i}}{2}\sin\theta\left[\sqrt{(\ell-s)(\ell+s+1)}\,{}_{s+1}Y_\ell^m(\theta,\phi)\right.\right.\\
&\quad\left.\left.+\sqrt{(\ell+s)(\ell-s+1)}\,{}_{s-1}Y_\ell^m(\theta,\phi)\right]-\mathrm{i}\,s\cos\theta\,{}_sY_\ell^m(\theta,\phi)\right\}
\end{aligned}
$$

$$\times \left\{ -\frac{\mathrm{i}}{2}\sin\theta' \left[\sqrt{(\ell-s')(\ell+s'+1)}\,{}_{s'+1}Y_\ell^{m*}(\theta',\phi') \right.\right.$$

$$\left.\left. + \sqrt{(\ell+s')(\ell-s'+1)}\,{}_{s'-1}Y_\ell^{m*}(\theta',\phi') \right] + \mathrm{i}\,s'\cos\theta'\,{}_{s'}Y_\ell^{m*}(\theta',\phi') \right\}$$

$$= -\sum_{m=-\ell}^{\ell} \left\{ \frac{1}{4}\sin\theta\,\sin\theta' \left[\sqrt{(\ell-s)(\ell+s+1)(\ell-s')(\ell+s'+1)}\,(-1)^{s+1}\,{}_{s+1}Y_\ell^{m}(\theta,\phi)\,{}_{s'+1}Y_\ell^{m*}(\theta',\phi') \right.\right.$$

$$- \sqrt{(\ell-s)(\ell+s+1)(\ell+s')(\ell-s'+1)}\,(-1)^{s+1}\,{}_{s+1}Y_\ell^{m}(\theta,\phi)\,{}_{s'-1}Y_\ell^{m*}(\theta',\phi')$$

$$- \sqrt{(\ell+s)(\ell-s+1)(\ell-s')(\ell+s'+1)}\,(-1)^{s-1}\,{}_{s-1}Y_\ell^{m}(\theta,\phi)\,{}_{s'+1}Y_\ell^{m*}(\theta',\phi')$$

$$\left.\left. + \sqrt{(\ell+s)(\ell-s+1)(\ell+s')(\ell-s'+1)}\,(-1)^{s-1}\,{}_{s-1}Y_\ell^{m}(\theta,\phi)\,{}_{s'-1}Y_\ell^{m*}(\theta',\phi') \right]$$

$$- \frac{s'}{2}\sin\theta\,\cos\theta' \left[\sqrt{(\ell-s)(\ell+s+1)}\,(-1)^{s+1}\,{}_{s+1}Y_\ell^{m}(\theta,\phi) \right.$$

$$\left. + \sqrt{(\ell+s)(\ell-s+1)}\,(-1)^{s-1}\,{}_{s-1}Y_\ell^{m}(\theta,\phi) \right]\,{}_{s'}Y_\ell^{m*}(\theta',\phi')$$

$$+ \frac{s}{2}\cos\theta\,\sin\theta' \left[\sqrt{(\ell-s')(\ell+s'+1)}\,{}_{s'+1}Y_\ell^{m*}(\theta',\phi') \right.$$

$$\left. + \sqrt{(\ell+s')(\ell-s'+1)}\,{}_{s'-1}Y_\ell^{m*}(\theta',\phi') \right]\,(-1)^{s}\,{}_{s}Y_\ell^{m}(\theta,\phi)$$

$$\left. - ss'\,(-1)^{s}\,{}_{s}Y_\ell^{m}(\theta,\phi)\,{}_{s'}Y_\ell^{m*}(\theta',\phi')\cos\theta\,\cos\theta' \right\}$$

$$= -\sqrt{\frac{2\ell+1}{4\pi}} \left\{ \frac{1}{4}\sin\theta\,\sin\theta' \left[\sqrt{(\ell-s)(\ell+s+1)(\ell-s')(\ell+s'+1)}\,\mathrm{e}^{-\mathrm{i}(s+1)\alpha}\,{}_{s+1}Y_\ell^{-s'-1}(\beta,\gamma) \right.\right.$$

$$+ \sqrt{(\ell-s)(\ell+s+1)(\ell+s')(\ell-s'+1)}\,\mathrm{e}^{-\mathrm{i}(s+1)\alpha}\,{}_{s+1}Y_\ell^{-s'+1}(\beta,\gamma)$$

$$+ \sqrt{(\ell+s)(\ell-s+1)(\ell-s')(\ell+s'+1)}\,\mathrm{e}^{-\mathrm{i}(s-1)\alpha}\,{}_{s-1}Y_\ell^{-s'-1}(\beta,\gamma)$$

$$\left.\left. + \sqrt{(\ell+s)(\ell-s+1)(\ell+s')(\ell-s'+1)}\,\mathrm{e}^{-\mathrm{i}(s-1)\alpha}\,{}_{s-1}Y_\ell^{-s'+1}(\beta,\gamma) \right]$$

$$- \frac{s'}{2}\sin\theta\,\cos\theta' \left[\sqrt{(\ell-s)(\ell+s+1)}\,\mathrm{e}^{-\mathrm{i}(s+1)\alpha}\,{}_{s+1}Y_\ell^{-s'}(\beta,\gamma) \right.$$

$$\left. + \sqrt{(\ell+s)(\ell-s+1)}\,\mathrm{e}^{-\mathrm{i}(s-1)\alpha}\,{}_{s-1}Y_\ell^{-s'}(\beta,\gamma) \right]$$

$$+ \frac{s}{2}\cos\theta\,\sin\theta' \left[\sqrt{(\ell-s')(\ell+s'+1)}\,\mathrm{e}^{-\mathrm{i}s\alpha}\,{}_{s}Y_\ell^{-s'-1}(\beta,\gamma) \right.$$

$$\left. \left. + \sqrt{(\ell+s')(\ell-s'+1)}\,\mathrm{e}^{-\mathrm{i}s\alpha}\,{}_{s}Y_\ell^{-s'+1}(\beta,\gamma) \right] - ss'\,\mathrm{e}^{-\mathrm{i}s\alpha}\,{}_{s}Y_\ell^{-s'}(\beta,\gamma)\cos\theta\,\cos\theta' \right\}.$$

5.3.5 Theorem. *The new addition theorem obtained when multiplying by m and taking a derivative respect to θ on one term is:*

$$(-1)^s \sum_{m=-\ell}^{\ell} m\Big[\frac{\partial}{\partial\theta}\,{}_{s}Y_\ell^{m}(\theta,\phi)\Big]\,{}_{s'}Y_\ell^{m*}(\theta',\phi')$$

$$= -\frac{1}{4}\sqrt{\frac{2\ell+1}{4\pi}} \left\{ \left[\sqrt{(\ell-s)(\ell+s+1)(\ell-s')(\ell+s'+1)}\,\mathrm{e}^{-\mathrm{i}(s+1)\alpha}\,{}_{s+1}Y_\ell^{-s'-1}(\beta,\gamma) \right.\right.$$

$$\left. - \sqrt{(\ell+s)(\ell-s+1)(\ell-s')(\ell+s'+1)}\,\mathrm{e}^{-\mathrm{i}(s-1)\alpha}\,{}_{s-1}Y_\ell^{-s'-1}(\beta,\gamma) \right.$$

$$+\sqrt{(\ell-s)(\ell+s+1)(\ell+s')(\ell-s'+1)}\,\mathrm{e}^{-\mathrm{i}(s+1)\alpha}{}_{s+1}Y_\ell^{-s'+1}(\beta,\gamma)$$
$$-\sqrt{(\ell+s)(\ell-s+1)(\ell+s')(\ell-s'+1)}\,\mathrm{e}^{-\mathrm{i}(s-1)\alpha}{}_{s-1}Y_\ell^{-s'+1}(\beta,\gamma)\Big]\sin\theta'$$
$$-2s'\Big[\sqrt{(\ell-s)(\ell+s+1)}\,\mathrm{e}^{-\mathrm{i}(s+1)\alpha}{}_{s+1}Y_\ell^{-s'}(\beta,\gamma)$$
$$-\sqrt{(\ell+s)(\ell-s+1)}\,\mathrm{e}^{-\mathrm{i}(s-1)\alpha}{}_{s-1}Y_\ell^{-s'}(\beta,\gamma)\Big]\cos\theta'\Big\}. \quad (5.37)$$

Its derivation and proof can be obtained from the following calculation:

$$(-1)^s\sum_{m=-\ell}^{\ell} m\Big[\frac{\partial}{\partial\theta}{}_sY_\ell^m(\theta,\phi)\Big]{}_{s'}Y_\ell^{m*}(\theta',\phi')$$
$$=\mathrm{i}\,(-1)^s\sum_{m=-\ell}^{\ell}\Big[\frac{\partial}{\partial\theta}{}_sY_\ell^m(\theta,\phi)\Big]\Big[\frac{\partial}{\partial\phi'}{}_{s'}Y_\ell^{m*}(\theta',\phi')\Big]$$
$$=-\frac{\mathrm{i}}{2}\,(-1)^s\sum_{m=-\ell}^{\ell}\Big[{}_s\eth\;{}_sY_\ell^m(\theta,\phi)+{}_s\overline{\eth}\;{}_sY_\ell^m(\theta,\phi)\Big]$$
$$\times\Big\{\frac{\mathrm{i}}{2}\sin\theta'\Big[{}_{s'}\eth'-{}_{s'}\overline{\eth}'\Big]{}_{s'}Y_\ell^m(\theta',\phi')-\mathrm{i}\,s'\cos\theta'\,{}_{s'}Y_\ell^m(\theta',\phi')\Big\}^*$$
$$=\frac{(-1)^s}{4}\sum_{m=-\ell}^{\ell}\Big[\sqrt{(\ell-s)(\ell+s+1)}\,{}_{s+1}Y_\ell^m(\theta,\phi)-\sqrt{(\ell+s)(\ell-s+1)}\,{}_{s-1}Y_\ell^m(\theta,\phi)\Big]$$
$$\times\Big\{\Big[\sqrt{(\ell-s')(\ell+s'+1)}\,{}_{s'+1}Y_\ell^{m*}(\theta',\phi')$$
$$+\sqrt{(\ell+s')(\ell-s'+1)}\,{}_{s'-1}Y_\ell^{m*}(\theta',\phi')\Big]\sin\theta'-2s'\cos\theta'\,{}_{s'}Y_\ell^{m*}(\theta',\phi')\Big\}$$
$$=-\frac{1}{4}\sum_{m=-\ell}^{\ell}\Big\{\Big[\sqrt{(\ell-s)(\ell+s+1)(\ell-s')(\ell+s'+1)}\,(-1)^{s+1}{}_{s+1}Y_\ell^m(\theta,\phi)$$
$$-\sqrt{(\ell+s)(\ell-s+1)(\ell-s')(\ell+s'+1)}\,(-1)^{s-1}{}_{s-1}Y_\ell^m(\theta,\phi)$$
$$+\sqrt{(\ell-s)(\ell+s+1)(\ell+s')(\ell-s'+1)}\,(-1)^{s+1}{}_{s+1}Y_\ell^m(\theta,\phi)$$
$$-\sqrt{(\ell+s)(\ell-s+1)(\ell+s')(\ell-s'+1)}\,(-1)^{s-1}{}_{s-1}Y_\ell^m(\theta,\phi)\Big]\sin\theta'$$
$$-2s'\Big[\sqrt{(\ell-s)(\ell+s+1)}\,(-1)^{s+1}{}_{s+1}Y_\ell^m(\theta,\phi)$$
$$-\sqrt{(\ell+s)(\ell-s+1)}\,(-1)^{s-1}{}_{s-1}Y_\ell^m(\theta,\phi)\Big]{}_{s'}Y_\ell^{m*}(\theta',\phi')\cos\theta'\Big\}$$
$$=-\frac{1}{4}\sqrt{\frac{2\ell+1}{4\pi}}\Big\{\Big[\sqrt{(\ell-s)(\ell+s+1)(\ell-s')(\ell+s'+1)}\,\mathrm{e}^{-\mathrm{i}(s+1)\alpha}{}_{s+1}Y_\ell^{-s'-1}(\beta,\gamma)$$
$$-\sqrt{(\ell+s)(\ell-s+1)(\ell-s')(\ell+s'+1)}\,\mathrm{e}^{-\mathrm{i}(s-1)\alpha}{}_{s-1}Y_\ell^{-s'-1}(\beta,\gamma)$$

$$+\sqrt{(\ell-s)(\ell+s+1)(\ell+s')(\ell-s'+1)}\,\mathrm{e}^{-\mathrm{i}(s+1)\alpha}{}_{s+1}Y_\ell^{-s'+1}(\beta,\gamma)$$
$$-\sqrt{(\ell+s)(\ell-s+1)(\ell+s')(\ell-s'+1)}\,\mathrm{e}^{-\mathrm{i}(s-1)\alpha}{}_{s-1}Y_\ell^{-s'+1}(\beta,\gamma)\Big]\sin\theta'$$
$$-2s'\Big[\sqrt{(\ell-s)(\ell+s+1)}\,\mathrm{e}^{-\mathrm{i}(s+1)\alpha}{}_{s+1}Y_\ell^{-s'}(\beta,\gamma)$$
$$-\sqrt{(\ell+s)(\ell-s+1)}\,\mathrm{e}^{-\mathrm{i}(s-1)\alpha}{}_{s-1}Y_\ell^{-s'}(\beta,\gamma)\Big]\cos\theta'\Big\}. \quad (5.38)$$

The addition theorems just presented all involve one derivative of a spin-weighted spherical harmonics. Similar theorems involving two or more derivatives acting on the same spin-weighted spherical harmonics can be deduced from the above, together with the differential equation governing the spin-weighted spherical harmonics [3, 56, 99, 118, 129]

$$\Big\{\frac{1}{\sin\theta}\,\partial_\theta\Big[\sin\theta\,\partial_\theta\Big]-\frac{1}{\sin^2\theta}\Big[s^2-2\mathrm{i}\,s\cos\theta\,\partial_\phi-\partial_\phi^2\Big]\Big\}\,{}_sY_\ell^m(\theta,\phi)=$$
$$=-\ell\Big[\ell+1\Big]\,{}_sY_\ell^m(\theta,\phi). \quad (5.39)$$

We will now take the coincidence limit $\theta'=\theta$, $\phi'=\phi$ in each of the results in the previous equations. We will explain the first result step by step, while for the following ones we will highlight the differences in the same manner as we did previously. Using Equation (5.20), Theorems 5.3.2, 5.3.1, 5.3.4, 5.3.3 and 5.3.5 gives:

5.3.6 Corollary.

$$\sum_{m=-\ell}^{\ell}\Big[\frac{\partial}{\partial\theta}\,{}_sY_\ell^m(\theta,\phi)\Big]\,{}_{s'}Y_\ell^{m*}(\theta,\phi)$$
$$=\frac{1}{2}\sqrt{\frac{2\ell+1}{4\pi}}\Big\{\sqrt{(\ell-s)(\ell+s+1)}\,\mathrm{e}^{-\mathrm{i}(s+1)\alpha}{}_{s+1}Y_\ell^{-s'}(\beta,\gamma)$$
$$-\sqrt{(\ell+s)(\ell-s+1)}\,\mathrm{e}^{-\mathrm{i}(s-1)\alpha}{}_{s-1}Y_\ell^{-s'}(\beta,\gamma)\Big\}, \quad (5.40)$$

where we have used the result of Theorem 5.3.1,

$$=\frac{1}{2}\sqrt{\frac{2\ell+1}{4\pi}}\Big\{\sqrt{(\ell-s)(\ell+s+1)}\,\mathrm{e}^{-\mathrm{i}(s+1)\alpha}{}_{s+1}Y_\ell^{-s'}(0,0)$$
$$-\sqrt{(\ell+s)(\ell-s+1)}\,\mathrm{e}^{-\mathrm{i}(s-1)\alpha}{}_{s-1}Y_\ell^{-s'}(0,0)\Big\}, \quad (5.41)$$

where we have taken the coincidence limit that takes the Euler angles to be zero as previously mentioned,

$$=\frac{2\ell+1}{8\pi}\Big\{\sqrt{(\ell-s)(\ell+s+1)}\,\delta_{s+1,s'}-\sqrt{(\ell+s)(\ell-s+1)}\,\delta_{s-1,s'}\Big\}, \quad (5.42)$$

where we have used the result in Equation (5.20),

$$= -\frac{2\ell+1}{8\pi}\left\{\sqrt{(\ell-s)(\ell+s+1)}\,\delta_{s+1,s'} - \sqrt{(\ell-s')(\ell+s'+1)}\,\delta_{s,s'+1}\right\}, \tag{5.43}$$

where we have used $\delta_{s-1,s'} = \delta_{s,s'+1}$ in order to make the result symmetric in s and s' and replaced s by $s'+1$ in the second form.

5.3.7 Corollary.

$$\begin{aligned}\sum_{m=-\ell}^{\ell} m\,{}_sY_\ell^m(\theta,\phi)\,{}_{s'}Y_\ell^{m*}(\theta,\phi)&\\ = -\frac{1}{2}\sqrt{\frac{2\ell+1}{4\pi}}\Bigg\{&\sqrt{(\ell-s)(\ell+s+1)}\,\mathrm{e}^{-\mathrm{i}(s+1)\alpha}\,{}_{s+1}Y_\ell^{-s'}(\beta,\gamma)\\ &+\sqrt{(\ell+s)(\ell-s+1)}\,\mathrm{e}^{-\mathrm{i}(s-1)\alpha}\,{}_{s-1}Y_\ell^{-s'}(\beta,\gamma)\Bigg\}\sin\theta\\ &-s\sqrt{\frac{2\ell+1}{4\pi}}\,\mathrm{e}^{-\mathrm{i}s\alpha}\,{}_sY_\ell^{-s'}(\beta,\gamma)\cos\theta,\end{aligned} \tag{5.44}$$

where we have used the result of Theorem 5.3.2,

$$\begin{aligned}= \frac{2\ell+1}{8\pi}\Bigg\{&\sqrt{(\ell-s)(\ell+s+1)}\,\delta_{s+1,s'}\\ &+\sqrt{(\ell-s')(\ell+s'+1)}\,\delta_{s,s'+1}\Bigg\}\sin\theta - \frac{2\ell+1}{4\pi}s\,\delta_{s,s'}\cos\theta,\end{aligned} \tag{5.45}$$

where we have used the same steps as in Corollary 5.3.6.

5.3.8 Corollary.

$$\begin{aligned}\sum_{m=-\ell}^{\ell}\left[\frac{\partial}{\partial\theta}{}_sY_\ell^m(\theta,\phi)\right]\left[\frac{\partial}{\partial\theta}{}_{s'}Y_\ell^{m*}(\theta,\phi)\right]&\\ = -\frac{1}{4}\sqrt{\frac{2\ell+1}{4\pi}}\Bigg[&\sqrt{(\ell-s)(\ell+s+1)(\ell-s')(\ell+s'+1)}\,\mathrm{e}^{-\mathrm{i}(s+1)\alpha}\,{}_{s+1}Y_\ell^{-s'-1}(\beta,\gamma)\\ &-\sqrt{(\ell-s)(\ell+s+1)(\ell+s')(\ell-s'+1)}\,\mathrm{e}^{-\mathrm{i}(s+1)\alpha}\,{}_{s+1}Y_\ell^{-s'+1}(\beta,\gamma)\\ &-\sqrt{(\ell+s)(\ell-s+1)(\ell-s')(\ell+s'+1)}\,\mathrm{e}^{-\mathrm{i}(s-1)\alpha}\,{}_{s-1}Y_\ell^{-s'-1}(\beta,\gamma)\\ &+\sqrt{(\ell+s)(\ell-s+1)(\ell+s')(\ell-s'+1)}\,\mathrm{e}^{-\mathrm{i}(s-1)\alpha}\,{}_{s-1}Y_\ell^{-s'+1}(\beta,\gamma)\Bigg],\end{aligned} \tag{5.46}$$

where we used the result of Theorem 5.3.3,

$$= -\frac{2\ell+1}{16\pi}\Bigg[\sqrt{(\ell-s)(\ell+s+1)(\ell-s')(\ell+s'+1)}\,\delta_{s+1,s'+1} - \sqrt{(\ell-s)(\ell+s+1)(\ell+s')(\ell-s'+1)}\,\delta_{s+1,s'-1} - \sqrt{(\ell+s)(\ell-s+1)(\ell-s')(\ell+s'+1)}\,\delta_{s-1,s'+1} + \sqrt{(\ell+s)(\ell-s+1)(\ell+s')(\ell-s'+1)}\,\delta_{s-1,s'-1}\Bigg], \quad (5.47)$$

where we have used the coincidence limit and the result in Equation (5.20),

$$= \frac{2\ell+1}{16\pi}\Bigg[2\Big(\ell^2+\ell-s^2\Big)\,\delta_{s,s'} - \sqrt{(\ell-s)(\ell+s+1)(\ell+s')(\ell-s'+1)}\,\delta_{s+1,s'-1} - \sqrt{(\ell+s)(\ell-s+1)(\ell-s')(\ell+s'+1)}\,\delta_{s-1,s'+1}\Bigg], \quad (5.48)$$

where we have used the fact that $\delta_{s+1,s'+1} = \delta_{s,s'}$ and $\delta_{s-1,s'-1} = \delta_{s,s'}$,

$$= \frac{2\ell+1}{16\pi}\Bigg[2\Big(\ell^2+\ell-s^2\Big)\,\delta_{s,s'} - \sqrt{(\ell-s-1)(\ell-s)(\ell+s+1)(\ell+s+2)}\,\delta_{s+2,s'} - \sqrt{(\ell-s'-1)(\ell-s')(\ell+s'+1)(\ell+s'+2)}\,\delta_{s,s'+2}\Bigg], \quad (5.49)$$

where we have substituted s' with $s+2$ in the coefficient of $\delta_{s+2,s'}$ and replaced s by $s'+2$ in the coefficient of $\delta_{s,s'+2}$, using the fact that $\delta_{s+1,s'-1} = \delta_{s+2,s'}$ and $\delta_{s-1,s'+1} = \delta_{s,s'+2}$.

5.3.9 Corollary.

$$\sum_{m=-\ell}^{\ell} m^2\,{}_sY_\ell^m(\theta,\phi)\,{}_{s'}Y_\ell^{m*}(\theta,\phi) = \frac{2\ell+1}{4\pi}\Bigg\{\Big[\frac{1}{2}\Big(\ell^2+\ell-s^2\Big)\sin^2\theta + s^2\cos^2\theta\Big]\,\delta_{s,s'} + \frac{1}{4}\sin^2\theta\Bigg[\sqrt{(\ell-s)(\ell+s+1)(\ell+s')(\ell-s'+1)}\,\delta_{s+1,s'-1} + \sqrt{(\ell+s)(\ell-s+1)(\ell-s')(\ell+s'+1)}\,\delta_{s-1,s'+1}\Bigg] - \frac{1}{2}\sin\theta\cos\theta\Bigg[\Big(2s'+1\Big)\sqrt{(\ell-s')(\ell+s'+1)}\,\delta_{s,s'+1} + \Big(2s+1\Big)\sqrt{(\ell-s)(\ell+s+1)}\,\delta_{s+1,s'}\Bigg]\Bigg\}, \quad (5.50)$$

where this is the result starting from Theorem 5.3.4.

5.3.10 Corollary.

$$\sum_{m=-\ell}^{\ell} m \left[\frac{\partial}{\partial\theta}{}_sY_\ell^m(\theta,\phi)\right] {}_{s'}Y_\ell^{m*}(\theta,\phi)$$
$$= \frac{2\ell+1}{16\pi}\Bigg\{\Bigg[-2s\,\delta_{s,s'}$$
$$- \sqrt{(\ell-s'-1)(\ell-s')(\ell+s'+1)(\ell+s'+2)}\,\delta_{s,s'+2}$$
$$+ \sqrt{(\ell-s-1)(\ell-s)(\ell+s+1)(\ell+s+2)}\,\delta_{s+2,s'}\Bigg]\sin\theta$$
$$- 2s'\Bigg[\sqrt{(\ell-s)(\ell+s+1)}\,\delta_{s+1,s'}$$
$$- \sqrt{(\ell-s')(\ell+s'+1)}\,\delta_{s,s'+1}\Bigg]\cos\theta\Bigg\}, \quad (5.51)$$

where this is the result starting from Theorem 5.3.5.

We have attempted to put every result in a symmetric expression in (s, s'), however, the last Corollary 5.3.10 is not symmetric.

Finally, if we also set the spins equal, $s' = s$, which is the case we will be interest in studying later in the thesis, the results reduce further, giving, respectively:

5.3.11 Corollary.

$$\sum_{m=-\ell}^{\ell}\left[\frac{\partial}{\partial\theta}{}_sY_\ell^m(\theta,\phi)\right]{}_sY_\ell^{m*}(\theta,\phi) = 0, \quad (5.52a)$$

$$\sum_{m=-\ell}^{\ell} m\,|{}_sY_\ell^m(\theta,\phi)|^2 = -\frac{(2\ell+1)\,s}{4\pi}\cos\theta, \quad (5.52b)$$

$$\sum_{m=-\ell}^{\ell}\left|\frac{\partial}{\partial\theta}{}_sY_\ell^m(\theta,\phi)\right|^2 = \frac{2\ell+1}{8\pi}\left(\ell^2+\ell-s^2\right), \quad (5.52c)$$

$$\sum_{m=-\ell}^{\ell} m^2\,|{}_sY_\ell^m(\theta,\phi)|^2 = \frac{2\ell+1}{8\pi}\left[\left(\ell^2+\ell-s^2\right)\sin^2\theta + 2s^2\cos^2\theta\right], \quad (5.52d)$$

$$\sum_{m=-\ell}^{\ell} m\left[\frac{\partial}{\partial\theta}{}_sY_\ell^m(\theta,\phi)\right]{}_sY_\ell^{m*}(\theta,\phi) = -\frac{(2\ell+1)\,s}{8\pi}\sin\theta. \quad (5.52e)$$

Our results hold for both integer and half-integer spins s. When s is a half-integer, the factor $(-1)^s$ in Equation (5.1) is purely imaginary (see, for example, [15] for specific examples of spin-weighted spherical harmonics in this case). When $s = 0$, the results in Equations (5.52) reduce to

5.3.12 Corollary.

$$\sum_{m=-\ell}^{\ell} \left[\frac{\partial}{\partial\theta}{}_0Y_\ell^m(\theta,\phi)\right] {}_0Y_\ell^{m*}(\theta,\phi) = 0, \tag{5.53a}$$

$$\sum_{m=-\ell}^{\ell} m\ |{}_0Y_\ell^m(\theta,\phi)|^2 = 0, \tag{5.53b}$$

$$\sum_{m=-\ell}^{\ell} \left|\frac{\partial}{\partial\theta}{}_0Y_\ell^m(\theta,\phi)\right|^2 = \frac{2\ell+1}{8\pi}\left(\ell^2+\ell\right), \tag{5.53c}$$

$$\sum_{m=-\ell}^{\ell} m^2\ |{}_0Y_\ell^m(\theta,\phi)|^2 = \frac{2\ell+1}{8\pi}\left[\left(\ell^2+\ell\right)\sin^2\theta\right], \tag{5.53d}$$

$$\sum_{m=-\ell}^{\ell} m\left[\frac{\partial}{\partial\theta}{}_0Y_\ell^m(\theta,\phi)\right] {}_0Y_\ell^{m*}(\theta,\phi) = 0. \tag{5.53e}$$

These results can also be found in Appendix C of [143] (see also [144, §5.10]). Notably, Equation (5.52a) is zero for all s. Although the precise form of the addition theorems in Equations (5.40), (5.44), (5.46), (5.50), and (5.51) depends on the conventions used for defining the spin-weighted spherical harmonics, the final results in Equations (5.52) remain independent of the choice of phase.

Summary

In this chapter, we have presented the main properties of the spin-weighted spherical harmonic functions. We have restricted our attention to the properties needed to prove the addition theorems in Equation (5.19) and to those required to present the new addition theorems that we have derived in Theorems 5.3.1, 5.3.2, 5.3.3, 5.3.4, and 5.3.5. These calculations will be pivotal in simplifying the analysis of the scalar field on a curved background, as we will see in Chapter 6 and 8.

We were able to prove these new addition theorems thanks to the properties of the differential operators ${}_s\eth$ and ${}_s\overline{\eth}$ and also thanks to the differential operators that we have introduced, ${}_{s'}\eth'$ and ${}_{s'}\overline{\eth}'$. We then took the coincidence limit and examined the result when $s = s'$. While all the previous results are general, this particular case is the one that we are going to use in later calculations in the thesis (see Chapter 8).

Chapter 6

Classical scalar field

In this chapter, we will present a comprehensive analysis of the classical scalar field on the black hole spacetime discussed in Chapter 4. Specifically, we will discuss the Klein-Gordon equation on this curved background and outline the procedure for solving it. Our approach follows the work of [43, 57, 85, 109].

In the first section, we will provide a general overview of the Klein-Gordon equation (6.1). We will demonstrate how the separability of this differential equation allows us to find the angular part, which depends on θ, and the radial part, which depends on r, separately.

In the second section, we will present the calculations required to solve the angular part of the Klein-Gordon equation (6.8). We will outline two possible methods for solving it: one using hypergeometric functions, in Section 6.2.1, and another using spin-weighted spherical harmonics, in Section 6.2.2. For the remaining of the thesis, we will use only the solution in the form of spin-weighted spherical harmonics.

In Section 6.3, we will present methods for solving the radial part of the Klein-Gordon equation (6.41), again showing two different approaches. The first method transforms the radial equation into the form of a Schrödinger equation in Section 6.3.1, allowing us to study the potential $V(r)$. This is useful for understanding the behaviour of the scalar field modes, especially near the event horizon. The second method employs the theory of Heun functions. In Section 6.3.2 we will solve the radial part of the Klein-Gordon equation by transforming it into a Heun differential equation, which has known solutions in the form of Heun functions. This solution will be used for the rest of the thesis.

In Section 6.4, we will present the normalization procedure for the scalar field modes and introduce the observable that we will focus on later in the thesis: the classical stress-energy tensor. We will show how the symmetries of the spacetime we are working in simplify the form of the stress-energy tensor.

6.1 Scalar field equation

We now consider a scalar field on Kerr-AdS in five-dimensional spacetime where the line element is given in Equation (4.6). To achieve this, we must solve the Klein-Gordon equation on a curved background, expressed as:

$$\Box\Phi - (\mu^2 + \xi_\Phi R)\Phi = 0, \tag{6.1}$$

where $\Box$ represents the d'Alembertian operator, defined by two covariant derivatives dependent on the Christoffel symbols and, consequently, on the metric of the background itself. In the equation, μ denotes the mass of the scalar field, ξ_Φ is the coupling constant of the scalar field with the curvature of the background, and we also report again $R = -\frac{20}{L^2}$, (4.3), which is the scalar curvature of the spacetime. To simplify the notation, we introduce a parameter

$$\mu_0^2 = (\mu^2 + \xi_\Phi R), \tag{6.2}$$

since R is constant (4.3).

There are two important couplings ξ_Φ: one is the minimal coupling case, where $\xi_\Phi = 0$, and the other is the conformal coupling $\xi_\Phi = \xi_c(D)$, where $\xi_c(D)$ is defined in Equation (2.23) and depends on the number of spacetime dimensions. We report the explicit formula for convenience that can be found in [41]. It is given by:

$$\xi_c(D) = \frac{1}{4}\left(\frac{D-2}{D-1}\right). \tag{6.3}$$

For the five-dimensional case we are considering, this results in $\xi_c(5) = \frac{3}{16}$.

In order to solve the Klein-Gordon equation in curved spacetime, we will use a method called separation of variables. This mathematical method is well known and is frequently used to solve partial differential equations (PDEs). The method assumes that the solution can be written as a product of functions depending only on one variable of the original equation. We assume the form of Φ as reported in [43, 57, 85, 109]:

$$\Phi(r, \theta, \phi, \psi, t) = e^{im\phi + ip\psi - it\omega} X(r) Y(\theta), \tag{6.4}$$

where ω represents the frequency of the field, and m and p are parameters linked to the quantum numbers associated with ϕ and ψ, respectively, with $2m \in \mathbb{Z}$ and $p \in \mathbb{Z}$, given the range of $\phi \in [0, 4\pi)$ and $\psi \in [0, 2\pi)$. Additionally, $Y(\theta)$ and $X(r)$ denote the angular and radial functions in five dimensions respectively. We proceed by writing the Klein-Gordon equation (6.1) as:

$$\frac{1}{\sqrt{-g}}\partial_\mu(\sqrt{-g}\partial^\mu\Phi) - \mu_0^2\Phi = 0. \tag{6.5}$$

Using (6.4) in (6.5), we can rewrite it as:

$$F[r, X(r), X'(r), X''(r)] + G[\theta, Y(\theta), Y'(\theta), Y''(\theta)] = 0, \tag{6.6}$$

where $F[r, X(r), X'(r), X''(r)]$ is the "radial part" of the Klein-Gordon differential equation, depending only on the variable r, and $G[\theta, Y(\theta), Y'(\theta), Y''(\theta)]$ is the "angular part", depending only on the variable θ. We have divided by Φ as in Equation (6.4), which gets rid of the common exponential factor $e^{im\phi+ip\psi-it\omega}$ obtaining a form in Equation (6.6) that only depends on r and θ. Hence, we set one part equal to λ and the other to $-\lambda$:

$$F[r, X(r), X'(r), X''(r)] = \lambda, \quad G[\theta, Y(\theta), Y'(\theta), Y''(\theta)] = -\lambda, \tag{6.7}$$

where λ is the separation constant. In this way, we have used the theory behind the separation of variables to obtain two ordinary differential equations (ODEs) to solve instead of a PDE. In the following sections, we will focus on solving the angular part in Section 6.2 and the radial part in Section 6.3.

6.2 Angular equation

Using Equation (6.5) together with the explicit expressions for the metric and the inverse metric given in Equation (4.11) and Equation (4.12), we can evaluate the box operator and obtain an explicit expression for the function $G[\theta, Y(\theta), Y'(\theta), Y''(\theta)]$. In this section, we will demonstrate how this equation can be solved and discuss the types of solutions it can have. The variety of possible forms of the solution is somewhat hidden in the freedom of choosing the form of the constant λ, which will also affect the radial equation.

6.2.1 Angular equation and hypergeometric function

We start our analysis showing the form of the angular ordinary differential equation:

$$\lambda + \frac{(p-2m)^2}{2(\cos\theta - 1)} - \frac{(p+2m)^2}{2(\cos\theta + 1)} + \frac{4\left[Y''(\theta) + \cot\theta Y'(\theta)\right]}{Y(\theta)} = 0. \tag{6.8}$$

Before we solve Equation (6.8), it is important to highlight that there is an alternative way to do it that we are not going to study in this thesis. In [85], the metric is treated slightly differently, as shown in (4.14). In this case, the authors take full advantage of the metric expression resembling a two-dimensional metric describing CP^1 [152]. They successfully solved the angular equation using the theory of harmonics on CP^N. We are not going to analyse this method in detail, but we verified that our results matched theirs. As we will see later in Section 6.3.1, the behaviour of the radial potential can also be matched with the analysis performed in [85].

To simplify the differential equation (6.8), we introduce a change of variable, setting $x = \cos\theta$. This yields:

$$4\,(1-x^2)^2\,Y''(x) - 8x\,(1-x^2)\,Y'(x) + \left[4mpx - p^2 - 4m^2 + \lambda(1-x^2)\right]Y(x) = 0. \tag{6.9}$$

We identify two regular singular points, one at $x = 1$ and the other at $x = -1$. In this scenario, we can apply the Frobenius method to solve this differential equation in a neighbourhood of each of the regular singular points.

This technique is used to find series solutions to linear differential equations, particularly when the differential equation has a regular singular point, as is the case here. The method extends the power series approach by allowing the solution to take the form of a generalised series, in which each term is multiplied by $(x-\alpha)^{\upsilon}$, where α represents the singular point, and υ may be non-integer. This allows the method to handle equations with regular singular points. The procedure begins by substituting the Frobenius series

$$Y(x) = (x-\alpha)^{\upsilon} \sum_{n=0}^{\infty} a_n (x-\alpha)^n, \tag{6.10}$$

into the differential equation. By balancing terms and equating powers of $(x-\alpha)$, the indicial equation is obtained, and we can determine the coefficients a_n of the series and the value of υ. The coefficient $a_0 \neq 0$ is usually fixed by normalization, and the other coefficients $\{a_n\}_{n\in\mathcal{M}'\setminus\{0\}}$ are computed recursively.

In order to study the behaviour of the solution near the singular points, $\alpha = 1, -1$, we focus only on the leading order term of the series expansion. This approximation leads to the following expression for the solution near $x = \alpha$:

$$Y(x) \sim a_0 (x-\alpha)^{\upsilon}, \tag{6.11}$$

where a_0 is a nonzero constant coefficient, α is the position of the regular singular point, and υ is determined from the indicial equation. Since there are two singular points, we perform the procedure for both, resulting in two distinct values for υ, denoted as σ_θ and τ for $\alpha = +1$ and $\alpha = -1$, respectively. Now we can substitute (6.11) in the Equation (6.9) to find the indicial equation:

$$a_0(x-\alpha)^{\upsilon}\{-4m^2 + 4mpx - p^2 - (x^2-1)\lambda + (x-\alpha)^{-1}[8x(x^2-1)\upsilon] \\ + 4\left(x^2-1\right)^2 (x-\alpha)^{-2}(\upsilon-1)\upsilon\} = 0. \tag{6.12}$$

If we substitute for $\alpha = 1$ and simplify a bit we get the following equation

$$a_0(x-1)^{\sigma_\theta}\{-4m^2 + 4mpx - p^2 + (x+1)[(1-x)\lambda + 4\sigma_\theta(x-1+\sigma_\theta + x\sigma_\theta)]\} = 0, \tag{6.13}$$

while if we substitute for $\alpha = -1$ we get the following equation

$$a_0(x+1)^{\tau}\{-4m^2 + 4mpx - p^2 + (x-1)[-(x+1)\lambda + 4\tau(x+1-\tau + x\tau)]\} = 0. \tag{6.14}$$

We then divide Equation (6.13) and Equation (6.14) by $a_0(x-1)^{\sigma_\theta}$ and $a_0(x+1)^{\tau}$ respectively,

$$-4m^2+4mpx-p^2+(x+1)[(1-x)\lambda+4\sigma_\theta(x-1+\sigma_\theta+x\sigma_\theta)]=0, \tag{6.15}$$
$$-4m^2+4mpx-p^2+(x-1)[-(x+1)\lambda+4\tau(x+1-\tau+x\tau)]=0. \tag{6.16}$$

We then substitute $x=1$ in Equation (6.15) and $x=-1$ in Equation of (6.16), and we obtain

$$\begin{aligned}-4m^2+4mp-p^2+16\sigma_\theta^2=0,\\ -4m^2-4mp-p^2+16\tau^2=0.\end{aligned} \tag{6.17}$$

If we solve the system of equations (6.17) for σ_θ and τ respectively we find:

$$\sigma_\theta=\frac{|p-2m|}{4}\quad \tau=\frac{|p+2m|}{4}, \tag{6.18}$$

where we have chosen σ_θ and τ to be always positive preventing divergences in the angular function $Y(x)$.

From this analysis, we obtain that the solution to the angular equation (6.8) should have the form of:

$$Y(x)=(1-x)^{\sigma_\theta}\ (1+x)^{\tau}\ Z(x), \tag{6.19}$$

where $Z(x)$ is an arbitrary function regular in $x=\pm1$. We introduce a change of coordinate that will aid us in retrieving the hypergeometric differential equation form:

$$w=\frac{x+1}{2}, \tag{6.20}$$

from which we obtain

$$\widetilde{Y}(w)=(2-2w)^{\sigma_\theta}\ (2w)^{\tau}\ Z(w). \tag{6.21}$$

We then substitute this new form of $Y(w)$ in (6.9) and we obtain:

$$\begin{aligned}0=&w(1-w)Z''(w)+(1+2\tau-2w(1+\sigma_\theta+\tau))Z'(w)\\ &+\left\{\frac{4m^2+p^2+4mp(1-2w)}{16(w-1)w}+\right.\\ &\left.\frac{4(-4\tau^2+w^2(\lambda-4(\sigma_\theta+\tau)(1+\sigma_\theta+\tau))+w(-\lambda+4(\sigma_\theta+\tau)(1+2\tau)))}{16(w-1)w}\right\}Z(w)\end{aligned} \tag{6.22}$$

After some computation, we can see that this equation can be simplified into:

$$w(1-w)\ Z''(w)+[c-(a+b+1)w]\ Z'(w)-ab\ Z(w)=0, \tag{6.23}$$

where

$$\begin{aligned}a&=-\frac{1}{2}\sqrt{\lambda+1}+\sigma_\theta+\tau+\frac{1}{2},\\ b&=\frac{1}{2}\sqrt{\lambda+1}+\sigma_\theta+\tau+\frac{1}{2},\\ c&=1+2\tau.\end{aligned} \tag{6.24}$$

Finally, we obtain the solution for the angular equation of the scalar field in terms of hypergeometric function:

$$Y(x) = (1-x)^{\sigma_\theta}\ (1+x)^{\tau}\ {}_2F_1(a,b;c;w), \tag{6.25}$$

where both x and w can be expressed as functions of the variable θ

$$\begin{aligned} x &= \cos(\theta) \\ w &= \frac{\cos(\theta)+1}{2}. \end{aligned} \tag{6.26}$$

The hypergeometric function ${}_2F_1(a,b;c;w)$ is defined by the Gauss series on the disk $|w| < 1$, and by analytic continuation elsewhere. On the circle of convergence, $|w| = 1$, the Gauss series, see [1]

- Converges absolutely when $c - a - b > 0$.
- Converges conditionally when $-1 < c - a - b \leq 0$ for $w \neq 1$.
- Diverges when $c - a - b \leq -1$.

While for $w = 0$ the solution always converges, see [1], for $w = 1$ we are looking at one of the possible three available cases defined above. Now, we determine the eigenvalue for Equation (6.8). We do this using the properties of the hypergeometric function ${}_2F_1$, looking specifically at the behaviour at the singular points [1]:

$$\begin{aligned} &w = 0 \to x = -1 \to {}_2F_1(a,b;c;0) = 1 \\ &w = 1 \to x = +1 \to {}_2F_1(a,b;c;1) \to \infty. \end{aligned} \tag{6.27}$$

In our case we can check that $c - a - b = -2\sigma_\theta$, which is clearly always negative from (6.18). Therefore, the angular function $Y(w)$ diverges at $w = 1$, it can only converge if the hypergeometric series terminates, and this occurs when $a = -n$, where n is a positive natural number [1],

$$-\frac{1}{2}\sqrt{\lambda+1} + \sigma_\theta + \tau + \frac{1}{2} = -n. \tag{6.28}$$

Hence, we obtain the values of the eigenvalues:

$$\lambda = [2n + 1 + 2(\sigma_\theta + \tau)]^2 - 1. \tag{6.29}$$

This result corresponds exactly to the one evaluated in [57] and [85].

6.2.2 Angular function and spin-weighted spherical harmonics

We now introduce the form of the angular function that we will use for our numerical computations in Chapter 8. We have already introduced the spin-weighted spherical harmonics in Chapter 5, and now we are going to show how we will utilise their properties

in our analysis. To do this, let us take a step back and properly introduce the subject. In Equation (5.1), the spin-weighted spherical harmonics are defined as depending on the angles θ and ϕ. In order to match this definition, we need to modify the way we look at the separation of variables in Equation (6.4). To this end, we define:

$$\widetilde{Y}(\theta,\phi) = e^{im\phi}Y(\theta), \tag{6.30}$$

so that Equation (6.4) becomes

$$\Phi(r,\theta,\phi,\psi,t) = e^{ip\psi-i\omega t}X(r)\widetilde{Y}(\theta,\phi). \tag{6.31}$$

Substituting the separable mode ansatz in Equation (6.31) for the scalar field into Equation (6.1) and separating variables, the resulting equation for the angular function $\widetilde{Y}(\theta,\phi)$ can be written as

$$0 = \frac{\partial^2\widetilde{Y}}{\partial\theta^2} + \cot\theta\frac{\partial\widetilde{Y}}{\partial\theta} - ip\cot\theta\csc\theta\frac{\partial\widetilde{Y}}{\partial\phi} + \csc^2\theta\frac{\partial^2\widetilde{Y}}{\partial\phi^2} - \frac{1}{4}p^2\widetilde{Y}\cot^2\theta + \widetilde{\lambda}\widetilde{Y}, \tag{6.32}$$

where $\widetilde{\lambda} = \frac{1}{4}(\lambda - p^2)$ is the separation constant.

We compare Equation (6.32) with the governing equation for the spin-weighted spherical harmonics (5.39) ${}_sY_\ell^n(\theta,\phi)$, which have spin s, total angular momentum quantum number ℓ, and azimuthal quantum number $\mathfrak{n}$ [28, 42, 56, 77, 99, 108, 118]:

$$0 = \frac{\partial^2{}_s\widetilde{Y}_\ell^{\mathfrak{n}}}{\partial\theta^2} + \cot\theta\frac{\partial_s\widetilde{Y}_\ell^{\mathfrak{n}}}{\partial\theta} + 2is\cot\theta\csc\theta\frac{\partial_s\widetilde{Y}_\ell^{\mathfrak{n}}}{\partial\phi} + \csc^2\theta\frac{\partial^2{}_s\widetilde{Y}_\ell^{\mathfrak{n}}}{\partial\phi^2} - s^2{}_s\widetilde{Y}_\ell^{\mathfrak{n}}\cot^2\theta + \left[\ell^2+\ell-s^2\right]{}_s\widetilde{Y}_\ell^{\mathfrak{n}}. \tag{6.33}$$

Here, s is a, positive or negative, integer or half-integer, $\ell = |s|, |s|+1, |s|+2, \ldots$ is a positive integer or half-integer, and $m = -\ell, -\ell+1, \ldots, \ell-1, \ell$ is also an integer or half-integer, taking both positive and negative values.

Comparing Equations (6.32) and (6.33), we see that the spin s is related to the quantum number p by

$$s = -\frac{p}{2}, \tag{6.34}$$

and the separation constant $\widetilde{\lambda}$ is given by

$$\widetilde{\lambda} = \ell^2 + \ell - s^2 = \ell^2 + \ell - \frac{1}{4}p^2. \tag{6.35}$$

We can also substitute back the form of the angular function in Equation (6.30) and divide by the exponential $e^{im\phi}$ to obtain a differential equation that depends only on θ:

$$Y''(\theta) + \cot\theta\, Y'(\theta) + \left\{\csc^2\theta\left[-(m+s\cos\theta)^2\right] + (\ell-s)(\ell+s+1) + s\right\}Y(\theta) = 0. \tag{6.36}$$

From this, we can highlight two important points. First, we can identify $m = \mathfrak{n}$ in Equation (6.33). Secondly, this corresponds exactly to our Equation (6.8), where

$$\widetilde{\lambda} \to \frac{1}{4}(\lambda - p^2), \tag{6.37}$$

$$p \to -2s. \tag{6.38}$$

It is also important to note the different form of the separation constant this being λ or $\widetilde{\lambda}$. This difference arises because there is a choice in selecting the eigenvalue's form, as we previously mentioned. While all choices are valid, maintaining consistency is vital. Hence, we will use Equation (6.35) throughout this thesis.

The advantage of working with spin-weighted spherical harmonics is the existence of addition theorems proven in Chapter 5 for sums over the azimuthal quantum number m, see Section 5.3. These theorems will enable us, in Chapter 8, to simplify the expressions for the vacuum polarisation and stress–energy tensor for the quantum scalar field.

Finally, we introduce the normalisation of the angular function of the quantum scalar field. The standard normalisation for the spin–weighted spherical harmonics having integer spin s is

$$\int_{\phi=0}^{2\pi}\int_{\theta=0}^{\pi} {}_s\widetilde{Y}_{\ell}^{m*}(\theta,\phi)\, {}_{s'}\widetilde{Y}_{\ell'}^{m'}(\theta,\phi)\, \sin\theta\, d\theta\, d\phi = \delta_{ss'}\, \delta_{\ell\ell'}\, \delta_{mm'}. \tag{6.39}$$

We use this normalisation so that the addition theorems in Chapter 5 can be applied. However, since we have $\phi \in [0, 4\pi)$ rather than $\phi \in [0, 2\pi)$, our normalisation is

$$\int_{\phi=0}^{4\pi}\int_{\theta=0}^{\pi} {}_s\widetilde{Y}_{\ell}^{m*}(\theta,\phi)\, {}_{s'}\widetilde{Y}_{\ell'}^{m'}(\theta,\phi)\, \sin\theta\, d\theta\, d\phi = 2\,\delta_{ss'}\, \delta_{\ell\ell'}\, \delta_{mm'}. \tag{6.40}$$

This normalisation condition is valid for both half-integer and integer spin. It is important to note that, from now on the indexes that will then be used in Chapter 7 as quantum numbers will be ℓ, m and $-p/2$, and ω as the frequency.

6.3 Radial equation

Now that we have discussed the angular equation, we can focus on the radial part of Equation (6.1). From the separation of variables introduced earlier in this chapter, we now look at the function $F[r, X(r), X'(r), X''(r)]$. This is expressed as follows:

$$0 = X''(r) + \left[\frac{3}{r} - \frac{2g'(r)}{g(r)}\right] X'(r) + g(r)^2 \left[\frac{\{\omega - p\Omega(r)\}^2}{f(r)^2} - \frac{p^2}{h(r)^2} - \frac{4\lambda}{r^2} - \mu_0^2\right] X(r), \tag{6.41}$$

where λ is the separation constant in Equation (6.7) and μ_0 is defined in Equation (6.2).

The analysis of the radial equation can be done following two different approaches. The first one is to write Equation (6.41) as a Schrödinger equation. This will give us insights into the behaviour of the modes, helping us defining an orthonormal basis of field modes for the canonical quantization of the scalar field in Chapter 7. The second one, is performed choosing an appropriate change of variables and writing the differential equation (6.41) as a Heun differential equation [1, Eq.31.2.1]. This will be useful for our numerical computations in Chapter 8.

6.3.1 Schrödinger equation form

Firstly, we are going to use the tortoise coordinate $r_\star$, and simplify the differential equation [85]. Let us define

$$\frac{dr_\star}{dr} = \frac{g(r)}{f(r)} \quad \text{and} \quad X(r) = \frac{R(r_\star)}{r\ h(r)^{1/2}}, \tag{6.42}$$

where the functions f, g and h are the ones defined in (4.7). We can see that:

$$r_\star \to -\infty \quad \text{when} \quad r \to r_+, \tag{6.43}$$

$$r_\star \to 0 \quad \text{when} \quad r \to +\infty. \tag{6.44}$$

Using this variable we have re-derived the fact that the radial equation can be written as a Schrödinger equation as shown in [85]

$$\frac{d^2}{dr_\star^2} R(r_\star) + V(r) R(r_\star) = 0, \tag{6.45}$$

where $V(r)$ is the potential of this equation, which is

$$V(r) = [\omega - p\Omega(r)]^2 - f(r)^2 \left[\mu_0^2 + \frac{4\lambda}{r^2} + \frac{p^2}{h(r)^2}\right] - \frac{f(r)^2\sqrt{h(r)}}{r^2}\frac{d}{dr}\left[\frac{f(r)^2 h(r)}{r}\frac{d}{dr}\left\{r\sqrt{h(r)}\right\}\right], \tag{6.46}$$

where we have used the relationship between the metric functions f, g and h, in Equation (4.7). We can now give some insights on the asymptotic behaviour of the potential.

- For $r \to \infty$,

$$V(r) \sim -\frac{15r^2}{4L^4} - \frac{\mu_0^2 r^2}{L^2}. \tag{6.47}$$

We can see that this expression is valid for finite values of L. Furthermore, we can show the behaviour in the minimally coupled case and in the conformally coupled case of the potential $V(r)$ when $r \to \infty$,

$$\text{Minimally coupled case: } \xi_\Phi = 0 \ \to\ V(r) \sim -\frac{15r^2}{4L^4} - \frac{\mu^2 r^2}{L^2}. \tag{6.48}$$

$$\text{Conformally coupled case: } \xi_\Phi = \xi_c(5) = \frac{3}{16} \ \to\ V(r) \sim -\frac{\mu^2 r^2}{L^2}. \tag{6.49}$$

We can see that $V(r)$ diverges like r^2 as $r \to +\infty$ unless the field is massless and conformally coupled, we will not consider this case in this thesis.

- For $f \to 0$, $r \to r_+$,

$$V(r) \sim (\omega - p\Omega_H)^2, \tag{6.50}$$

which gives us the behaviour of the potential at the horizon r_+ and this is constant. We can also define:

$$\widetilde{\omega} = \omega - p\Omega_H, \tag{6.51}$$

where ω is the frequency of the mode. This quantity will be pivotal for the evaluation of observables in the following chapters.

In case L goes to infinity, given the relation to the cosmological constant $L \propto \Lambda^{-1}$, the spacetime becomes asymptotically flat rather than asymptotically AdS. This will bring the potential $V(r)$ to zero as $r \to \infty$ and to be (6.50) on the event horizon [85].

Near the horizon, as $r \to r_+$ and $r_\star \to -\infty$, the solutions of the radial equation (6.45) take the form

$$R(r_\star) \sim \mathcal{C}_+ \, e^{i\widetilde{\omega}\, r_\star} + \mathcal{C}_- \, e^{-i\widetilde{\omega}\, r_\star}, \tag{6.52}$$

where $\mathcal{C}_\pm$ are complex constants, representing ingoing and outgoing plane waves. As $r \to \infty$ and $r_\star \to 0$, the solutions of Equation (6.45) are [85]

$$R(r_\star) \sim \mathcal{D}_+ \, r_\star^{1/2+L\widetilde{\mu_0}} + \mathcal{D}_- \, r_\star^{1/2-L\widetilde{\mu_0}}, \tag{6.53}$$

where $\mathcal{D}_\pm$ are complex constants, and

$$\widetilde{\mu_0}^2 = \mu_0^2 + \frac{4}{L^2}. \tag{6.54a}$$

In order for the scalar field to exhibit no classical mode instabilities, the Breitenlöhner–Freedman bound [25, 26] must be satisfied, namely:

$$\widetilde{\mu_0}^2 > 0. \tag{6.54b}$$

From this point forward, we will assume that this condition holds. We then consider only the regular, decaying solution in (6.53); that is, we assume $\widetilde{\mu_0} > 0$ and

$$R(r_\star) \sim \mathcal{D}_+ \, r_\star^{1/2+L\widetilde{\mu_0}}, \tag{6.55}$$

as $r \to \infty$ and $r_\star \to 0$. When $\widetilde{\mu_0} = 0$, although the Breitenlöhner–Freedman bound is still satisfied, the radial equation no longer yields solutions of the form (6.53). This change arises because terms in the potential $V(r)$ that are subleading when $\widetilde{\mu_0} \neq 0$ become the leading-order terms. We will not consider this possibility in this thesis.

Finally we will present the analysis for the normalization of the radial function. We can absorb the constant $\mathcal{C}_+$ in Equation (6.52) into an overall normalisation constant, and we can, without loss of generality, take the radial function $R(r)$ to have the form

$$R_{\omega p\ell}(r) \sim \begin{cases} e^{i\widetilde{\omega}\, r_\star} + \mathcal{R}_{\omega p\ell}\, e^{-i\widetilde{\omega}\, r_\star}, & r_\star \to -\infty, \\ \mathcal{T}_{\omega p\ell}\, r_\star^{1/2+L\widetilde{\mu_0}}, & r_\star \to 0, \end{cases} \tag{6.56}$$

where $\mathcal{R}_{\omega p\ell}$ and $\mathcal{T}_{\omega p\ell}$ are complex constants, and the subscripts indicate that the radial function depends only on the frequency ω and the quantum numbers p and ℓ. Since Equation (6.45) is a Schrödinger-like form equation, the Wronskian of any two linearly independent solutions is a nonzero constant. In particular, by considering the Wronskian of $R_{\omega p\ell}$ and its complex conjugate, we obtain

$$\widetilde{\omega}\left(|\mathcal{R}_{\omega p\ell}|^2 - 1\right) = 0, \tag{6.57}$$

which implies that either $|\mathcal{R}_{\omega p\ell}|^2 = 1$ or $\widetilde{\omega} = 0$.

This is a good moment to pause and introduce one of the choices made in our analysis of a quantum scalar field on a five-dimensional Kerr-AdS black hole. Given that the AdS structure generates a boundary at infinity, as discussed in Chapter 3, we must impose boundary conditions. In this work, we adopt the reflective boundary conditions introduced in Section 3.2; specifically, we impose Dirichlet boundary conditions by picking Equation (6.56) as the radial equation for the scalar field. As a result, the scalar field flux through the boundary at $r \to \infty$ is zero, and the field is reflected at the boundary. This implies that, unlike the case of rotating asymptotically flat black holes, there is no classical superradiance in this setup, and hence no superradiant instability for slowly rotating black holes (e.g. for $0 < a < a_{\text{min}}$) [68, 83].

With this analysis, we also highlight that we have only one set of modes, which simplifies the study of this case considerably compared to other black hole cases, such as the Schwarzschild black hole, see Section 1.3. In particular, these are the ingoing and outgoing modes at the horizon. All of this is consistent with the analysis performed in [85]. This will be the key point for constructing quantum states, in particular, the Hartle–Hawking state for this background.

6.3.2 Heun equation form

In order to solve the differential equation (6.41), we will use a different method than the one introduced for the angular part (namely, the Frobenius method in Equation (6.11)). However, we will still focus on the singular points of Equation (6.41) in order to solve it. In fact, we will attempt to transform the radial equation (6.41) into the form of a Heun differential equation [124]. To this end, we follow the method of [6,8,83,109]. In [6,8,83,109],

the authors use a different coordinate system from that employed here; this means that their expressions for the various constants introduced below differ from ours.

Initially, we observe that $g(r)^{-2}$, as defined in Equation (4.7), constitutes a cubic function in r^2, multiplied by r^{-4}:

$$g(r)^{-2} = \frac{1}{r^4}\left(\frac{r^6}{L^2} + r^4 - 2Mr^2\Xi + 2Ma^2\right). \tag{6.58}$$

The roots of the equation $g(r)^{-2} = 0$ are $r_+^2 > r_-^2 > 0$ and $r_0^2 < 0$. We also know that (see Chapter 4)

$$r_+^2 + r_-^2 + r_0^2 = -L^2. \tag{6.59}$$

The radial equation (6.41) has four regular singular points, at $r^2 = r_+^2$, $r^2 = r_-^2$, $r^2 = r_0^2$ and $r^2 = \infty$. Since the Heun differential equation also has four regular singular points, we are confident that it will be possible to transform the form of the radial equation (6.41) into the Heun form using an appropriate change of variables. To this end, we first define an independent variable [109]:

$$z = \frac{r^2 - r_+^2}{r^2 - r_0^2}. \tag{6.60}$$

The regular singular points are then at $z = 0$ ($r = r_+$), $z = 1$ ($r = \infty$), $z = z_0$ ($r = r_-$) and $z = \infty$ ($r = r_0$), where

$$z_0 = \frac{r_-^2 - r_+^2}{r_-^2 - r_0^2}. \tag{6.61}$$

Here, r_+, r_- and r_0 are the roots of $g(r)$ defined above, which also provide information about the surfaces of the black hole, as explained in Chapter 4. We can then define a new function $H(z)$ by writing the radial function as

$$X(z) = z^{\theta_+}(z-1)^{\sigma}(z-z_0)^{\theta_-}H(z), \tag{6.62}$$

where θ_+, σ and θ_-, corresponding to the singular points 0, 1 and z_0, are possibly complex constants to be determined. Instead of constructing the indicial equation for each singular point as we did for the angular differential equation, we substitute this form of the radial function into Equation (6.41); this gives us

$$0 = H''(z) + \left[\frac{\gamma}{z} + \frac{\delta}{z-1} + \frac{\epsilon}{z-z_-}\right]H'(z) + \mathfrak{V}(z)H(z), \tag{6.63}$$

where the constants γ, δ and ϵ are given by

$$\gamma = 1 + 2\theta_+, \quad \delta = -1 + 2\sigma, \quad \epsilon = 1 + 2\theta_-, \tag{6.64}$$

and $\mathfrak{V}(z)$ is a function of z that is too lengthy to display here, serving the purpose of transforming Equation (6.41) into a Heun differential equation. To this end, we require $\mathfrak{V}(z)$ to take the form

$$\mathfrak{V}(z) = \frac{\alpha\beta z - q}{z(z-1)(z-z_0)}, \tag{6.65}$$

where α and β are constants such that

$$\alpha + \beta + 1 = \gamma + \delta + \epsilon. \tag{6.66}$$

The constraint (6.66) is satisfied for α and β given by

$$\begin{aligned} \alpha &= \theta_+ + \theta_- + \sigma + \theta_0, \\ \beta &= \theta_+ + \theta_- + \sigma - \theta_0, \end{aligned} \tag{6.67}$$

where θ_0 is another constant to be determined. Now we must determine the constants θ_+, θ_-, σ and θ_0. These are found by requiring $\mathfrak{V}(z)$ to have the form given in Equation (6.65). After a considerable amount of lengthy algebra, we find

$$\theta_+ = \frac{i}{2\kappa_+}\left(\omega - p\Omega_H\right), \tag{6.68a}$$

$$\theta_- = \frac{i}{2\kappa_-}\left(\omega - p\Omega_-\right), \tag{6.68b}$$

$$\theta_0 = \frac{i}{2\kappa_0}\left(\omega - p\Omega_0\right), \tag{6.68c}$$

$$\sigma = 1 + \sqrt{1 + \frac{1}{4}\mu_0^2 L^2}, \tag{6.68d}$$

where μ_0 is given in Equation (6.2), the constants κ_+ in Equation (4.54) and Ω_H in Equation (4.37) can be written in the alternative form

$$\kappa_+ = \frac{\left(r_+^2 - r_-^2\right)\left(r_+^2 - r_0^2\right)}{L r_+^2 \sqrt{\left(r_+^2 + r_-^2\right)\left(r_-^2 + L^2\right)}}, \tag{6.68e}$$

$$\Omega_H = \frac{i r_- r_0 \sqrt{r_+^2 + L^2}}{L r_+ \sqrt{\left(r_+^2 + r_-^2\right)\left(r_-^2 + L^2\right)}}, \tag{6.68f}$$

and we have defined the quantities κ_-, Ω_-, κ_0 and Ω_0 in a similar way:

$$\kappa_- = \frac{\left(r_-^2 - r_0^2\right)\left(r_-^2 - r_+^2\right)}{L r_-^2 \sqrt{\left(r_+^2 + L^2\right)\left(r_-^2 + r_+^2\right)}}, \tag{6.68g}$$

$$\Omega_- = \frac{i r_+ r_0 \sqrt{r_-^2 + L^2}}{L r_- \sqrt{\left(r_+^2 + L^2\right)\left(r_-^2 + r_+^2\right)}}, \tag{6.68h}$$

$$\kappa_0 = \frac{i\left(r_0^2 - r_+^2\right)\left(r_0^2 - r_-^2\right)}{L r_0^2 \sqrt{\left(r_+^2 + L^2\right)\left(r_-^2 + L^2\right)}}, \tag{6.68i}$$

$$\Omega_0 = \frac{i r_+ r_- \sqrt{r_+^2 + r_-^2}}{L r_0 \sqrt{\left(r_+^2 + L^2\right)\left(r_-^2 + L^2\right)}}. \tag{6.68j}$$

All quantities under a square-root sign in Equation (6.68) are positive, and since $r_0^2 < 0$, we have that r_0 is purely imaginary. Therefore, $\kappa_\pm$ and $\Omega_\pm$ are real, while κ_0 and Ω_0 are

purely imaginary. This means that both $\theta_\pm$ are purely imaginary but θ_0 is real. Since $\mu_0^2 L^2 > -\frac{15}{4}$ in Equation (6.54), we also have that σ is real. Finally, the constant q is given by

$$q = \frac{L^2}{4\left(r_-^2 - r_0^2\right)}\left[\omega^2 L^2 - p^2 - 4\widetilde{\lambda} - r_+^2\mu_0^2\right] + z_-\left(2\theta_+\sigma + \sigma - \theta_+\right) + \left(\theta_+ + \theta_-\right)\left(\theta_+ + \theta_- + 1\right) - \theta_0^2, \quad (6.69)$$

where μ_0 can be found in Equation (6.2) and $\widetilde{\lambda}$ in Equation (6.35). Now that we have successfully matched our radial equation to the Heun differential equation and determined the form of every parameter, we can use this to our advantage. We know that the solutions to Equation (6.63) are the Heun functions, specifically,

$$\begin{aligned} H_{01}(z) &= Hl(z_0, q; \alpha, \beta, \gamma, \delta; z), \\ H_{02}(z) &= z^{1-\gamma}\, Hl\Big(z_0, (z_0\delta + \epsilon)(1-\gamma) + q; \alpha + 1 - \gamma, \beta + 1 - \gamma, 2 - \gamma, \delta; z\Big), \end{aligned} \quad (6.70)$$

in a neighbourhood of $z = 0$, while

$$\begin{aligned} H_{11}(z) &= Hl(1 - z_0, \alpha\beta - q; \alpha, \beta, \delta, \gamma; 1 - z), \\ H_{12}(z) &= (1-z)^{1-\delta}\, Hl\Big(1 - z_0,\ ((1-z_0)\gamma + \epsilon)(1-\delta) + \alpha\beta - q; \\ &\qquad \alpha + 1 - \delta, \beta + 1 - \delta, 2 - \delta, \gamma; 1 - z\Big), \end{aligned} \quad (6.71)$$

in a neighbourhood of $z = 1$. These results can be matched with those reported by [109]. $H_{01}(z)$ and $H_{02}(z)$ are two linearly independent solutions of Equation (6.63) with $\mathfrak{V}(z)$ given by Equation (6.65). $H_{11}(z)$ and $H_{12}(z)$ are also two linearly independent solutions of the radial equation (6.63). We see that $H_{01}(z)$ is regular at $z = 0$ and $H_{11}(z)$ is regular at $z = 1$, since

$$H_{01}(z) = Hl(z_0, q; \alpha, \beta, \gamma, \delta; 0) = 1 \quad \text{as } z \to 0, \quad (6.72)$$

$$H_{11}(z) = Hl(1 - z_0, \alpha\beta - q; \alpha, \beta, \delta, \gamma; 0) = 1 \quad \text{as } z \to 1, \quad (6.73)$$

for any parameters z_0, q, α, β, γ, δ. However,

$$H_{02}(z) \sim z^{2(1-\gamma)} \quad \text{as } z \to 0, \quad (6.74)$$

$$H_{12}(z) \sim (1-z)^{2(1-\sigma)} \quad \text{as } z \to 1, \quad (6.75)$$

where σ is given by Equation (6.68d) and γ is given by Equation (6.64). We focus on the solutions in a neighbourhood of $z = 1$, since $\sigma > 1$, we see that $H_{12}(z)$ diverges as $z \to 1$. We therefore choose the solution $H_{11}(z)$ to be the appropriate radial function, so that

$$X_{\omega p\ell}(r) = \mathfrak{X}_{\omega p\ell}\, z^{\theta_+}\,(z-1)^{\sigma}\,(z - z_0)^{\theta_-}\, \mathsf{H}l(1 - z_0, \alpha\beta - q; \alpha, \beta, \delta, \gamma; 1 - z), \quad (6.76)$$

where $\mathfrak{X}_{\omega p\ell}$ is a constant that we will determine in the next section. The choice of this radial function corresponds to reflective boundary conditions. In particular, we use the Dirichlet boundary conditions, which we have introduced in Section 3.2. We assume that the radial function tends to zero as rapidly as possible as $r \to \infty$. The form of the radial function given in Equation (6.76) is the one that we shall use for our numerical computations in Chapter 8, since the Heun functions $Hl(z_0, q; \alpha, \beta, \gamma, \delta; z)$ are built into `Mathematica`.

Another important property of the Heun functions, these being solutions of a second order linear ODE, is that we can relate the solution in Equation (6.70) at $z = 0$ to the solution in Equation (6.71) at $z = 1$ via linear combinations,

$$H_{01}(z) = C_{11}\, H_{11}(z) + C_{12}\, H_{12}(z), \tag{6.77}$$

$$H_{02}(z) = C_{21}\, H_{11}(z) + C_{22}\, H_{12}(z), \tag{6.78}$$

where C_{ij}, with $i = 1, 2$ and $j = 1, 2$ are constants which can be expressed as the ratios of Wronskians $W\{,\}$ of Heun functions as

$$C_{11} = \frac{W_z[H_{01}, H_{12}]}{W_z[H_{11}, H_{12}]}, \quad C_{12} = \frac{W_z[H_{01}, H_{11}]}{W_z[H_{12}, H_{11}]}, \tag{6.79}$$

$$C_{21} = \frac{W_z[H_{02}, H_{12}]}{W_z[H_{11}, H_{12}]}, \quad C_{22} = \frac{W_z[H_{02}, H_{11}]}{W_z[H_{12}, H_{11}]}, \tag{6.80}$$

and where

$$W_z[u, v] = u\,\frac{dv}{dz} - \frac{du}{dz}\,v, \tag{6.81}$$

is the Wronskian. If we use the form of the radial function in Equation (6.63), it holds that

$$z^{\theta_+}(z-1)^{\sigma}(z-z_0)^{\theta_-}\, W_z[H_a, H_b] = \text{const.} \tag{6.82}$$

This means that the Wronskian itself is not constant, but the ratio between Wronskians is [109]. On the other hand, in a neighbourhood of $z = 1$ we can express the solutions as

$$H_{11}(z) = D_{11}\, H_{01}(z) + D_{12}\, H_{02}(z), \tag{6.83}$$

$$H_{12}(z) = D_{21}\, H_{01}(z) + D_{22}\, H_{02}(z), \tag{6.84}$$

where D_{ij}, with $i = 1, 2$ and $j = 1, 2$ are constants which can be expressed as the ratios of Wronskians $W\{,\}$ of Heun functions as

$$D_{11} = \frac{W_z[H_{11}, H_{02}]}{W_z[H_{01}, H_{02}]}, \quad D_{12} = \frac{W_z[H_{11}, H_{01}]}{W_z[H_{02}, H_{01}]}, \tag{6.85}$$

$$D_{21} = \frac{W_z[H_{12}, H_{02}]}{W_z[H_{01}, H_{02}]}, \quad D_{22} = \frac{W_z[H_{12}, H_{01}]}{W_z[H_{02}, H_{01}]}. \tag{6.86}$$

We will make use of this property in the next subsection, where we will see why it is important that one Heun function can be written as a linear combination of the others.

6.3.3 Matching the two forms of the radial equation

In the previous two subsections, we have derived two forms of the radial function $X_{\omega p\ell}(r)$. What we do now is to match their definitions, since Equation (6.76) and Equation (6.42) need to represent the same function. We report them here for simplicity:

$$X_{\omega p\ell}(r) = \frac{R_{\omega p\ell}(r_\star)}{r\sqrt{h(r)}}, \tag{6.87a}$$

$$X_{\omega p\ell}(r) = \mathfrak{X}_{\omega p\ell}\, z^{\theta_+}\,(z-1)^{\sigma}\,(z-z_-)^{\theta_-}\, H_{11}(z), \tag{6.87b}$$

where $R_{\omega p\ell}(r_\star)$ has the asymptotic forms given in (6.56), the variable z is defined in Equation (6.60), and $H_{11}(z)$ is the Heun function in Equation (6.71). In Section 6.4, we will use the form in Equation (6.87a) near the past event horizon to determine the overall normalisation of the modes. In this subsection we would like to find the constant $\mathfrak{X}_{\omega p\ell}$ so that, near the past horizon (where $r = r_+$), the two asymptotic forms in Equation (6.87) match. Our analysis follows that in [109], although we use different coordinates. In particular, our definition of the tortoise coordinate in Equation (6.42) differs from that in [109].

Since we know the behaviour of Equation (6.87a) near the past horizon, we can write

$$X_{\omega p\ell}(r) \sim \frac{e^{i\widetilde{\omega}\, r_\star}}{r_+\sqrt{h(r_+)}}, \tag{6.88}$$

where the tortoise coordinate $r_\star$ is determined by the differential equation (6.42). As $r \sim r_+$, we have, for $r > r_+$,

$$r_\star \sim \frac{1}{2\kappa_+}\log\left(\frac{r-r_+}{r_+}\right) + C, \tag{6.89}$$

where κ_+ is the surface gravity in Equation (6.68e) and C is a constant, which leads to a phase in Equation (6.88) which we will not consider. Effectively we are putting $C = 0$. If we substitute Equation (6.89) into Equation (6.88), we obtain

$$X_{\omega p\ell}(r) \sim \frac{1}{r_+\sqrt{h(r_+)}}\left(\frac{r-r_+}{r_+}\right)^{\frac{i\widetilde{\omega}}{2\kappa_+}}. \tag{6.90}$$

This is the form we wish to match to the expression in Equation (6.87b) for $X_{\omega p\ell}(r)$ involving a Heun function.

The expression (6.87b) involves a Heun function whose asymptotics as $z \to 0$ is not easily obtainable. However, we can use the fact that the solution defined in a neighbourhood of $z = 1$ can be rewritten as a linear combination of the solutions in Equation (6.70), as shown in Equation (6.83). Hence, substituting Equation (6.83) for $H_{11}(z)$ in Equation (6.87b) we obtain, for $z \sim 0$ (noting that θ_+ in Equation (6.68a) is purely imaginary),

$$X_{\omega p\ell}(r) \sim \mathfrak{X}_{\omega p\ell}\, D_{11}\, z^{\theta_+}\,(-1)^{\sigma}\,(-z_0)^{\theta_-}. \tag{6.91}$$

Next, since for $r \sim r_+$

$$z \sim \frac{2r_+(r-r_+)}{r_+^2 - r_0^2}, \tag{6.92}$$

we have

$$X_{\omega p\ell}(r) \sim \mathfrak{X}_{\omega p\ell}\, D_{11}\, (-1)^{\sigma}\, (-z_0)^{\theta_-} \left(\frac{2r_+(r-r_+)}{r_+^2 - r_0^2}\right)^{\theta_+}. \tag{6.93}$$

Comparing Equation (6.90) and Equation (6.93), the constant $\mathfrak{X}_{\omega p\ell}$ is determined to be

$$\mathfrak{X}_{\omega p\ell} = \frac{1}{D_{11}\, r_+ \sqrt{h(r_+)}}\, (-1)^{-\sigma}\, (-z_0)^{-\theta_-} \left(\frac{1}{2r_+^2}\left[r_+^2 - r_0^2\right]\right)^{\theta_+}. \tag{6.94}$$

We have already chosen the overall phase in our derivation of the form (6.90) of the radial function near the past horizon. As a result, we need to retain all the phases in the constant $\mathfrak{X}_{\omega p\ell}$. Notably, the ratios of Wronskians in Equation (6.85) will be convenient for our numerical computations in Chapter 8.

6.4 Normalization of the scalar field

We have solved the Klein–Gordon equation (6.1), finding solutions for both the angular part (6.8) and the radial part (6.41). The final step in constructing an orthonormal basis of scalar field modes is to ensure that the modes are normalised. We have already discussed the normalisation of the angular function in Section 6.2.2, which follows from the properties of spin-weighted spherical harmonics introduced in Chapter 5. In order to complete the analysis, let us consider the scalar field modes which take the form

$$\Phi(r,\theta,\phi,\psi,t) = \mathcal{N}_{\omega p\ell}\, e^{-i\omega t}\, e^{ip\psi}\, X_{\omega p\ell}(r)\, {}_{-p/2}Y_\ell^m(\theta,\phi), \tag{6.95}$$

where the quantum numbers are as follows: the frequency $\omega \in \mathbb{R}$; the azimuthal quantum number $p \in \mathbb{Z}$; the total angular momentum quantum number ℓ, which takes the values $|p/2|$, $|p/2|+1$, $|p/2|+2, \ldots$; and the additional angular quantum number m, ranging from $-\ell$ to ℓ in integer steps. In Equation (6.95), the constant $\mathcal{N}_{\omega p\ell}$ is a normalisation constant that depends only on ω, p and ℓ. Notably, the only dependence on the quantum number m is contained in the spin-weighted spherical harmonics ${}_{-p/2}Y_\ell^m(\theta,\phi)$, which will be useful for simplifying the expectation values of observables in Chapter 8.

The modes in Equation (6.95) are normalised using the inner product $\langle \Phi_1, \Phi_2 \rangle$ of any two solutions of the scalar field equation (6.1), which is defined by

$$\langle \Phi_1, \Phi_2 \rangle = i \int_\Sigma \left[(\nabla_\mu \Phi_1^*)\, \Phi_2 - \Phi_1^* \nabla_\mu \Phi_2\right] d\Sigma^\mu, \tag{6.96}$$

where the star denotes complex conjugation. Consider a spacelike hypersurface Σ that extends from the event horizon to the spacetime boundary. In an asymptotically AdS black hole, this hypersurface is not a Cauchy surface. However, by imposing appropriate

boundary conditions on the radial function $X_{\omega p\ell}(r)$, we ensure that the scalar field modes vanish as $r \to \infty$. Consequently, the inner product defined in Equation (6.96) is independent of the choice of the surface Σ.

We choose the hypersurface Σ to lie near the past horizon, where the Kruskal coordinate V is set to zero, and we parameterise this surface using the Kruskal coordinate U (as defined in Equation (4.67)). On Σ, by employing the radial function given in Equation (6.87a) together with its asymptotic behaviour from Equation (6.56), we obtain

$$\begin{aligned}\phi_{\omega p\ell m}(t,r,\theta,\phi,\psi) &= \frac{1}{r\sqrt{h(r)}}\mathcal{N}_{\omega p\ell}e^{-i\omega t}e^{ip\psi}e^{i\widetilde{\omega}r_\star}{}_{-p/2}Y_\ell^m(\theta,\phi) \\ &= \frac{1}{r\sqrt{h(r)}}\mathcal{N}_{\omega p\ell}e^{-i\widetilde{\omega}u}e^{ip\psi_+}{}_{-p/2}Y_\ell^m(\theta,\phi), \end{aligned} \tag{6.97}$$

where the corotating angle $\psi_\star$ is given by (4.57). The surface element is $d\Sigma^\mu = n^\mu\, d\Sigma$, where n^μ is the normal

$$n^\mu = -\frac{2\kappa_+^2 UV}{f(r)^2}\delta^\mu_U \tag{6.98}$$

where κ_+ is the surface gravity in Equation (4.54), and

$$d\Sigma = \sqrt{-g_{\mathrm{K}}}\, dU\, d\theta\, d\phi\, d\psi_+, \tag{6.99}$$

where $\sqrt{-g_{\mathrm{K}}}$ is defined in Equation (4.71). Substituting (4.71) into (6.99), we obtain

$$\begin{aligned} d\Sigma^\mu &= -\frac{r^2h(r)}{4\kappa_+ f(r)^2}\left[2\kappa_+ f(r)^2 + \{\Omega(r)-\Omega_H\}^2 h(r)^2\right]\sin\theta\,\delta^\mu_U\, dU\, d\theta\, d\phi\, d\psi_+ \\ &\sim -\frac{1}{2}r^2h(r)\sin\theta\,\delta^\mu_U\, dU\, d\theta\, d\phi\, d\psi_+, \end{aligned} \tag{6.100}$$

where in the last line we give the leading-order expression near the past event horizon, where $r \to r_+$. Changing the integration variable to u (4.61), the inner product of two scalar field modes is

$$\begin{aligned}&\langle \phi_{\omega p\ell m}(t,r,\theta,\phi,\psi), \phi_{\omega' p'\ell' m'}(t,r,\theta,\phi,\psi)\rangle \\ &\quad= \frac{1}{2}\int_{u=-\infty}^{\infty}\int_{\theta=0}^{\pi}\int_{\phi=0}^{4\pi}\int_{\psi_+=0}^{2\pi}\mathcal{N}^*_{\omega p\ell}\mathcal{N}_{\omega' p'\ell'}\left[\widetilde{\omega}+\widetilde{\omega}'\right]e^{i(\widetilde{\omega}-\widetilde{\omega}')u}e^{-i(p-p')\psi_+} \\ &\qquad\times X^*_{\omega p\ell}(r)X_{\omega' p'\ell'}(r)\,{}_{-p/2}Y_\ell^{m*}(\theta,\phi)\,{}_{-p'/2}Y_{\ell'}^{m'}(\theta,\phi)\, du\, d\theta\, d\phi\, d\psi. \end{aligned} \tag{6.101}$$

Using the normalisation shown in Equation (6.40) of the spin-weighted spherical harmonics and that

$$\int_0^{2\pi} e^{-i(p-p')\psi_+}\, d\psi_+ = 2\pi\delta_{pp'}, \tag{6.102a}$$

$$\int_{-\infty}^{\infty} e^{i(\widetilde{\omega}-\widetilde{\omega}')u}\, du = 2\pi\delta\left(\widetilde{\omega}-\widetilde{\omega}'\right), \tag{6.102b}$$

the inner product (6.101) becomes

$$\langle \phi_{\omega p \ell m}(t,r,\theta,\phi,\psi), \phi_{\omega' p' \ell' m'}(t,r,\theta,\phi,\psi) \rangle = 8\pi^2 \widetilde{\omega} \left| \mathcal{N}_{\omega p \ell} \right|^2 \delta\left(\widetilde{\omega} - \widetilde{\omega}'\right) \delta_{pp'} \delta_{\ell \ell'} \delta_{m m'}, \quad (6.103)$$

and requiring orthonormality takes the normalisation constant to be,

$$\mathcal{N}_{\omega p \ell} = \frac{1}{2\sqrt{2}\pi \left| \widetilde{\omega} \right|}, \quad (6.104)$$

where we have taken $\mathcal{N}_{\omega p \ell}$ to be positive. Note that, from (6.103), modes having $\widetilde{\omega} > 0$ have positive "norm", whereas those with $\widetilde{\omega} < 0$ have negative "norm". Now that we have evaluated the normalisation constant, we are ready for the construction of the quantum states. In particular, in the next chapter, we will display the procedure to derive the Boulware state and the Hartle-Hawking state for the system.

Summary

In this chapter, we have presented a comprehensive analysis of the classical scalar field on Kerr–AdS in five dimensions. We have provided a general overview of the Klein–Gordon equation (6.1), and, using the separability of this differential equation, we have solved both the angular and the radial parts.

We have detailed the calculations required to solve the angular part of the Klein–Gordon equation (6.8) using two methods: one utilising hypergeometric functions (6.25) and the other employing spin–weighted spherical harmonics (6.32). We have also shown that there is a choice associated with selecting the eigenvalue form (6.29), thanks to these two methods.

We have also shown how to solve the radial part of the Klein–Gordon equation (6.41) using two different approaches. The first method transformed the radial equation into the form of a Schrödinger equation (6.45), which allowed us to study the potential $V(r)$ and provided insights into the behaviour of the modes close to the event horizon. The second method transformed the radial equation into a Heun differential equation, whose solutions are given in terms of Heun functions (6.76). This form of the radial function is the one that we will use to evaluate the observables in Chapter 8, as the Heun functions are implemented in `Mathematica`, providing an advantage in the numerical calculations.

Finally, we have presented the normalisation procedure for the scalar field modes, which was the last step required to create an orthonormal basis of modes. This was the first step towards constructing the quantum states over the Kerr–AdS five-dimensional background, which will be the topic of the next chapter.

Chapter 7

Canonical quantisation on Kerr-AdS$_5$

In Chapter 6, we introduced the properties of a classical scalar field with general coupling on a classical background 5D Kerr-AdS spacetime. In this chapter, we quantize the scalar field in order to define quantum states while maintaining the background 5D Kerr-AdS spacetime as classical. We will achieve this by following the prescription of quantum field theory on curved backgrounds, using the canonical quantization method.

The process of canonically quantizing the scalar field involves decomposing the field Φ into sets of modes that are positive-frequency or negative-frequency with respect to a time coordinate, as we discussed in Part I. We will then define quantum operators for the positive-frequency modes, which will be annihilation operators, and quantum operators for the negative-frequency modes, which will be creation operators. A key aspect in the construction of these operators relies on the fact that positive-frequency modes have positive norm, while negative-frequency modes have negative norm. Only under these conditions will the canonical commutation relations associated with the operators be valid. In this manner, we will define the two quantum states, the Boulware [23] state and the Hartle-Hawking state [64].

We will also present a method to evaluate observables in a manner that does not require renormalization. We will use the two quantum states that we have defined, and we will exploit the fact that both these quantum states are Hadamard states (see Section 2.4), which means that their two-point functions share the same divergent part. This divergence depends only on the field and on the geometry of the spacetime, which are the same for both quantum states. This means that we can subtract the two expectation values of an observable in two different quantum states and obtain a quantity which is finite.

In Section 7.1, we will introduce the canonical quantization procedure, providing an easy example of its application. We will also display results to show how working in an asymptotically AdS five-dimensional spacetime can actually simplify the whole calculation. In

Sections 7.2 and 7.3, we will describe the construction of the Boulware state and the Hartle-Hawking state, which are quantum states that are going to be pivotal in the evaluation of observables. Finally, in Sections 7.4 and 7.5, we will evaluate the vacuum polarization and the renormalized stress-energy tensor.

7.1 Canonical quantization procedure

In the previous chapter, we solved the Klein-Gordon equation on the 5D Kerr-AdS black hole, giving us this form for the scalar field modes:

$$\Phi(r,\theta,\phi,\psi,t) = e^{im\phi+ip\psi-it\omega}X(r)Y(\theta), \tag{7.1}$$

where we now know the form of $X(r)$ (6.76) and $Y(\theta)$ (6.33). We have also evaluated the normalisation constant (6.104). (7.1) provides us with an orthonormal basis of modes in which we can decompose our field.

In order to canonically quantise the field, we need to decompose the scalar field modes introduced in Chapter 6 into sets of positive- and negative-frequency modes, following Section 2.2. We remind the reader that in Minkowski spacetime, there is a unique choice for the vacuum state. On the other hand, in QFTCS, this is not the case, as we discussed in Section 3.4. This arises from the diffeomorphism invariance of GR, which allows the scalar field to be decomposed into positive- and negative-frequency modes with respect to different time coordinates, depending on the chosen coordinate system. For this reason, we will present the construction of two quantum states, based on the coordinate system used for the field decomposition. Specifically, we will discuss the Boulware state and the Hartle–Hawking state, both introduced in Section 3.4.

We are about to reach one of the main goals of the analysis, which is the possibility of evaluating observables, such as the stress-energy tensor or the vacuum polarization. In order to do this, we have to define suitable quantum states to evaluate the expectation value of these quantum objects. These calculations are new in the literature since, as far as we know, no one has constructed the Hartle-Hawking or the Boulware states on a five dimensional Kerr-AdS black hole.

We start the analysis by giving a definition:

7.1.1 Definition. *Let us consider the Fourier transform of an arbitrary integrable function* $f : \mathbb{R} \to \mathbb{C}$,

$$\int_{-\infty}^{\infty} d\mathcal{X} e^{-i\mathfrak{p}\mathcal{X}} f(\mathcal{X}) = F(\mathfrak{p}) \quad \forall \mathfrak{p} \in \mathbb{R}, \tag{7.2}$$

where $F(\mathfrak{p})$ is the Fourier transform. Then if

$$\int_{-\infty}^{\infty} d\mathcal{X} e^{-i\mathfrak{p}\mathcal{X}} f(\mathcal{X}) = 0, \quad \mathfrak{p} > 0, \tag{7.3}$$

holds, the function $f(\mathcal{X})$ is defined to be ***positive frequency*** *w.r.t the variable $\mathcal{X}$. In the same way we can define the* ***negative frequency*** *w.r.t the variable $\mathcal{X}$ as*

$$\int_{-\infty}^{\infty} d\mathcal{X} e^{-i\mathfrak{p}\mathcal{X}} f(\mathcal{X}) = 0, \quad \mathfrak{p} < 0. \tag{7.4}$$

In order to define quantum states, we need to separate the positive frequency modes from the negative frequency modes. In our case, the frequency is denoted by the parameter ω, and from this we will construct the creation and annihilation operators as described in Section 2.2. We would like these modes to be defined with respect to the Kruskal coordinates (U, V), see Section 7.3. However, the modes are not well defined throughout the entire spacetime as the Kruskal coordinates. To overcome this problem, we are going to use the Heaviside function, so that we can write the following Lemma [110].

7.1.2 Lemma. *Let us take the Heaviside function $\Theta(\mathcal{X})$ w.r.t a variable $\mathcal{X}$,*

$$\Theta(\mathcal{X}) = \begin{cases} 1, & \mathcal{X} \geq 0 \\ 0, & \mathcal{X} < 0, \end{cases} \tag{7.5}$$

then

$$\int_{-\infty}^{\infty} d\mathcal{X} e^{-i\mathfrak{p}\mathcal{X}} \left\{ e^{-i\mathfrak{q}\ln(\mathcal{X})}\Theta(\mathcal{X}) + e^{-\pi q} e^{-i\mathfrak{q}\ln(-\mathcal{X})}\Theta(-\mathcal{X}) \right\} = 0, \tag{7.6}$$

for positive real $\mathfrak{p}$ and arbitrary $\mathfrak{q} \in \mathbb{R}$. By Definition 7.1.1 the quantity inside the curly brackets is defined to be positive frequency w.r.t $\mathcal{X}$. For the same reason we can define negative frequency taking the complex conjugate of Equation 7.6,

$$\int_{-\infty}^{\infty} d\mathcal{X} e^{i\mathfrak{p}\mathcal{X}} \left\{ e^{i\mathfrak{q}\ln(\mathcal{X})}\Theta(\mathcal{X}) + e^{-\pi q} e^{i\mathfrak{q}\ln(-\mathcal{X})}\Theta(-\mathcal{X}) \right\} = 0, \tag{7.7}$$

for positive real $\mathfrak{p}$ and arbitrary $\mathfrak{q} \in \mathbb{R}$.

Lastly, we want to emphasise once again that, due to the AdS boundary of the Kerr-AdS five-dimensional black hole, we have only one set of modes, as observed in the previous chapter. This greatly simplifies the analysis, and we do not encounter superradiance effects, which are typically expected in Kerr black holes. To visualise this, let us focus on Region I in Figure 4.6, see Figure 7.1. Given that the radial function takes the form in Equation (6.56), we can see that we have only one set of modes and that, due to the reflective boundary conditions we have chosen (Dirichlet boundary conditions), the modes are reflected back into the black hole. We have only one set of modes going "in" and "out". We are now ready to define and construct the quantum states. We begin by constructing the Boulware state.

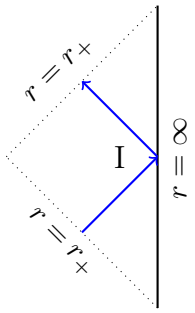

Figure 7.1: Region I of the Penrose diagram in Figure 4.6, where the blue lines indicates the scalar field modes.

7.2 Boulware state

In order to define the Boulware state [23], which corresponds to the vacuum state of the system defined w.r.t. the Schwarzschild-like coordinate t, we report the scalar field modes in terms of these coordinates. We find it useful for later calculation to also use the corotating coordinate $\psi_\star$ introduced in Equation (4.57). Hence, we have

$$\Phi = \frac{1}{2\sqrt{2}\pi\,|\widetilde{\omega}|\,r\sqrt{h(r)}} e^{-i\widetilde{\omega}t+ip\psi_\star} e^{i\widetilde{\omega}r_\star}\,{}_{-p/2}Y_\ell^m(\theta,\phi), \tag{7.8}$$

where this expression is valid only near the past event horizon since we are assuming that the radial function $R(r_\star)$ is of the form (6.56). The modes in Equation (7.8) are already an orthonormal basis and we can define $\Phi_{\widetilde{\omega}\ell mp}$ to have positive frequency with positive norm and $\Phi^\star_{\widetilde{\omega}\ell mp}$ to have negative frequency with negative norm when $\widetilde{\omega} > 0$. We will call them respectively $\Phi^+_{\widetilde{\omega}\ell mp}$ and $\Phi^-_{\widetilde{\omega}\ell mp}$.

$$\Phi^+ = \frac{1}{2\sqrt{2}\pi\,|\widetilde{\omega}|} e^{-i\widetilde{\omega}t+ip\psi_\star} e^{i\widetilde{\omega}r_\star}\,{}_{-p/2}Y_\ell^m(\theta,\phi), \quad \widetilde{\omega} > 0, \tag{7.9}$$

$$\Phi^- = \frac{1}{2\sqrt{2}\pi\,|\widetilde{\omega}|} e^{-i\widetilde{\omega}t+ip\psi_\star} e^{i\widetilde{\omega}r_\star}\,{}_{-p/2}Y_\ell^m(\theta,\phi), \quad \widetilde{\omega} < 0, \tag{7.10}$$

where these are defined in a neighbourhood of the *past event horizon*, where the coordinates $(t, r_\star, \theta, \phi, \psi_\star)$ remain regular and the solutions are well behaved. So the classical scalar field Φ can be written as a sum of modes as,

$$\Phi = \sum_{p=-\infty}^{\infty} \sum_{\ell=|p|/2}^{\infty} \sum_{m=-\ell}^{\ell} \left\{ \int_{-\infty}^{\infty} d\widetilde{\omega} \left[a_{\widetilde{\omega}\ell mp}\Phi^+_{\widetilde{\omega}\ell mp} + a^\dagger_{\widetilde{\omega}\ell mp}\Phi^-_{\widetilde{\omega}\ell mp} \right] \right\}, \tag{7.11}$$

where a and $a^\dagger$ are constants for the classical field. Since we were able to define the scalar field using an orthonormal basis of field modes, we can now proceed with the canonical quantization and promote the field and the expansion coefficients to operators,

$$\hat{\Phi} = \sum_{p=-\infty}^{\infty} \sum_{\ell=|p|/2}^{\infty} \sum_{m=-\ell}^{\ell} \left\{ \int_{-\infty}^{\infty} d\widetilde{\omega} \left[\hat{a}_{\widetilde{\omega}\ell mp}\Phi^+_{\widetilde{\omega}\ell mp} + \hat{a}^\dagger_{\widetilde{\omega}\ell mp}\Phi^-_{\widetilde{\omega}\ell mp} \right] \right\}, \tag{7.12}$$

where $\hat{a}$ and $\hat{a}^\dagger$ are respectively annihilation and creation operators, which satisfy the usual commutation relations,

$$[\hat{a}_{\widetilde{\omega}\ell mp}, \hat{a}^\dagger_{\widetilde{\omega}'\ell' m' p'}] = \delta(\widetilde{\omega} - \widetilde{\omega}')\delta_{\ell\ell'}\delta_{mm'}\delta_{pp'} \quad \text{for} \quad \widetilde{\omega} > 0, \tag{7.13}$$

$$[\hat{a}^\dagger_{\widetilde{\omega}\ell mp}, \hat{a}^\dagger_{\widetilde{\omega}'\ell' m' p'}] = 0, \tag{7.14}$$

$$[\hat{a}_{\widetilde{\omega}\ell mp}, \hat{a}_{\widetilde{\omega}'\ell' m' p'}] = 0 \tag{7.15}$$

We can then define the Boulware state by,

$$\hat{a}_{\widetilde{\omega}\ell mp} |B\rangle = 0 \quad \text{for} \quad \widetilde{\omega} > 0. \tag{7.16}$$

The Boulware state, defined as in Equation (7.16), is the natural definition of a ground state for an observer at constant $(r, \theta, \phi, \psi_\star)$, in other words, an observer corotating with the event horizon of the black hole. It has the physical interpretation of being as empty as possible to an observer far from the black hole who is also corotating with the event horizon.

7.3 Hartle-Hawking state

In order to define the Hartle-Hawking state, which corresponds to the vacuum state of the system defined w.r.t. the Kruskal coordinate U (see Equation (4.67)), we first need to report the expression for the scalar field modes in terms of these coordinates. The choice to use the Kruskal coordinate system has been motivated in Section 3.4.

Now in order to define positive and negative frequency, we should express the scalar field modes near the past event horizon in term of the Kruskal coordinates, we first introduce the coordinate $\widetilde{U}$ that will simplify the notation later on,

$$u = -\frac{1}{\kappa}\ln(-\widetilde{U}), \quad \text{where} \quad \widetilde{U} = \kappa U, \quad \widetilde{U} \in (-\infty, 0), \tag{7.17}$$

then for the outgoing modes near the past event horizon, we can write

$$\Phi_{\widetilde{\omega}p\ell m} = \frac{1}{2\sqrt{2}\pi\,|\widetilde{\omega}|\,r\sqrt{h(r)}} \exp\left[i\frac{\widetilde{\omega}}{\kappa_+}\ln\left(-\widetilde{U}\right)\right] e^{ip\psi_\star}{}_{-p/2}Y^m_\ell(\theta,\phi)\Theta\left(-\widetilde{U}\right), \tag{7.18}$$

where we again referred to a system of coordinates that is corotating with the black hole as in the construction of the Boulware state, using $\psi_\star$ defined in Equation (4.57) and we have included the Heaviside step function $\Theta(\mathsf{X})$ so that the argument of the logarithm is positive. The quantity κ_+ is the surface gravity (4.54), and $\widetilde{\omega}$ the shifted frequency (6.51). The scalar field modes that we have constructed in Equation (7.18) are nonzero in Region I and vanish in Region IV in Figure 4.6. From Equation (6.103) the modes (7.18) have positive "norm" when $\widetilde{\omega} > 0$ and negative "norm" when $\widetilde{\omega} < 0$. We want to construct positive and negative frequency modes that can be defined in both Region I and Region

IV. To achieve this, we need to define a set of modes that is nonvanishing in Region IV. This can be constructed by applying the transformation $\Psi = \Phi_{|_{(\widetilde{U},V)\to(-\widetilde{U},-V)}}$. The coordinate V does not appear in Equation (7.18) because we are considering the form of the modes near past event horizon where $V = 0$. Hence after the transformation we get:

$$\Psi_{\widetilde{\omega}p\ell m} = \frac{1}{2\sqrt{2}\pi\,|\widetilde{\omega}|\,r\sqrt{h(r)}} \exp\left[i\frac{\widetilde{\omega}}{\kappa_+}\ln\left(\widetilde{U}\right)\right] e^{ip\psi_\star}{}_{-p/2}Y_\ell^m(\theta,\phi)\Theta\left(\widetilde{U}\right), \tag{7.19}$$

where the modes have positive norm for negative $\widetilde{\omega}$ and negative norm for positive $\widetilde{\omega}$, as we can see from the inner product

$$\langle\Psi_{\widetilde{\omega}_1\ell_1m_1p_1}, \Psi_{\widetilde{\omega}_2\ell_2m_2p_2}\rangle = -\text{sign}(\widetilde{\omega})\delta(\widetilde{\omega}_1 - \widetilde{\omega}_2)\delta_{m_1m_2}\delta_{p_1p_2}\delta_{\ell_1\ell_2}. \tag{7.20}$$

For the construction of the Hartle-Hawking state, we are going to use Lemma 7.1.2. The second term of the Lemma can be built from (7.19) choosing the variables as,

$$\mathcal{X} = \widetilde{U} \quad \text{and} \quad \mathfrak{q} = -\frac{\widetilde{\omega}}{\kappa_+}, \tag{7.21}$$

this means that

$$\int_{-\infty}^{\infty} d\widetilde{U} e^{-i\mathfrak{p}\widetilde{U}} \left\{e^{i\widetilde{\omega}/\kappa\ln(\widetilde{U})}\Theta(\widetilde{U}) + e^{\pi\widetilde{\omega}/\kappa}e^{i\widetilde{\omega}/\kappa\ln(-\widetilde{U})}\Theta(-\widetilde{U})\right\} = 0, \tag{7.22}$$

where this is valid for arbitrary positive $\mathfrak{p}$. Then from (7.22), since the $\Phi_{\widetilde{\omega}\ell mp}$ are already normalized, we have

$$\int_{-\infty}^{\infty} d\widetilde{U} e^{-i\mathfrak{p}\widetilde{U}} \chi^+_{\widetilde{\omega}\ell mp} = 0 \quad \text{where} \quad \chi^+_{\widetilde{\omega}\ell mp} = \Psi_{\widetilde{\omega}\ell mp} + e^{\pi\widetilde{\omega}/\kappa}\Phi_{\widetilde{\omega}\ell mp}, \tag{7.23}$$

which are the positive frequency modes w.r.t. $\widetilde{U}$ for all $\widetilde{\omega}$. In regard of the negative frequency modes we can apply the same principle, and apply the Lemma 7.1.2 with the choice of

$$\mathcal{X} = \widetilde{U} \quad \text{and} \quad \mathfrak{q} = \frac{\widetilde{\omega}}{\kappa}, \tag{7.24}$$

giving

$$\int_{-\infty}^{\infty} d\widetilde{U} e^{i\mathfrak{p}\widetilde{U}} \left\{e^{i\widetilde{\omega}/\kappa\ln(\widetilde{U})}\Theta(\widetilde{U}) + e^{-\pi\widetilde{\omega}/\kappa}e^{i\widetilde{\omega}/\kappa\ln(-\widetilde{U})}\Theta(-\widetilde{U})\right\} = 0, \tag{7.25}$$

where this is valid for arbitrary positive $\mathfrak{p}$. Then from (7.25) we have

$$\int_{-\infty}^{\infty} d\widetilde{U} e^{-i\mathfrak{p}\widetilde{U}} \chi^-_{\widetilde{\omega}\ell mp} = 0, \quad \text{where} \quad \chi^-_{\widetilde{\omega}\ell mp} = \Psi_{\widetilde{\omega}\ell mp} + e^{-\pi\widetilde{\omega}/\kappa}\Phi_{\widetilde{\omega}\ell mp} \tag{7.26}$$

which define negative frequency modes w.r.t. $\widetilde{U}$ for all $\widetilde{\omega}$.

We have defined positive and negative frequency modes w.r.t. $\widetilde{U}$, hence we have a set of modes that can act as a basis, however, we need to normalize these in order to be able to quantize the field w.r.t. this basis. We introduce two normalization constant to be determined $\mathcal{N}^+_{\widetilde{\omega}\ell mp}$ and $\mathcal{N}^-_{\widetilde{\omega}\ell mp}$, which for simplicity we will report only with the $\widetilde{\omega}$

dependence in the following calculation. So, let us start with the positive frequency modes and consider,

$$\begin{aligned}
&\langle \mathcal{N}^{+}_{\widetilde{\omega}_1}\chi^{+}_{\widetilde{\omega}_1\ell mp}, \mathcal{N}^{+}_{\widetilde{\omega}_2}\chi^{+}_{\widetilde{\omega}_2\ell mp}\rangle \qquad (7.27)\\
&= e^{-\pi(\widetilde{\omega}_1+\widetilde{\omega}_2)/2\kappa}\mathcal{N}^{+}_{\widetilde{\omega}_1}\mathcal{N}^{+\star}_{\widetilde{\omega}_2}\left\langle \Psi_{\widetilde{\omega}_1\ell mp}, \Psi_{\widetilde{\omega}_2\ell mp}\right\rangle + e^{\pi(\widetilde{\omega}_1+\widetilde{\omega}_2)/2\kappa}\mathcal{N}^{+}_{\widetilde{\omega}_1}\mathcal{N}^{+\star}_{\widetilde{\omega}_2}\left\langle \Phi_{\widetilde{\omega}_1\ell mp}, \Phi_{\widetilde{\omega}_2\ell mp}\right\rangle\\
&= 2\mathcal{N}^{+}_{\widetilde{\omega}_1}\mathcal{N}^{+\star}_{\widetilde{\omega}_2}|\sinh(\pi\widetilde{\omega}/\kappa)|\delta(\widetilde{\omega}_1-\widetilde{\omega}_2),
\end{aligned}$$

where we used the facts that Ψ and Φ are orthonormal and the fact that $\langle\Psi|\Psi\rangle < 0$ for $\widetilde{\omega} > 0$. If we require normalized modes this means,

$$\mathcal{N}^{+}_{\widetilde{\omega}\ell mp} = \frac{1}{\sqrt{2|\sinh(\pi\widetilde{\omega}/\kappa)|}}. \qquad (7.28)$$

We can apply the same procedure to the negative frequency modes which gives us

$$\mathcal{N}^{-}_{\widetilde{\omega}\ell mp} = \frac{1}{\sqrt{2|\sinh(\pi\widetilde{\omega}/\kappa)|}}. \qquad (7.29)$$

Now that we have an orthonormal basis of positive and negative frequency modes we can write the field as a sum of these modes as

$$\Phi = \sum_{p=-\infty}^{\infty}\sum_{\ell=|p|/2}^{\infty}\sum_{m=-\ell}^{\ell}\left\{\int_{-\infty}^{\infty}d\widetilde{\omega}\frac{1}{\sqrt{2|\sinh(\pi\widetilde{\omega}/\kappa)|}}\left[b_{\widetilde{\omega}\ell mp}\chi^{+}_{\widetilde{\omega}\ell mp} + b^{\dagger}_{\widetilde{\omega}\ell mp}\chi^{-}_{\widetilde{\omega}\ell mp}\right]\right\}, \qquad (7.30)$$

where b and $b^{\dagger}$ are constants. In the same manner as before since we are able to define the scalar field using an orthonormal basis of field modes, we can now proceed with the canonical quantization and promote the field and the expansion coefficients to operators,

$$\hat{\Phi} = \sum_{p=-\infty}^{\infty}\sum_{\ell=|p|/2}^{\infty}\sum_{m=-\ell}^{\ell}\left\{\int_{-\infty}^{\infty}d\widetilde{\omega}\frac{1}{\sqrt{2|\sinh(\pi\widetilde{\omega}/\kappa)|}}\left[\hat{b}_{\widetilde{\omega}\ell mp}\chi^{+}_{\widetilde{\omega}\ell mp} + \hat{b}^{\dagger}_{\widetilde{\omega}\ell mp}\chi^{-}_{\widetilde{\omega}\ell mp}\right]\right\}, \qquad (7.31)$$

where $\hat{b}_{\widetilde{\omega}\ell mp}$ and $\hat{b}^{\dagger}_{\widetilde{\omega}\ell mp}$ are respectively annihilation and creation operators, which satisfy the usual commutation relations,

$$[\hat{b}_{\widetilde{\omega}\ell mp}, \hat{b}^{\dagger}_{\widetilde{\omega}'\ell'm'p'}] = \delta(\widetilde{\omega}-\widetilde{\omega}')\delta_{\ell\ell'}\delta_{mm'}\delta_{pp'}, \qquad (7.32)$$

$$[\hat{b}^{\dagger}_{\widetilde{\omega}\ell mp}, \hat{b}^{\dagger}_{\widetilde{\omega}'\ell'm'p'}] = 0, \qquad (7.33)$$

$$[\hat{b}_{\widetilde{\omega}\ell mp}, \hat{b}_{\widetilde{\omega}'\ell'm'p'}] = 0. \qquad (7.34)$$

Let us focus on Region I in Figure 4.6 of the spacetime, so that the modes $\Psi_{\widetilde{\omega}\ell mp}$ vanish, then the scalar field reduces to

$$\begin{aligned}
\hat{\Phi} = \sum_{p=-\infty}^{\infty}\sum_{\ell=|p|/2}^{\infty}\sum_{m=-\ell}^{\ell}\int_{-\infty}^{\infty}d\widetilde{\omega}\ &\frac{1}{\sqrt{2|\sinh(\pi\widetilde{\omega}/\kappa)|}}\\
&\times\left[\ \hat{b}_{\widetilde{\omega}\ell mp}e^{-\pi\widetilde{\omega}/2\kappa}\Phi_{\widetilde{\omega}\ell mp} + \ \hat{b}^{\dagger}_{\widetilde{\omega}\ell mp}e^{\pi\widetilde{\omega}/2\kappa}\Phi_{\widetilde{\omega}\ell mp}\right], \qquad (7.35)
\end{aligned}$$

Now we can define the Hartle-Hawking state by,

$$\hat{b}_{\widetilde{\omega}\ell mp}\,|HH\rangle = 0. \tag{7.36}$$

The Hartle-Hawking state $|HH\rangle$ is the natural definition of a ground state for an observer freely falling towards the event horizon of the black hole. It has the physical interpretation of exhibiting outgoing thermal radiation at infinity.

7.4 Vacuum polarization

Now that we have defined $|B\rangle$ and $|HH\rangle$, we can evaluate observables. The first and easiest observable to evaluate is the expectation value of the square of the quantum scalar field operator (also known as the "vacuum polarization" or the "scalar condensate"), and it is given by $\frac{1}{2}\langle\psi|\,\hat{\Phi}^\dagger\hat{\Phi}+\hat{\Phi}\hat{\Phi}^\dagger\,|\psi\rangle$ for a generic quantum state ψ. This quantity will need to be renormalized, but before that, let us start with evaluating the quantity $\langle B|\,\hat{\Phi}^\dagger\hat{\Phi}\,|B\rangle$. We will use the expression for the field operator as reported in Equation (7.12). Hence, since $|\Phi^-_{\widetilde{\omega}\ell mp}|^2 = |\Phi^+_{\widetilde{\omega}\ell mp}|^2$, we can write

$$\langle B|\,\hat{\Phi}^\dagger\hat{\Phi}\,|B\rangle = \sum_{p=-\infty}^{\infty}\sum_{\ell=|p|/2}^{\infty}\sum_{m=-\ell}^{\ell}\int_{-\infty}^{\infty}d\widetilde{\omega}\;|\Phi_{\widetilde{\omega}\ell mp}|^2\,\langle B|\,\hat{a}_{\widetilde{\omega}\ell mp}\hat{a}^\dagger_{\widetilde{\omega}\ell mp}\,|B\rangle\,, \tag{7.37}$$

and using the commutation rules,

$$\begin{aligned}\langle B|\,\hat{\Phi}^\dagger\hat{\Phi}\,|B\rangle &= \sum_{p=-\infty}^{\infty}\sum_{\ell=|p|/2}^{\infty}\sum_{m=-\ell}^{\ell}\int_{-\infty}^{\infty}d\widetilde{\omega}\;|\Phi_{\widetilde{\omega}\ell mp}|^2\,\langle B|\,(1-\hat{a}^\dagger_{\widetilde{\omega}\ell mp}\hat{a}_{\widetilde{\omega}\ell mp})\,|B\rangle\\ &= \sum_{p=-\infty}^{\infty}\sum_{\ell=|p|/2}^{\infty}\sum_{m=-\ell}^{\ell}\int_{-\infty}^{\infty}d\widetilde{\omega}\;|\Phi_{\widetilde{\omega}\ell mp}|^2.\end{aligned} \tag{7.38}$$

In the same way we can also evaluate the quantity $\langle B|\,\hat{\Phi}\hat{\Phi}^\dagger\,|B\rangle$ which gives us the same result. Hence we can write

$$\frac{1}{2}\,\langle B|\,\hat{\Phi}\hat{\Phi}^\dagger+\hat{\Phi}^\dagger\hat{\Phi}\,|B\rangle = \sum_{p=-\infty}^{\infty}\sum_{\ell=|p|/2}^{\infty}\sum_{m=-\ell}^{\ell}\int_{-\infty}^{\infty}d\widetilde{\omega}\;|\Phi_{\widetilde{\omega}\ell mp}|^2. \tag{7.39}$$

We can do the same analysis for $|HH\rangle$, so using (7.35), we can write

$$\begin{aligned}&\langle HH|\,\hat{\Phi}^\dagger\hat{\Phi}\,|HH\rangle =\\ &\quad= \sum_{p=-\infty}^{\infty}\sum_{\ell=|p|/2}^{\infty}\sum_{m=-\ell}^{\ell}\int_{-\infty}^{\infty}d\widetilde{\omega}\;\frac{e^{\pi\widetilde{\omega}/\kappa}}{2|\sinh(\pi\widetilde{\omega}/\kappa)|}|\Phi_{\widetilde{\omega}\ell mp}|^2\,\langle HH|\,\hat{b}_{\widetilde{\omega}\ell mp}\hat{b}^\dagger_{\widetilde{\omega}\ell mp}\,|HH\rangle\,,\end{aligned} \tag{7.40}$$

and using the commutation rules,

$$\begin{aligned}\langle HH|\,\hat{\Phi}^\dagger\hat{\Phi}\,|HH\rangle &= \sum_{p=-\infty}^{\infty}\sum_{\ell=|p|/2}^{\infty}\sum_{m=-\ell}^{\ell}\int_{-\infty}^{\infty}d\widetilde{\omega}\;\frac{e^{\pi\widetilde{\omega}/\kappa}|\Phi_{\widetilde{\omega}\ell mp}|^2}{2|\sinh(\pi\widetilde{\omega}/\kappa)|}\,\langle HH|\,(1-\hat{b}^\dagger_{\widetilde{\omega}\ell mp}\hat{b}_{\widetilde{\omega}\ell mp})\,|HH\rangle\\ &= \sum_{p=-\infty}^{\infty}\sum_{\ell=|p|/2}^{\infty}\sum_{m=-\ell}^{\ell}\int_{-\infty}^{\infty}d\widetilde{\omega}\;\frac{e^{\pi\widetilde{\omega}/\kappa}|\Phi_{\widetilde{\omega}\ell mp}|^2}{2|\sinh(\pi\widetilde{\omega}/\kappa)|}.\end{aligned} \tag{7.41}$$

In the same way as before we can also evaluate the quantity $\langle HH|\,\hat{\Phi}\hat{\Phi}^\dagger\,|HH\rangle$. We find

$$\langle HH|\,\hat{\Phi}\hat{\Phi}^\dagger\,|HH\rangle = \sum_{p=-\infty}^{\infty}\sum_{\ell=|p|/2}^{\infty}\sum_{m=-\ell}^{\ell}\int_{-\infty}^{\infty} d\widetilde{\omega}\ \frac{e^{-\pi\widetilde{\omega}/\kappa}|\Phi_{\widetilde{\omega}\ell mp}|^2}{2|\sinh(\pi\widetilde{\omega}/\kappa)|}. \tag{7.42}$$

Finally, we can evaluate the quantity $\langle HH|\,\hat{\Phi}^\dagger\hat{\Phi}+\hat{\Phi}\hat{\Phi}^\dagger\,|HH\rangle$,

$$\frac{1}{2}\langle HH|\,\hat{\Phi}^\dagger\hat{\Phi}+\hat{\Phi}\hat{\Phi}^\dagger\,|HH\rangle = \sum_{p=-\infty}^{\infty}\sum_{\ell=|p|/2}^{\infty}\sum_{m=-\ell}^{\ell}\int_{-\infty}^{\infty} d\widetilde{\omega}\ |\Phi_{\widetilde{\omega}\ell mp}|^2|\coth(\pi\widetilde{\omega}/\kappa)|. \tag{7.43}$$

The vacuum polarization in Equation (7.39) and in Equation (7.43) needs to be renormalized. However, in this thesis we will not present a renormalization procedure for this quantity; instead, we are going to exploit the properties of the Hadamard states introduced in Chapter 2. In fact, we can subtract the vacuum polarization evaluated in Equation (7.39) from that in Equation (7.43) to obtain a finite quantity that does not need renormalization. This is due to the fact that both the Boulware and Hartle-Hawking states are Hadamard states, which means that the divergent part of the expectation value of an observable is the same for both (see Section 2.6). Hence, we can write

$$\begin{aligned}\langle HH|\,\hat{\Phi}^\dagger\hat{\Phi}+\hat{\Phi}\hat{\Phi}^\dagger\,|HH\rangle - \langle B|\,\hat{\Phi}^\dagger\hat{\Phi}+\hat{\Phi}\hat{\Phi}^\dagger\,|B\rangle =\\ = \sum_{p=-\infty}^{\infty}\sum_{\ell=|p|/2}^{\infty}\sum_{m=-\ell}^{\ell}\int_{-\infty}^{\infty} d\widetilde{\omega}\ |\Phi_{\widetilde{\omega}\ell mp}|^2(|\coth(\pi\widetilde{\omega}/\kappa)|-1) =\\ = \sum_{p=-\infty}^{\infty}\sum_{\ell=|p|/2}^{\infty}\sum_{m=-\ell}^{\ell}\int_{-\infty}^{\infty} d\widetilde{\omega}\ |\Phi_{\widetilde{\omega}\ell mp}|^2\frac{1}{e^{2\pi|\widetilde{\omega}|/\kappa}-1},\end{aligned} \tag{7.44}$$

where we can see that the thermal factor is in the form of a Bose-Einstein distribution. We have finally retrieved the expression for the difference between the vacuum polarizations evaluated in two different ground states, which is finite and can be studied. This procedure can be used to evaluate all kinds of observables on the Kerr–AdS spacetime in five dimensions, and it gives us a sum over the scalar field modes that, with some manipulation, can be evaluated numerically (see Chapter 8).

7.5 Renormalized stress energy tensor

Now that we have presented the formula for the evaluation of vacuum polarization, we can introduce the next observable we would like to evaluate: the renormalized stress-energy tensor (RSET). As is known, the stress-energy tensor possesses divergences in the quantum picture, see Chapter 2. To eliminate these divergences, we can renormalize the stress-energy tensor using a prescription given by the theory of QFTCS. However, this process has some complications in the case of a rotating black hole, for which a more practical implementation has yet to be developed.

In this case, we will use the results we have obtained for the vacuum polarization and evaluate the stress-energy tensor again as a difference between quantum states, which circumvents the problem of renormalization. Indeed, we will have a finite observable that we can study; however, this will be a combination of the finite parts of the two quantum states we have defined earlier, the Boulware state and the Hartle-Hawking state. While we would also like to study a method to renormalize the stress-energy tensor utilizing just the Hartle-Hawking state, since the Boulware state is ill-defined on the event horizon, we still think this quantity is interesting to understand the behaviour of the scalar field in the 5D Kerr-AdS spacetime.

As we can see in Section 2.6, the vacuum polarisation appears directly in the expression of the renormalized stress–energy tensor; this is also why we decided to evaluate it before this observable. Applying the same method presented in the previous section, we obtain

$$\Delta\hat{T}_{\mu\nu} = \langle \mathrm{H}|\hat{T}_{\mu\nu}|\mathrm{H}\rangle - \langle \mathrm{B}|\hat{T}_{\mu\nu}|\mathrm{B}\rangle = \\ = \sum_{p=-\infty}^{\infty} \sum_{\ell=|p|/2}^{\infty} \sum_{m=-\ell}^{\ell} \int_{\widetilde{\omega}=-\infty}^{\infty} d\widetilde{\omega}\, \frac{{}^{\aleph}T_{\mu\nu}}{\exp\left(2\pi|\widetilde{\omega}|/\kappa_+\right) - 1}, \quad (7.45)$$

where ${}^{\aleph}T_{\mu\nu}$ is the classical SET for a scalar field mode in Equation (6.4). We use the notation $\aleph = \{\widetilde{\omega}, p, \ell, m\}$ to denote the quantum numbers on which the mode contribution to the SET depends. We will study the symmetries and the components of this quantity in Section 8.2, where we will also give the explicit analytical expression for each component.

Summary

In this chapter, we have quantised the scalar field and defined quantum states while maintaining the background 5D Kerr–AdS spacetime as classical. We achieved this using the canonical quantisation procedure. We then defined quantum operators corresponding to the positive-frequency modes, which are annihilation operators, and quantum operators corresponding to the negative-frequency modes, which are creation operators. We constructed the Boulware state and the Hartle–Hawking state, which we then used to evaluate observables. We presented the analysis to calculate the expectation values of the vacuum polarisation and of the renormalized stress–energy tensor through subtraction of the expectation values of the two quantum states.

Chapter 8

Numerical results

Having defined the Boulware $|\mathrm{B}\rangle$ and Hartle-Hawking $|\mathrm{H}\rangle$ states in the previous chapter, we now present the calculation, numerical evaluation, and results for the expectation values of the vacuum polarisation, evaluated in Section 7.4, and the SET evaluated in Section 7.5. In this chapter, we also describe the steps carried out using Mathematica to compute the numerical results for the stress-energy tensor and the vacuum polarisation, taking also a closer look at the HPC implementation and the numerical side of this calculation.

8.1 Vacuum polarization

The simplest non-trivial expectation value that we are going to numerically evaluate is the square of the scalar field $\langle\hat{\Phi}^2\rangle$, the vacuum polarization. We have presented the sum over the modes in Section 7.4. In this thesis, we will not provide a demonstration of how to renormalize this quantity, as this technique is yet to be developed, we will provide some discussion of this in the conclusion of the thesis, see Part III. Instead, we consider the difference between the two expectation values in Equation (7.44), which, being a finite quantity, gives us insightful information. This will give us important insights into the behaviour of the quantum field in this curved background. For convenience, we report the equation for the expectation value of the vacuum polarisation in Equation (7.44):

$$\frac{1}{2}\langle HH|\,\hat{\Phi}^\dagger\hat{\Phi}+\hat{\Phi}\hat{\Phi}^\dagger\,|HH\rangle-\frac{1}{2}\langle B|\,\hat{\Phi}^\dagger\hat{\Phi}+\hat{\Phi}\hat{\Phi}^\dagger\,|B\rangle= \\ =\sum_{p=-\infty}^{\infty}\sum_{\ell=|p|/2}^{\infty}\sum_{m=-\ell}^{\ell}\int_{-\infty}^{\infty}d\widetilde{\omega}\;|\Phi_{\widetilde{\omega}\ell mp}|^2\frac{1}{e^{2\pi|\widetilde{\omega}|/\kappa}-1}. \tag{8.1}$$

This difference in expectation values does not require renormalization, as the singular terms in the Green's function for the scalar field are independent of the quantum state [41].

In the next sections, we first describe the numerical method employed to compute (8.1), and then we will discuss the numerical results.

8.1.1 Mathematica computation

To evaluate Equation (8.1), we use the separated form of the scalar field, derived in Chapter 6, for the scalar field modes:

$$\Delta\hat{\Phi}^2 = \frac{1}{8\pi^2}\sum_{p=-\infty}^{\infty}\sum_{\ell=|p|/2}^{\infty}\sum_{m=-\ell}^{\ell}\int_{\widetilde{\omega}=-\infty}^{\infty} d\widetilde{\omega}\,\frac{|X_{\omega p\ell}(r)|^2\left|{}_{-p/2}Y_\ell^m(\theta,\varphi)\right|^2}{|\widetilde{\omega}|\left[\exp\left(2\pi|\widetilde{\omega}|/\kappa_+\right)-1\right]}, \tag{8.2}$$

where we know the form of the angular and radial function to be respectively a spin-weighted spherical harmonic and a Heun function. We observe that there is no dependence on the time coordinate t or the azimuthal coordinate ψ. Furthermore, as shown in Chapter 5, the norm of the spin-weighted spherical harmonics does not depend on φ, so the final expression of Equation (8.2) depends only on the radial coordinate r and the polar angle θ. In our numerical work, we use the coordinate z (6.60) instead of r as the radial coordinate. This choice is advantageous because the radial function $X_{\omega p\ell}(r)$ can be expressed in terms of the Heun function when applying the coordinate transformation $r \to z$, as described in Section 6.3.2. With this transformation, the entire region exterior to the event horizon, $r \in [r_+, \infty)$, is mapped to $z \in [0, 1]$. This approach not only simplifies the representation but also facilitates numerical computation, particularly as the Heun functions are built into `Mathematica`.

In Equation (8.2), we first evaluate the sum over m, which can be performed analytically using the addition theorem for spin-weighted spherical harmonics, as detailed in Chapter 5, see Equation (5.19). This yields:

$$\Delta\hat{\Phi}^2 = \frac{1}{32\pi^3}\sum_{p=-\infty}^{\infty}\sum_{\ell=|p|/2}^{\infty}\int_{\widetilde{\omega}=-\infty}^{\infty} d\widetilde{\omega}\,\frac{(2\ell+1)\,|X_{\omega p\ell}(r)|^2}{|\widetilde{\omega}|\left[\exp\left(2\pi|\widetilde{\omega}|/\kappa_+\right)-1\right]}. \tag{8.3}$$

We have obtained an analytical expression that we can now analyse numerically. As a first step in the numerical computation, it is useful to examine the behaviour of the integral over the shifted frequency $\widetilde{\omega}$. To do this, we define:

$$I_{p\ell}(r) = \int_{\widetilde{\omega}=-\infty}^{\infty} d\widetilde{\omega}\,\frac{|X_{\omega p\ell}(r)|^2}{|\widetilde{\omega}|\left[\exp\left(2\pi|\widetilde{\omega}|/\kappa_+\right)-1\right]}. \tag{8.4}$$

We must fix the parameters of the black hole and the scalar field. We select:

$$a = \frac{1}{2}, \quad L = 1, \quad M = 10, \quad \mu_0 = \frac{1}{100}, \tag{8.5}$$

and these values will be used throughout this chapter unless otherwise specified. They have been chosen to respect the bound imposed at the beginning of the analysis, namely that the light surface does not exist when $a < a_{\min}$. In this manner, we obtain a numerical expression for the integrand in Equation (8.4), which depends only on z, $\widetilde{\omega}$, ℓ, p, and m, where ℓ is either an integer or a half-integer and p is an integer. Specifically, we plotted

the integrand for a given mode, fixing the value of the radial coordinate to $z = \frac{1}{10}$, as shown in Figure 8.1. The qualitative behaviour of the integrand is unchanged when we modify the values of z, ℓ or p, with the cusp that we see in Figure 8.1 due to the presence of $|\widetilde{\omega}|$ in the denominator of Equation (8.4).

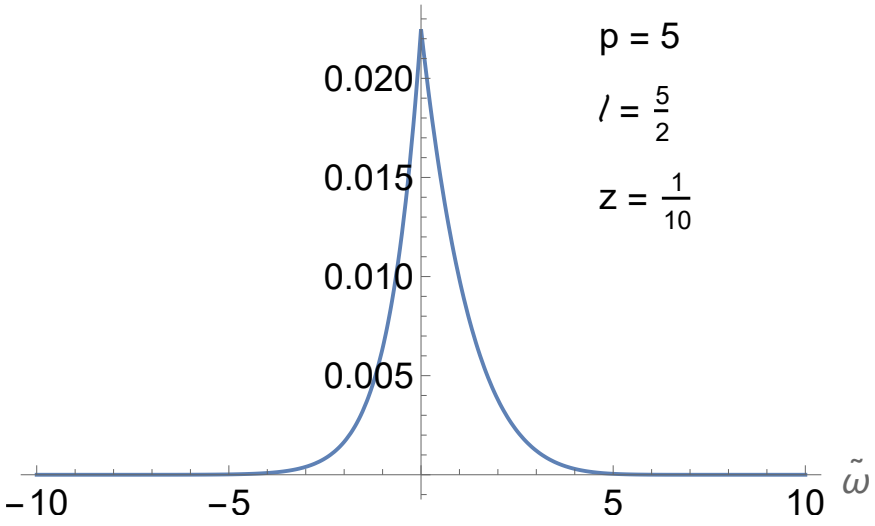

Figure 8.1: Integrand of Equation (8.4) as a function of the shifted frequency $\widetilde{\omega}$ (6.51). The integrand is evaluated at the radial coordinate $z = 1/10$ (6.60), for the scalar field mode with $p = 5$ and $\ell = 5/2$.

Notably, it is integrable, but there are three important aspects to consider. Firstly, the integrand converges quickly to zero for $|\widetilde{\omega}| \to \infty$, which is an important feature for numerical analysis because it allows us to limit the interval of integration significantly. Secondly, the integrand is not symmetric in $\widetilde{\omega}$, which is something to consider while limiting the integral interval. Lastly, the peak of this curve is quite sharp, so during the numerical analysis we had to implement the function `Exclusions` in the code to exclude this point in the calculation of the integral.

The integrals $I_{p\ell}(r)$ are computed using `Mathematica`'s built-in `NIntegrate` function. We have used a working precision of 32 digits, and the integration is performed over $|\widetilde{\omega}| \leq 30$. We picked this value for the integration interval in the convergence test on the integrand to see after which value of $\widetilde{\omega}$ the function get close to zero. The relative errors due to truncating the integration interval at this value are negligible. For instance, we estimate this truncation error to be less than 10^{-12} for the mode shown in Figure 8.1. The peak in Figure 8.1 typically increases as z decreases and decreases as either p or ℓ increases. While it is convenient from a coding perspective that the radial functions are expressed in terms of Heun functions, the evaluation of the integrals $I_{p\ell}(r)$ requires significant computational effort due to the numerical evaluation of these Heun functions. The integrals $I_{p\ell}(r)$ are evaluated on an evenly spaced grid of 99 points for $z \in (0, 1)$, for values of p and ℓ that

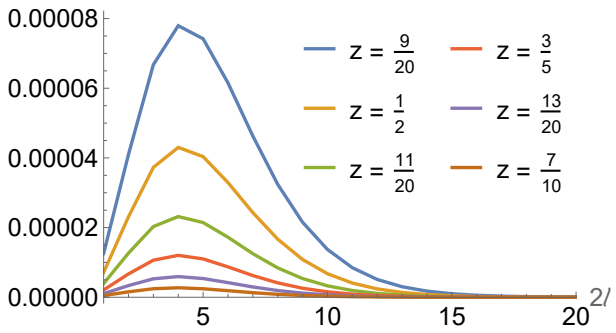

Figure 8.2: Summand $S_\ell(r)$ (8.7) as a function of 2ℓ for a selection of values of z (6.60).

we will discuss shortly. This translates to more than 1 hour of numerical computation per mode to derive the value of the integral for each of the 99 points of z.

Now that we have studied the integrand of $I_{p\ell}(r)$ and performed the integrals, we need to perform the summation over the quantum numbers p and ℓ. We can express Equation (8.3) as

$$\begin{aligned}\Delta\hat{\Phi}^2 &= \frac{1}{32\pi^3}\sum_{p=-\infty}^{\infty}\sum_{\ell=|p|/2}^{\infty}(2\ell+1)\,I_{p\ell}(r)\\ &= \frac{1}{32\pi^3}\sum_{2\ell=0}^{\infty}\sum_{p=-2\ell}^{2\ell}(2\ell+1)\,I_{p\ell}(r),\end{aligned} \tag{8.6}$$

where in the second line we have rewritten the two infinite sums over ℓ and p in an equivalent form. Using the second line is advantageous because it reduces the summation to a finite range of the quantum number p for each value of ℓ, with only the final summation over the infinite range of ℓ. The finite sum over p is, in this way, straightforward to compute for each value of ℓ and z. Defining

$$S_\ell(r) = \frac{1}{32\pi^3}\sum_{p=-2\ell}^{2\ell}(2\ell+1)\,I_{p\ell}(r), \tag{8.7}$$

the final step in our computation of the vacuum polarization is to evaluate

$$\Delta\hat{\Phi}^2 = \sum_{2\ell=0}^{\infty} S_\ell(r), \tag{8.8}$$

which will be discussed in Section 8.4. Typical summands $S_\ell(r)$ are shown in Figure 8.2 for a selection of values of the radial coordinate z (see Equation (6.60)). The profiles of S_ℓ as a function of 2ℓ have similar shapes for all values of z in Figure 8.2. In particular, there is a peak in the value of S_ℓ at $\ell \sim 4$ for each value of z, and S_ℓ then decreases rapidly as ℓ increases. The value of S_ℓ at the peak increases as z decreases, and S_ℓ is significantly greater than zero for larger values of ℓ as z decreases.

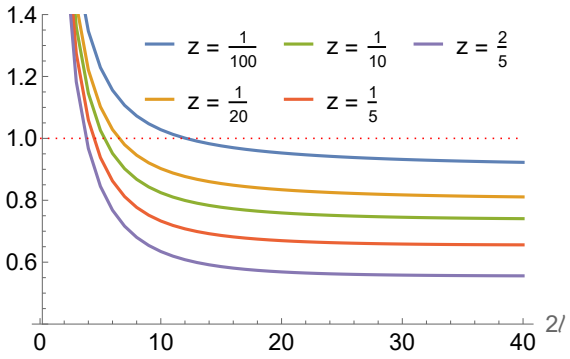

Figure 8.3: Ratio of the summands $S_{\ell+1}/S_\ell$ (8.7) as a function of 2ℓ for a selection of values of z (6.60).

8.1.2 Convergence test

In order to understand where we could truncate the numerical evaluation of the infinite sum over ℓ, we conducted a series of convergence tests. If the sum is convergent and we can determine the value of ℓ after which the terms become negligible, we can make a more precise approximation of the infinite sum. To this end, we employed three different methods, which are explained below.

The ratio method

The ratio method for series convergence involves calculating the limit of the absolute ratio of consecutive terms in the series. We define $\mathcal{L}$ as

$$\mathcal{L} = \lim_{n\to\infty} \left| \frac{f_{j+1}}{f_j} \right| \tag{8.9}$$

where f_j is a sequence in which each term is a real or complex number. The ratio method states that:

- if $\mathcal{L} < 1$ then the series converges absolutely,
- if $\mathcal{L} > 1$ then the series diverges,
- if $\mathcal{L} = 1$ the test is inconclusive.

To illustrate this, we evaluated and plotted the ratio of the summands $S_{\ell+1}/S_\ell$ for our specific case. In Figure 8.3, we show this ratio as a function of 2ℓ for a selection of values of z. We find that the ratio is less than 1 for sufficiently large 2ℓ, confirming that the sum is convergent. However, the sums over 2ℓ are not uniformly convergent as z varies, with the rate of convergence decreasing as z decreases.

Shanks method

We have also employed a series acceleration method called the Shanks method [69, 127, 130], which utilises partial sums. This transformation is a non-linear series acceleration

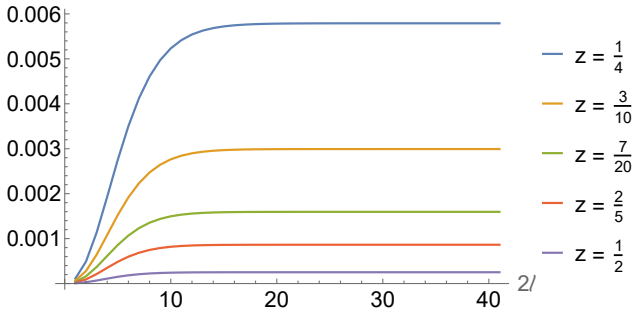

Figure 8.4: Partial sums $\widetilde{S}_\ell$ (8.11) as a function of 2ℓ for a selection of values of z (6.60).

technique designed to increase the rate of convergence of a sequence, at the expense of precision. We first introduce the partial sums

$$p_j = \sum_{k=1}^{j} f_k, \tag{8.10}$$

where f_k is a sequence in which each term is a real or complex number and j could, in principle, take any sufficiently large value. As in the previous case f_k will be represented by S_ℓ in Equation (8.8) in our analysis. For the vacuum polarization in our case, the partial sums are defined as

$$\widetilde{S}_\ell(r) = \sum_{2\ell'=0}^{2\ell} S_{\ell'}(r), \tag{8.11}$$

and are shown in Figure 8.4 for a selection of values of z. We can see that in this plot for each value of z, the partial sums converge for sufficiently large 2ℓ, with the limiting value increasing as z decreases. This is a crucial point for the employment of the series acceleration method, such as the Shanks method, because the series and the partial sums need to be convergent to accelerate the rate of convergence.

The Shanks method involves the sequence:

$$\mathcal{P}_j = \frac{p_{j+1}p_{j-1} - p_j^2}{p_{j+1} + p_{j-1} - 2p_j}, \tag{8.12}$$

where the p_j are the partial sums of f_k in Equation (8.10). The sequence $\mathcal{P}_j$ converges faster than the original series, providing valuable insights into the convergence of f_k. Another test that can be performed involves using the resulting sequence as the initial sum and repeating the construction process. However, due to the way this sequence is defined, the accelerated convergence comes at a price: precision loss. This is because the sequence in Equation (8.12) is nonlinear, which results in increasing the error. This is accentuated even more when looking at multiple iterations of this method.

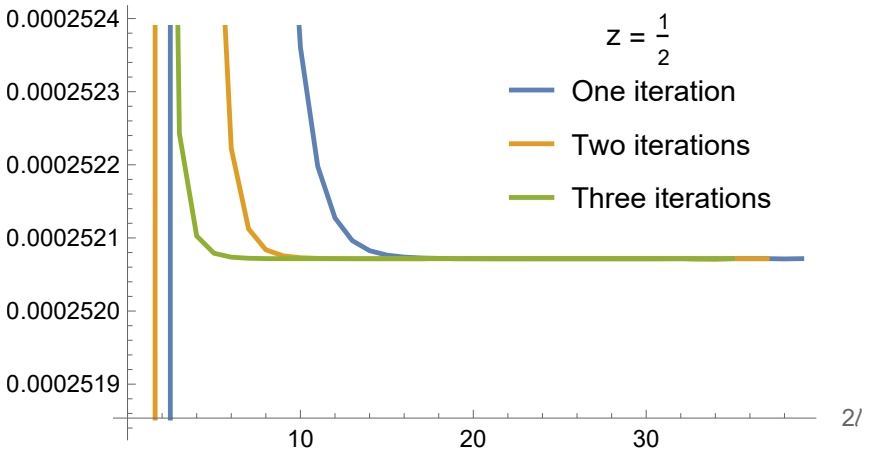

Figure 8.5: $\mathcal{S}_\ell$ plotted for $z = \frac{1}{2}$, showing the results for each of the three iterations of the Shanks method.

We can apply this method directly to our definition of the partial sums for the vacuum polarization in Equation (8.11). Hence, we can write

$$\mathcal{S}_\ell = \frac{\widetilde{S}_{\ell+1}\widetilde{S}_{\ell-1} - \widetilde{S}_\ell^2}{\widetilde{S}_{\ell+1} + \widetilde{S}_{\ell-1} - 2\widetilde{S}_\ell}. \tag{8.13}$$

We can see from Figure 8.4 that at $2\ell = 40$, $\mathcal{S}_\ell$ is convergent. Hence, we truncate the sum in Equation (8.8), which yields small relative errors, estimated to be of the order of 10^{-8} for $z = \frac{1}{2}$ at $2\ell = 40$. We can use $\mathcal{S}_\ell$ as the initial sum and repeat the process. In this iteration, the number of "modes" considered is reduced, with the maximum index decreasing from 40 to 38, and the process can be repeated for as many iterations as the initial maximum value of the summation index permits. In our case, an example of three iteration of the Shanks method is shown in Figure 8.5, which illustrates the convergence of the sum.

8.2 Stress-energy tensor

We now turn our attention to the expectation value of the quantum stress-energy tensor, $\hat{T}_{\mu\nu}$, as presented in Equation (7.45). We report the result for convenience here:

$$\Delta\hat{T}_{\mu\nu} = \langle \mathrm{H}|\hat{T}_{\mu\nu}|\mathrm{H}\rangle - \langle \mathrm{B}|\hat{T}_{\mu\nu}|\mathrm{B}\rangle = \\ = \sum_{p=-\infty}^{\infty} \sum_{\ell=|p|/2}^{\infty} \sum_{m=-\ell}^{\ell} \int_{\widetilde{\omega}=-\infty}^{\infty} d\widetilde{\omega}\, \frac{{}^{\aleph}T_{\mu\nu}}{\exp\left(2\pi|\widetilde{\omega}|/\kappa_+\right) - 1}, \tag{8.14}$$

where ${}^{\aleph}T_{\mu\nu}$ is the classical SET for a scalar field mode in Equation (6.4). We use the notation $\aleph = \{\widetilde{\omega}, p, \ell, m\}$ to denote the quantum numbers on which the mode contribution to the SET depends. Before delving into the numerical analysis we performed, let us focus on the properties and symmetries of this particular SET, which will simplify the study later on.

8.2.1 General properties of the stress-energy tensor

Symmetries

In five-dimensional spacetime, there are fifteen independent components of the stress-energy tensor, as it is a symmetric tensor. Using the mode solutions in Equation (6.4) of the scalar field equation, the form of these components, ${}^{\aleph}T_{\mu\nu}$, can be expressed in terms of the radial and angular functions $X_{\omega p\ell}(r)$ and ${}_s\widetilde{Y}^m_\ell(\theta)$. We will use the symmetries of the spacetime, given in Equation (4.6), to constrain the form and to find information about the components of the stress-energy tensor in Equation (8.14). We assume that the SET shares the symmetries of the underlying background.

We use the Killing vectors in Equation (4.19), so that the Lie derivatives of the SET along each of these Killing vectors vanish, given the properties shown in Chapter 1:

$$\mathcal{L}_{\xi_i}\langle\hat{T}^{\mu\nu}\rangle = 0, \qquad i = 0, 1, \ldots, 5. \tag{8.15}$$

We apply this to the first three Killing vectors in Equation (4.19). From this, we conclude that the components of $\langle\hat{T}^{\mu\nu}\rangle$ are independent of the coordinates t, φ, and ψ. The remaining independent Killing vectors, ξ_3 and ξ_4 in Equation (4.19), impose more complex constraints. Writing the Lie derivative $\mathcal{L}_{\xi_i}\langle\hat{T}_{\mu\nu}\rangle$ as

$$\begin{aligned} 0 &= \mathcal{L}_{\xi_i}\langle\hat{T}_{\mu\nu}\rangle \\ &= \xi_i^\alpha\partial_\alpha\langle\hat{T}^{\mu\nu}\rangle - (\partial_\alpha\xi_i^\mu)\langle\hat{T}^{\alpha\nu}\rangle - (\partial_\alpha\xi_i^\nu)\langle\hat{T}^{\mu\alpha}\rangle, \end{aligned} \tag{8.16}$$

gives fifteen equations for each of the two remaining Killing vectors. Considering the combination $\mathcal{L}_{\xi_4}\langle\hat{T}^{\mu\nu}\rangle\sin\varphi + \mathcal{L}_{\xi_5}\langle\hat{T}^{\mu\nu}\rangle\cos\varphi$ leads us to conclude that the following SET components vanish:

$$\langle\hat{T}^{t\theta}\rangle = \langle\hat{T}^{t\varphi}\rangle = \langle\hat{T}^{r\theta}\rangle = \langle\hat{T}^{r\varphi}\rangle = \langle\hat{T}^{\theta\varphi}\rangle = \langle\hat{T}^{\theta\psi}\rangle = 0. \tag{8.17}$$

In addition, it also gives us the following relations:

$$\langle\hat{T}^{\varphi\varphi}\rangle = \frac{\langle\hat{T}^{\theta\theta}\rangle}{\sin^2\theta}, \tag{8.18a}$$

$$\langle\hat{T}^{\varphi\psi}\rangle = -\frac{\langle\hat{T}^{\theta\theta}\rangle}{2\tan\theta\sin\theta}. \tag{8.18b}$$

Next, we consider $\mathcal{L}_{\xi_4}\langle\hat{T}^{\mu\nu}\rangle\cos\varphi - \mathcal{L}_{\xi_5}\langle\hat{T}^{\mu\nu}\rangle\sin\varphi$, which also tells us that the following

components do not depend on θ:

$$\frac{\partial}{\partial\theta}\langle\hat{T}^{rt}\rangle = 0, \tag{8.19a}$$
$$\frac{\partial}{\partial\theta}\langle\hat{T}^{rr}\rangle = 0, \tag{8.19b}$$
$$\frac{\partial}{\partial\theta}\langle\hat{T}^{\theta\theta}\rangle = 0, \tag{8.19c}$$
$$\frac{\partial}{\partial\theta}\langle\hat{T}^{tt}\rangle = 0, \tag{8.19d}$$
$$\frac{\partial}{\partial\theta}\langle\hat{T}^{t\psi}\rangle = 0, \tag{8.19e}$$
$$\frac{\partial}{\partial\theta}\langle\hat{T}^{r\psi}\rangle = 0. \tag{8.19f}$$

There is one further relation arising from this combination of Lie derivatives, which takes the form

$$\partial_\theta\langle\hat{T}^{\psi\psi}\rangle = -\frac{\langle\hat{T}^{\theta\theta}\rangle}{2\tan\theta\sin^2\theta}, \tag{8.20a}$$

and which is readily integrated to give

$$\langle\hat{T}^{\psi\psi}\rangle = \frac{\langle\hat{T}^{\theta\theta}\rangle}{4\sin^2\theta} + \mathcal{F}^{\psi\psi}(r), \tag{8.20b}$$

where $\mathcal{F}^{\psi\psi}(r)$ is an arbitrary function of r. In summary, we can write the SET in matrix form as follows:

$$\langle\hat{T}^{\mu\nu}\rangle = \begin{pmatrix} \mathcal{F}^{tt}(r) & \mathcal{F}^{tr}(r) & 0 & 0 & \mathcal{F}^{t\psi}(r) \\ \mathcal{F}^{tr}(r) & \mathcal{F}^{rr}(r) & 0 & 0 & \mathcal{F}^{r\psi}(r) \\ 0 & 0 & \mathcal{F}^{\theta\theta}(r) & 0 & 0 \\ 0 & 0 & 0 & \dfrac{\mathcal{F}^{\theta\theta}(r)}{\sin^2\theta} & -\dfrac{\mathcal{F}^{\theta\theta}(r)}{2\tan\theta\sin\theta} \\ \mathcal{F}^{t\psi}(r) & \mathcal{F}^{r\psi}(r) & 0 & -\dfrac{\mathcal{F}^{\theta\theta}(r)}{2\tan\theta\sin\theta} & \dfrac{\mathcal{F}^{\theta\theta}(r)}{4\sin^2\theta} + \mathcal{F}^{\psi\psi}(r) \end{pmatrix}, \tag{8.21}$$

where the $\mathcal{F}^{\bullet\bullet}(r)$ are arbitrary functions of r. We also note that the order in which the coordinates are displayed has changed from the previous choice $(r, \theta, \phi, \psi, t)$, see Equation (4.11), to the standard ordering $(t, r, \theta, \phi, \psi)$. This change is purely conventional and does not affect the results in any way. The important thing to notice is that the underlying symmetries of the black hole geometry have completely fixed the dependence of the SET components on the angle θ. This resembles the case of the static spherically symmetric black holes, and we are left with seven arbitrary functions of r, which are to be determined. We will determine these numerically later in this chapter.

Conservation

Before doing this, we can further constrain these seven arbitrary functions of r by imposing the requirement that the SET is conserved:

$$\nabla_\nu\langle\hat{T}_\mu{}^\nu\rangle = 0, \tag{8.22}$$

which we write in the alternative form

$$\partial_\nu \left(\mathsf{g} \langle \hat{T}_\mu{}^\nu \rangle \right) = \frac{1}{2} \mathsf{g} \left(\partial_\mu g_{\alpha\beta} \right) \langle \hat{T}^{\alpha\beta} \rangle, \tag{8.23}$$

where g is the determinant of the metric given by Equation (4.13). Utilizing the expressions of these quantities, we notice that the $\mu = \theta$ equation is trivial. Since the metric in Equation (4.6) does not depend on t, φ, or ψ, there are three simple conservation equations arising from Equation (8.23). The φ and ψ equations are identical and give

$$\frac{d}{dr}\mathcal{F}_1(r) + \left[\frac{2}{r} + \frac{f'(r)}{f(r)} + \frac{g'(r)}{g(r)} + 3\frac{h'(r)}{h(r)} \right] \mathcal{F}_1(r) = 0, \tag{8.24}$$

where we have defined

$$\mathcal{F}_1(r) = \mathcal{F}^{r\psi}(r) - \Omega(r)\mathcal{F}^{tr}(r) \tag{8.25}$$

and $f(r)$, $g(r)$, $h(r)$, and $\Omega(r)$ are the metric functions given in Equation (4.7). If we integrate Equation (8.2.1), we obtain

$$\mathcal{F}_1(r) = \frac{\mathcal{Y}}{r^2 f(r) g(r) h(r)^3} = \frac{\mathcal{Y}}{r^3 h(r)^2}, \tag{8.26}$$

where $\mathcal{Y}$ is an arbitrary constant. The $\mu = t$ equation arising from Equation (8.23) then takes the form

$$\frac{d}{dr}\mathcal{F}^{tr}(r) + \left(\frac{2}{r} + \frac{3f'(r)}{f(r)} + \frac{g'(r)}{g(r)} + \frac{h'(r)}{h(r)} \right) \mathcal{F}^{tr}(r) + \frac{\mathcal{Y}\Omega'(r)}{r^3 f(r)^2} = 0. \tag{8.27}$$

This is also readily integrated to give

$$\mathcal{F}^{tr}(r) = \frac{\mathcal{Z} - \mathcal{Y}\Omega(r)}{r^2 f(r)^3 g(r) h(r)} = \frac{\mathcal{Z} - \mathcal{Y}\Omega(r)}{r^3 f(r)^2}, \tag{8.28}$$

where $\mathcal{Z}$ is an arbitrary constant. Hence, using (8.25), we have

$$\mathcal{F}^{r\psi}(r) = \frac{1}{r^3 f(r)^2 h(r)^2} \left\{ \mathcal{Y} f(r)^2 + h(r)^2 \Omega(r) \left[\mathcal{Z} - \mathcal{Y}\Omega(r) \right] \right\}. \tag{8.29}$$

The remaining conservation equation (8.23) has $\mu = r$ and is more complicated:

$$\begin{aligned} 0 = {} & \frac{d}{dr}\mathcal{F}^{rr}(r) + \left[\frac{2}{r} + \frac{f'(r)}{f(r)} + \frac{2g'(r)}{g(r)} + \frac{h'(r)}{h(r)} \right] \mathcal{F}^{rr}(r) - \frac{1}{4g(r)^2} \left[2r + h(r)h'(r) \right] \mathcal{F}^{\theta\theta}(r) \\ & + \frac{1}{g(r)^2} \left\{ \left[f(r)f'(r) - h(r)h'(r)\Omega(r)^2 - h(r)^2\Omega(r)\Omega'(r) \right] \mathcal{F}^{tt}(r) \right. \\ & \left. + \left[2h(r)h'(r)\Omega(r) + h(r)^2\Omega'(r) \right] \mathcal{F}^{t\psi}(r) - h(r)h'(r)\mathcal{F}^{\psi\psi}(r) \right\}. \end{aligned} \tag{8.30}$$

We can integrate Equation (8.30) to obtain $\mathcal{F}^{rr}(r)$:

$$\mathcal{F}^{rr}(r) = \frac{1}{r^3 g(r)} \left[\mathcal{K} + \int_{r'=r_+}^{r} \Theta(r')\, dr' \right], \tag{8.31}$$

where $\mathcal{K}$ is an arbitrary constant, and we have defined

$$\Theta(r) = \frac{r^3}{g(r)}\Big\{ \left[f(r)f'(r) - h(r)h'(r)\Omega(r)^2 - h(r)^2\Omega(r)\Omega'(r)\right]\mathcal{F}^{tt}(r) + \left[2h(r)h'(r)\Omega(r) + h(r)^2\Omega'(r)\right]\mathcal{F}^{t\psi}(r) - h(r)h'(r)\mathcal{F}^{\psi\psi}(r) - \frac{1}{4}\left[2r + h(r)h'(r)\right]\mathcal{F}^{\theta\theta}(r)\Big\}. \quad (8.32)$$

We have found, by only using the symmetries of the spacetime and the properties of the SET, that the SET is determined by three arbitrary constants ($\mathcal{K}$, $\mathcal{Y}$ and $\mathcal{Z}$) and four arbitrary functions of the radial coordinate r only, namely $\mathcal{F}^{\theta\theta}(r)$, $\mathcal{F}^{tt}(r)$, $\mathcal{F}^{t\psi}(r)$ and $\mathcal{F}^{\psi\psi}(r)$. This is again a place where we can see the power of working in five dimensions. The enhanced symmetries that we were able to impose on the metric and on the spacetime compared to the four-dimensional Kerr metric managed to simplify tremendously the evaluation of the SET, enabling us to constrain the SET much more than in the Kerr case [111]. Studying the Kerr black hole introduced in Section 1.3, using the Killing vectors and the conservation equations in the same way we did for the five-dimensional case, gives the four-dimensional SET in terms of two arbitrary functions of the angle θ and six functions of both θ and r, which are constrained by two coupled equations [111]. In our scenario, the enhanced symmetry of the metric in Equation (4.6) managed to completely fix the dependence over the angular coordinates, especially θ, and reduced the components that we have to evaluate to just four unknown functions of r. However, the structure of the SET is more complex than the static spherically symmetric black hole case introduced in Section 1.3 and studied in [101], which is determined by just two arbitrary constants and two arbitrary functions of the radial coordinate.

Components

We now outline the computations that are needed to find the analytical expressions of these functions starting from the classical SET components (2.68) evaluated for a scalar field mode (6.4) with angular function ${}_s\widetilde{Y}^m_\ell(\theta)$. We omit the indices on the radial and angular functions for simplicity, as these equations, as the reader will see, are quite lengthy. In terms of the metric functions $f(r)$, $g(r)$, $h(r)$ and $\Omega(r)$ in Equation (4.7), the SET components are:

$${}^{\aleph}T_{tt} = \omega^2 |X(r)|^2 \widetilde{Y}(\theta)^2 + \frac{2\xi}{g(r)^2}\left[f(r)f'(r) - h(r)\Omega(r)\frac{d}{dr}\Big\{h(r)\Omega(r)\Big\}\right]\mathrm{Re}\Big\{X^*(r)X'(r)\Big\}\widetilde{Y}(\theta)^2 - \Big[f(r)^2 - h(r)^2\Omega(r)^2\Big]\mathfrak{Z}(r,\theta)\,, \quad (8.33a)$$

$${}^{\aleph}T_{tr} = -\omega\ \mathrm{Im}\Big\{X^*(r)X'(r)\Big\}\widetilde{Y}(\theta)^2, \quad (8.33b)$$

$$^{\aleph}T_{t\theta} = 0, \tag{8.33c}$$

$$\begin{aligned}^{\aleph}T_{t\varphi} = &-m\omega \left|X(r)\right|^2 \widetilde{Y}(\theta)^2 - \frac{2\xi}{r^2} h(r)^2 \Omega(r) \left|X(r)\right|^2 \widetilde{Y}'(\theta)\widetilde{Y}(\theta) \sin\theta \\ &+ \frac{\xi h(r)}{2g(r)^2} \Big[h(r)\Omega'(r) + 2h'(r)\Omega(r)\Big] \mathrm{Re}\Big\{X^*(r)X'(r)\Big\} \widetilde{Y}(\theta)^2 \cos\theta \\ &- \frac{1}{2} h(r)^2 \Omega(r) \mathfrak{Z}(r,\theta) \cos\theta\,, \end{aligned} \tag{8.33d}$$

$$\begin{aligned}^{\aleph}T_{t\psi} = &-p\omega \left|X(r)\right|^2 \widetilde{Y}(\theta)^2 \\ &+ \frac{\xi h(r)}{g(r)^2} \Big[h(r)\Omega'(r) + 2h'(r)\Omega(r)\Big] \mathrm{Re}\Big\{X^*(r)X'(r)\Big\} \widetilde{Y}(\theta)^2 \\ &- h(r)^2 \Omega(r) \mathfrak{Z}(r,\theta)\,, \end{aligned} \tag{8.33e}$$

$$\begin{aligned}^{\aleph}T_{rr} = &(1-2\xi) \left|X'(r)\right|^2 \widetilde{Y}(\theta)^2 \\ &- 2\xi\, g(r)^2 \left[\frac{1}{r^2 h(r)^2} \Big\{p^2 r^2 + \big(4\lambda + r^2\nu^2\big) h(r)^2\Big\} - \frac{1}{f(r)^2} \Big\{\omega - p\Omega(r)\Big\}^2\right] \\ &\times \left|X(r)\right|^2 \widetilde{Y}(\theta)^2 + 2\xi \left[\frac{f'(r)}{f(r)} + \frac{2h(r) + rh'(r)}{rh(r)}\right] \mathrm{Re}\Big\{X^*(r)X'(r)\Big\} \widetilde{Y}(\theta)^2 \\ &+ g(r)^2 \mathfrak{Z}(r,\theta)\,, \end{aligned} \tag{8.33f}$$

$$^{\aleph}T_{r\theta} = \left[(1-4\xi)\, \mathrm{Re}\Big\{X^*(r)X'(r)\Big\} + \frac{2\xi}{r} \left|X(r)\right|^2\right] \widetilde{Y}'(\theta)\widetilde{Y}(\theta)\,, \tag{8.33g}$$

$$^{\aleph}T_{r\varphi} = m\ \mathrm{Im}\Big\{X^*(r)X'(r)\Big\} \widetilde{Y}(\theta)^2\,, \tag{8.33h}$$

$$^{\aleph}T_{r\psi} = p\ \mathrm{Im}\Big\{X^*(r)X'(r)\Big\} \widetilde{Y}(\theta)^2\,. \tag{8.33i}$$

$$\begin{aligned}^{\aleph}T_{\theta\theta} = &(1-2\xi) \left|X(r)\right|^2 \widetilde{Y}'(\theta)^2 - \frac{\xi r}{2g(r)^2} \mathrm{Re}\Big\{X^*(r)X'(r)\Big\} \widetilde{Y}(\theta)^2 \\ &+ 2\xi \left[\lambda - \frac{1}{4}\Big(p\cot\theta - 2m\csc\theta\Big)^2\right] \left|X(r)\right|^2 \widetilde{Y}(\theta)^2 \\ &+ 2\xi \cot\theta \left|X(r)\right|^2 \widetilde{Y}'(\theta)\widetilde{Y}(\theta) + \frac{1}{4} r^2 \mathfrak{Z}(r,\theta)\,, \end{aligned} \tag{8.33j}$$

$$^{\aleph}T_{\theta\varphi} = 0\,, \tag{8.33k}$$

$$^{\aleph}T_{\theta\psi} = 0\,, \tag{8.33l}$$

$$\begin{aligned}^{\aleph}T_{\varphi\varphi} = {}& m^2\,|X(r)|^2\,\widetilde{Y}(\theta)^2 \\ & - \frac{\xi}{2g(r)^2}\Big[r\sin^2\theta + h(r)h'(r)\cos^2\theta\Big]\mathrm{Re}\Big\{X^*(r)X'(r)\Big\}\widetilde{Y}(\theta)^2 \\ & + \frac{\xi}{r^2}\Big[h(r)^2 - r^2\Big]\,|X(r)|^2\,\widetilde{Y}'(\theta)\widetilde{Y}(\theta)\sin(2\theta) \\ & + \frac{1}{4}\Big[r^2\sin^2\theta + h(r)^2\cos^2\theta\Big]\mathfrak{Z}(r,\theta)\,,\end{aligned} \tag{8.33m}$$

$$\begin{aligned}^{\aleph}T_{\varphi\psi} = {}& mp\,|X(r)|^2\,\widetilde{Y}(\theta)^2 - \frac{\xi h(r)h'(r)}{g(r)^2}\mathrm{Re}\Big\{X^*(r)X'(r)\Big\}\widetilde{Y}(\theta)^2\cos\theta \\ & + \frac{2\xi h(r)^2}{r^2}\,|X(r)|^2\,\widetilde{Y}'(\theta)\widetilde{Y}(\theta)\sin\theta + \frac{1}{2}h(r)^2\mathfrak{Z}(r,\theta)\cos\theta\,,\end{aligned} \tag{8.33n}$$

$$^{\aleph}T_{\psi\psi} = p^2\,|X(r)|^2\,\widetilde{Y}(\theta)^2 - \frac{2\xi h(r)h'(r)}{g(r)^2}\mathrm{Re}\Big\{X^*(r)X'(r)\Big\}\widetilde{Y}(\theta)^2 + h(r)^2\mathfrak{Z}(r,\theta)\,. \tag{8.33o}$$

where

$$\begin{aligned}\mathfrak{Z}(r,\theta) &= \left(2\xi - \frac{1}{2}\right)g^{\rho\sigma}\Phi_{;\rho}\Phi_{;\sigma} + \frac{1}{2}\left(4\xi - 1\right)\mu^2\Phi^2 + \xi R\left(2\xi - \frac{3}{10}\right)\Phi^2 \\ &= \left(2\xi - \frac{1}{2}\right)\left[\left\{\frac{p^2}{h(r)^2} + \frac{1}{r^2}\left[p\cot\theta - 2m\csc\theta\right]^2 - \frac{1}{f(r)^2}\left[\omega - p\Omega(r)\right]^2\right\}|X(r)|^2\,\widetilde{Y}(\theta)^2\right. \\ &\quad \left. + \frac{1}{g(r)^2}\left|X'(r)\right|^2\widetilde{Y}(\theta)^2 + \frac{4}{r^2}\,|X(r)|^2\,\widetilde{Y}'(\theta)^2\right] \\ &\quad + \left[\frac{1}{2}\left(4\xi - 1\right)\mu^2 + \xi R\left(2\xi - \frac{3}{10}\right)\right]|X(r)|^2\,\widetilde{Y}(\theta)^2.\end{aligned} \tag{8.33p}$$

In Equation (8.33), the radial functions $X(r)$ depend on the frequency ω and the azimuthal quantum number $p \in \mathbb{Z}$, while the angular functions $\widetilde{Y}(\theta)$ depend on the quantum number $m = -\ell, -\ell+1, \ldots, \ell-1, \ell$, the spin $s = -p/2$ and the quantum number $\ell = |s|, |s|+1, |s|+2, \ldots$.

We now use the addition theorems for the spin-weighted spherical harmonics in Chapter 5 to perform the sum over m in each of the SET components. We define new quantities $t_{\mu\nu}$ by

$$\sum_{m=-\ell}^{\ell} {}^{\aleph}T_{\mu\nu} = \frac{2\ell+1}{4\pi}t_{\mu\nu} \tag{8.34}$$

where ${}^{\aleph}T_{\mu\nu}$ are the components given in Equations (8.33). A further simplification arises from the fact that, for our particular modes (6.56), we have $\mathrm{Im}\{X^*(r)X'(r)\} = 0$. This can be seen by taking advantage of the Schrödinger-like equation defined in Section 6.3. We know from that analysis (see Equation (6.42)) that

$$X(r) = \frac{R(r_\star)}{r\,h(r)^{1/2}} = \frac{R(r_\star)}{\mathcal{F}(r)}. \tag{8.35}$$

Hence,

$$\begin{aligned}\mathrm{Im}\left\{X^*(r)X'(r)\right\} &= \mathrm{Im}\left\{\frac{R^*(r_\star)}{\mathcal{F}(r)}\left(\frac{R'(r_\star)}{\mathcal{F}(r)} - \frac{R(r_\star)}{\mathcal{F}(r)^2}\mathcal{F}(r)'\right)\right\}\\ &= \mathrm{Im}\left\{\frac{R^*(r_\star)}{\mathcal{F}(r)}\frac{R'(r_\star)}{\mathcal{F}(r)}\right\} - \mathrm{Im}\left\{\frac{R^*(r_\star)}{\mathcal{F}(r)}\frac{R(r_\star)}{\mathcal{F}(r)^2}\mathcal{F}(r)'\right\}\\ &= \frac{1}{\mathcal{F}(r)^2}\,\mathrm{Im}\left\{R^*(r_\star)\,R'(r_\star)\right\}, \end{aligned}\tag{8.36}$$

where we took advantage of the linearity of the Im function and the fact that $\mathrm{Im}\{R^*(r_\star)\,R(r_\star)\} = 0$. Near the horizon, as $r \to r_+$, the radial equation takes the form (6.52):

$$R(r_\star) \sim \mathcal{C}_+\, e^{i\widetilde{\omega}\, r_\star} + \mathcal{C}_-\, e^{-i\widetilde{\omega}\, r_\star}. \tag{8.37}$$

Thus, close to the event horizon we have:

$$\begin{aligned}\frac{dr_\star}{dr}\,\mathrm{Im}\left\{R^*(r_\star)\,R'(r_\star)\right\} &= \frac{dr_\star}{dr}\,\mathrm{Im}\Big\{\left[\mathcal{C}_+^*\, e^{-i\widetilde{\omega}\, r_\star} + \mathcal{C}_-^*\, e^{i\widetilde{\omega}\, r_\star}\right]\left[\mathcal{C}_+\, i\widetilde{\omega}\, e^{i\widetilde{\omega}\, r_\star} - \mathcal{C}_-\, i\widetilde{\omega}\, e^{-i\widetilde{\omega}\, r_\star}\right]\Big\}\\ &= \frac{dr_\star}{dr}\,\mathrm{Im}\Big\{i\widetilde{\omega}\,|\mathcal{C}_+|^2 - i\widetilde{\omega}\,|\mathcal{C}_-|^2 + i\widetilde{\omega}\,\mathcal{C}_-^*\mathcal{C}_+\, e^{2i\widetilde{\omega}\, r_\star} - i\widetilde{\omega}\,\mathcal{C}_+^*\mathcal{C}_-\, e^{-2i\widetilde{\omega}\, r_\star}\Big\}. \end{aligned}\tag{8.38}$$

Given the analysis we performed (see Equation (6.56)) and the fact that there is no superradiance effect in the Kerr-AdS$_5$ black hole in the slow-rotation regime, when $a < a_{\mathrm{min}}$, we know that $|\mathcal{C}_+| = |\mathcal{C}_-|$. Also, the complex conjugate of $+i\widetilde{\omega}\,\mathcal{C}_-^*\mathcal{C}_+\, e^{2i\widetilde{\omega}\, r_\star}$ is $-i\widetilde{\omega}\,\mathcal{C}_+^*\mathcal{C}_-\, e^{-2i\widetilde{\omega}\, r_\star}$, this means that if we sum this two we always obtain something real. Hence,

$$\frac{dr_\star}{dr}\,\mathrm{Im}\left\{R^*(r_\star)\,R'(r_\star)\right\} = \frac{dr_\star}{dr}\,\widetilde{\omega}\,\left(|\mathcal{C}_+|^2 - |\mathcal{C}_-|^2\right) = 0. \tag{8.39}$$

Then we have

$$\begin{aligned} t_{tt} = \omega^2\,|X(r)|^2 + \frac{2\xi}{g(r)^2}\Big[f(r)f'(r) - h(r)\Omega(r)\frac{d}{dr}\{h(r)\Omega(r)\}\Big]\mathrm{Re}\{X^*(r)X'(r)\}\\ - \Big[f(r)^2 - h(r)^2\Omega(r)^2\Big]\widetilde{\mathfrak{Z}}(r), \end{aligned}\tag{8.40a}$$

$$t_{tr} = 0, \tag{8.40b}$$

$$t_{t\theta} = 0, \tag{8.40c}$$

$$t_{t\varphi} = \Bigg\{ \frac{1}{2} p\omega \, |X(r)|^2 + \frac{\xi h(r)}{2g(r)^2} \Big[h(r)\Omega'(r) + 2h'(r)\Omega(r) \Big] \times \mathrm{Re}\{X^*(r)X'(r)\} - \frac{1}{2} h(r)^2 \Omega(r) \widetilde{\mathfrak{Z}}(r) \Bigg\} \cos\theta, \quad (8.40d)$$

$$t_{t\psi} = -p\omega \, |X(r)|^2 + \frac{\xi h(r)}{g(r)^2} \Big[h(r)\Omega'(r) + 2h'(r)\Omega(r) \Big] \mathrm{Re}\{X^*(r)X'(r)\} - h(r)^2 \Omega(r) \widetilde{\mathfrak{Z}}(r) \, , \quad (8.40e)$$

$$t_{rr} = \Big(1 - 2\xi\Big) \big|X'(r)\big|^2 - 2\xi \, g(r)^2 \left[\frac{1}{r^2 h(r)^2} \Big\{ p^2 r^2 + \Big(4\lambda + r^2 \nu^2 \Big) h(r)^2 \Big\} - \frac{1}{f(r)^2} \Big\{ \omega - p\Omega(r) \Big\}^2 \right] |X(r)|^2 + 2\xi \left[\frac{f'(r)}{f(r)} + \frac{2h(r) + rh'(r)}{rh(r)} \right] \mathrm{Re}\{X^*(r)X'(r)\} + g(r)^2 \widetilde{\mathfrak{Z}}(r), \quad (8.40f)$$

$$t_{r\theta} = 0, \quad (8.40g)$$

$$t_{r\varphi} = 0, \quad (8.40h)$$

$$t_{r\psi} = 0 \, , \quad (8.40i)$$

$$t_{\theta\theta} = \frac{1}{8} \Big(1 - 4\xi \Big) \Big(4\ell^2 + 4\ell - p^2 \Big) \, |X(r)|^2 + 2\xi \, \lambda \, |X(r)|^2 - \frac{\xi r}{2g(r)^2} \mathrm{Re}\{X^*(r)X'(r)\} + \frac{1}{4} r^2 \widetilde{\mathfrak{Z}}(r), \quad (8.40j)$$

$$t_{\theta\varphi} = 0 \, , \quad (8.40k)$$

$$t_{\theta\psi} = 0 \, , \quad (8.40l)$$

$$t_{\varphi\varphi} = \frac{1}{2} \mathfrak{C} \, |X(r)|^2 \, \widetilde{Y}(\theta)^2 - \frac{\xi}{2g(r)^2} \Big[r \sin^2\theta + h(r)h'(r) \cos^2\theta \Big] \mathrm{Re}\{X^*(r)X'(r)\} + \frac{1}{4} \Big[r^2 \sin^2\theta + h(r)^2 \cos^2\theta \Big] \widetilde{\mathfrak{Z}}(r), \quad (8.40m)$$

$$t_{\varphi\psi} = -\left\{\frac{1}{2}p^2\,|X(r)|^2 + \frac{\xi h(r)h'(r)}{g(r)^2}\mathrm{Re}\{X^*(r)X'(r)\} - \frac{1}{2}h(r)^2\widetilde{\mathfrak{Z}}(r)\right\}\cos\theta\,, \tag{8.40n}$$

$$t_{\psi\psi} = p^2\,|X(r)|^2 - \frac{2\xi h(r)h'(r)}{g(r)^2}\mathrm{Re}\{X^*(r)X'(r)\} + h(r)^2\widetilde{\mathfrak{Z}}(r). \tag{8.40o}$$

where $\mathfrak{C}$ is given by

$$\mathfrak{C} = \left(\ell^2+\ell-s^2\right)\sin^2\theta + 2s^2\cos^2\theta, \tag{8.40p}$$

and

$$\begin{aligned}\widetilde{\mathfrak{Z}}(r) = \Bigg\{&\frac{p^2}{h(r)^2} + \frac{1}{2r^2}\left(4\ell^2+4\ell-p^2\right) - \frac{1}{f(r)^2}\left[\omega - p\Omega(r)\right]^2 \\ &+\frac{1}{2}\left(4\xi-1\right)\mu^2 + \xi R\left(2\xi-\frac{3}{10}\right)\Bigg\}\,|X(r)|^2 \\ &+\frac{1}{g(r)^2}\left|X'(r)\right|^2 + \frac{1}{2r^2}\left(4\ell^2+4\ell-p^2\right)|X(r)|^2\,,\end{aligned} \tag{8.40q}$$

and we have simplified using the result in Equation (6.35) that we report for convenience

$$\lambda = \ell^2+\ell-s^2 = \ell^2+\ell-\frac{1}{4}p^2. \tag{8.41}$$

It can be seen from Equations (8.40) that all the dependence on the angle θ is now determined in closed form.

We now wish to compare the components in Equations (8.40) with the form of the SET in Equations (8.21) derived from symmetry principles. Using the metric in Equation (4.6) to lower the indices on Equations (8.21), we find

$$\begin{aligned}\langle\hat{T}_{tt}\rangle = &\left[f(r)^2 - h(r)^2\Omega(r)^2\right]^2\mathcal{F}^{tt}(r) \\ &+2\,h(r)^2\Omega(r)\left[f(r)^2-h(r)^2\Omega(r)^2\right]\mathcal{F}^{t\psi}(r) \\ &+h(r)^4\Omega(r)^2\,\mathcal{F}^{\psi\psi}(r) + \frac{1}{4}h(r)^4\Omega(r)^2\,\mathcal{F}^{\theta\theta}(r)\,,\end{aligned} \tag{8.42a}$$

$$\langle\hat{T}_{tr}\rangle = -g(r)^2\left[f(r)^2-h(r)^2\Omega(r)^2\right]\mathcal{F}^{tr}(r) - g(r)^2h(r)^2\Omega(r)\,\mathcal{F}^{r\psi}(r)\,, \tag{8.42b}$$

$$\langle\hat{T}_{t\theta}\rangle = 0\,, \tag{8.42c}$$

$$\begin{aligned}\langle\hat{T}_{t\varphi}\rangle = \frac{1}{2}h(r)^2\Bigg\{&\Omega(r)\left[f(r)^2-h(r)^2\Omega(r)^2\right]\mathcal{F}^{tt}(r) \\ &-\left[f(r)^2-2h(r)^2\Omega(r)^2\right]\mathcal{F}^{t\psi}(r) \\ &-h(r)^2\Omega(r)\,\mathcal{F}^{\psi\psi}(r) - \frac{1}{4}h(r)^2\Omega(r)\,\mathcal{F}^{\theta\theta}(r)\Bigg\}\cos\theta\,,\end{aligned} \tag{8.42d}$$

$$\langle\hat{T}_{t\psi}\rangle = h(r)^2\Big\{\Omega(r)\Big[f(r)^2 - h(r)^2\Omega(r)^2\Big]\,\mathcal{F}^{tt}(r) - \Big[f(r)^2 - 2h(r)^2\Omega(r)^2\Big]\,\mathcal{F}^{t\psi}(r) - h(r)^2\Omega(r)\,\mathcal{F}^{\psi\psi}(r) - \frac{1}{4}h(r)^2\Omega(r)\,\mathcal{F}^{\theta\theta}(r)\Big\}\,, \quad (8.42e)$$

$$\langle\hat{T}_{rr}\rangle = g(r)^4\,\mathcal{F}^{rr}(r)\,, \quad (8.42f)$$

$$\langle\hat{T}_{r\theta}\rangle = 0\,, \quad (8.42g)$$

$$\langle\hat{T}_{r\varphi}\rangle = \frac{1}{2}g(r)^2h(r)^2\Big\{\mathcal{F}^{r\psi}(r) - \Omega(r)\,\mathcal{F}^{tr}(r)\Big\}\cos\theta\,, \quad (8.42h)$$

$$\langle\hat{T}_{r\psi}\rangle = g(r)^2h(r)^2\Big\{\mathcal{F}^{r\psi}(r) - \Omega(r)\,\mathcal{F}^{tr}(r)\Big\}\,, \quad (8.42i)$$

$$\langle\hat{T}_{\theta\theta}\rangle = \frac{r^4}{16}\,\mathcal{F}^{\theta\theta}(r)\,, \quad (8.42j)$$

$$\langle\hat{T}_{\theta\varphi}\rangle = 0\,, \quad (8.42k)$$

$$\langle\hat{T}_{\theta\psi}\rangle = 0\,, \quad (8.42l)$$

$$\langle\hat{T}_{\varphi\varphi}\rangle = \frac{1}{4}h(r)^4\Big\{\Omega(r)^2\,\mathcal{F}^{tt}(r) - 2\Omega(r)\,\mathcal{F}^{t\psi}(r) + \mathcal{F}^{\psi\psi}(r)\Big\}\cos^2\theta + \frac{1}{16}\Big[h(r)^4\cos^2\theta + r^4\sin^2\theta\Big]\mathcal{F}^{\theta\theta}(r)\,, \quad (8.42m)$$

$$\langle\hat{T}_{\varphi\psi}\rangle = \frac{1}{2}h(r)^4\Big\{\Omega(r)^2\,\mathcal{F}^{tt}(r) - 2\Omega(r)\,\mathcal{F}^{t\psi}(r) + \mathcal{F}^{\psi\psi}(r)\Big\}\cos\theta + \frac{1}{8}h(r)^4\,\mathcal{F}^{\theta\theta}(r)\cos\theta\,, \quad (8.42n)$$

$$\langle\hat{T}_{\psi\psi}\rangle = h(r)^4\Big\{\Omega(r)^2\,\mathcal{F}^{tt}(r) - 2\Omega(r)\,\mathcal{F}^{t\psi}(r) + \mathcal{F}^{\psi\psi}(r)\Big\} + \frac{1}{4}h(r)^4\,\mathcal{F}^{\theta\theta}(r)\,. \quad (8.42o)$$

from which it is clear that the dependence on the angle θ in all components is of the same form. Let $\mathfrak{F}^{\bullet\bullet}$ be the classical mode contribution to $\mathcal{F}^{\bullet\bullet}$ arising from the scalar field mode (6.4), with the sum over m completed. To find the $\mathfrak{F}^{\bullet\bullet}$, it is simplest to use the inverse

metric in Equation (4.12) to raise both indices on the components in Equations (8.40) and then compare with Equations (8.21). This gives us

$$\mathfrak{F}^{tt}(r) = \frac{1}{f(r)^4}\Big[\omega - p\Omega(r)\Big]^2 |X(r)|^2 + \frac{2\xi\, f'(r)}{f(r)^3 g(r)^2}\mathrm{Re}\Big\{X^*(r)X'(r)\Big\} - \frac{1}{f(r)^2}\widetilde{\mathfrak{Z}}(r), \tag{8.43a}$$

$$\mathfrak{F}^{tr}(r) = 0, \tag{8.43b}$$

$$\begin{aligned}\mathfrak{F}^{t\psi}(r) = {}& \frac{1}{f(r)^4 h(r)^2}\Big\{\omega - p\Omega(r)\Big\}\Big\{p\, f(r)^2 + h(r)^2\Omega(r)\Big[\omega - p\Omega(r)\Big]\Big\}|X(r)|^2 \\ & - \frac{\xi}{f(r)^3 g(r)^2}\Big\{f(r)\Omega'(r) - 2f'(r)\Omega(r)\Big\}\mathrm{Re}\Big\{X^*(r)X'(r)\Big\} - \frac{\Omega(r)}{f(r)^2}\widetilde{\mathfrak{Z}}(r)\,,\end{aligned} \tag{8.43c}$$

$$\begin{aligned}\mathfrak{F}^{rr}(r) = {}& \frac{1}{g(r)^4}\Big(1 - 2\xi\Big)\big|X'(r)\big|^2 \\ & - 2\xi\Bigg[\frac{1}{g(r)^2}\Big\{\frac{4\lambda}{r^2} + \nu^2 + \frac{p^2}{h(r)^2} - \frac{\Big[\omega - p\Omega(r)\Big]^2}{f(r)^2}\Big\}|X(r)|^2 \\ & - \frac{1}{g(r)^4}\Big\{\frac{2}{r} + \frac{f'(r)}{f(r)} + \frac{h'(r)}{h(r)}\Big\}\mathrm{Re}\Big\{X^*(r)X'(r)\Big\}\Bigg] + \frac{1}{g(r)^2}\widetilde{\mathfrak{Z}}(r)\,,\end{aligned} \tag{8.43d}$$

$$\mathfrak{F}^{r\psi}(r) = 0, \tag{8.43e}$$

$$\begin{aligned}\mathfrak{F}^{\theta\theta}(r) = {}& \frac{2}{r^4}\Big(1 - 4\xi\Big)\Big[4\ell^2 + 4\ell - p^2\Big]|X(r)|^2 \\ & - 8\xi\Bigg[\frac{1}{r^3 g(r)^2}\mathrm{Re}\Big\{X^*(r)X'(r)\Big\} - \frac{4\lambda}{r^4}|X(r)|^2\Bigg] + \frac{4}{r^2}\widetilde{\mathfrak{Z}}(r)\,,\end{aligned} \tag{8.43f}$$

$$\begin{aligned}\mathfrak{F}^{\psi\psi}(r) = {}& \frac{1}{f(r)^4 h(r)^4}\Big\{p\, f(r)^2 + h(r)^2\Omega(r)\Big[\omega - p\Omega(r)\Big]\Big\}^2|X(r)|^2 \\ & - \frac{2\xi}{g(r)^2}\Big\{\frac{h'(r)}{h(r)^3} + \frac{\Omega(r)\Omega'(r)}{f(r)^2} - \frac{f'(r)\Omega(r)^2}{f(r)^3} - \frac{1}{r^3}\Big\}\mathrm{Re}\Big\{X^*(r)X'(r)\Big\} \\ & + \Big[\frac{1}{h(r)^2} - \frac{\Omega(r)^2}{f(r)^2}\Big]\widetilde{\mathfrak{Z}}(r),\end{aligned} \tag{8.43g}$$

where the above expressions will need to be multiplied by an overall factor of $(2\ell + 1)/4\pi$ in the final mode sums. We have found the analytical expression of the functions of r that were left in the SET after the study based on the symmetries of the spacetime. We will show the numerical results in Section 8.4.

Trace

In addition to these studies, we can also introduce and discuss the trace of the stress-energy tensor. This can work as a constraint on the SET components. In the case of a massless, conformally coupled scalar field, we have already seen that the trace vanishes without anomalies in five spacetime dimensions [41]. When the scalar field has general mass μ and coupling ξ to the scalar curvature, the trace $\langle \hat{T}^{\mu}_{\mu} \rangle$ is given by [41]

$$\langle \hat{T}^{\mu}_{\mu} \rangle = -\mu^2 \langle \hat{\Phi}^2 \rangle + 4 \left(\xi - \frac{3}{16} \right) \Box \langle \hat{\Phi}^2 \rangle, \tag{8.44}$$

which depends on the vacuum polarisation $\langle \hat{\Phi}^2 \rangle$. When we look at the massless ($\mu = 0$) and conformally coupled ($\xi = 3/16$) case, this evidently vanishes. Since we will have to compute the vacuum polarisation numerically, Equation (8.44) does not reduce the number of unknown functions of the SET. However, we will use this constraint as a useful check of our numerical results. In particular, using the SET form in Equation (8.21) and the metric in Equation (4.6), we have

$$\begin{aligned} \langle \hat{T}^{\mu}_{\mu} \rangle = \left[-f(r)^2 + h(r)^2 \Omega(r)^2 \right] \mathcal{F}^{tt}(r) - 2h(r)^2 \Omega(r) \mathcal{F}^{t\psi}(r) + g(r)^2 \mathcal{F}^{rr}(r) \\ + \frac{1}{4} \left[2r^2 - h(r)^2 \right] \mathcal{F}^{\theta\theta}(r) + h(r)^2 \mathcal{F}^{\psi\psi}(r). \end{aligned} \tag{8.45}$$

8.2.2 Mathematica computation

In this subsection, we will present the steps taken to obtain a form of $\Delta \hat{T}_{\mu\nu}$ in Equation (8.14) that is suitable for numerical computations. As a first step, we will use our knowledge of the symmetries and the conservation equations discussed in the previous subsection. As we have seen, in order to determine the difference in expectation values of the SET between the Hartle–Hawking and Boulware states in Equation (8.14), we require the determination of three arbitrary constants ($\mathcal{K}$, $\mathcal{X}$, and $\mathcal{Z}$) and the numerical computation of four functions of the radial coordinate r: $\mathcal{F}^{\theta\theta}(r)$, $\mathcal{F}^{tt}(r)$, $\mathcal{F}^{t\psi}(r)$, and $\mathcal{F}^{\psi\psi}(r)$.

We will implement some of the studies carried out for the vacuum polarization in Section 8.1. First, we require mode-sum expressions for the functions $\mathcal{F}^{\bullet\bullet}(r)$. To find these, we start with the expressions for ${}^{\aleph}T_{\mu\nu}$, the classical SET components for a scalar field mode in Equation (6.4), which are given in Equation (8.33). We then utilize our knowledge of spin-weighted spherical harmonics and sum over m using the addition theorems as presented in Chapter 5. The resulting quantities can be found in Equation (8.40). From these, we can express each $\mathcal{F}^{\bullet\bullet}(r)$ as an integral over the shifted frequency $\widetilde{\omega}$ and a sum over the quantum numbers p and ℓ:

$$\mathcal{F}^{\bullet\bullet}(r) = \frac{1}{4\pi} \sum_{2\ell=0}^{\infty} \sum_{p=-2\ell}^{2\ell} \int_{\widetilde{\omega}=-\infty}^{\infty} d\widetilde{\omega} \, \frac{(2\ell+1)\, \mathfrak{F}^{\bullet\bullet}(r)}{\exp\left(2\pi |\widetilde{\omega}|/\kappa_{+}\right) - 1}, \tag{8.46}$$

where expressions for the individual $\mathfrak{F}^{\bullet\bullet}(r)$ can be found in Equation (8.43). Now, we can proceed in the same way as we did for the vacuum polarization in Equation (8.6) and rewrite the sums over $p = -\infty, \ldots, \infty$ and $2\ell = |p|, \ldots \infty$ as a sum over a finite number of values of p and a sum over $2\ell = 0, \ldots \infty$. Once we have rewritten Equation (8.46), we observe that $\mathfrak{F}^{tr}(r) = 0 = \mathfrak{F}^{r\psi}(r)$, and hence $\mathcal{F}^{tr}(r) = 0 = \mathcal{F}^{r\psi}(r)$. Using Equations (8.26) and (8.28), we can immediately fix two of our constants as $\mathcal{Y} = 0 = \mathcal{Z}$.

For the remaining constant $\mathcal{K}$, it is more convenient to compute $\mathcal{F}^{rr}(r)$ directly. The reason is that the following derivation will be carried out numerically, and the evaluation of $\mathcal{K}$ would in practice only reproduce part of the definition of $\mathcal{F}^{rr}(r)$, leaving the second part to be evaluated numerically as well, see Equation (8.31). By focusing on $\mathcal{F}^{rr}(r)$ from the beginning, we simply shift the numerical computation from $\mathcal{K}$ to $\mathcal{F}^{rr}(r)$, which makes the procedure more straightforward and convenient. This implies that we will compute **five functions of** r, namely $\mathcal{F}^{\theta\theta}(r)$, $\mathcal{F}^{tt}(r)$, $\mathcal{F}^{t\psi}(r)$, $\mathcal{F}^{\psi\psi}(r)$, and $\mathcal{F}^{rr}(r)$. As in Section 8.1, we first perform the integral over the shifted frequency $\widetilde{\omega}$ in Equation (8.46). This leads to the following integral expressions for each p and ℓ:

$$I^{(1)}_{p\ell}(r) = \int_{\widetilde{\omega}=-\infty}^{\infty} d\widetilde{\omega}\, \frac{\omega\, |X_{\omega p\ell}(r)|^2}{|\widetilde{\omega}|\left[\exp\left(2\pi|\widetilde{\omega}|/\kappa_+\right) - 1\right]}, \tag{8.47a}$$

$$I^{(2)}_{p\ell}(r) = \int_{\widetilde{\omega}=-\infty}^{\infty} d\widetilde{\omega}\, \frac{\omega^2\, |X_{\omega p\ell}(r)|^2}{|\widetilde{\omega}|\left[\exp\left(2\pi|\widetilde{\omega}|/\kappa_+\right) - 1\right]}, \tag{8.47b}$$

$$I^{(3)}_{p\ell}(r) = \int_{\widetilde{\omega}=-\infty}^{\infty} d\widetilde{\omega}\, \frac{\mathrm{Re}\{X^*_{p\ell}(r) X'_{p\ell}(r)\}}{|\widetilde{\omega}|\left[\exp\left(2\pi|\widetilde{\omega}|/\kappa_+\right) - 1\right]}, \tag{8.47c}$$

$$I^{(4)}_{p\ell}(r) = \int_{\widetilde{\omega}=-\infty}^{\infty} d\widetilde{\omega}\, \frac{\left|X'_{\omega p\ell}(r)\right|^2}{|\widetilde{\omega}|\left[\exp\left(2\pi|\widetilde{\omega}|/\kappa_+\right) - 1\right]}, \tag{8.47d}$$

$$I^{(5)}_{p\ell}(r) = \int_{\widetilde{\omega}=-\infty}^{\infty} d\widetilde{\omega}\, \frac{|X_{\omega p\ell}(r)|^2}{|\widetilde{\omega}|\left[\exp\left(2\pi|\widetilde{\omega}|/\kappa_+\right) - 1\right]}, \tag{8.47e}$$

where $I^{(5)}_{p\ell}(r)$ coincides exactly with the integral $I_{p\ell}(r)$ presented in the study of the vacuum polarization in Equation (8.4). This explicitly demonstrates why studying the vacuum polarization was a crucial first step towards the evaluation of the stress-energy tensor. Hence, we will need to evaluate these five integrals numerically to obtain both the vacuum polarization and the stress-energy tensor.

In the same way as the integrand in Equation (8.4) $I_{p\ell}(r)$ (see Figure 8.1), the integrands in Equations (8.47) are regular and rapidly decaying as $|\widetilde{\omega}| \to \infty$. We will use similar methods to evaluate these integrals numerically; hence, we will employ `Mathematica`'s built-in `NIntegrate` function. However, these computations require a longer runtime than that needed for $I_{p\ell}(r)$, approximately four hours for one integral. We will provide a more detailed discussion on obtaining these numerical results in Section 8.3.

Once we have computed the integrals in Equations (8.47), we need to take appropriate combinations of these to study a sum over the modes. Using Equation (8.43), we obtain

$$\widetilde{\mathfrak{F}}^{\bullet\bullet}_{p\ell}(r) = \int_{\widetilde{\omega}=-\infty}^{\infty} d\widetilde{\omega}\, \frac{\mathfrak{F}^{\bullet\bullet}(r)}{\exp\left(2\pi|\widetilde{\omega}|/\kappa_+\right) - 1}, \tag{8.48}$$

in terms of which we have

$$\mathcal{F}^{\bullet\bullet}(r) = \frac{1}{4\pi} \sum_{2\ell=0}^{\infty} \sum_{p=-2\ell}^{2\ell} (2\ell+1)\, \widetilde{\mathfrak{F}}^{\bullet\bullet}_{p\ell}(r). \tag{8.49}$$

The sums over the quantum number p in Equation (8.49) are again straightforward to compute, just as in the vacuum polarization case, leaving only the sum over 2ℓ. To determine where it is possible to truncate this infinite sum for the SET, we reproduce the same convergence analysis performed for the vacuum polarization. We found that, as in the vacuum polarization case, summing over values of 2ℓ from 0 to 40 yields results that are accurate enough for our purposes. This is because we have performed the same analysis presented for the vacuum polarization for each component of the SET in Equation (8.42), and we saw that for 2ℓ around 20 the sums start to converge, so we took 2ℓ to 40 for good measure. We had to come to a compromise between precision and time of evaluation, since these calculations require a long time to produce numerical results, as we will discuss in the next section.

8.2.3 Consistency checks

In order to test our results and verify that our numerical computations are consistent, we perform several consistency checks. First, we validate our results by computing the trace of $\Delta\hat{T}_{\mu\nu}$ in Equation (8.14) using Equation (8.45) and comparing it with the result in Equation (8.44), which involves the difference in vacuum polarization between the Hartle-Hawking and Boulware states. For a conformally coupled field with $\xi = 3/16$, we find that the relative error is 10^{-12}.

Another check that we could perform is to verify that the stress-energy tensor we have computed satisfies the conservation equations and that Equation (8.44) holds for values of ξ other than 3/16. However, performing any of these checks for our functions $\mathcal{F}^{\bullet\bullet}(r)$ requires derivatives of quantities computed numerically. We obtained these values by interpolating our results between the grid points in z and then differentiating the interpolating function. This procedure introduces additional numerical errors. In our case, these errors are compounded by the fact that both the difference in vacuum polarization $\Delta\hat{\Phi}^2$ and the functions $\mathcal{F}^{\bullet\bullet}(r)$ vary by several orders of magnitude over the range of values of z (see, for example, Figure 8.7). Furthermore, different functions $\mathcal{F}^{\bullet\bullet}(r)$ have very different orders of magnitude at the same value of z, see Figure 8.8 and Figure 8.9. As a result, neither the

conservation equation test nor the trace test (for nonconformally-coupled fields) is giving meaningful results. However, we do find that, at intermediate values of z, the relative error in evaluating the conservation equation (8.30) is several orders of magnitude smaller than the largest magnitude of the $\mathcal{F}^{\bullet\bullet}(r)$ functions. This at least gives some credibility to our numerical results.

8.3 HPC implementation

In this section, we describe in detail the procedure used for the numerical analysis of both the vacuum polarization and the stress-energy tensor, utilizing the HPC computing facilities at the University of Sheffield. We also outline the challenges encountered during the computations and the solutions implemented to address them. Building on the analysis presented in Section 8.1 and Section 8.2, we evaluate the sum over the modes in Equation (8.46).

Regarding the integral over $\widetilde{\omega}$, it is important to note that the integrand is not symmetric with respect to $\widetilde{\omega} = 0$, as illustrated in Figure 8.1. This means that the tails of the integrand are different for every mode that we look at; for this reason, the integration range must be large enough to minimise the error introduced by truncating the interval over which we integrate. Furthermore, the sum over p is also constrained, due to the properties of the spin-weighted spherical harmonics, to the range $-2\ell \leq p \leq 2\ell$.

The code

We are now going to present the code that has been used to conduct the numerical evaluation, focusing on its structure. In particular, we have integrated $\widetilde{\omega}$ between -30 and 30, summed ℓ between 0 and 20, and p between -2ℓ and 2ℓ, for 99 points of z ranging from $\frac{1}{100}$ to $\frac{99}{100}$. In Figure 8.6 we report the code used to evaluate a fraction of the modes needed, specifically with ℓ going from 0 to 5. This is because, as we will see later, splitting the evaluation into different codes sped up the numerical evaluation. The structure of the code is identical for each case, with the interval of ℓ changed accordingly; for example, the next code would have ℓ between 6 and 10.

In Figure 8.6 highlighted in yellow, we can see the `For` and the `Do` functions. The first fixes j, which is what we have called 2ℓ, and the second fixes a value of p that runs from -2ℓ to 2ℓ. Once these two quantum numbers are fixed, the code proceeds with performing the integral for $\widetilde{\omega}$ using the function `NIntegrate`, highlighted in red in Figure 8.6, for each of the 99 points of z, creating a table with all these values. It will export each of these evaluations in a file, in which we will have the numerical evaluation of the integral for 99 different points of z with fixed p and j. Once this is done for every p associated with the

```
Clear[list002];
For[j=0,j≤10,j++,Print["Processing 2l = ",j];
Do[Print["  Processing p = ",i[[1]]," to ",i[[-1]]];
ParallelDo[list002=ConstantArray[0,{99}];(*Initialize list002*)testsum1=Vacuum/. p→k/. l→j/2;
timingResult=Timing[
list002=Table[Quiet[Check[NIntegrate[testsum1,{ωt,-30,30},Exclusions→{0},
WorkingPrecision→20],0]],{z,1/100,99/100,1/100}]];
Print["Time taken for l=",j,", p=",k,": ",timingResult[[1]]," seconds"];
Export[StringJoin["HPC_Vacuum_2l",ToString[j],"_p",ToString[k],".dat"],list002];,{k,i}];
,{i,Partition[Range[-j,j,2],UpTo[10]]}]]
Clear[list002];
```

Figure 8.6: Sample of the code that has been used in HPC to perform the numerical integration.

respective value of j, the code will start again and fix the next j, repeating until completion. Notably, p is the quantum number associated with the spin in the spin-weighted spherical harmonics, so it increases by one each time. However, in Figure 8.6 we are considering the fact that $j = 2\ell$ for this reason the steps are set at two as we can see on the bottom line inside the `Range` function.

While we were attempting to generate this code, we encountered some complications. The integrals for one mode, with fixed values of p and j, took almost 4 days of computation to give a result, for all 99 points of z. This is due to the high complexity of the expression of the Heun functions, which are also very sensitive to changes in parameters. To overcome this problem, we not only requested more CPU resources from the HPC but also added a string to the code `ParallelDo` that allows us to parallelize the process, highlighted in green in Figure 8.6. This way, the code can use multiple cores of the HPC to evaluate the integrals, meaning that we were able to evaluate multiple integrals simultaneously. For fixed j, we were able to evaluate the integrals for 99 points of z for multiple values of p at the same time, which sped up the analysis significantly.

Another problem was related to the need for a safety net in case the code crashed during the evaluation of an integral. For this reason, we added the functions `Quiet` and `Check`, which prevent error messages from appearing in the final output. Additionally, if one of the integrals was not evaluated correctly, it assigns a value of zero to that integral. This allows the code to continue the loop until completion. Even though in a few instances most of the errors occurred because the integral was too small to evaluate, hence this approach also serves as a reasonable approximation. In particular, this was happening for extremal values of p, specifically when p is equal to -2ℓ or 2ℓ. The integral was giving quite small results. To address this issue, other that introducing a safety net we needed to improve the working precision to twenty decimal digits. Fortunately, this can be easily

done by adding the function `WorkingPrecision` in Mathematica.

8.4 Final results

We now present the results of our numerical computations obtained using the HPC code described in the previous section. First, we display the vacuum polarisation results, followed by an analysis of the five functions of r that form the components of the SET. Throughout this chapter, the spacetime parameters are fixed as given in Equation (8.5).

8.4.1 Vacuum polarisation numerical results

The vacuum polarisation, as expressed in Equation (8.1), is shown in Figure 8.7. The upper plot in Figure 8.7 shows the difference in vacuum polarisation between the Hartle-Hawking and Boulware states using a linear scale. It can be seen that this difference tends to zero as $z \to 1$, corresponding to the Anti-de Sitter boundary at $r \to \infty$, while it diverges as $z \to 0$, close to the event horizon. In the upper plot of Figure 8.7, the difference in vacuum polarisation becomes indistinguishable from zero for $z \gtrsim 0.2$. In order to clarify its behaviour near the event horizon, we present the lower plot in Figure 8.7 which gives the representation of the same data on a log-log scale. This highlights the rate of divergence as $z \to 0$.

This divergence is expected because the Boulware state $|\mathrm{B}\rangle$ diverges on the event horizon since it is ill-defined there, while the Hartle-Hawking state is expected to be regular on the event horizon. This is in agreement with the divergence of $\langle \mathrm{B}|\hat{\Phi}^2|\mathrm{B}\rangle$ at the event horizon of, for example, a Schwarzschild black hole [29,89]. This is because the Boulware state $|\mathrm{B}\rangle$ is expected to be a vacuum state and to be as empty of particles as possible, far from the black hole, see Section 7.2. We expect that $\langle \mathrm{B}|\hat{\Phi}^2|\mathrm{B}\rangle$ tends to zero very quickly as $r \to \infty$ and $z \to 1$. Hence, we can infer that $\langle \mathrm{H}|\hat{\Phi}^2|\mathrm{H}\rangle$ tends to zero as $z \to 1$ from Figure 8.7.

On the other hand, the Hartle-Hawking state $|\mathrm{H}\rangle$ represents a black hole in thermal equilibrium with a heat bath at the Hawking temperature $\kappa_+/2\pi$, which, at the event horizon, is regular, see Section 7.3. The vacuum polarisation for a quantum scalar field in a thermal equilibrium state in pure Anti-de Sitter spacetime tends to its vacuum expectation value at the boundary [7,10,18,103,107]. This is also the case for the 5D Kerr-AdS black hole in which the vacuum polarisation in the Hartle-Hawking state approaches that in the Boulware state far from the black hole.

8.4.2 Stress energy tensor numerical results

In this section, we present our numerical results for the difference in expectation values between the Hartle–Hawking and Boulware quantum states of the stress-energy tensor, as

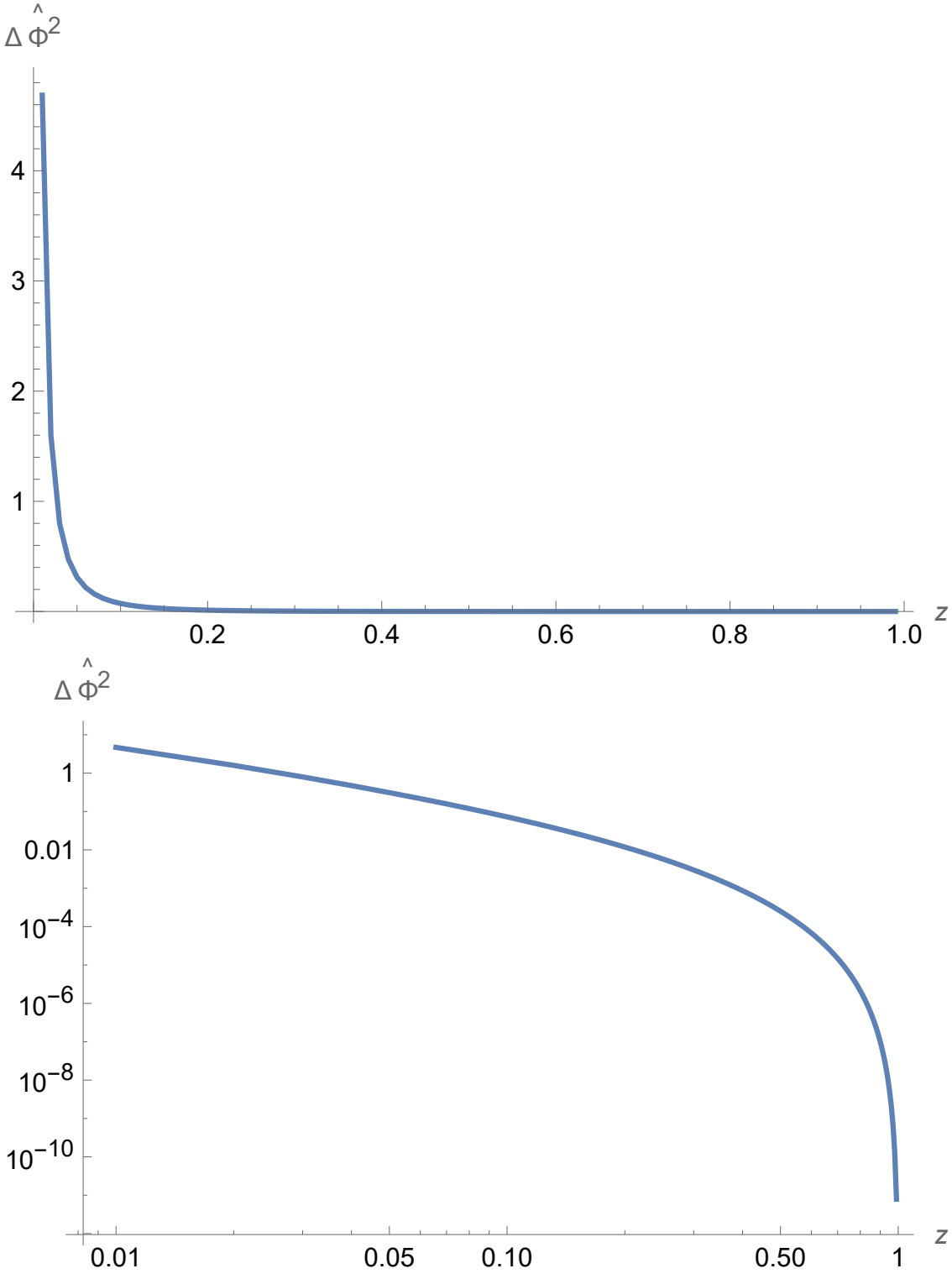

Figure 8.7: Difference in expectation values of the vacuum polarisation in the Hartle-Hawking and Boulware states, shown in Equation (8.2), as a function of the radial coordinate z (defined in Equation (6.60)). The upper plot displays the values on a linear scale, while the lower plot uses a log-log scale.

expressed in Equation (8.14).

We first plot the functions $\mathcal{F}^{\bullet\bullet}$ as functions of z in the conformally coupled case $\xi = 3/16$, in Figure 8.8. What we can see is that the resulting graphs are not particularly informative and resemble the vacuum polarisation shown in Figure 8.7. In particular, these functions diverge at the event horizon and decay rapidly to zero as $z \to 1$, confirming the behaviour of the field both at the event horizon and at infinity as described for the vacuum polarisation. Notably, the range of values is very different for each component of the SET and the $\mathcal{F}^{\theta\theta}_{\xi=3/16}(r)$ becomes negative after a certain value of z. We also plot the functions $\mathcal{F}^{\bullet\bullet}$ in a log-log plot, as we did for the vacuum polarization (see Figure 8.9). This again confirms the asymptotic behaviour at infinity that we expected from the analysis of the vacuum polarization, and does not provide any additional insight into the behaviour of the $\mathcal{F}^{\bullet\bullet}$ functions.

To gain more insight into the behaviour of the SET components, we instead consider ratios of the functions $\mathcal{F}^{\bullet\bullet}$ for selected values of the coupling constant ξ, normalised by their corresponding values when $\xi = 3/16$, where the scalar field is conformally coupled, see Figure 8.10. This operation brought the numerical values to be comparable, allowing us to see the behaviour of each component more clearly.

The radial functions $X_{\omega p\ell}(r)$, found from the radial equation (6.76), and the vacuum polarisation in Equation (8.2) depend on the scalar field mass μ and coupling ξ only through the combination μ_0 in Equation (6.2). However, as seen in Equation (8.43), the SET components and functions $\mathcal{F}^{\bullet\bullet}(r)$ depend separately on μ^2 and ξ. Given the computational intensity of our numerical calculations, as described in Section 8.3, we present results for a fixed value of $\mu_0 = 1/100$. With this fixed μ_0, we can vary both the coupling constant ξ and the mass μ, allowing us to study how the SET changes with different couplings to the scalar curvature.

A similar approach was taken in [13,138], where the SET on four-dimensional Schwarzschild and Reissner-Nordström backgrounds was analysed. In those cases, the Ricci scalar curvature vanishes identically, meaning that ξ does not appear in the scalar field equation, and the scalar field mass plays a role analogous to our μ_0. The results in [13,138] indicate that varying the scalar field mass does not significantly alter the qualitative behaviour of the SET components. However, changes in the coupling constant ξ can have a substantial effect, influencing whether the SET components increase or decrease monotonically with radius, as well as determining the presence of maxima or minima. In Figure 8.10, we explore the effect of varying the coupling constant ξ, and consequently the scalar field mass μ, while keeping the effective mass μ_0 fixed. We find that changes in ξ have a sig-

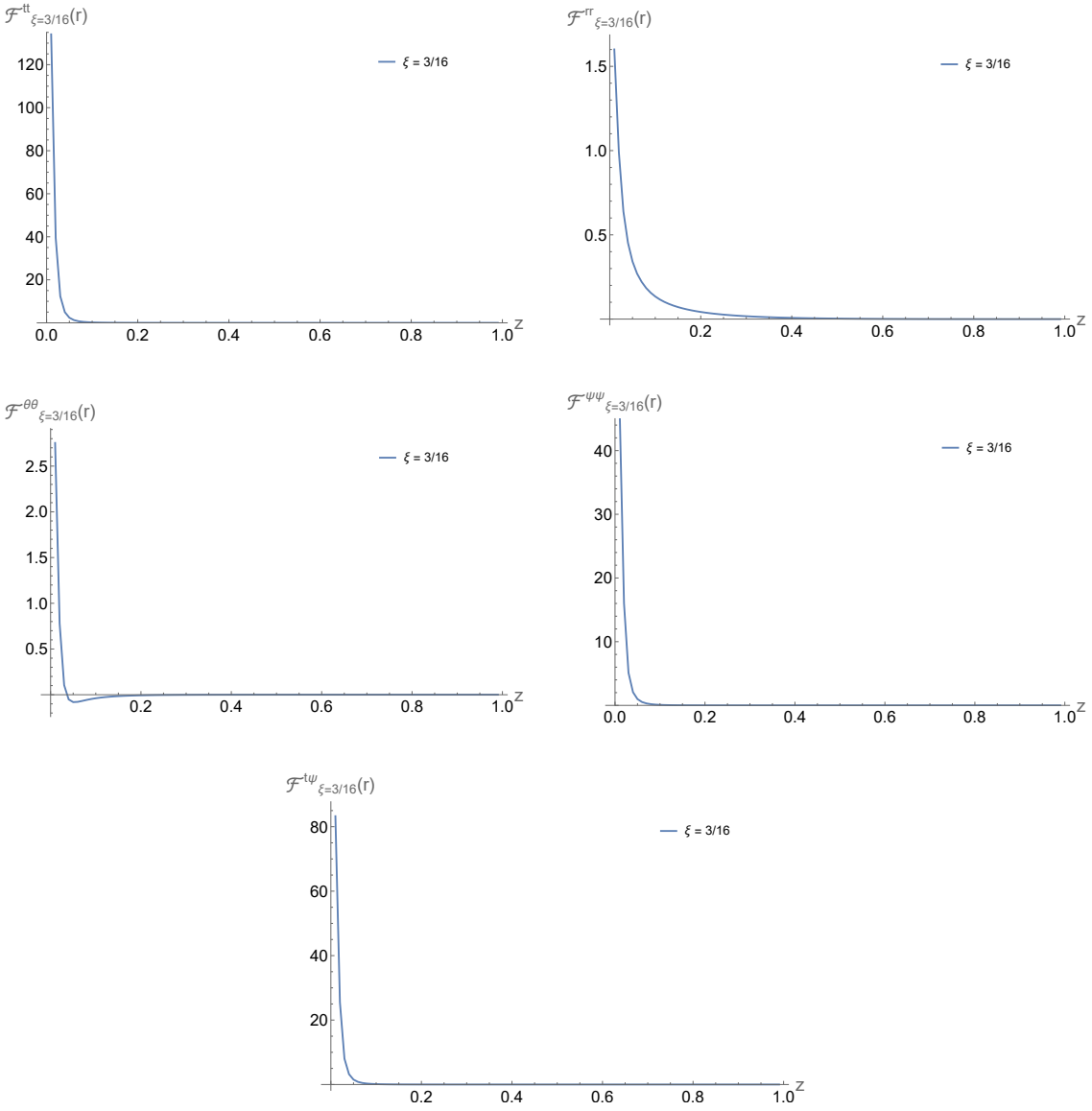

Figure 8.8: Functions $\mathcal{F}^{\bullet\bullet}_{\xi=3/16}(r)$ in the SET, shown in Equation (8.21), for $\xi = 3/16$, where the scalar field is conformally coupled.

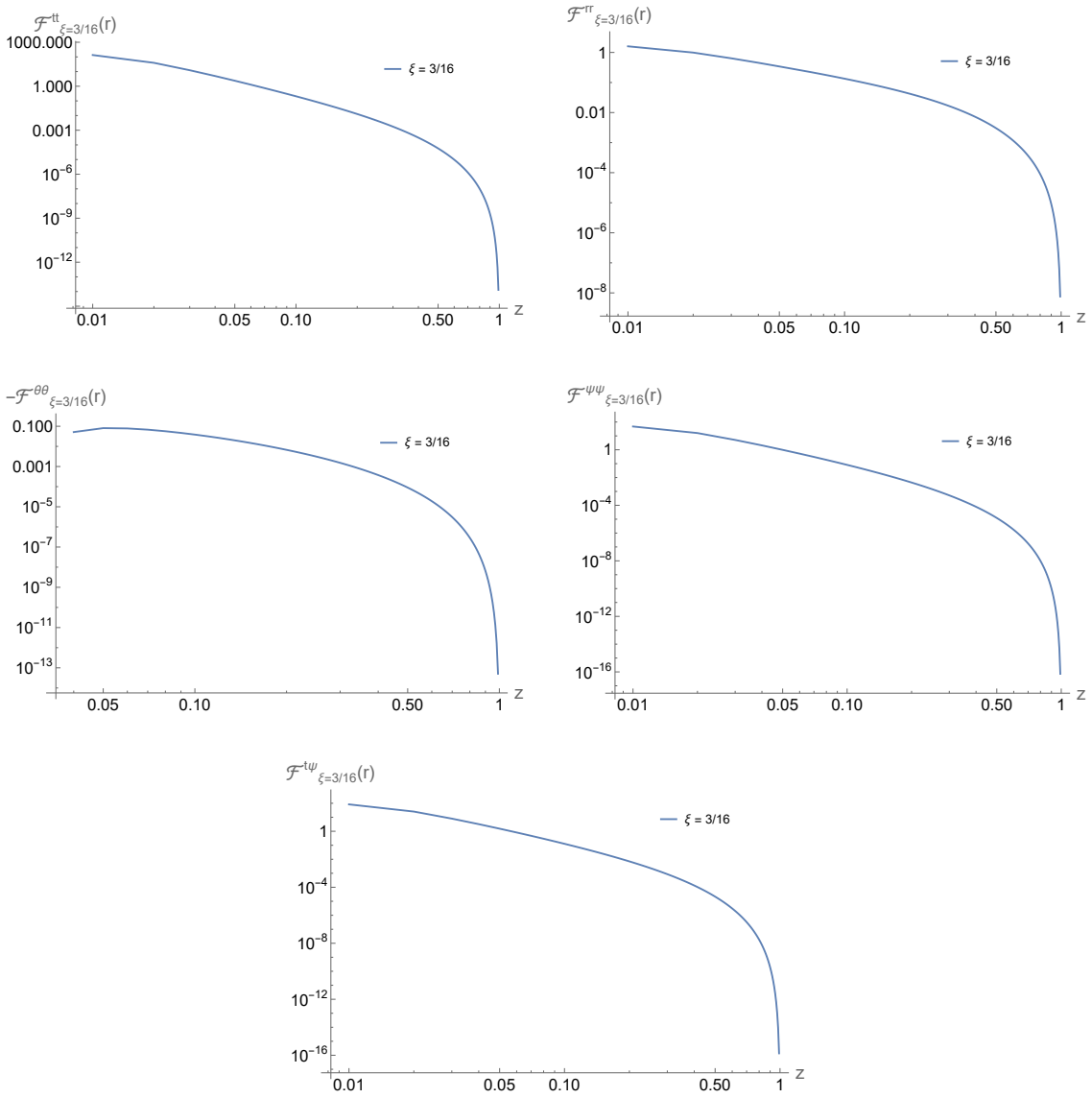

Figure 8.9: Functions $\mathcal{F}^{\bullet\bullet}_{\xi=3/16}(r)$ in the SET, shown in Equation (8.21), for $\xi = 3/16$, where the scalar field is conformally coupled, in a log-log plot. Since the function $\mathcal{F}^{\theta\theta}_{\xi=3/16}(r)$ is negative for the majority of the data points, it is displayed here with a minus sign, $-\mathcal{F}^{\theta\theta}_{\xi=3/16}(r)$, to make it positive.

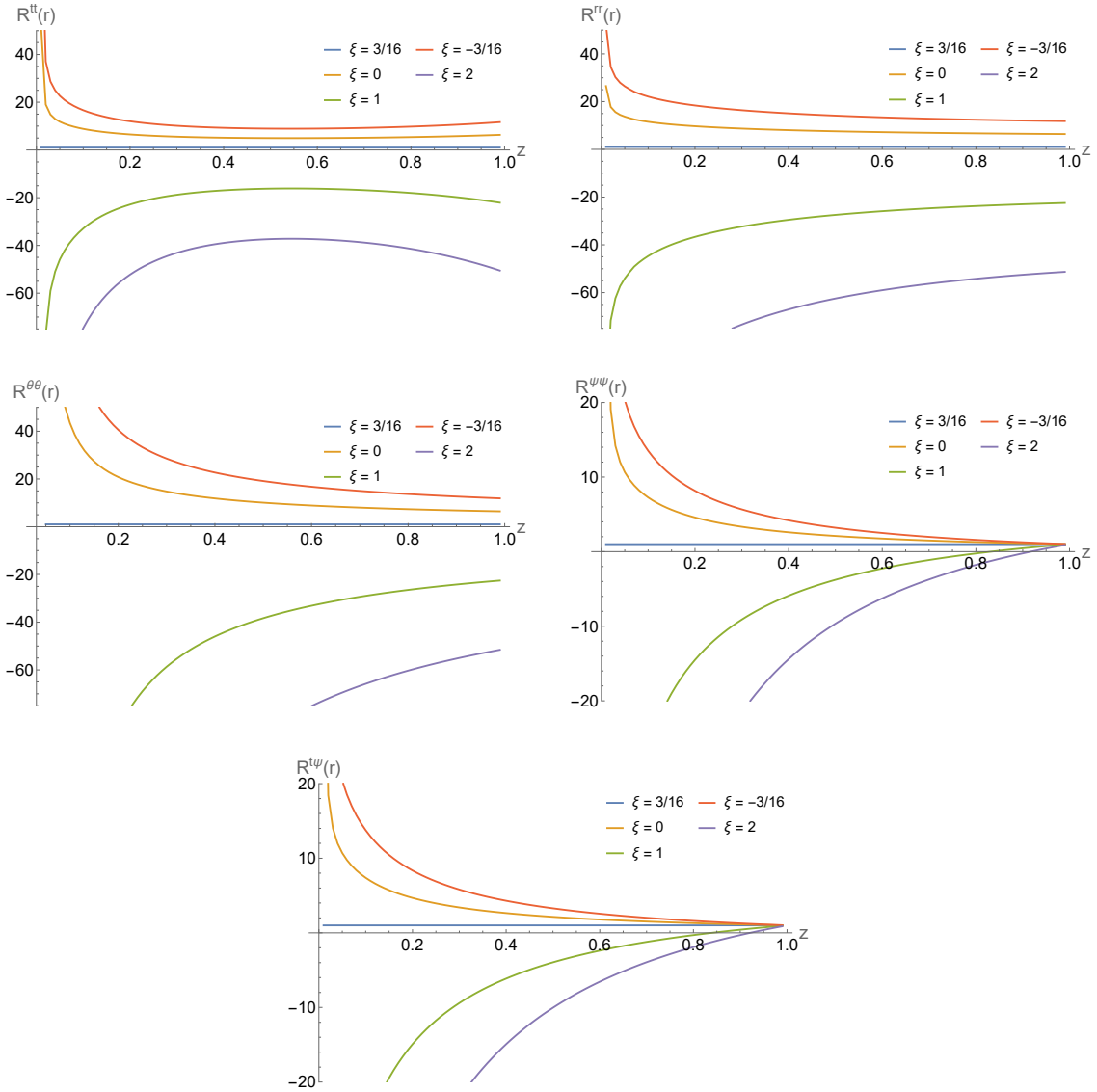

Figure 8.10: Ratios $\mathsf{R}(r)^{\bullet\bullet} = \mathcal{F}^{\bullet\bullet}(r)/\mathcal{F}^{\bullet\bullet}_{\xi=3/16}(r)$ of the functions $\mathcal{F}^{\bullet\bullet}(r)$ in the SET, shown in Equation (8.21), for selected values of the coupling constant ξ, normalised by the corresponding functions for $\xi = 3/16$, where the scalar field is conformally coupled.

nificant impact on the difference in expectation values of the SET operator and can even alter the sign of the functions $\mathcal{F}^{\bullet\bullet}(r)$. As expected, all the ratios $\mathsf{R}^{\bullet\bullet}(r)$ are identically equal to unity when $\xi = 3/16$, where the field is conformally coupled. Decreasing the coupling constant ξ below $3/16$ increases all the ratios $\mathsf{R}^{\bullet\bullet}(r)$ for every value of the radial coordinate z, while increasing ξ above $3/16$ decreases these ratios. Notably, all five ratios are negative for nearly all values of z when $\xi = 1$ or $\xi = 2$.

Near the horizon, as $z \to 0$, the ratios $\mathsf{R}^{\bullet\bullet}(r)$ all diverge, implying that the SET components exhibit a stronger divergence when the field is not conformally coupled. The rate of divergence increases as $|\xi - 3/16|$ grows. The ratios $\mathsf{R}^{\bullet\bullet}(r)$ display distinct behaviours as $z \to 1$, where the spacetime boundary is approached. The ratios $\mathsf{R}^{tt}(r)$ increase slightly in magnitude as $z \to 1$, but appear to remain finite. In contrast, $\mathsf{R}^{rr}(r)$ and $\mathsf{R}^{\theta\theta}(r)$ decrease slightly in magnitude as the boundary is approached, tending towards nonzero limits. Finally, the ratios $\mathsf{R}^{t\psi}(r)$ and $\mathsf{R}^{\psi\psi}(r)$ approach unity for all values of ξ as $z \to 1$. Another notable feature is that the ratios $\mathsf{R}^{t\psi}(r)$ and $\mathsf{R}^{\psi\psi}(r)$ are very similar, while not exactly the same, they are indistinguishable in the plots, even though the functions $\mathcal{F}^{t\psi}(r)$ and $\mathcal{F}^{\psi\psi}(r)$ are not.

On a four-dimensional Reissner-Nordström black hole, it was found in [13] that for all nonzero components of the renormalized SET in the Hartle-Hawking, Boulware, or Unruh states, changing the value of ξ does not alter the expectation value far from the black hole. In our case, this behaviour appears to hold only for certain components of the SET. Furthermore, in [13], varying the coupling constant ξ does not affect the regularity or rate of divergence of the SET components, depending on the quantum state under consideration. However, this result does not seem to be fully replicated in our set-up. A complete computation of the renormalized SET would be necessary to examine this issue in greater detail, but that will need new methodologies and a brand new method on renormalization on curved spacetime for rotating black holes which we leave for future studies.

Summary

In this chapter, we have presented the numerical analysis that we have performed on the difference in expectation values for the vacuum polarization and the stress–energy tensor of a scalar field. We have shown the steps to take in order to proceed with a numerical evaluation from Equation (8.1) and from Equation (8.14).

For the vacuum polarization, we have shown a detailed analysis of the integrand and discussed the convergence test that we have utilised to study the sum over the modes. We have then introduced the SET tensor, particularly focusing on the symmetries. We have

exploited the fact that we are working on an enhanced symmetry Kerr–AdS spacetime in five dimensions, to our advantage. We have showed how it was possible through the properties of the SET and the symmetries of the background to reduce what was the evaluation of fifteen independent components to the evaluation of just five functions that depend only on r.

We have also displayed all the analytical expressions for each component of the SET. We have discussed the code that was utilised in HPC to retrieve the numerical results, with all the difficulties that arose from this analysis and the solutions that we have implemented. Finally, we have displayed the numerical results that we obtained in Figure 8.7 and Figure 8.10.

Part III

Final considerations

Conclusion

'Ti sei mai chiesto come dovremmo fare a lasciare andare qualcosa che un tempo significava tutto? Una persona, un momento, una vita che pensavi sarebbe durata per sempre. La gente ti dice di andare avanti, di lasciar andare, ma nessuno ti dice mai come. Come si lascia andare ciò che ci ha plasmato? Forse la verità è che non siamo destinati a dimenticare. Lasciare andare non significa cancellare il passato. Significa imparare a portarlo con sé. Perché anche i capitoli più belli devono finire affinché la storia possa continuare. E forse è proprio da qui che nasce la forza. Non nel fingere che non faccia male, ma nel trovare il coraggio di voltare pagina, anche quando sembra impossibile, perché la vita non aspetta che noi guariamo. Va avanti e in qualche modo lo facciamo anche noi.'

- Kynd.

'Have you ever wondered how we are supposed to let go of something that once meant everything? A person, a moment, a life you thought would last forever. People tell you to move on, to let go, but no one ever tells you how. How do you let go of what has shaped us? Perhaps the truth is that we are not destined to forget. Letting go does not mean erasing the past. It means learning to carry it with us. Because even the most beautiful chapters must come to an end for the story to continue. And perhaps it is from this that strength is born—not in pretending that it doesn't hurt, but in finding the courage to turn the page, even when it seems impossible, because life doesn't wait for us to heal. It goes on, and somehow, so do we.'

We have reached the end of our journey. So let us summarise what we have done and the possible ramifications of this research.

In this thesis, we studied a massive quantum scalar field on a rotating black hole spacetime in five dimensions, utilising the framework of quantum field theory on curved spacetimes. We have performed a numerical evaluation for the difference in expectation values of the vacuum polarisation and the stress–energy tensor between two quantum states, taking advantage of the fact that these quantities do not need renormalization. The main goals of this thesis were

- to study a quantum massive scalar field on the Kerr–AdS$_5$ black hole spacetime by solving the Klein–Gordon equation and proceeding with the canonical quantisation of the field,
- to present new results on the addition theorems for the spin–weighted spherical harmonics,
- to construct the Boulware and the Hartle–Hawking quantum states for the massive scalar field on the Kerr–AdS$_5$ black hole spacetime,
- to evaluate the difference in the expectation values of the vacuum polarisation and the stress–energy tensor for the massive scalar field evaluated in the Boulware state and the Hartle-Hawking state,
- to present a numerical evaluation of the difference in the expectation values of the vacuum polarisation and the stress–energy tensor.

Before analysing the results, let us take a moment to summarise why we have chosen a five-dimensional rotating black hole. We have picked this background because, against all odds, studying the scalar field on this spacetime is easier than studing it on its four-dimensional counterpart. This is because, in a five-dimensional spacetime, we can exploit the extra symmetry provided by the fifth dimension to impose an enhanced symmetry on the background, which simplifies the calculation of observables, as we have seen throughout Part II. We selected the equal angular momentum Kerr–AdS five-dimensional metric (Equation (4.7)), which, as its name suggests, has the rotational parameters for ϕ and ψ equal. This gives us a shell structure for the geometry of the spacetime, resembling the symmetry of a static black hole while being a stationary one. It is also important to point out that in QFTCS theory, working in odd dimensions simplifies both the analysis and the renormalization procedure. Although we have not considered renormalization in this thesis, it remains a goal for future work. This is because a Hadamard state in odd dimensions does not exhibit logarithmic divergences in the two-point function, as we have seen in Chapter 2.

We have also chosen to study the case of an asymptotically AdS black hole. This can be thought of as if our black hole were enclosed in a "box", meaning that we have a boundary at infinity. This makes, on one side, the analysis slightly more complicated because QFTCS theory is based on the hypothesis that the background we are studying is globally hyperbolic, which is not the case for AdS black holes. However, this simply translates to imposing boundary conditions at the boundary. The asymptotically AdS spacetimes offer multiple advantages. Firstly, working in AdS gives us only one set of modes for the scalar field, as we have seen in Chapter 6. This means that no superradiance occurs, in contrast to what happens in four-dimensional Kerr black holes. We thus avoid the possible complication of canonical quantisation shown in [111, 143]. Another important aspect is the fact that asymptotically AdS black holes seem to have a regime (which is when the angular momentum of the black hole is sufficiently small) in which the speed-of-light surface does not exist. As we have discussed in the beginning of Part II, the absence of this surface allows us to define a Killing vector which is timelike everywhere outside the event horizon. This is pivotal for our analysis because it allowed us to proceed with the canonical quantisation procedure for the scalar field, and to construct quantum states for it, as we have seen in Chapter 7. Particularly, the Boulware state $|B\rangle$ and the Hartle–Hawking state $|HH\rangle$ do not exist in Kerr spacetime.

To this end, we have solved the Klein–Gordon equation by splitting the differential equation into a radial part and an angular part, exploiting the separability of the scalar field. We have studied the radial part potential to discover the behaviour of the modes, showing that no superradiant modes appear in this scenario. We have then identified the radial part as a Heun differential equation, which was useful for our numerical analysis since Heun functions are implemented in `Mathematica`. Then, we found that the angular part is a spin–weighted spherical harmonics differential equation (see Chapter 6). We have proved new addition theorems for these functions, which we have displayed in Chapter 5. We have used the addition theorems of the spin–weighted spherical harmonics to simplify the numerical analysis of observables.

Thanks to our studies of the background, we were able to use the QFTCS framework to canonical quantise the scalar field, by expressing our field as a sum over modes split between positive and negative-frequency modes, as shown in Chapter 7. Once we had quantised the scalar field, we were able to construct the Boulware and the Hartle–Hawking quantum states on the Kerr–AdS$_5$ black hole. This was an important step in continuing the analysis and study observables.

Once we obtained the ground states, we evaluated the difference in expectation values of the stress–energy tensor and the vacuum polarisation evaluated both in the Boulware and

the Hartle–Hawking states (see Equation (7.44) and (7.45)). We then showed the numerical evaluation of the stress–energy tensor and the vacuum polarisation obtained in this way in Chapter 8. We used HPC for the numerical evaluation of the sum over the modes. We needed to sum over the quantum numbers m, p and ℓ, and integrate over ω. The sum over the quantum number m was resolved by the addition theorems of the spin–weighted spherical harmonics that we have found, and the sum over p was limited by the quantum number ℓ thanks to the properties of the spin–weighted spherical harmonics. We then limited the integral over the frequencies ω and the infinite sum over ℓ. We have shown the asymptotic behaviour through numerical analysis, and we have plotted the results.

Possible future avenues for this work include, as a first step, varying the black hole parameters—the mass M, the angular momentum parameter a, and the scalar field effective mass μ_0 (see Equation (6.2)). In this thesis, we have only shown results for a fixed set of these values, as the numerical computations were quite lengthy. This was considering all the simplifications brought by the symmetries of the five-dimensional Kerr-AdS black hole. It would be interesting to study the behaviour of the SET and the vacuum polarisation while varying these parameters.

Another generalisation regards the boundary conditions. Being an AdS black hole, we had to impose boundary conditions. In our analysis, we chose the simplest one, the Dirichlet boundary condition (which is a reflective boundary condition). This means that the scalar field modes tend to zero near infinity. While these boundary conditions are the most commonly used in the literature and serve as a good first step, it would be interesting to study the behaviour of the SET and vacuum polarisation when changing these boundary conditions to Neumann boundary conditions. This can be motivated by some studies that have been conducted in pure AdS spacetimes in three and four dimensions [103, 107]. Another possibility is to consider the most general case, the Robin boundary conditions, which have been implemented in asymptotically AdS spacetime before, see [102–104, 106, 107].

Furthermore, we can extend this analysis not only to the exterior of the event horizon but also to the interior. This has been the focus of many papers in the literature (see for example [81, 82, 97, 98, 156, 157]). In our case, the Boulware state diverges at the event horizon. However, the Hartle–Hawking state is regular across the horizon. It might be possible to extend the definition we have presented to also include the interior of the black hole. Usually, this would not be possible since the Hartle–Hawking state does not exist on four-dimensional Kerr black holes, see [78].

Another possibility could be to analyse the case in lower dimensionality. We have briefly introduced the BTZ black hole in Part I. This is a rotating black hole that is asymp-

totically AdS in three dimensions. The lower dimensionality allows us to build the SET expectation value of a quantum scalar field using the method of images [133]. It has been shown that it is possible to construct a Hartle–Hawking state on a BTZ spacetime, and such a state has been used to compute the renormalized SET for both the interior and exterior of the black hole (see [32, 46, 92, 133]). This result can also be used to study the back-reaction of the scalar field [32].

A natural extension of this work would be to use the definition of the Hartle–Hawking state for the scalar field on this background to evaluate a renormalized SET and vacuum polarisation for this state, and to verify whether these quantities are regular across the horizon. This would entail, that instead of exploiting the Hadamard properties and studying the differences in the expectation values of observables between quantum states, one could attempt to find a renormalization method for the stress–energy tensor and the vacuum polarisation. This has yet to be done for the Kerr AdS_5 black hole. The full computation of the SET expectation value on Kerr black holes has been performed only relatively recently [87, 88, 156–159]. This is because the techniques that were implemented for static black holes were not easily extendable to the stationary ones. The method used in [87, 88] still faces formidable practical challenges; for example, four million scalar field modes are required to produce results. However, progress has been made in the static case for the renormalization of the SET using a method called the "extended coordinates method" [135, 136]. This method is the only one that has been used to find renormalized expectation values in more than four dimensions. Our suggestion for proceeding from here is to use this method to achieve renormalization. This would overcome the numerical difficulties of the method shown in [87, 88] and provide a renormalized SET. To do this, we need to extend this method to rotating black holes. This is where we think that our setup comes to our aid. In fact, the fifth dimension could be the key to generalising this method to any Kerr black hole, not just the five-dimensional one. This is because the symmetries of this spacetime, as mentioned earlier, resemble those of a static black hole. We believe that the enhanced symmetry could be exploited even further to help find a generalisation of the "extended coordinates method", which extends to also the four dimensional case.

Bibliography

[1] *NIST Digital Library of Mathematical Functions*. https://dlmf.nist.gov/, Release 1.2.1 of 2024-06-15. F. W. J. Olver, A. B. Olde Daalhuis, D. W. Lozier, B. I. Schneider, R. F. Boisvert, C. W. Clark, B. R. Miller, B. V. Saunders, H. S. Cohl, and M. A. McClain, eds.

[2] H. K. Kunduri A. Al Balushi, R. A. Hennigar and R. B. Mann. Holographic complexity and thermodynamic volume. *Phys. Rev. Lett.*, 126:101601, 2021.

[3] A. Challinor A. Lewis and N. Turok. Analysis of CMB polarization on an incomplete sky. *Phys. Rev. D*, 65:023505, 2002.

[4] A. Pound A. Spiers and B. Wardell. Second-order perturbations of the Schwarzschild spacetime: Practical, covariant, and gauge-invariant formalisms. *Phys. Rev. D*, 110:064030, 2024.

[5] K. Akiyama et al. First M87 Event Horizon Telescope Results. I. The Shadow of the Supermassive Black Hole. *Astrophys. J. Lett.*, 875:L1, 2019.

[6] A. N. Aliev and O. Delice. Superradiant instability of five-dimensional rotating charged AdS black holes. *Phys. Rev. D*, 79:024013, 2009.

[7] B. Allen, A. Folacci, and G. W. Gibbons. Anti-de Sitter space at finite temperature. *Phys. Lett. B*, 189:304, 1987.

[8] J. Barragán Amado, B. Carneiro Da Cunha, and E. Pallante. Scalar quasinormal modes of Kerr-AdS$_5$. *Phys. Rev. D*, 99(10):105006, 2019.

[9] V. E. Ambruş and E. Winstanley. Rotating quantum states. *Phys. Lett. B*, 734:296–301, 2014.

[10] V. E. Ambrus, C. Kent, and E. Winstanley. Analysis of scalar and fermion quantum field theory on anti-de Sitter spacetime. *Int. J. Mod. Phys. D*, 27:1843014, 2018.

[11] P. R. Anderson, W. A. Hiscock, and D. A. Samuel. Stress energy tensor of quantized scalar fields in static black hole space-times. *Phys. Rev. Lett.*, 70:1739–1742, 1993.

[12] P. R. Anderson, W. A. Hiscock, and D. A. Samuel. Stress-energy tensor of quantized scalar fields in static spherically symmetric space-times. *Phys. Rev. D*, 51:4337–4358, 1995.

[13] J. Arrechea, C. Breen, A. Ottewill, and P. Taylor. Renormalized stress-energy tensor for scalar fields in Hartle-Hawking, Boulware, and Unruh states in the Reissner-Nordström spacetime. *Phys. Rev. D*, 108:125004, 2023.

[14] S. J. Avis, C. J. Isham, and D. Storey. Quantum Field Theory in anti-De Sitter Space-Time. *Phys. Rev. D*, 18:3565, 1978.

[15] W. Lee B.-H. Lee and Y.-H. Qi. Superradiance in the Kerr-Taub-NUT spacetime. 11 2023.

[16] M. Banados, M. Henneaux, C. Teitelboim, and J. Zanelli. Geometry of the (2+1) black hole. *Phys. Rev. D*, 48:1506–1525, 1993.

[17] M. Banados, C. Teitelboim, and J. Zanelli. The black hole in three-dimensional space-time. *Phys. Rev. Lett.*, 69:1849–1851, 1992.

[18] V. S. Barroso and J. P. M. Pitelli. Boundary conditions and vacuum fluctuations in AdS_4. *Gen. Rel. Grav.*, 52:29, 2020.

[19] A. O. Barut and R. Raczka. *Theory of group representations and applications*. 1986.

[20] C. A. Bayona and N. R. F. Braga. Anti-de Sitter boundary in Poincare coordinates. *Gen. Rel. Grav.*, 39:1367–1379, 2007.

[21] M. Benini, C. Dappiaggi, and A. Schenkel. Algebraic quantum field theory on spacetimes with timelike boundary. *Annales Henri Poincare*, 19(8):2401–2433, 2018.

[22] N. D. Birrell and P. C. W. Davies. *Quantum Fields in Curved Space*. Cambridge Monographs on Mathematical Physics. Cambridge University Press, Cambridge, UK, 1982.

[23] D. G. Boulware. Quantum Field Theory in Schwarzschild and Rindler Spaces. *Phys. Rev. D*, 11:1404, 1975.

[24] M. Boyle. How should spin-weighted spherical functions be defined? *J. Math. Phys.*, 57:092504, 2016.

[25] P. Breitenlohner and D. Z. Freedman. Positive energy in anti-de Sitter backgrounds and gauged extended supergravity. *Phys. Lett. B*, 115:197–201, 1982.

[26] P. Breitenlohner and D. Z. Freedman. Stability in gauged extended supergravity. *Annals Phys.*, 144:249, 1982.

[27] M. M. Caldarelli, G. Cognola, and D. Klemm. Thermodynamics of Kerr-Newman-AdS black holes and conformal field theories. *Class. Quant. Grav.*, 17:399–420, 2000.

[28] W. B. Campbell. Tensor and spinor spherical harmonics and the spin-s harmonics ${}_sY_{lm}(\theta, \phi)$. *J. Math. Phys.*, 12:1763–1770, 1971.

[29] P. Candelas. Vacuum polarization in Schwarzschild space-time. *Phys. Rev. D*, 21:2185–2202, 1980.

[30] S. M. Carroll. *Spacetime and Geometry: An Introduction to General Relativity.* Cambridge University Press, 7 2019.

[31] M. Casals, A. Fabbri, C. Martínez, and J. Zanelli. Quantum dress for a naked singularity. *Phys. Lett. B*, 760:244–248, 2016.

[32] M. Casals, A. Fabbri, C. Martínez, and J. Zanelli. Quantum backreaction on three-dimensional black holes and naked singularities. *Phys. Rev. Lett.*, 118:131102, 2017.

[33] O. Mišković and J. Zanelli. Negative spectrum of the $2 + 1$ black hole. *Phys. Rev. D*, 79:105011, May 2009.

[34] C. Dappiaggi, H. Ferreira, and A. Marta. Ground states of a Klein-Gordon field with Robin boundary conditions in global anti–de Sitter spacetime. *Phys. Rev. D*, 98(2):025005, 2018.

[35] C. Dappiaggi and H. R. C. Ferreira. On the algebraic quantization of a massive scalar field in anti-de-Sitter spacetime. *Rev. Math. Phys.*, 30(02):1850004, 2017.

[36] C. Dappiaggi, H. R. C. Ferreira, and C. A. R. Herdeiro. Superradiance in the BTZ black hole with Robin boundary conditions. *Phys. Lett. B*, 778:146–154, 2018.

[37] C. Dappiaggi, H. R. C. Ferreira, and B. A. Juárez-Aubry. Mode solutions for a Klein-Gordon field in anti–de Sitter spacetime with dynamical boundary conditions of Wentzell type. *Phys. Rev. D*, 97(8):085022, 2018.

[38] C. Dappiaggi and A. Marta. Fundamental solutions and Hadamard states for a scalar field with arbitrary boundary conditions on an asymptotically AdS spacetimes. *Math. Phys. Anal. Geom.*, 24(3):28, 2021.

[39] C. C. de Oliveira, R. A. Mosna, and J. P. M. Pitelli. Robin boundary conditions in acoustic BTZ black holes. *Phys. Rev. D*, 107(6):064018, 2023.

[40] L. de S. Campos, C. Dappiaggi, and L. Sinibaldi. Hidden freedom in the mode expansion on static spacetimes. *Gen. Rel. Grav.*, 55(3):50, 2023.

[41] Y. Decanini and A. Folacci. Hadamard renormalization of the stress-energy tensor for a quantized scalar field in a general spacetime of arbitrary dimension. *Phys. Rev. D*, 78:044025, 2008.

[42] G. F. Torres del Castillo. Spin-weighted spherical harmonics and their applications. *Rev. Mex. Fis.*, 53:125–134, 2007.

[43] T. Delsante, J. V. Rocha, and R. Santarelli. Geodesic motion in equal angular momenta Myers-Perry-AdS spacetimes. *Phys. Rev. D*, 92(8):084028, 2015.

[44] G. Denardo and R. Percacci. Quantum Field Theory for a Rotating Observer. *Nuovo Cim. B*, 48:81–89, 1978.

[45] B. S. DeWitt. Quantum Field Theory in Curved Space-Time. *Phys. Rept.*, 19:295–357, 1975.

[46] O. J. C. Dias, H. S. Reall, and J. E. Santos. The BTZ black hole violates strong cosmic censorship. *JHEP*, 2019(12):097, 2019.

[47] P. A. M. Dirac. Quantised singularities in the electromagnetic field. *Proc. Roy. Soc. Lond. A*, 133:60–72, 1931.

[48] T. Dray. The relationship between monopole harmonics and spin-weighted spherical harmonics. *J. Math. Phys.*, 26:1030–1033, 1985.

[49] T. Dray. A unified treatment of Wigner D-functions, spin-weighted spherical harmonics, and monopole harmonics. *J. Math. Phys.*, 27:781–792, 1986.

[50] G. Duffy and A. C. Ottewill. The rotating quantum thermal distribution. *Phys. Rev. D*, 67:044002, 2003.

[51] G. Duffy and A. C. Ottewill. The renormalized stress tensor in Kerr space-time: Numerical results for the Hartle-Hawking vacuum. *Phys. Rev. D*, 77:024007, 2008.

[52] A. Einstein. On the electrodynamics of moving bodies. *Annalen Phys.*, 17:891–921, 1905.

[53] A. Einstein. Zur Allgemeinen Relativitätstheorie. *Sitzungsber. Preuss. Akad. Wiss. Berlin (Math. Phys.)*, 1915:778–786, 1915. [Addendum: Sitzungsber.Preuss.Akad.Wiss.Berlin (Math.Phys.) 1915, 799–801 (1915)].

[54] E. Elizalde, S. D. Odintsov, A. Romeo, A. A. Bytsenko, and S. Zerbini. *Zeta regularization techniques with applications.* World Scientific Publishing, Singapore, 1994.

[55] C. W. F. Everitt et al. Gravity Probe B: Final Results of a Space Experiment to Test General Relativity. *Phys. Rev. Lett.*, 106:221101, 2011.

[56] W. Freeden and M. Schreiner. *Spin-weighted spherical harmonics, in: Spherical Functions of Mathematical Geosciences.* Birkhauser, Berlin, Heidelberg, 2022.

[57] V. P. Frolov and D. Stojkovic. Quantum radiation from a five-dimensional rotating black hole. *Phys. Rev. D*, 67:084004, 2003.

[58] D. N. Page G. W. Gibbons, H. Lu and C. N. Pope. Rotating black holes in higher dimensions with a cosmological constant. *Phys. Rev. Lett.*, 93:171102, 2004.

[59] O. Gannot and M. Wrochna. Propagation of singularities on AdS spacetimes for general boundary conditions and the holographic Hadamard condition. *J. Inst. Math. Jussieu*, 21(1):67–127, 2022.

[60] C. Gérard. The Hartle-Hawking-Israel state on spacetimes with stationary bifurcate Killing horizons. *Rev. Math. Phys.*, 33:2150028, 2021.

[61] G. W. Gibbons, H. Lu, D. N. Page, and C. N. Pope. The general Kerr-de Sitter metrics in all dimensions. *J. Geom. Phys.*, 53:49–73, 2005.

[62] G. W. Gibbons, M. J. Perry, and C. N. Pope. The first law of thermodynamics for Kerr-anti-de Sitter black holes. *Class. Quant. Grav.*, 22:1503–1526, 2005.

[63] S. Gielen and E. Nash. Quantum cosmology of pure connection general relativity. *Class. Quant. Grav.*, 40(11):115009, 2023.

[64] J. B. Hartle and S. W. Hawking. Path Integral Derivation of Black Hole Radiance. *Phys. Rev. D*, 13:2188–2203, 1976.

[65] S. W. Hawking. Particle creation by black holes. *Commun. Math. Phys.*, 43:199–220, 1975.

[66] S. W. Hawking and G. F. R. Ellis. *The Large Scale Structure of Space-Time.* Cambridge Monographs on Mathematical Physics. Cambridge University Press, 2 2023.

[67] S. W. Hawking and D. N. Page. Thermodynamics of Black Holes in anti-De Sitter Space. *Commun. Math. Phys.*, 87:577, 1983.

[68] S. W. Hawking and H. S. Reall. Charged and rotating AdS black holes and their CFT duals. *Phys. Rev. D*, 61:024014, 2000.

[69] K. W. Howard. Vacuum $\langle T_{\mu\nu} \rangle$ in Schwarzschild space-time. *Phys. Rev. D*, 30:2532–2547, 1984.

[70] K. W. Howard and P. Candelas. Quantum stress tensor in Schwarzschild space-time. *Phys. Rev. Lett.*, 53:403–406, 1984.

[71] W. Hu and M. J. White. CMB anisotropies: total angular momentum method. *Phys. Rev. D*, 56:596–615, 1997.

[72] A. Ishibashi and R. M. Wald. Dynamics in nonglobally hyperbolic static space-times. 2. General analysis of prescriptions for dynamics. *Class. Quant. Grav.*, 20:3815–3826, 2003.

[73] A. Ishibashi and R. M. Wald. Dynamics in nonglobally hyperbolic static space-times. 3. Anti-de Sitter space-time. *Class. Quant. Grav.*, 21:2981–3014, 2004.

[74] W. Israel. Event horizons in static vacuum space-times. *Phys. Rev.*, 164:1776–1779, 1967.

[75] W. Israel. Event horizons in static electrovac space-times. *Commun. Math. Phys.*, 8:245–260, 1968.

[76] W. Israel. Thermo field dynamics of black holes. *Phys. Lett. A*, 57:107–110, 1976.

[77] E. T. Newman F. Rohrlich J. N. Goldberg, A. J. MacFarlane and E. C. G. Sudarshan. Spin-s spherical harmonics and $\eth$. *J. Math. Phys.*, 8:2155–2161, 1967.

[78] B. S. Kay and R. M. Wald. Theorems on the Uniqueness and Thermal Properties of Stationary, Nonsingular, Quasifree States on Space-Times with a Bifurcate Killing Horizon. *Phys. Rept.*, 207:49–136, 1991.

[79] C. Kent. *Quantum scalar field theory on anti-de Sitter space.* PhD thesis, Sheffield U., 2013.

[80] R. P. Kerr. Gravitational field of a spinning mass as an example of algebraically special metrics. *Phys. Rev. Lett.*, 11:237–238, 1963.

[81] C. Klein, M. Soltani, M. Casals, and S. Hollands. Infinite quantum twisting at the Cauchy horizon of rotating black holes. *Phys. Rev. Lett.*, 132:121501, 2024.

[82] C. Klein and J. Zahn. Long-range correlations of the stress tensor near the Cauchy horizon. *Phys. Rev. D*, 109:L061702, 2024.

[83] I. Koga, N. Oshita, and K. Ueda. Global study of the scalar quasinormal modes of Kerr-AdS$_5$ black holes: Stability, thermality, and horizon area quantization. *Phys. Rev. D*, 105:124044, 2022.

[84] S. Konewko and E. Winstanley. Charge superradiance on charged BTZ black holes. *Eur. Phys. J. C*, 84(6):594, 2024.

[85] H. K. Kunduri, J. Lucietti, and H. S. Reall. Gravitational perturbations of higher dimensional rotating black holes: Tensor perturbations. *Phys. Rev. D*, 74:084021, 2006.

[86] F. Gonzalez Ledesma and M. Mewes. Spherical-harmonic tensors. *Phys. Rev. Res.*, 2:043061, 2020.

[87] A. Levi. Renormalized stress-energy tensor for stationary black holes. *Phys. Rev. D*, 95(2):025007, 2017.

[88] A. Levi, E. Eilon, A. Ori, and M. van de Meent. Renormalized stress-energy tensor of an evaporating spinning black hole. *Phys. Rev. Lett.*, 118:141102, 2017.

[89] A. Levi and A. Ori. Pragmatic mode-sum regularization method for semiclassical black-hole spacetimes. *Phys. Rev. D*, 91:104028, 2015.

[90] G. Lifschytz and M. Ortiz. Scalar field quantization on the (2+1)-dimensional black hole background. *Phys. Rev. D*, 49:1929–1943, Feb 1994.

[91] B. C. Nolan A. C. Ottewill M. Casals, S. R. Dolan and E. Winstanley. Quantization of fermions on Kerr space-time. *Phys. Rev. D*, 87:064027, 2013.

[92] C. Martínez M. Casals, A. Fabbri and J. Zanelli. Quantum-corrected rotating black holes and naked singularities in (2+1) dimensions. *Phys. Rev. D*, 99(10):104023, 2019.

[93] J. M. Maldacena. The Large N limit of superconformal field theories and supergravity. *Adv. Theor. Math. Phys.*, 2:231–252, 1998.

[94] C. Martínez, C. Teitelboim, and J. Zanelli. Charged rotating black hole in three spacetime dimensions. *Phys. Rev. D*, 61:104013, Apr 2000.

[95] C. Martínez and J. Zanelli. Conformally dressed black hole in 2 + 1 dimensions. *Phys. Rev. D*, 54:3830–3833, Sep 1996.

[96] C. Martínez and J. Zanelli. Back reaction of a conformal field on a three-dimensional black hole. *Phys. Rev. D*, 55:3642–3646, Mar 1997.

[97] T. McMaken. Backreaction from quantum fluxes at the Kerr inner horizon. *Phys. Rev. D*, 110:045019, 2024.

[98] T. McMaken and A. J. S. Hamilton. Renormalization of $\langle\phi^2\rangle$ at the inner horizon of rotating, accreting black holes. *Phys. Rev. D*, 105:125020, 2022.

[99] V. Michel and K. Seibert. *A mathematical view on spin-weighted spherical harmonics and their applications in geodesy, in: Mathematische Geodäsie/Mathematical Geodesy. Springer Reference Naturwissenschaften, W. Freeden (Ed.)*. Springer Spektrum, Berlin, Heidelberg, 2020.

[100] J. Michell. On the Means of Discovering the Distance, Magnitude, &c. of the Fixed Stars, in Consequence of the Diminution of the Velocity of Their Light, in Case Such a Diminution Should be Found to Take Place in any of Them, and Such Other Data Should be Procured from Observations, as Would be Farther Necessary for That Purpose. *Phil. Trans. Roy. Soc. Lond.*, 74:35–57, 1784.

[101] D. Morgan, S. Thom, E. Winstanley, and P. M. Young. Some general properties of the renormalized stress-energy tensor for static quantum states on $(n+1)$-dimensional spherically symmetric black holes. *Gen. Rel. Grav.*, 39:1719–1734, 2007.

[102] T. Morley, S. Namasivayam, and E. Winstanley. Renormalized stress-energy tensor on global anti-de Sitter space-time with Robin boundary conditions. *Gen. Rel. Grav.*, 56:38, 2024.

[103] T. Morley, P. Taylor, and E. Winstanley. Quantum field theory on global anti-de Sitter space-time with Robin boundary conditions. *Class. Quant. Grav.*, 38:035009, 2021.

[104] T. Morley, P. Taylor, and E. Winstanley. Vacuum polarization on topological black holes with Robin boundary conditions. *Phys. Rev. D*, 103(4):045007, 2021.

[105] R. C. Myers and M. J. Perry. Black Holes in Higher Dimensional Space-Times. *Annals Phys.*, 172:304, 1986.

[106] S. Namasivayam. *Quantum scalar field theory on anti-de Sitter space-time with Robin boundary conditions*. PhD thesis, The University of Sheffield, Faculty of Science (Sheffield), School of Mathematics and Statistics (Sheffield), United Kingdom, Sheffield U., 2024.

[107] S. Namasivayam and E. Winstanley. Vacuum polarization on three-dimensional anti-de Sitter space-time with Robin boundary conditions. *Gen. Rel. Grav.*, 55:13, 2023.

[108] E. T. Newman and R. Penrose. Note on the Bondi-Metzner-Sachs group. *J. Math. Phys.*, 7:863–870, 1966.

[109] S. Noda and H. Motohashi. Spectroscopy of Kerr-AdS5 spacetime with the Heun function: Quasinormal modes, greybody factor, and evaporation. *Phys. Rev. D*, 106(6):064025, 2022.

[110] I. D. Novikov and V. P. Frolov. *Physics of Black Holes*, volume 27. Kluwer Academic, Dordrecht, Netherlands, 1989.

[111] A. C. Ottewill and E. Winstanley. The Renormalized stress tensor in Kerr spacetime: general results. *Phys. Rev. D*, 62:084018, 2000.

[112] D. N. Page P. Krtous, D. Kubiznak and V. P. Frolov. Killing-Yano tensors, rank-2 Killing tensors, and conserved quantities in higher dimensions. *JHEP*, 02:004, 2007.

[113] L. Parker. Quantized fields and particle creation in expanding universes. 1. *Phys. Rev.*, 183:1057–1068, 1969.

[114] L. Parker and S. A. Fulling. Adiabatic regularization of the energy momentum tensor of a quantized field in homogeneous spaces. *Phys. Rev. D*, 9:341–354, 1974.

[115] W. Pauli and F. Villars. On the Invariant regularization in relativistic quantum theory. *Rev. Mod. Phys.*, 21:434–444, 1949.

[116] J. D. Pendleton. Euler angle geometry, helicity basis vectors, and the Wigner D-function addition theorem. *Am. J. Phys.*, 71:1280–1291, 2003.

[117] M. E. Peskin and D. V. Schroeder. *An Introduction to quantum field theory.* Addison-Wesley, Reading, USA, 1995.

[118] M. P. Ryan Jr. R. A. Breuer and S. Waller. Some properties of spin-weighted spheroidal harmonics. *Proc. R. Soc. Lond.*, A 358:71–86, 1977.

[119] K. Fredenhagen J. Yngvason K. Rejzner M. Benini C. J. Fewster R. Verch I. Khavkine V. Moretti T. P. Hack N. Pinamonti D. Bahns S. Doplicher G. Morsella G. Piacitelli K. H. Rehren P. Naaijkens R. Brunetti, C. Dappiaggi and G. Lechner. *Advances in Algebraic Quantum Field Theory.* Mathematical Physics Studies. Springer, 2015.

[120] S. Kurien R. Rubinstein and C. Cambon. Scalar and tensor spherical harmonics expansion of the velocity correlation in homogeneous anisotropic turbulence. *J. Turbulence*, 16:1058–1075, 2015.

[121] M. J. Radzikowski. Micro-local approach to the Hadamard condition in quantum field theory on curved space-time. *Commun. Math. Phys.*, 179:529–553, 1996.

[122] H. Reissner. Über die Eigengravitation des elektrischen Feldes nach der Einsteinschen Theorie. *Annalen Phys.*, 355(9):106–120, 1916.

[123] D. C. Robinson. Uniqueness of the Kerr black hole. *Phys. Rev. Lett.*, 34:905–906, 1975.

[124] A. Ronveaux, editor. *Heun's differential equations.* Oxford Science Publications. The Clarendon Press, Oxford University Press, New York, 1995. With contributions by F. M. Arscott, S. Yu. Slavyanov, D. Schmidt, G. Wolf, P. Maroni and A. Duval.

[125] C. J. Hunter S. W. Hawking and M. Taylor. Rotation and the AdS-CFT correspondence. *Phys. Rev. D*, 59:064005, 1999.

[126] J. J. G. Scanio. Spin-weighted spherical harmonics and electromagnetic multipole expansions. *Am. J. Phys.*, 45:173, 1977.

[127] R. J. Schmidt. On the numerical solution of linear simultaneous equations by an iterative method. *Phil. Mag.*, 32:369–383, 1941.

[128] K. Schwarzschild. On the gravitational field of a mass point according to Einstein's theory. *Sitzungsber. Preuss. Akad. Wiss. Berlin (Math. Phys.)*, 1916:189–196, 1916.

[129] K. Seibert. *Spin-weighted spherical harmonics and their application for the construction of tensor Slepian functions on the spherical cap*. PhD thesis, Universität Siegen, 2018.

[130] D. Shanks. Non-linear transformation of divergent and slowly convergent sequences. *J. of Math. and Phys.*, 34:1–42, 1955.

[131] S. K. Sharma and U. Khanal. Perturbation of FRW spacetime in NP formalism. *Int. J. Mod. Phys. D*, 23:1450017, 2014.

[132] M. Shiraishi. *Probing the Early Universe with the CMB Scalar, Vector and Tensor Bispectrum*. Springer Theses. Springer, 2013.

[133] A. R. Steif. The Quantum stress tensor in the three-dimensional black hole. *Phys. Rev. D*, 49:585–589, 1994.

[134] G. 't Hooft and M. J. G. Veltman. Regularization and Renormalization of Gauge Fields. *Nucl. Phys. B*, 44:189–213, 1972.

[135] P. Taylor and C. Breen. Mode-sum prescription for the vacuum polarization in odd dimensions. *Phys. Rev. D*, 94:125024, 2016.

[136] P. Taylor and C. Breen. Mode-sum prescription for vacuum polarization in black hole spacetimes in even dimensions. *Phys. Rev. D*, 96(10):105020, 2017.

[137] P. Taylor and C. Breen. Semiclassical backreaction on asymptotically anti–de Sitter black holes. *Phys. Rev. D*, 103:025006, 2021.

[138] P. Taylor, C. Breen, and A. Ottewill. Mode-sum prescription for the renormalized stress energy tensor on black hole spacetimes. *Phys. Rev. D*, 106:065023, 2022.

[139] K. S. Thorne. Multipole expansions of gravitational radiation. *Rev. Mod. Phys.*, 52:299–339, 1980.

[140] W. G. Unruh. Second quantization in the Kerr metric. *Phys. Rev. D*, 10:3194–3205, 1974.

[141] W. G. Unruh. Notes on black hole evaporation. *Phys. Rev. D*, 14:870, 1976.

[142] W. G. Unruh. Has Hawking radiation been measured? *Found. Phys.*, 44:532–545, 2014.

[143] R. P. Bernar V. Balakumar and E. Winstanley. Quantization of a charged scalar field on a charged black hole background. *Phys. Rev. D*, 106:125013, 2022.

[144] A. N. Moskalev V. K. Khersonskii and D. A. Varshalovich. *Quantum Theory Of Angular Momentum.* World Scientific Publishing Company, 1988.

[145] P. Krtous V. P. Frolov and D. Kubiznak. Black holes, hidden symmetries, and complete integrability. *Living Rev. Rel.*, 20:6, 2017.

[146] R. M. Wald. Dynamics in nonglobally hyperbolic, static space-times. *J. Math. Phys.*, 21:2802–2805, 1980.

[147] R. M. Wald. *General Relativity.* Chicago Univ. Pr., Chicago, USA, 1984.

[148] R. M. Wald. Quantum field theory in curved space-time. In *14th International Conference on General Relativity and Gravitation (GR14)*, pages 401–415, 8 1995.

[149] S. Weinberg. *The Quantum theory of fields. Vol. 1: Foundations.* Cambridge University Press, 6 2005.

[150] E. P. Wigner. On Unitary Representations of the Inhomogeneous Lorentz Group. *Annals Math.*, 40:149–204, 1939.

[151] E. Witten. Anti-de Sitter space and holography. *Adv. Theor. Math. Phys.*, 2:253–291, 1998.

[152] T. T. Wu and C. N. Yang. Dirac monopole without strings: Monopole harmonics. *Nuclear Physics B*, 107(3):365–380, 1976.

[153] T. T. Wu and C. N. Yang. Some properties of monopole harmonics. *Phys. Rev. D*, 16:1018–1021, 1977.

[154] L. Jacques Y. Wiaux and P. Vandergheynst. Fast directional correlation on the sphere with steerable filters. *Astrophys. J.*, 652:820–832, 2006.

[155] L. Jacques Y. Wiaux and P. Vandergheynst. Fast spin +-2 spherical harmonics transforms. *J. Comput. Phys.*, 226:2359–2371, 2007.

[156] N. Zilberman, M. Casals, A. Levi, A. Ori, and A. C. Ottewill. Computation of $\langle\Phi^2\rangle$ and quantum fluxes at the polar interior of a spinning black hole. *Phys. Rev. D*, 111:124054, Jun 2025.

[157] N. Zilberman, M. Casals, A. Ori, and A. C. Ottewill. Quantum fluxes at the inner horizon of a spinning black hole. *Phys. Rev. Lett.*, 129:261102, 2022.

[158] N. Zilberman, M. Casals, A. Ori, and A. C. Ottewill. Two-point function of a quantum scalar field in the interior region of a Kerr black hole. *Phys. Rev. D*, 106:125011, 2022.

[159] N. Zilberman and A. Ori. Quantum fluxes at the inner horizon of a near-extremal spherical charged black hole. *Phys. Rev. D*, 104:024066, 2021.